The Role of the Ciliary Protein IFT88 in Post-Natal Joint Development, Homeostasis and Disease





Clarissa R. Coveney
Green Templeton College
University of Oxford

Supervised by
Dr Angus Wann
Professor Tonia Vincent

A thesis submitted in partial fulfilment of the requirements for the degree of Doctor of Philosophy

Michaelmas Term, 2019

Abstract

The Role of the Ciliary Protein IFT88 in Post-Natal Joint Development, Homeostasis and Disease

Clarissa R. Coveney

Green Templeton College, Michaelmas Term 2019

A thesis submitted in partial fulfilment of the requirements for the degree of Doctor of Philosophy of the University of Oxford

More than 50% of the UK population over 75 suffers from the degenerative cartilage disease osteoarthritis, but the mechanisms of pathogenesis remain elusive. While it is appreciated that joint mechanics are hugely influential to osteoarthritis and fundamental for cartilage development and homeostasis, the chondrocyte/cartilage 'mechanostat' is unknown. Chondrocytes assemble a primary cilium, a microtubule-based organelle reliant on intraflagellar transport (IFT). Mutations to ciliary genes alter the chondrocyte's anabolic matrix response to compression *in vitro*. Perturbations to IFT *in vivo* alter embryonic and early post-natal skeletal development, but little is known of its cartilaginous influence in adulthood. The main aim of this thesis was to explore whether the core ciliary gene IFT88, and therefore likely the primary cilium itself, maintains influence beyond development in the contexts of adolescent and adult cartilage. A sub-aim preliminarily explored a role of IFT88 in cartilage matrix catabolism *in vitro*.

Experiments *in vitro* identified putative, novel regulation of aggrecaneolysis by IFT88, through control of the endocytic clearance of proteases. Establishment and validation of a cartilage-specific, inducible knockout mouse model (cKO) enabled the deletion of IFT88. Deletion during adolescence, resulted in longer growth plates, with large bilateral cartilaginous holes where the normal ossification programme associated with growth plate closure was inhibited. Thinner articular cartilage in cKO mice was exhibited throughout adolescence and adulthood and its progressive calcification was inhibited. The effects on cartilage thickness were most pronounced in plateaus that experience the highest compressive loads. Following deletion at skeletal maturity, some joints exhibited total loss of cartilage, associated with features of osteoarthritis 28-weeks later. Experimental osteoarthritis, instigated by destabilisation of the joint, was exacerbated in cKO animals.

These studies demonstrate that IFT88, and by extension the primary cilium, has a critical role in cartilaginous tissues, sustained throughout adolescence into adulthood. The results in this thesis suggest that in the growth plate and articular cartilage, IFT88 could be an integrator and dampener of extrinsic, physiological, mechanical cues and intrinsic ciliary signalling pathways such as hedgehog signalling, and thus critical to the maturation, homeostasis and health of the post-natal joint.

Acknowledgements

Life is what happens when you're busy making other plans- John Lennon

I have many people to acknowledge for their support and guidance in the production of this thesis. It takes a village to raise a child, but an institute and establishment to produce a scientist. I think words are insufficient to express my gratitude to my supervisor, Angus Wann, who challenged me daily, developed my ideas, my confidence, and transformed me as both a person and a scientist. I also am indebted to Tonia Vincent whose continuous support and insights into my project were invaluable.

I am grateful to the Kennedy Trust Prize Studentship which enable me to do my research. I could not have asked for a better place to conduct my research, and am thankful to those who gave me the opportunity to work at the Kennedy Institute of Rheumatology. In particular I would like to highlight Afsie Sakobar, Chris Murphy, Chris Sauer and Fiona Powrie for helping me through a difficult start to my DPhil and to Mark Coles for continued support. Throughout my DPhil I have been fortunate enough to have an unrivalled team to support my work and I would like to thank in particular, Jadwiga, Tino, Bryony, Ida, Claudia, Marcia, Vicky, Heba and Tas.

Additionally, the University of Oxford gave me many opportunities outside of academia, and this led me to be part of the team that initiated the start-up WattsonBlue, a platform that has unexpectedly enabled future scientific collaborations. I would, of course, not have been able to do this without having been a part of the Oxford University Women's and Men's Boat Clubs during my time at Oxford. The amazing women and men I have met through these activities have inspired me every day to pursue excellence as a habit and not a chore. I'll be forever a Dark Blue. My continued involvement with the clubs has been spurred on by Filipe Salbany who nurtured my love of sports psychology and physiology. I hope to continue working in this area of research in the future.

I'd like to thank Robert Price, for initiating me into the world of science whilst I was still at school, and who has been a constant source of guidance throughout my career thus far. I'd also like to thank my family and friends for their never-ending support, encouraging me to pursue what ever I set my mind to.

I would like to dedicate this thesis to my grandmother, Joan Bridger.

Declarations

Originality
I declare that, unless otherwise stated, all work presented in this thesis is my own. Wherever I received assistance, I have appropriately acknowledged within the Materials and Methods Chapter. All experimental work was undertaken in line with the regulations outlined by the Kennedy Institute of Rheumatology at the University of Oxford.

Copyright
Permissions for material used within this thesis that was not my own were requested and granted by all relevant authors and publishers. All material was appropriately cited and acknowledged in the relevant sections throughout this thesis.

Submitted Abstracts

- **FASEB Cilia Conference, Oral presentation**
  Snow Mass Village, Colorado, USA, 2019
  Travel Award Winner
  Oral presentation and poster: *The ciliary protein IFT88 is profoundly influential in the post-natal joint, through joint maturation, adult life, and disease as a mechanoeffector of cartilage*
  Coveney CR, Miotla-Zabreska J, Stott B, Parisi I, Curtinha M, Duarte C, Vincent TL, Wann AKT

- **Cutting Edge Osteoarthritis, Oral presentation**
  Oxford, United Kingdom, 2019
  Runner up prize winner for best oral presentation: *The ciliary protein IFT88 is profoundly influential in the post-natal joint, through joint maturation, adult life, and disease as a mechanoeffector of cartilage*
  Coveney CR, Miotla-Zabreska J, Stott B, Parisi I, Curtinha M, Duarte C, Vincent TL, Wann AKT

- **OARSI World Congress on Osteoarthritis**
  Toronto, Ontario, Canada, 2019
  Poster:*The primary cilia protein IFT88, exerts a profound and evolving influence in the post-natal joint through joint maturation, adult life and in disease*
  Coveney CR, Miotla-Zabreska J, Stott B, Parisi I, Curtinha M, Duarte C, Vincent TL, Wann AKT

- **STEM for Britain Competition**
  London, United Kingdom, 2019
  I was competitively selected to present my work at the House of Commons to Members of Parliament.
  Poster:*The cell's antenna and its novel role in joint health and disease*
  Coveney CR, Jadwiga Miotla-Zarebska, Claudia Duarte, Ida Parisi, Bryony Stott, Vincent TL, Wann AKT

- **EMBO Cilia Conference**
  Copenhagen, Denmark, 2018
  Poster:*The role of IFT88 in joint maturation, homeostasis and disease*
  Coveney CR, Jadwiga Miotla-Zarebska, Marcia Curtinha, Ida Parisi, Bryony Stott, Anastasios Chanalaris, Vincent TL, Wann AKT

- **OARSI World Congress on Osteoarthritis**
  Liverpool, United Kingdom, 2018
  Poster:*Exploring and exploiting a ciliome protease matrix regulatory axis disturbed in osteoarthritis*

Collins I, **Coveney CR**, Bangs FK, Troeberg L, Vincent TL, Wann AKT

- **OARSI World Congress on Osteoarthritis**
  Las Vegas, Nevada, 2017
  Poster: *Postnatal influence of the ciliome in the joint*
  Coveney CR, I. Collins, M. McFie, A. Chanalaris, T.L. Vincent, A.K. Wann

- **Cutting Edge Osteoarthritis, Oral presentation**
  Oxford, United Kingdom, 2017
  Poster: *The role of the ciliome in joint homeostasis and disease*
  Coveney CR, Chanalaris A, Yamamoto K, Vincent TL, Wann AKT

- **British Society of Matrix Biology**
  Oxford, United Kingdom, 2017
  Poster: *Regulation of matrix catabolism by intraflagellar transport proteins and LRP-1*
  Collins I, McFie M, **Coveney CR**, Chanalaris A, Yamamoto K, Vincent TL, Wann AKT

- **EMBO Cilia**
  Amsterdam, The Netherlands, 2016
  Poster: *Primary cilia influence in mature joints and matrix turnover*
  Coveney CR, Chanalaris A, Yamamoto K, Vincent TL, Wann AKT

- **British Society of Matrix Biology**
  Cardiff, United Kingdom, 2016
  Poster: *The evolving roles of chondrocyte IFT in joint homeostasis and disease*
  Coveney CR, McFie M, Stott B, Curtinha M, Parisi I, Miotla-Zarebska J, Chanalaris A, Vincent TL, Wann AKT

Associated Publications

1. Non-canonical functions of the ciliome tune NF$\kappa\beta$ to define the cellular inflammatory response, (2020). McFie M, Koneva L, Collins I, **Coveney CR**, Clube AM, Chanalaris A, Vincent TL, Bezbradica JS, Sansom SN, Wann AKT. (Accepted.)
Journal of Cell Science

2. Prominin-1 controls stem cell activation by orchestrating ciliary dynamics, (2019). Singer D, Thamm K, Zhuang H, Karbanová J, Gao Y, Walker JV, Jin H, Wu X, **Coveney CR**, Marangoni P, Lu D, Grayson PRC, Gulsen T, Liu KJ, Ardu S, Wann AK, Luo S, Zambon AC, Jetten AM, Tredwin C, Klein OD, Attanasio M, Carmeliet P, Huttner WB, Corbeil D, Hu B.
EMBO Journal

3. Cilia protein IFT88 regulates extracellular protease activity by optimizing LRP-1 mediated endocytosis, (2018). **Coveney, CR**, Collins I, McFie M, Chanalaris A, Yamamoto K, Wann AKT.
FASEBJ

Contents

Abstract i

Acknowledgements ii

Declarations iii

Submitted Abstracts iv

Associated Publications vi

Contents vii

List of Figures viii

List of Tables ix

Abbreviations x

1 Introduction 1
1.1 Overview . . . 1
1.2 Skeleton . . . 3
1.3 Cartilage . . . 6
1.4 Primary Cilium . . . 26
1.5 Aims . . . 55

2 Materials and Methods 56
2.1 Experimental animals . . . 56
2.2 Surgical procedures . . . 66
2.3 Tissue collection . . . 70
2.4 Gene expression analysis . . . 73
2.5 Micro-computed tomography (MicroCT) imaging and radiography 77
2.6 Histological and histomorphometric analyses . . . 82
2.7 Western blotting . . . 92
2.8 Cell Culture and Experiments . . . 99
2.9 Data presentation and statistics . . . 104

3 The role of IFT88 in the regulation of matrix turnover *in vitro* 105
3.1 Introduction . . . 105
3.2 Aims . . . 110
3.3 Results . . . 110
3.4 Discussion . . . 131
3.5 Conclusion . . . 139

4 Cartilage-specific inducible deletion of IFT88 140
4.1 Introduction . . . 140
4.2 Aims . . . 146

4.3 Results . . . 147
4.4 Protein . . . 165
4.5 Histology of hip articular cartilage . . . 168
4.6 AggrecanCreER^{T2};TdTomato reporter . . . 170
4.7 *In vitro* deletion of IFT88 in primary rib chondrocytes . . . 178
4.8 Discussion . . . 183
4.9 Summary . . . 194

5 The role of IFT88 in the adolescent growth plate and metaphysis 197
5.1 Introduction . . . 197
5.2 Aims . . . 205
5.3 Results . . . 206
5.4 Discussion . . . 235
5.5 Summary . . . 245

6 The role of IFT88 in post-natal articular cartilage 247
6.1 Introduction . . . 247
6.2 Aims . . . 252
6.3 Results . . . 254
6.4 Discussion . . . 285
6.5 Summary . . . 291

7 Is IFT88 a regulator of the cartilage response to loading 293
7.1 Introduction . . . 293
7.2 Aims . . . 297
7.3 Results . . . 297
7.4 Discussion . . . 312
7.5 Summary . . . 317

8 General Discussion 318
8.1 Project Rationale . . . 318
8.2 IFT88 as a novel regulator of chondrocyte protease activity . . . 320
8.3 The peri-ciliary region as a 'hotspot' for endocytotic clearance . . . 320
8.4 The role of IFT88 in the adolescent growth plate . . . 325
8.5 The role of IFT88 in articular cartilage . . . 329
8.6 IFT88 supports mechanotransduction *in vivo* . . . 331
8.7 IFT88 and the remodelling of cartilage matrix . . . 333
8.8 Preliminary studies linking *in vivo* phenotypes to *in vitro* protease activity and LRP-1 localisation . . . 336
8.9 Non-canonical roles . . . 339
8.10 Future Work . . . 342
8.11 Concluding remarks . . . 343

Appendices 345

A Appendices 345

Bibliography 358

List of Figures

1.2.1.1 The structure of the knee joint . . . 6
1.3.1.1 Signalling in the growth plate . . . 8
1.3.2.1 Cross section of articular cartilage . . . 10
1.3.4.1 The structure of the knee joint and the effects of OA . . . 16
1.4.1.1 The primary cilium . . . 26
1.4.2.1 Intraflagellar transport in the primary cilium . . . 29
1.4.3.1 IFT88 is crucial to cilia formation . . . 30
1.4.4.1 Schematic of Hedgehog signalling at the primary cilium . . . 34
1.4.4.2 The primary cilium responds to fluid flow . . . 35
1.4.6.1 Ihh disruption in the mouse . . . 42
1.4.6.2 Disruption of IFT88 results in changes to cartilage deposition and joint formation . . . 44
1.4.6.3 Deletion of IFT88 in the limb bud mesenchyme . . . 45
1.4.6.4 Cartilage specific deletion of IFT88 . . . 46
1.4.6.5 Cartilage specific deletion of Kif3a . . . 47
1.4.6.6 Deletion of BBS proteins in mice . . . 48
1.4.6.7 Cartilage specific post-natal deletion of IFT80 . . . 49

2.1.3.1 Generation of a conditional knockout mouse model using the Cre-LoxP system. . . . 60
2.2.2.1 The destabilisation of the medial meniscus surgery. . . . 68
2.5.2.1 MicroCT growthplate measurements. . . . 78
2.5.3.1 Thresholded MicroCT growthplate measurements. . . . 79
2.5.4.1 Analysis of epiphysis and epiphyseal plate. . . . 81
2.6.4.1 Representation of histological sections for analysis. . . . 85
2.6.4.2 Histological sections illustrating method for articular cartilage measurements. . . . 86
2.6.5.1 Histological sections illustrating method for growth plate cartilage measurements. . . . 87
2.6.6.1 Representative images of 6 osteoarthritis histological scores taken from the medial compartment: . . . 89

3.1.0.1 A schematic representation of aggrecan monomers forming a larger proteoglycan aggregate with hyaluronic acid. . . . 107
3.3.1.1 Western blot analysis of aggrecan degradation over a time-course. 113
3.3.1.2 Validation of anti-AGEG antibody in human articular chondrocytes. . . . 114
3.3.1.3 AGEG and ARGS production by Osteoarthritic (OA) HACs over a time-course. . . . 115
3.3.1.4 Overlay assay in chondrocyte cell line. . . . 116
3.3.1.5 siRNA targeting of IFT88 in primary human articular chondrocytes and its effects on cilia. . . . 118
3.3.1.6 IFT88 deletion in HACs and its effects on AGEG neoepitope production. . . . 119
3.3.1.7 WT and ORPK AGEG production over a time-course. . . . 120

3.3.2.1 ORPK chondrocytes have reduced rate of clearance of TS-5-FLAG from the media than WT chondrocytes 123
3.3.3.1 Total LRP-1 protein expression is not affected by ORPK mutation. 125
3.3.4.1 Distribution of LRP-1 receptor is qualitatively altered in ORPK cell line. 126
3.3.4.2 LRP-1β localises to the base of the primary cilium/ periciliary region in cell line, primary mouse chondrocytes and human articular chondrocytes. 127
3.3.5.1 LRP-1α chain is shed more in ORPK chondrocytes and this is associated with higher presence of sheddase proteins. 129
3.3.6.1 Schematic illustrating hypothesised mechanism behind elevated aggrecanase degradation observed in OPRK chondrocytes. 130
3.4.0.1 TIMP-3 protein expression is higher in WT than ORPK lysates. . 139

4.1.0.1 IFT88fl/fl and AggrecanCreER^{T2} mice. 146
4.3.1.1 Cre and IFT88fl/fl identification of DNA isolated from mice. . . . 147
4.3.2.1 No reduction in IFT88 expression observed in cartilaginous tissues by end stage PCR. 150
4.3.3.1 Aggrecan is expressed in cartilage and soft tissues in both humans and mice. 151
4.3.4.1 IFT88 is expressed across both human and mouse tissues. 153
4.3.5.1 Relative expression of IFT88 across different tissues. 154
4.3.6.1 Hip cartilage IFT88 expression decreases between 6-and 10-weeks of age. 155
4.3.7.1 Hip articular cartilage. 157
4.3.7.2 Tamoxifen induced a 35% knockdown of IFT88 in hip cartilage. . 159
4.3.7.3 No measurable deletion of IFT88 observed in 10-week old mice. . 161
4.3.8.1 No off-target deletion of IFT88 in liver and kidney samples. . . . 163
4.3.9.1 Deletion of IFT88 in liver and kidney samples. 165
4.4.1.1 Deletion of IFT88 in xiphoid cartilage analysed by western blot. . 167
4.4.2.1 Deletion of IFT88 in hip articular cartilage analysed by western blot. 168
4.5.0.1 Histological sections of hip joints and hip articular cartilage. . . . 170
4.6.1.1 Cre recombination in cartilaginous tissue 2-weeks post-tamoxifen in AggrecanCreERT2;TdTomato reporter mice (6-weeks of age). . 172
4.6.1.2 Cre recombination in kidney and liver 2-weeks post-tamoxifen in AggrecanCreERT2;TdTomato reporter mice (6-weeks of age). . . . 173
4.6.2.1 Activity of Cre in cartilaginous tissue 2-weeks post-tamoxifen in AggrecanCreERT2;TdTomato reporter mice (10-weeks of age). . . 176
4.6.2.2 Activity of Cre in kidney and liver 2-weeks post-tamoxifen in AggrecanCreERT2;TdTomato reporter mice (10-weeks of age). . . 177
4.7.1.1 Deletion *in vitro* of IFT88 in rib chondrocytes analysed by qPCR. 179
4.7.2.1 Deletion in vitro of IFT88 in rib chondrocytes analysed by western blot. 180
4.7.3.1 Immunofluorescent staining of rib chondrocytes. 182
4.8.0.1 Aggrecan expression in xiphoid cartilage. 188

5.1.0.1 A schematic representation of tibial growth plate closure between 4-10-weeks of age. . . . 199
5.1.0.2 The growth plate . . . 201
5.3.1.1 Raw (un-thresholded) and thresholded MicroCT images. . . . 207
5.3.1.2 Tibial growth plate closure and tibial growth curves. . . . 208
5.3.1.3 Characterisation of growth plate morphology: hypertrophic and proliferative chondrocyte populations. . . . 210
5.3.2.1 Histological measurements compared with MicroCT measurements. 212
5.3.3.1 Experimental timeline. . . . 213
5.3.3.2 Deletion of IFT88 results in morphological changes to the growth plate. . . . 216
5.3.3.3 Effect of IFT88 deletion of growth plate length. . . . 219
5.3.3.4 Deletion of IFT88 results in morphological changes to the growth plate. . . . 222
5.3.3.5 Histological measurements of hypertrophic and proliferative regions of the growth plate. . . . 224
5.3.3.6 Effects of IFT88 deletion on the growth plate and hypertrophic chondrocyte regions. . . . 226
5.3.4.1 Histological coronal sections of 6-week old knee joints revealed longer growth plates in cKO animals. . . . 229
5.3.4.2 Longer growth plates in cKO animals associated with larger regions of col X staining. . . . 230
5.3.4.3 Histological coronal sections of 10-week old knee joints revealed growth plates filled with ColX expressing chondrocytes in both control and cKO animals. . . . 231
5.3.5.1 Deletion of IFT88 results in changes to the bone beneath the cartilage in the epiphysis and bone beneath growth plate. . . . 234
5.4.0.1 Growth plate cartilage fails to calcify in cKO. . . . 239

6.1.0.1 Articular cartilage dissipates mechanical load equally across the tissue. . . . 249
6.3.1.1 Tibial articular cartilage thickness. . . . 255
6.3.1.2 Articular cartilage is significantly thicker on the medial plateau at every age between 6- and 34-weeks. . . . 256
6.3.1.3 Articular cartilage calcifies with age. . . . 258
6.3.1.4 Articular cartilage calcifies with age, replacing uncalcified cartilage with calcified cartilage. . . . 259
6.3.1.5 Calcified and uncalcified measurements differ between lateral and medial plateaus, but this difference is not reflected as a proportion of total cartilage thickness. . . . 260
6.3.2.1 Effects of IFT88 deletion in articular cartilage. . . . 262
6.3.2.2 Removal of IFT88 results in decreased calcified cartilage thickness by 8-weeks. . . . 264
6.3.3.1 Experimental timeline. . . . 265
6.3.3.2 Deletion of IFT88 results in complete inhibition of cartilage thickening followed by progressive cartilage loss within two-weeks. 266
6.3.3.3 Spontaneous osteoarthritis observed 6 months post-deletion of IFT88 at 8-weeks of age. . . . 267

6.3.3.4 Deletion of IFT88 results in complete inhibition of cartilage thickening followed by progressive cartilage loss within two-weeks predominantly on the medial plateau. 269
6.3.3.5 Removal of IFT88 results in significantly thinner calcified cartilage, prior to spontaneous disease 271
6.3.3.6 Percentage ratios of uncalcified and calcified cartilage reveal changes in cartilage composition on the lateral and medial plateau. 273
6.3.4.1 No observed differences in ColX staining on deletion of IFT88 at 4-weeks of age. 276
6.3.4.2 No observed differences in ColX staining on deletion of IFT88 at 6-weeks of age.. 278
6.3.4.3 No observed differences in ColX staining on deletion of IFT88 at 8-weeks of age. 280
6.3.4.4 Neoepitope (NITEGE) staining in articular cartilage. 283
6.3.4.5 Neoepitope (NITEGE) staining in articular cartilage. 284

7.3.1.1 Representative histological sections of control and cKO medial compartments 8- and 12- week post DMM surgery. 299
7.3.1.2 DMM surgery results in significantly higher OARSI scores 12-week post-surgery in cKO animals. 300
7.3.2.1 Histological staining of ipsilateral (immobilised) and contralateral joints. 302
7.3.2.2 Contralateral and ipsilateral growth plate length measurements of cKO and control animals. 303
7.3.2.3 Articular cartilage measurements of contralateral and ipsilateral knee joints. 305
7.3.2.4 Lateral and medial cartilage measurements of contralateral and ipsilateral knee joints. 307
7.3.2.5 Uncalcified and calcified cartilage measurements of contralateral and ipsilateral knee joints. 309
7.3.2.6 Total cartilage thickness measurements from naive contralateral and ipsilateral hindlimbs. 311

8.8.0.1 No observed differences in LRP-1 staining on deletion of IFT88. . 339

List of Tables

1.1 Table summary of mouse model phenotypes. 50
1.1 Table summary of mouse model phenotypes. 51

2.1 Primers for mouse genotyping 64
2.2 Taqman primers for mouse tissues. 76
2.3 OARSI guidelines for histological scoring 90
2.4 Table of primary antibodies used in this thesis. IHC: Immunohistochemistry, IF: immunofluorescence, WB: western blotting 96
2.4 Table of primary antibodies used in this thesis. IHC: Immunohistochemistry, IF: immunofluorescence, WB: western blotting 97
2.5 Table of secondary antibodies used in this thesis. IHC: Immunohistochemistry, IF: immunofluorescence, WB: western blotting. 98

4.1 Challenges of validation and approach taken to understand the AggrecanCreER^{T2} system 148
4.1 Challenges of validation and approach taken to understand the AggrecanCreER^{T2} system 149
4.2 Summary of the challenges of validating this mouse model and how they were addressed. 195
4.2 Summary of the challenges of validating this mouse model and how they were addressed. 196

Abbreviations

β-actin	Beta-actin
18S	Eukaryotic rRNA18S
4-OH	4-hydroxy-tamoxifen
AcαTUB	Acetylated-α-tubulin
ACAN	Aggrecan
ADAM17	ADAM Metallopeptidase Domain 17
ADAMTS-4	A Disintegrin and Metalloproteinase with Thrombospondin Motif 4
ADAMTS-5	A Disintegrin and Metalloproteinase with Thrombospondin Motif 5
Arl13b	ADP-ribosylation factor-like protein 13B
ARRIVE	Animal research reporting of *in vivo* experiments
ATP	Adenosine triphosphate
BBS	Bardet biedel syndrome
BMP	Bone morphogenetic protein
BSA	Bovine serum albumin
BV	Bone volume
cAMP	Cyclic adenosine monphosphate
cDNA	Complementary deoxyribonucleic acid
Col2	Type II collagen
ColX	Type X collagen
COX-2	Cyclo-oxygenase-2
Cre	Cre recombinase
DAPI	4',6-Diamidino-2-Phenylindole, Dihydrochloride
DMEM	Dulbeccos modified eagles medium
DMM	Destabilisation of the medial meniscus
DNA	Deoxyribonucleic acid
DNA	Double neurectomy
ECL	Enhanced chemiluminescence
ES	Embryonic stem cells
ECM	Extracellular matrix
EDTA	Ethylenediaminetetraacetic acid
ERK	Extracellular signal-regulated kinase
FCS	Fetal calf serum
FDA	Food and Drug Administration
FGF	Fibroblast growth factor
FGFR	Fibroblast growth factor receptor
GAG	Glycosaminoglycan
GAPDH	Glyceraldehyde-3-phosphate dehydrogenase

GLI-1	Zinc finger protein GLI1, glioma-associated oncogene
Gli-1	Glioma associated-oncogene-1
GPCR	G-protein coupled receptor
HACs	Human articular chondrocytes
HEPES	4-(2-hydroxyethyl)-1-piperazineethanesulfonic acid
Hh	Hedgehog
IF	Immunofluorescence
IFT	Intraflagellar transport
IFT-A	Intraflagellar protein transport complex A
IFT-B	Intraflagellar protein transport complex B
IFT88	Intraflagellar transport protein 88
IGF-1	Insulin growth factor-1
IGFR	Insulin like growth factor
IHC	Immunohistochemistry
Ihh	Indian Hedgehog
IL-1	Interleukin-1
IGD	Immunoglobular domain
IMS	Industrial methylated spirit
INF-γ	Interferon-gamma
JNK	c-Jun N-terminal kinase
Kif3a	Kinesin like protein 3a
LRP-1	Lipoprotein receptor-related protein-1
MAPK	Mitogen activated protein kinase
MEK	Mitogen-activated protein kinase/ERK kinase
MicroCT	Micro computer tomography
MM	Medial meniscus
MMTL	Medial menisco tibial ligament
MMP	Matrix metalloproteinase
MMP-13	Matrix metalloproteinase-13
MMP-14	Matrix metalloproteinase-14
mRNA	messenger RNA
MSCs	Mesenchymal stem cells
MSK	Musculoskeletal
NG2	Neuron glia antigen-2
NHS	National Health Service
OA	Osteoarthritis
OARSI	Osteoarthritis research society international
ORPK	Oak Ridge Polycystic Kidney
PBS	Phosphate buffered saline

PC1	Polycytsin-1
PC2	Polycytsin-2
PCM	Pericellular matrix
PCR	Polymerase chain reaction
PDGFR	Platelet-derived growth factor
PDGFR	Platelet derived growth factor receptor
PFA	Paraformaldehyde
PKD	Polycystic kidney disease
Prx1	Paired related homeobox 1
PTCH-1	Protein patched homolog 1
PTCH1	Patched1
PTHrP	Parathyroid hormone related peptide
PTHrPR	Parathyroid hormone related peptide receptor
PTOA	Post-traumatic osteoarthritis
q-PCR	Quantitative reverse transcription polymerase chain reaction
RA	Rheumatoid arthritis
RNA	Ribonucleic acid
RT-PCR	Reverse transcriptase polymerase chain reaction
Runx-2	Runt-related transcription factor 2
SDS	Sodium dodecyl sulfate polyacrylamide gel electrophoresis
Shh	Sonic Hedgehog
Smo	Smoothened
Somatostatin R	Somatostatin receptor
Sox-9	Transcription factor SOX-9
SPAG17	Sperm associated antigen 17
SuFu	Suppressor of fused
TAZ	Transcriptional coactivator with PDZ-binding motif
TB.N	Trabecular number
Tb.Sp	Trabecular spacing
TGF-B	Transformation growth factor β
TIMP	Tissue inhibitors of metalloproteinases
TNF-α	Tumor necrosis factor-alpha
TRPV	Transient receptor potential cation channel subfamily V
TS-5 -FLAG	FLAG tagged TS-5
TTBK2	Tau tubulin kinase 2
TV	Total volume
VEGF	Vascular endothelial growth factor
VEGFR	Vascular endothelial growth factor receptor
YAP	Yes associated protein

1

Introduction

Science makes people reach selflessly for truth and objectivity; it teaches people to accept reality with wonder and admiration- Lise Meitner

Contents

1.1 Overview 1
1.2 Skeleton 3
1.3 Cartilage 6
1.4 Primary Cilium 26
1.5 Aims 55

1.1 Overview

Cartilage is a unique tissue with properties exceeding those of any man-made material. Cartilage lines the ends of long bones, allowing for smooth articulation over the joints whilst absorbing and dissipating mechanical loads. Physiological mechanics has been shown to be important for cartilage development and homeostasis, upregulating anabolic matrix-building programmes in cartilage, but pathophysiological mechanics can lead to cartilage destruction in osteoarthritic disease. Despite the importance of

mechanics to cartilage and the musculoskeletal (MSK) system in general, it is currently not known what could be the joint 'mechanostat,' safeguarding cartilage homeostasis.

The primary cilium, a microtubule-based organelle that relies on intraflagellar transport (IFT), is assembled by chondrocytes. Perturbations to ciliary proteins or ciliary function result in congenital, developmental joint malformation associated with cartilage abnormalities. In humans, mutations to ciliary proteins result in a group of human congenital diseases called 'ciliopathies.' Ciliopathies result in multiple pathologies, including MSK phenotypes such as polydactyly and shortening of the long bones. These developmental phenotypes are largely ascribed to alterations to Hh signalling, which is regulated at the primary cilium. The primary cilium has also been associated with mechanotransduction, most famously in the context of the ciliopathy polycystic kidney disease (PKD) where the current dogma is that ciliary dysfunction impairs epithelial ciliary mechanotransduction downstream of fluid flow, resulting in dysregulation of downstream calcium signalling and a raft of other cell behaviours. The ciliary protein IFT88 is crucial to cilia formation and its developmental removal in murine models recapitulates many of the elements seen in ciliopathies including MSK phenotypes attributed to Hh and kidney phenotypes attributed to faulty mechanotransduction. The

role of IFT88 in adult tissues is far less well-described.

1.2 Skeleton

The skeleton is the supporting structure of an organism that provides support and protection of soft tissues. Bone has a very specific function depending on location within the body. Bones protect organs, allow for movement at the joints, provide the body with a framework and can be manipulated by the muscles that attach to them. Bone is a very dynamic and rigid connective tissue, but one that is constantly remodelling in response to external cues, exquisitely sensitive to remodelling stimuli. It is also responsible for the production of red and white blood cells and minerals.

The skeleton develops by means of a complex process, a coordinated response to many biological and physico-chemical signals. The skeleton is intricately designed during embryogenesis, limbs arising from limb bud patterning, a process dictated by signalling pathways and downstream programs of gene transcription. The signalling pathway Hedgehog (Hh), which will be discussed in more detail later, is crucial to the development of the skeleton in conjunction with mechanical cues from contracting muscles in the embryo.

During development and post-natal life, genetic and environmental factors affect bone and joint health. Bone formation is influenced

by hormones, cytokines and other extrinsic signalling molecules. These include growth factors such as Ihh, PTHrP, BMPs, FGFs, Wnts and key transcription factors such as Sox9 and Runx2. These factors and their associated pathways interact with each other to regulate the coordinated proliferation and differentiation of chondrocytes and osteoblasts (Berendsen and Olsen, 2015).

There are two types of osteogenesis; endochondral ossification and intramembranous. Intramembranous ossification arises directly from mesenchymal condensations without a cartilage intermediate, differentiating directly into osteoblasts (Crombrugghe et al., 2001). This process results in the formation of flat bones such as the skull and clavicle. However, the majority of the skeleton is formed through endochondral ossification involving a cartilage intermediate/template known as anlagen. Generally, mesenchymal stem cells form endochondral condensations that differentiate into chondrocytes (Crombrugghe et al., 2001). These differentiated chondrocytes go on to form the cartilaginous anlagen of the forming bone (Haycraft and Serra, 2008). Chondrocytes eventually undergo hypertrophy, swelling, expressing and secreting collagen X and producing alkaline phosphatase, an enzyme required for mineral deposition that triggers calcification of the bone (Melrose et al., 2016). Hypertrophic chondrocytes also promote and attract the development of the vasculature by secreting factors such as VEGF,

a vital process for bone formation. The interzone is a region of condensing mesenchymal cells that is the precursor to the joint site (Holder, 1977).

1.2.1 Articular joints

Articular joints are intricate structures and organs, that enable smooth articulation at the point where two bones meet. They are able to both lubricate these movements and transmit and withstand great mechanical forces, through cartilage matrix.

The long bone of the femur meets the long bone of the tibia at the knee joint as shown in Fig. 1.2.1.1. The knee joint is stabilised by a network of ligaments, tendons and muscles holding this composite structure together. Where the two bones meet, there are two menisci, named after the side of the joint that it is on; the medial and lateral menisci (Fig. 1.2.1.1). Stretching over the plateaus they form a protective layer over the cartilage lining both ends of the long bones.

The knee joint is also able to withstand huge compressive forces, experiencing up to 12x an individual's body weight during elite sporting events such as gymnastics and even greater loads in localised regions. Whilst we know the structure of this unrivalled material, we currently do not fully understand how the joint is able to sense and respond to these forces to create and maintain

cartilage.

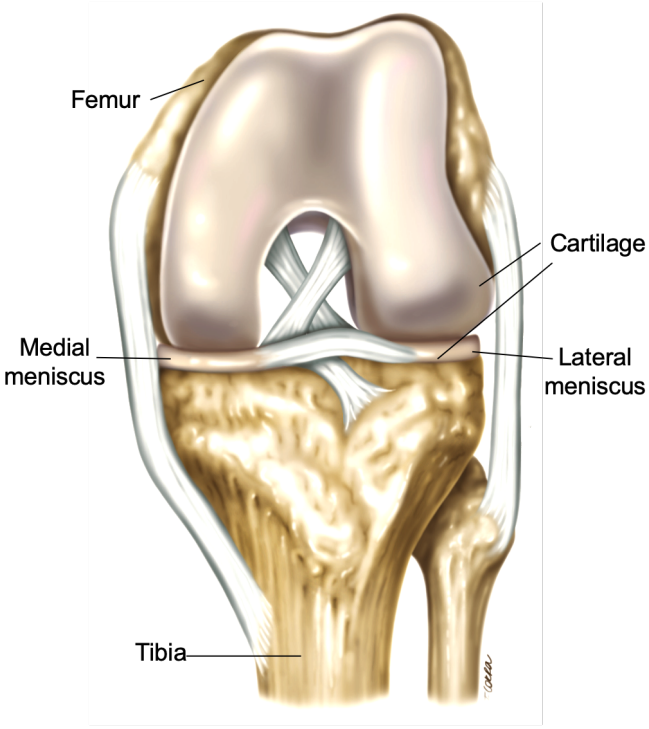


Figure 1.2.1.1: The structure of the knee joint.
Artistic schematic of the knee joint revealing exposed femoral cartilage, the medial and lateral meniscus, and tibia. Drawn by Kennedy Institute artist F. Corra.

1.3 Cartilage

1.3.1 Growth plate

1.3.1.1 Growth plate development

The growth plate is a region of dynamic tissue below the epiphysis of the long bone (Fig. 1.3.1.1). The growth plate is cartilaginous and located at either end of the long bone and facilitates longitudinal bone growth. In humans after birth the growth plate remains active and 'open' until the skeleton is fully formed. On reaching skeletal

maturity the growth plate cartilage is no longer and maintained, ossifying to fuse the diaphysis with the epiphysis. This closure usually occurs between 13 and 18 years of age in humans. However, the mouse growth plate never closes completely, but does reduce in size and activity, forming boney bridges between the epiphysis and diaphysis, as the animal reaches skeletal maturity around 8-10 weeks of age.

1.3.1.2 Signalling

Whilst the growth plate has been fairly well characterised during development, less is known about the final stages of endochondral ossification at growth plate closure. During development, proliferating chondrocytes at the epiphysis continually replenish the cell population, whereas older cells further away from the epiphysis undergo hypertrophy and eventually apoptose or transdifferentiate into osteoblasts forming bone (Zhou et al., 2014). These hypertrophic chondrocytes characteristically express type X collagen and calcify their surrounding matrix. Indian hedgehog (Ihh) also acts to signal to resting and proliferating chondrocytes at the diaphysis to secrete parathyroid hormone receptor protein (PTHrP) which, in turn, simulates proliferation and inhibits the Ihh signal from stimulating hypertrophy in cells in this region. Thereby, the PTHrP-Ihh axis is crucial to the regulation of growth plate dynamics (Fig. 1.3.1.1).

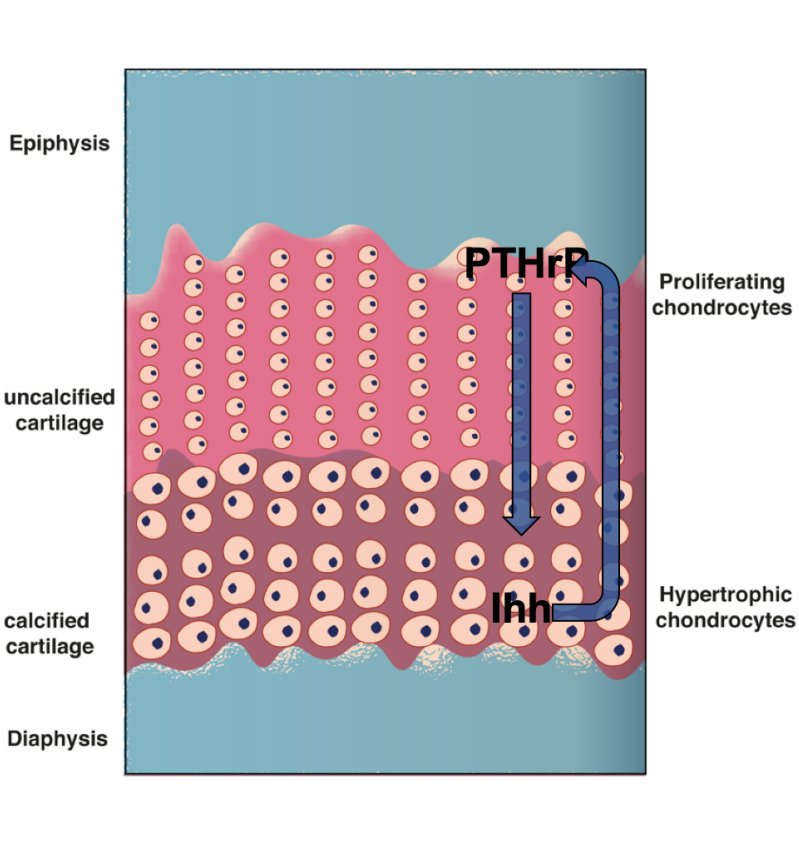


Figure 1.3.1.1: Signalling in the growth plate.
Schematic illustrates the composition of growth plate cartilage showing proliferating chondrocytes located within uncalcified cartilage beneath the epiphysis and hypertrophic chondrocytes close to the diaphysis in the calcified cartilage region. Indian hedgehog (Ihh) is expressed by hypertrophic chondrocytes stimulating the expression of parathyroid receptor related protein (PTHrP) by proliferating chondrocytes. PTHrP promotes proliferation and inhibits differentiation of chondrocytes to hypertrophic chondrocytes, whilst Ihh signalling acts to stimulate chondrocyte hypertrophic differentiation.

1.3.2 Articular cartilage

1.3.2.1 Joints

The bones of the synovial joint are covered by articular cartilage. Human articular cartilage is a relatively acellular (1-10%) and completely avascular tissue. This matrix layer consists of proteoglycans, collagens, ions, water, and its only resident cell, the chondrocyte. Aggrecan is the chief cartilage proteoglycan,

providing a fixed density of anionic chondroitin sulfate sidechains. These charged sidechains promote water retention which is fundamental for the ability of cartilage to resist compression. The most abundant structural molecule of the extracellular matrix (ECM) is collagen. Approximately 90% of the collagen in the ECM is Type II collagen, wound into fibrils. These fibrils form matrices with proteoglycan aggrecans providing stability to the matrix and giving the articular cartilage tensile strength. The fibril arrangement changes with depth, and can be divided into zones (Fig. 1.3.2.1). In the superficial zone fibrils are arranged parallel to the surface; in the transitional zone there is a less prescript organisation; whilst the deep zone consists of fibrils perpendicular to the articular surface.

1.3.2.2 Chondrocyte phenotypes

Whilst the chondrocyte is often described as the sole cell type in cartilage, the different zones within the articular cartilage matrix are home to distinct subsets of chondrocytes with particular phenotypes. Within human articular cartilage these are often subdivided into the superficial, transitional, and deep zones (Fig. 1.3.2.1). The calcified cartilage acts as a bridge between cartilage and the subchondral bone. The chondrocytes within each zone have different morphologies; superficial zone chondrocytes are flatter and more oval shaped compared with transitional zone

chondrocytes, which are rounder. Beneath the transition zone, is the deep zone, consisting of round and columnar chondrocytes. The chondrocytes closest to the subchondral bone are hypertrophic, having an enlarged pericellular matrix (Fig. 1.3.1.1).

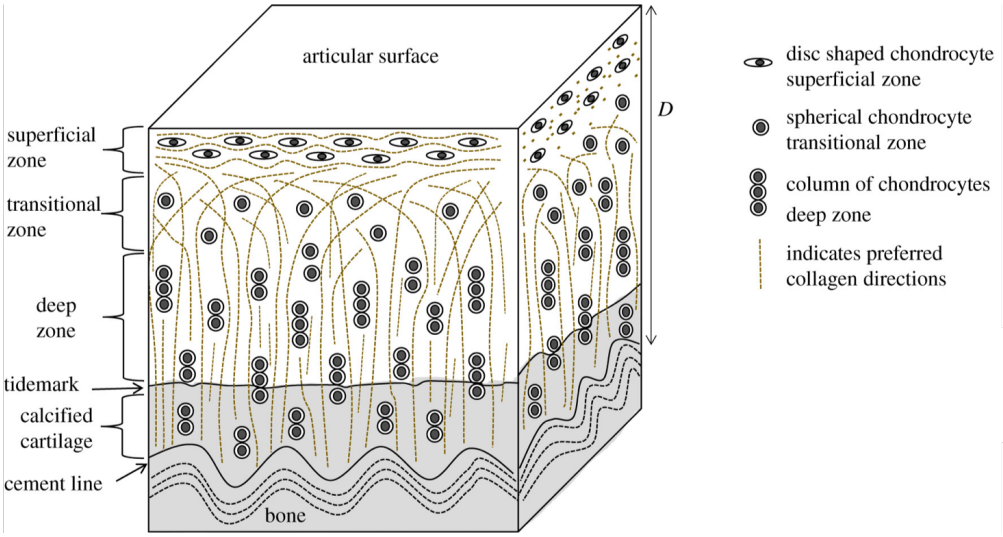


Figure 1.3.2.1: Cross section of articular cartilage.
Schematic illustrates the composition of articular cartilage, including collagen fibres, the zones: superficial, transitional, deep and calcified cartilage. Chondrocytes in each zone are depicted by shape (see key). Reproduced from (Mansfield et al., 2019).

1.3.2.3 Calcified and uncalcified cartilage

Articular cartilage can be demarcated by histological staining into uncalcified and calcified cartilage. The superficial, transitional and part of the deep zone makes up a region of the cartilage that is uncalcified. The 'tidemark' is the interface between the calcified and uncalcified cartilage. This region of calcified cartilage forms an intermediary between uncalcified cartilage and bone, creating a transition between the two different tissues. This transitionary calcified cartilage region is also present in the growth plate (Fig.

1.3.2.1).

1.3.3 Chondrocyte

1.3.3.1 Characterisation of phenotype

The chondrocyte is the only cell type found in the cartilage and is responsible for both secretion and turnover of extracellular matrix components. Chondrocytes vary in shape, size and function depending on their anatomical location within the articular cartilage. Superficial zone articular chondrocytes are flatter and smaller and have greater density than the columnar or hypertrophic chondrocytes. Columnar chondrocytes are rounder than superficial chondrocytes, whilst hypertrophic chondrocytes are the largest chondrocytes with an extended pericellular matrix and large nucleus.

At each stage of development, expression of specific genes characterises chondrocyte cell type; type II collagen (Col2) and aggrecan for early chondrocytes; parathyroid hormone related protein (PTHrP), Indian Hedgehog (Ihh), Type X collagen (ColX) for pre-hypertrophic chondrocytes and only ColX for hypertrophic chondrocytes. Pre-hypertrophic chondrocytes will undergo subsequent differentiation directed by Runx2 (Takeda et al., 2001) and Osterix (Osx) (Nakashima et al., 2002), which is necessary for osteoblast specification and differentiation (Yang et al., 2014).

When chondrocytes undergo hypertrophy, they express type X collagen and begin to produce alkaline phosphatase, an enzyme required for mineral deposition that triggers calcification of the cartilage (Melrose et al., 2016). These osteogenic cells undergo apoptosis and cartilage matrix is displaced with bone tissue by osteoblasts (Song et al., 2007). Osteoprogenitors secrete osteoid to form trabeculae and osteoclasts form the bone marrow cavity leading to elongation of the long bone. Many of these processes have been studied during development, but they are likely to also be relevant to articular cartilage.

Chondrocytes and osteoblasts develop from mesenchymal precursors, expressing SRY box 9 (Sox-9) transcription factor or runt-related transcription factor 2 (Runx2) respectively, committing them to these two different lineages. Sox-9 expression is necessary and required for chondrocyte specification and early differentiation, its expression maintained throughout chondrocyte maturation until pre-hypertrophy, but is switched off in other lineages arising from the ectoderm or the endoderm (Akiyama et al., 2002; Bi et al., 1999).

1.3.4 Cartilage health and homeostasis

1.3.4.1 Diseases of cartilage

1.3.4.2 Achondrodysplasia

Developmental musculoskeletal disorders include chondrodysplasias, which are hereditary disorders of which there is no treatment or cure. Despite this, distraction of the joint surgery, which eliminates contact between the joint surfaces, has been reported to have successful results in treating chondrodysplasias (Ornitz and Legeai-Mallet, 2017; Schiedel and Rodl, 2012). Chondrodysplasias are associated with developmental dysregulation of signalling pathways regulating growth plate dynamics. This often results in alterations in long bone growth. Achondrodysplasia, otherwise known as dwarfism, affects elongation of the long bones, resulting in shortness of stature. Achondrodysplasia arises from a single point mutation in FGFR3, a negative regulator of bone growth, resulting in the down regulation of chondrocyte proliferation (Ornitz and Marie, 2002; Ornitz and Marie, 2019). Hh disruption also leads to chondrodysplasias (Schmidts, 2014).

1.3.4.3 Osteoarthritis

The two most prevalent forms of arthritis are historically, simplistically, classified into their inflammatory, rheumatoid arthritis (RA) and non-inflammatory OA forms. RA is an

autoimmune disease, and has a very different aetiology to OA, associated with inflammation driving the pathological destruction of cartilage and joints. Treatments include immune suppressants, pain relief and anti-TNF therapy. OA is a multifactorial disease, with proposed risks including, genetics, age, gender, inflammation, BMI, smoking, alcohol, diet, and exercise or injury. The heterogeneity of OA has inhibited the scientific community thus far from finding an effective treatment beyond late stage intrusive interventions such as knee replacement surgery. Whilst the large majority of sufferers are in older patients, there are juvenile sufferers of OA. Additionally, post-traumatic OA (PTOA) arises following a significant acute trauma to the joint, commonly incurred during sporting accidents (Whittaker et al., 2015), such as tearing of the anterior cruciate ligament, which results in aberrant mechanical loading of the joint and substantial inflammation.

Osteoarthritis is the most common musculoskeletal disease with over 30% of the UK population over 45 years of age affected. Over 50% of those over 75 years of age (Arthritis Research UK 2013) will seek treatment for OA. The cost of OA to the UK economy is estimated at 1% of gross national product. Hip and knee replacements alone cost the NHS £890 million pounds in 2010. There are also additional costs to include sick days, GP consultations, hospital admissions and money spent on community

and social services. As such, the Osteoarthritis Research Society International (2016) (OARSI) submitted a white paper to the Federal Drug Administration (FDA) in the United States, to persuade the government to class OA as a serious disease.

OA is largely considered by the non-scientific community to be a wear and tear disease with the loss of cartilage as a gradual degradation of the soft tissue lining the articular surfaces (Fig. 1.3.4.3). However, we now know that articular cartilage is a dynamic tissue capable of repair and continuously adapting to its biophysico-chemical cues (Loeser et al., 2012; Moskowitz, 1972). Osteoarthritis is also a whole joint disease, not just affecting the cartilage, but also the meniscus, synovium and bone, with subchondral bone thickening, osteophyte formation and thickened joint capsule (Loeser et al., 2012) (Fig. 1.3.4.1).

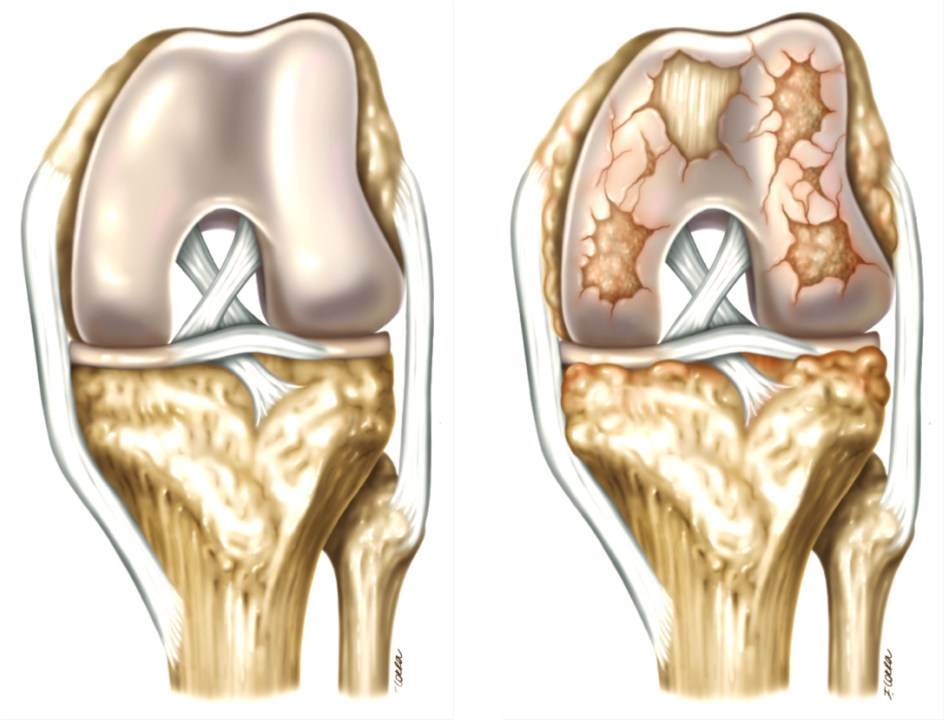


Figure 1.3.4.1: The structure of the knee joint and the effects of OA.
Artistic schematic of the knee joint revealing exposed femoral cartilage, the medial and lateral meniscus, and tibia (Left). OA results in the destruction of articular cartilage and formation of boney outgrowths (osteophytes) (Right). Drawn by Kennedy Institute artist F. Corra.

1.3.4.4 Clinical relevance

Patients often present to the clinic with joint pain, when already the pathological and destructive processes behind OA have already begun. Additionally, we are currently unable to visualise cartilage and monitor cartilage thickness during early disease processes. Therefore, we have a lack of understanding about the early mechanisms behind the pathology of OA or indeed what regulates the homeostasis of the cartilage. Understanding these regulators of homeostasis could help to elucidate processes that become dysregulated during disease pathogenesis. In particular, not

enough is known about the role of mechanics and its integration with signalling programs such as those driven by growth factors in the extracellular matrix. A large outstanding question is what senses this mechanical input within the joint. This is fundamental to understanding these disease processes, without which new targets for drug discovery to artificially augment disease progression cannot be developed.

1.3.4.5 Animal models of osteoarthritis

To study OA, there are several widely used methods to model OA in animals, including spontaneous OA onset, intra articular injections, immobilisation and surgical induction methods (Fang and Beier, 2014; Vincent et al., 2012). The STR/ort mouse was identified in a random mutagenesis screen in the 1950s. The STR/ort mouse spontaneously develops OA in early life and is thought to be genetically predisposed to the disease, exhibiting characteristic OA pathology including loss of proteoglycan staining, articular cartilage fibrillation, increased matrix turnover and osteophyte development. Research is still ongoing to elucidate what mechanisms are responsible for causing this spontaneous degradation of the articular cartilage, which so closely resembles human OA (Staines et al., 2017a).

The majority of surgical mouse induction methods resemble human

post-traumatic OA (PTOA), by introducing joint instability, hence altering mechanical loading. The destabilisation of the medial meniscus (DMM) model is the most widely used surgical induction model for OA in mice (Fang and Beier, 2014). During the DMM model, the medial meniscus is cut, resulting in joint destabilisation, and thereby focusing mechanical loading to a narrower area predominantly affecting the posterior femur and central tibia (Glasson et al., 2007). These models have been validated as robust and reproducible, with degradation of the cartilage and disease developing between 4-16-weeks post-surgery. However, this is clearly an accelerated model, not reflective of the majority of human osteoarthritic disease which can take many decades to develop and materialise. Current animals models of the disease manifest more rapidly even when accounting for animal life expectancy (Little and Hunter, 2013). Genetic modification has been an extremely useful tool to manipulate the genome of mice and to target specific tissues. Within this thesis I use genetic modification to target chondrocytes within the articular cartilage. The most well characterised method of OA introduction within the field of OA research today is the surgical induction model. In the latter part of this thesis, this method was used to challenge the joint with aberrant mechanics.

1.3.4.6 Maintenance of cartilage matrix regulation and turnover

Articular cartilage is a tissue that, contrary to popular belief, is constantly turning itself over. The principal ECM proteins, aggrecan and collagen, are degraded by specific proteases produced by chondrocytes. The most prominent of these that are also dysregulated during the pathologic destruction of mouse articular cartilage is the 'A Disintegrin And Metalloproteinase ThromboSpondin motif' (ADAMTS)-5 targeting aggrecan and matrix metallopeptidase (MMP)-13 predominantly targeting collagen. As the chondrocyte is responsible for both the production of ECM and also enzymes that break down the ECM, these two opposing processes must be tightly controlled. Continued exposure of the cartilage to these potent enzymes, over time, causes significant destruction of the cartilage to result in cartilage degenerative diseases such as OA. They are hence tightly controlled by transcription. However, a more immediate means of regulation is at the post-transcriptional level. For example, removal of enzymes from their substrates or inhibiting their activity could be a means of regulating enzyme activity.

1.3.4.7 Matrix proteases

Both the production and destruction (turnover) of matrix are important for the maintenance and homeostasis of the cartilage.

Chondrocytes express several members from families of proteases responsible for cleaving collagens and proteoglycans, such as aggrecan. The most-relevant proteases are MMPs and ADAMTSs (Fosang et al., 2008; Little et al., 2009; Little et al., 2007). These enzymes cleave their substrates at specific sites and can be regulated by transcription, activation of proenzymes, by their cleavage by other proteases such as MMP-14, inhibition by tissue resident inhibitors of activity, or by their cellular endocytotic clearance from the ECM.

Aggrecanases degrade the proteoglycan aggrecan, of which the primary site is Glu373-Ala374 to produce fragments containing neoepitopes. Both ADAMTS-4 and -5 have shown to be associated with cartilage degradation in OA. However, ADAMTS-4 null mice are not protected from cartilage degradation in a model of OA (Glasson et al., 2004). Conversely, ADAMTS-5 knockout mice exhibit undamaged cartilage in models of OA (Glasson et al., 2005a). This suggests ADAMTS-5, at least in the mouse, is the major contributing enzyme to pathogenic catabolism of cartilage, making it a focus of OA research. Additionally, to ADAMTS-4 and -5, there are other ADAMTSs that contribute to the differentiation and proliferation of chondrocytes as well as to the balance between anabolism and catabolism of the matrix (Yang et al., 2017).

Collagenases or MMPs are also important for matrix turnover.

Interestingly, destruction of aggrecan stimulates MMP activity (Troeberg and Nagase, 2012). Evidence links MMP-13 in particular to cartilage destruction, for example, conditional expression of MMP-13 in murine cartilage results in the spontaneous development of OA (Neuhold et al., 2001). Additionally, Mmp-13-/- mice are protected from cartilage degradation in a surgical model of OA (Little et al., 2009).

There are other control mechanisms for regulating tissue turnover. Tissue inhibitors of metalloproteinases (TIMPs), inhibit the activity of both MMPs and ADAMTSs, protecting the cartilage matrix, and hence is potentially a regulator of cartilage destruction in OA (Sahebjam et al., 2007). A recently explored system at the Kennedy Institute of Rheumatology found endogenous protease activity increased when cells were dead. This phenomenon was later found to be owing to the cell membrane actively removing proteases by clathrin dependent endocytosis; a process dependent on the low-density lipoprotein receptor-related protein 1 (LRP-1), a cell surface receptor. This system was identified to be impaired in OA chondrocytes, resulting in failed removal of ADAMTS-5 and MMP-13 from the ECM leading to exacerbated degradation (Yamamoto et al., 2016; Yamamoto et al., 2013a). Specifically, this impairment in the OA context was found to be owing to the ligand-binding portion of LRP-1 to be shed by 'sheddases,' to

include ADAM17 and MMP-14. This shed portion of LRP-1 can also increase the activity of ADAMTS-5 (Yamamoto et al., 2017).

1.3.4.8 The role of mechanics in cartilage thickness, health, and homeostasis

Musculoskeletal research has identified mechanical forces as crucial to development and health and homeostasis of the skeleton. During development, formation of bone is driven by a constant interaction with mechanical forces emanating from both muscular contractions and, later, load-bearing. This is evidenced by a reduction in the number of proliferating chondrocytes and ECM production in growth plates when paralysis is induced during development (Shwartz et al., 2013). Additionally, aforementioned signalling molecules associated with the growth plate, Ihh and PTHrP, are known to be mechanosensitive and have been shown to regulate the size of the growth plate through the differentiation of proliferating chondrocytes to hypertrophic chondrocytes in developmental and adult mouse models (Kronenberg, 2003; Lanske et al., 1999a; Mak et al., 2008). Ihh is thought to act as a mechanotransduction mediator translating mechanical forces into the upregulation of anabolic production of the ECM (Ng et al., 2006).

Articular cartilage health is often associated with the thickness of the cartilage. When patients present with knee pain in the clinic,

CT-scans will be taken to determine what stage of OA disease an individual may have. The distance between end of the tibia and femur in the knee joint defines the joint gap and represents cartilage thickness. The narrower the gap, the higher the level of disease. There is substantial evidence to support the role of mechanics in cartilage thickness and health, with aberrant joint loading or cartilage injury commonly resulting in arthritic disease within a few years (Muthuri et al., 2011). A clear distinction must be made here between the loss of cartilage volume (atrophy) to loss of cartilage observed during the pathological destruction of cartilage in arthritic disease. Atrophy has been documented in large animals and humans with disuse (reduced loading), whereas joints that were 'over-loaded' suffered from arthritic disease. Both conditions result in cartilage thinning, but owing to very different mechanical inputs.

Studies in both humans and animal models have observed that joint disuse can lead to cartilage thinning. Disuse of joints can result in atrophy of hip articular cartilage by up to 50%, such as that documented in bed ridden patients suffering from flaccid paralysis (Pool, 1974). This loss of cartilage owing to joint immobilisation has also been observed in animal models, where disuse for less than a week was sufficient to reduce proteoglycan content of the cartilage, and with 8-weeks of immobilisation up to a 50%

reduction in cartilage thickness was observed (Palmoski et al., 1979). Additionally, in another study, immobilisation was found to affect the calcified cartilage layer in the medial compartment, leaving uncalcified largely unaffected. Interestingly, the reverse was true in the contralateral limb/joint, with increases in proteoglycan content observed in the uncalcified cartilage (Kiviranta et al., 1987).

Conversely, physiological loading of the knee joint, for example during exercise, is associated with an increase in cartilage thickness. The daily exercising of dogs over three months was enough to increase cartilage thickness by over 11% in loaded regions, coinciding with increased cartilage stiffness (Jurvelin et al., 1986). Training over a longer period of time led to a ~20% increase in uncalcified cartilage thickness coinciding with an increase in glycosaminoglycan production (Kiviranta et al., 1988).

Further supportive evidence includes cartilage responses following joint distraction, where the joint is 'unloaded' post-injury or surgical intervention. In these experiments joint space widening can be observed on a radiograph, indicative of cartilage thickening, and hence repair, even in the setting of osteoarthritic disease (Wiegant et al., 2015). However, whilst exercise has been shown to increase cartilage thickness, aberrant or pathophysiological loading has also been associated with arthritic disease. It has been hypothesised that this is owing to an intrinsic 'mechanostat'

within the tissue, continuously monitoring mechanical inputs and adapting the cartilage accordingly within a physiological window of appropriate forces (Vincent and Wann, 2018).

This large body of evidence for the role of compression induced mechanics in articular cartilage is convincing, yet the molecular mechanisms underlying these processes are less explored. Mechanical stimulation of cartilaginous tissue leads to activation of integrins, stretch and cation-sensitive channels leading to the upregulation of anabolic cartilage programmes (Kamkin and Kiseleva, 2005). The master chondrocyte/cartilage 'mechanosensor' remains elusive, and associated mechanotransduction machinery remains undefined.

1.4 Primary Cilium

1.4.1 Structure

The primary cilium is a highly conserved microtubule based organelle present on the majority of eukaryotic cells, analogous in structure to flagellar (Brinkmann and Philippe, 2007). It is present on the majority of cell types in the mammalian body, protruding out into the extracellular matrix, projecting alongside the cell or invaginated within the cell membrane to form a ciliary pocket (Fig. 1.4.1.1).

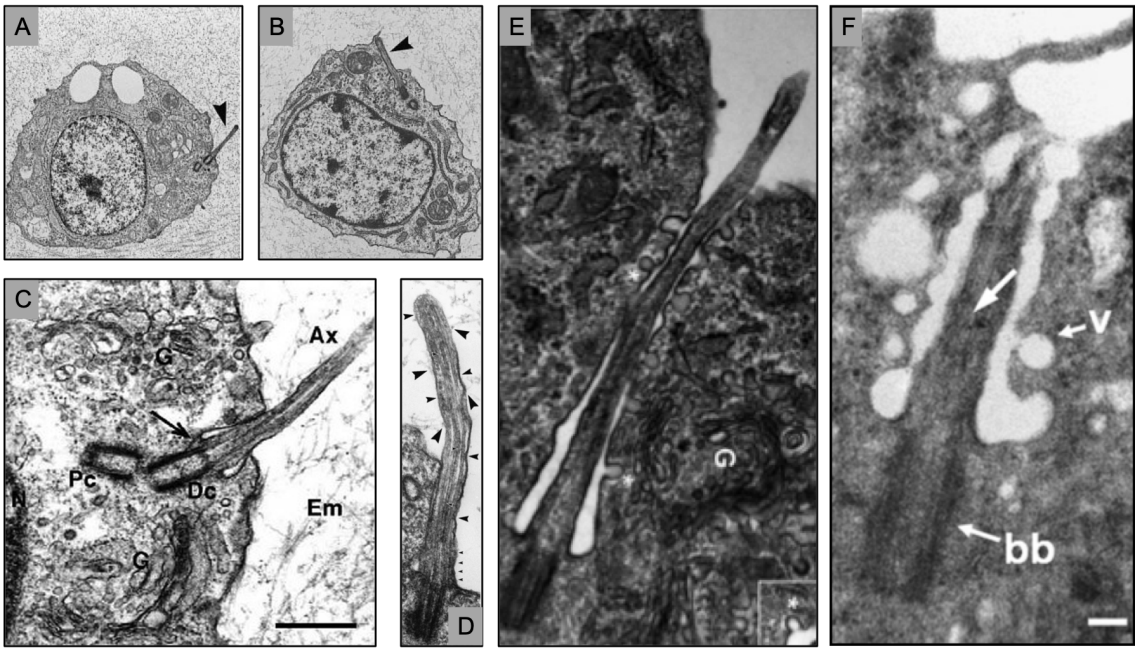


Figure 1.4.1.1: The primary cilium.
Chick chondrocyte primary cilia can be projecting into the extracellular matrix (A) or alongside the cell (B&D): adapted from (Poole et al., 2001). Chondrocyte primary cilium (C) adapted from (Ruhlen and Marberry, 2014) showing proximity to golgi apparatus. Other joint cells, such as the synoviocyte also present with a primary cilium, here within a deep ciliary pocket, lined with apparent vesicular activity marked by white stars (E) adapted from (Rattner et al., 2010). Mouse chondrocyte primary cilium (marked with white arrow) within the cilia pocket. V marks suspected vesicular activity at the pocket. The basal body is labelled as 'bb' (F). Image adapted from (Rich and Clark, 2012).

The primary cilium was first documented by in mammalian cells by Zimmermann in 1898 (Zimmermann, 1898). Until the beginning of the 21st century, the primary cilium was thought to be a vestigial organelle, a remnant from evolution. Through the identification of the role of cilia proteins in the rare human congenital diseases 'ciliopathies,' it is now irrefutable that the primary cilium is crucial to embryonic development and broadly, metazoan life. In 2001 the primary cilium was found to have a sensory role for kidney epithelial cells, bending in response to fluid flow, initiating intracellular calcium signalling (Praetorius and Spring, 2001), a hypothesis that still holds support in the field despite some conflicting evidence (Delling et al., 2013a; Delling et al., 2016a; Norris and Jackson, 2016). Polycystic kidney disease was hence coined as the very first ciliopathy and highlighted the importance of the primary cilium.

1.4.2 Primary cilia proteins

Primary cilia, motile cilia and flagella are highly conserved microtubule-based structures differing only in arrangement and prevalence. In normal circumstances, only one primary cilium can be formed per cell, originating from the mother (older) centriole of the cell and it is immotile, in contrast with motile cilia of multi-ciliated cells. The ciliary axoneme comprises 9 doublet

microtubules, associating in a ring around none, two or more central singlet microtubules. This structure is often denoted as 9 + 2 for motile or 9 + 0 for non-motile cilia and flagella. Additional accessory proteins, such as radial spokes and dynein arms confer axonemal motility and are lacking in primary cilia (Satir and Christensen, 2007). At the base of the primary cilium is a modified mother (older) centriole, which is adapted through the addition of protein appendages, to become the basal body. This structure nucleates the formation of the primary cilium, and disruption to the protein complex at its base, known as the BBSome, results in aberrant primary cilia function. Mutations to these basal body/BBSome proteins result in a human congenital disease known as Bardet-Biedl syndrome (BBS).

The primary cilium forms its own separate compartment away from the rest of the cell and hence has to actively import and actively export proteins required for its structure and function. To accomplish this, the structure relies heavily on intraflagellar transport (IFT) proteins for trafficking of proteins to the ciliary tip (anterograde) and back to the cell body (retrograde) (Fig. 1.4.2.1). IFT proteins assemble to form two larger complexes responsible for carrying cargo proteins, associating with kinesins and dynein motor proteins to do so. In anterograde transport the IFT-B complex comprises of several IFTs, notably including IFT88. As the IFTB

complex is crucial for anterograde transport, mutations to these proteins and in particular, IFT88, results in an inability to assemble a primary cilium. Additionally, mutations to the motor proteins, kinesins and dyneins responsible for powering this trafficking, results in an inability to assemble cilia.

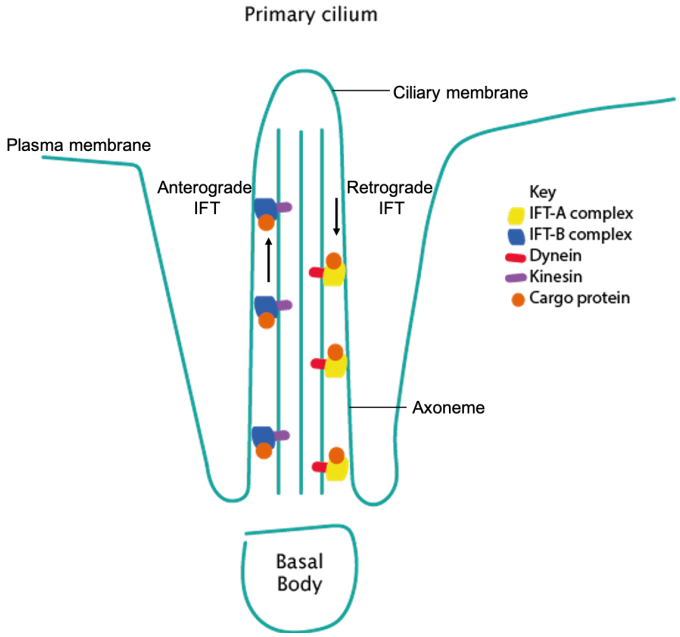


Figure 1.4.2.1: Intraflagellar transport in the primary cilium.
A schematic illustrating intraflagellar transport within the primary cilium. The IFT-B complex associates with cargo proteins and binds to the motor protein kinesin in order to transport cargo proteins from the cell body to the tip of the primary cilium in anterograde transport. The IFT-A complex associates with cargo proteins and binds to the motor protein dynein to return proteins from the cilia tip to back to the cell body in retrograde transport.

1.4.3 IFT88

The IFT protein IFT88 (intraflagellar transport 88) is a crucial component of the IFT-B complex, responsible for anterograde transport of proteins to the ciliary tip and as such vital for cilium growth and function (Fig. 1.4.3.1). The relevance of mammalian

IFT88 was discovered through a large-scale insertional mutagenesis project at the Oak Ridge Laboratories in 1994, generating a mouse that exhibited polycystic kidney disease, subsequently called the Oak Ridge Polycystic kidney disease mouse (ORPK mouse). This IFT88 mutation (IFt88Tg737Rpw) arose from transgene integration near the 3' end, subsequently interfering with the expression of the (IFT88/polaris/Tg737) protein. IFT88 null mutants are embryonic lethal owing to failed hedgehog signalling during embryonic patterning and organogenesis. The hypomorphic mutation in IFT88 (ORPK) in one allele is sufficient for an embryo to progress to the foetus stage and beyond to adulthood, during which time polycystic kidney disease develops. The ORPK mouse is therefore an interesting model to investigate the role of cilia in disease pathogenesis (Lehman et al., 2008).

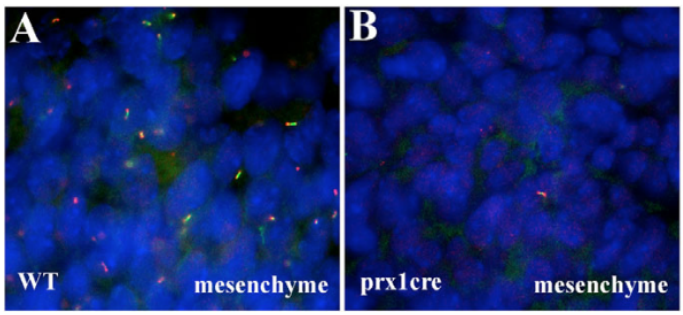


Figure 1.4.3.1: IFT88 is crucial to cilia formation.
Cilia were identified in WT (A) and prx1cre;Ift88fl/n (B) frozen sections from E11.5 limbs by immunofluorescence. Acetylated-tubulin (green) and Ift88 (red) and nuclei shown in blue (DAPI). Figure adapted from (McGlashan 2007).

Beyond canonical ciliary roles, the ORPK mutation in chondrocytes results in cytoskeletal re-organisation, specifically in regards

to F-actin filaments, resulting in stress fibre formation, failed hypertrophic chondrocyte differentiation, and reduced cell density (McGlashan et al., 2007). These cytoskeletal changes have also been associated with disruption to cell biomechanics (Wang et al., 2016). Specifically, in chondrocytes, IFT88 has been shown to regulate actin organisation and stiffness of the actin cortex. Disruption to actin cortex stiffness results in changes to cell deformation, mechanical properties and formation of cellular protrusions.

Additionally, IFT88 is thought to be involved in microtubule transport of the poles by localising to them during cell division (Robert et al., 2007). IFT88 also associates with the centrosome by attaching to the proximal ends of centrioles controlling G1-S phase transition (Robert et al., 2007). This function of IFT88 is conserved in non-ciliated cells. Therefore, IFT88 is important for correct mitosis and spindle formation (Delaval et al., 2011). Furthermore, IFT88 has been implicated in controlling the orientation of polarised cell divisions at both gastrulation and neurulation in zebrafish embryos, a function that is independent of the primary cilium (Borovina and Ciruna, 2013).

1.4.4 Primary cilia function

Most of our understanding of primary cilia biology so far has arisen from aberrations to the ciliary structure, and the cilium has

subsequently been found to either regulate or be connected to many signalling pathways. These include hedgehog signalling (Corbit et al., 2005; Huangfu et al., 2003), cellular mechanotransduction (Wann et al., 2012), polycystins (Nauli et al., 2003), Wnt signalling (Ross et al., 2005; Praetorius and Spring, 2003; Praetorius and Spring, 2001; Tatsumi et al., 2007), and TGF-β signalling (Clement et al., 2013a). The ciliary membrane, a continuation of the cell's plasma membrane, embeds many receptors including PDGFR, SOMATOSTATIN R, frizzled, IGFR and patched demonstrating its potential to influence many cellular signalling pathways. This evidence can be collated to support theories as to how the primary cilium functions including as a sensor, a transducer and compartmentalisation of signalling molecules.

1.4.4.1 Hedgehog signalling

As one of the receptors in the ciliary membrane is Patched, the Hedgehog receptor, the primary cilium is involved in Hedgehog (Hh) signalling, a very important developmental pathway. The primary cilium is fundamental to correct embryonic patterning which was first demonstrated in mammalian systems using mouse models in 2005 (Huangfu and Anderson, 2005). Phenotypes of ciliary mutant mouse models demonstrated that the role of IFT proteins, and crucially for this thesis, IFT88, are important for the transduction of Hh signals (Clement et al., 2009a).

In the absence of Hedgehog (Hh) ligand, Smoothened (Smo), a transmembrane protein, is inhibited by the hedgehog ligand receptor Patched (Ptch). Gli2 and Gli3, the main transcription factors of the pathway, are cleaved to their repressor forms (Fig. 1.4.4.1). However, ligand, e.g Shh, binding to Ptch causes the transmembrane protein to leave the cilium, allowing, by an unknown mechanism, for the entry and activatiPthc1on of Smo (Rohatgi et al., 2007a). This enables for Gli2/3 to dissociate from Sufu, a negative regulator of the pathway, and the unprocessed full-length form is actively transported to the nucleus, where it activates transcription of effector genes which include *Ptch1* and *Gli1*.

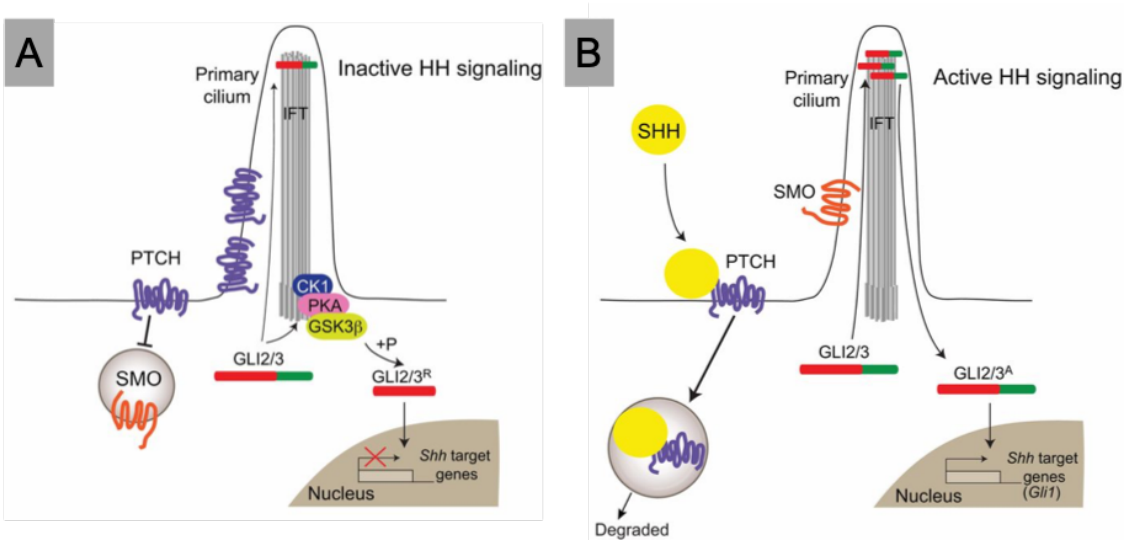


Figure 1.4.4.1: Schematic of Hedgehog signalling at the primary cilium.
Inactive: The Hedgehog (Hh) binding receptor patched 1 (PTCH) localises to the primary cilium where it inhibits the activation of smoothened (Smo). Intraflagellar transport (IFT) proteins traffic components of the Hh signalling pathway including glioma associated oncogene proteins (GLIs), in and out of the ciliary structure. Phosphorylation of Glis by protein kinase A (PKA), casein kinase 1α (CK1) and glycogen synthase kinase 3β (GSK3β), leads to their proteolytic cleavage to their repressor forms (Gli2R and Gli3R), which suppresses transcription of Hh target genes (A). Active: Hh ligand binding to Ptch1, leads to its exit from the primary cilium and degradation, removing the suppression on Smo. Smo enters the primary cilium, and Glis accumulate at the ciliary tip where they are processed to their transcriptional activator form (Gli2A and Gli3A). They then translocate to the nucleus to activate Hh targeting genes including the transcriptional activator Gli1. Figure adapted from (Petrova et al. 2014).

1.4.4.2 Mechanotransduction

At present, the majority of research on the primary cilium's role as a potential mechanotransducer focusses on the response to shear stress created by fluid flow (Fig. 1.4.4.2). There are a number of channels that localise to the primary ciliary membrane that are potential candidate sensors and are the focus of investigation which include; the polycystins PC1 and PC2 and other transient receptor potential (TRP) channels.

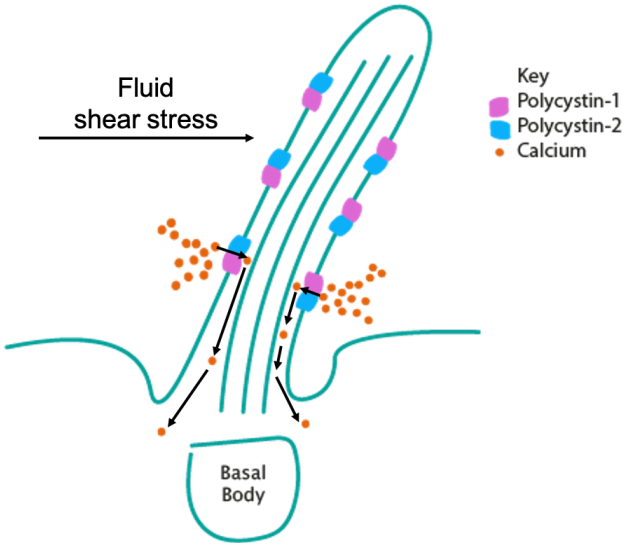


Figure 1.4.4.2: The primary cilium responds to fluid flow.
A schematic illustrating the response of the primary cilium to fluid shear stress in kidney epithelial cells. Fluid flow in the kidney bends the primary cilium activating the mechanosensitive channels polycystin-1 and polycystin-2, initiating calcium influx and initiating pathways downstream.

TRP proteins were first discovered in Drosophila melanogaster, but it has subsequently been found to have homologs in other species. The TRP proteins assemble cation channels that transduce cellular stimuli into chemical signals by changes to intracellular Ca^{2+} signals or electrical signals by membrane potential changes (Clapham, 2003). Subfamilies exist within the family of TRP proteins to include TRPV. This family of channels have largely been defined as thermosensors. TRPV1, TRPV2 TRPV3, TRPV4 are all responsive to heat and pH changes, but TRPV5 and TRPV6 are activated by Ca^{2+} ion changes (Clapham, 2003; Desai and Clapham, 2005). The majority of these TRP channels have some Ca^{2+} activity that is crucial to their regulation of cellular processes (Nilius, 2007).

Additionally, the TRP channels are often located within cilia and are non-selective cation channels activated by Ca^{2+} (Kottgen et al., 2008; Masuyama et al., 2008). How exactly these channels are specifically activated is unknown at present. Understanding their role is further complicated by their formation of complexes with PC2. TRPV4 in particular has been proposed as a ciliary ion channel. It has been proposed that as TRPV4 can sense changes in osmolarity, the primary cilium is also required for the cell to transduce signals about tonicity in the microenvironment.

The polycystins have been intensely studied owing to their links to polycystic kidney disease. PC1 colocalises to the primary cilium membrane with PC2, a Ca^{2+} cation channel (Fig. 1.4.4.2). This is achieved by the help of IFT proteins (Follit et al., 2006). Calcium signalling is lost in the cell when the functional properties of PC1 are disrupted (Lee and Somlo, 2014). Both PC1 and PC2 are involved in the maintenance of intracellular calcium concentrations. In turn this elevates the levels of adenylate cyclase, decreases phosphodiesterase activity resulting in an increase in cAMP concentration and subsequent increased PKA activity. Calcium signalling is a key regulator of many important signalling pathways including the Raf/MEK/ERK, PDGFR and Hh pathways, and disruptions to these are sufficient to induce pathogenesis; ciliary mutations are hence important to the cell's

function in general (Ko and Park, 2013). Until recently, it was thought that the PC1 and the primary cilium responded to fluid shear stress by initiating intracellular calcium signalling (Delling et al., 2013a; Praetorius and Spring, 2001). However, it has now been shown that whilst there is an increase in calcium concentration in the primary cilium, that is much higher than that of the cellular cytoplasm, this intra-ciliary change in calcium is thought to originate from intracellular calcium stores and not from the extracellular environment (Delling et al., 2016b). In chondrocytes the ORPK mutation to IFT88 renders them unable to elicit an appropriate calcium response downstream to ATP (which is released by strain) (Wann et al., 2012).The debate continues over whether the primary cilium could be sensing other molecules stimulated by this mechanical input (Norris and Jackson, 2016). In chondrocytes the IFT88 ORPK mutation renders them unable to elicit an appropriate calcium response downstream to ATP (Wann et al., 2012).

1.4.5 Ciliopathies

Ciliopathies are a group of rare human congenital diseases resulting from mutations to proteins associated with the cilium. Mutations to proteins that are crucial to the ciliary structure significantly impact Hh signalling, resulting in failed embryonic patterning

and are hence embryonic lethal. Mouse models targeting these vital components are embryonic lethal. However, there is one consanguineous family carrying a mutation to *IFT88* which was found to be autosomal recessive and resulted in retinal disease most resembling retinitis pigmentosa (Chekuri et al., 2018).

As cilia are present on the majority of cell types, aberrant signalling resulting from a ciliary protein mutation within each individual tissue leads to the development of multiple pathologies including, retinal degeneration, obesity, Type II diabetes, liver fibrosis, polycystic kidney disease and musculoskeletal phenotypes. Mutations to basal body proteins leads to Bardet-Biedl syndrome (BBS). Other ciliopathies include Alström syndrome (obesity, diabetes, vision and hearing loss), Joubert syndrome (brain), Meckel syndrome (renal cysts, hepatic developmental defects, and polydactyly) and polycystic kidney disease. Additionally, primary cilia dyskinesia, which effects motile cilia only, results in pulmonary and respiratory problems/infections, hearing loss and infections and infertility. Beyond the ciliopathies, recent research is beginning to associate the primary cilium with the pathogenesis and/or progression of a plethora of other human diseases including cancer (Liu et al., 2018), obesity (Siljee et al., 2018) and cardiovascular disease (Dinsmore and Reiter, 2016).

1.4.5.1 Musculoskeletal ciliopathies

Some ciliopathies present with musculoskeletal phenotypes. These phenotypes can largely be attributed to failed Hh signalling in embryonic limb bud patterning, and regulation of growth plate dynamics during long bone growth. In Jeune syndrome (asphyxiating thoracic dysplasia) patients present with shortened ribs, narrowing of the chest, shortened long bones, short stature, and polydactyly (extra fingers and toes). Most die early in childhood, suffocated by the restrictions on lung expansion owing to a narrow rib cage. If children do survive, they can live normal lives, but will likely present with kidney or heart complications later in life. Other ciliopathies presenting with dactyly defects are BBS, Meckel and Alström syndrome.

1.4.6 Cilia in musculoskeletal mouse models

1.4.6.1 Mouse models targeting Hh components in cartilage

In early development, using the *Prx1Cre* system, progenitors destined to form the limb bud mesenchyme can be targeted. Cartilage development requires the use of the hedgehog ligand known as Indian Hedgehog (Ihh). Deletion of Ihh in the limb bud mesenchyme (*Prx1Cre;Ihh*) results in impaired type X collagen expression and osteogenesis of digit growth plate cartilage (Amano et al., 2016). In the same study *Prx1Cre;PTHrP* null mice resulted in

inhibited growth plate formation and replacement of cartilaginous tissue with bone.

Later in development, other cartilage specific promoters are used to drive Cre activation including type II collagen. The cartilage specific inducible deletion of Ihh (*Col2a1CreER;Ihh*), removing Ihh signalling, resulted in dwarfism (Fig. 1.4.6.1.A) and complete loss of the growth plate by 2-weeks of age (Fig. 1.4.6.1.B) (Maeda et al., 2007). Loss of Ihh results in premature hypertrophic differentiation due to the loss of PTHrP expression in presumptive articular cartilage and perichondrium, leading to reduced chondrocyte proliferation and loss of vascularisation of the long bones. Interestingly, a similar phenotype emerges when Hh signalling is elevated. Removal of Ptch1 (*Col2Cre;Ptch1*) resulted in a removal of the inhibition on Smoothened and elevated Hh resulting in premature growth plate fusion (Mak et al., 2006).

Another study, targeting Ihh and PTHrP in embryonic skeletal development, resulted in altered growth plate formation and maturation of developing articular cartilage. By overexpressing Ihh in the cartilage, they found accelerated chondrocyte hypertrophy in PTHrP-/- embryos (Mak et al., 2008). Additionally, they showed that the upregulation of Hh signalling in postnatal cartilage (at one year) as a result of inducible deletion of Ptch1 specifically in chondrocytes (*Ptch1c/c;Col2a1-CreER*) resulted in accelerated

chondrocyte hypertrophy, a reduction in proteoglycan content in articular cartilage and thinner articular cartilage (Fig. 1.4.6.1 C). At this age there was no apparent disruption to the growth plates. Conversely, targeting of Smo (*Col2a1-CreER;Smo*) in the cartilage of adult mice, thus inhibiting Hh signalling, resulted in increased proteoglycan content and thicker cartilage (Fig. 1.4.6.1 D), implicating the role of Hh signalling in cartilage homeostasis potentially beyond development. Supporting this hypothesis, Hh blockade also attenuates OA progression in a surgically induced model of OA (Lin et al., 2009).

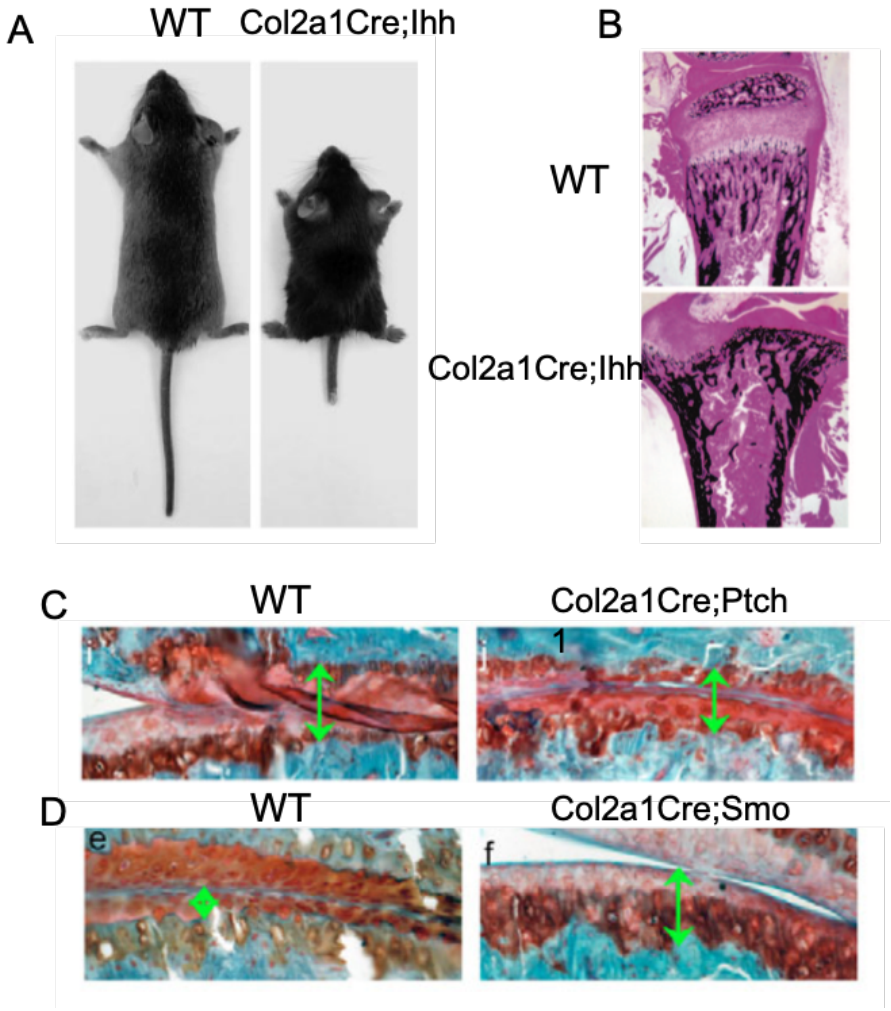


Figure 1.4.6.1: Ihh disruption in the mouse.
WT and Ihh null mice (A). Tibia of P14 knee mice in WT and Ihh null mice showing loss of growth plate in KO (B). Articular cartilage WT and Ptch1 null mice cartilage thickness (C). Articular cartilage of WT and Smo null mice (D). Green arrows represent difference in thickness in C and D. Figure adapted from Maeda et al. 2007 and Mak et al. 2008.

There is a strong relationship between primary cilia and Hh signalling, evidenced by the similarity in phenotypes observed from genetic models targeting components of either the primary cilium or Hh pathway. It is difficult to dissect the role of IFT and cilia in the regulation of Hh and other Hh-independent roles, for example mechanotransduction.

1.4.6.2 Mouse models targeting ciliary proteins in cartilage

The first mouse model to identify the primary cilium as having a role in disease processes, finally abolishing the hypothesis that the organelle was vestigial, was generated in a random mutagenesis screen at the Oak Ridge laboratories. The first noticeable phenotype in this mouse was polycystic kidney disease (PKD). Beyond PKD, this mouse has musculoskeletal developmental defects, resulting in shortened growth plates, differences in type II collagen deposition within articular cartilage, and changes to type X collagen expression in the hypertoric region of growth plates (Fig. 1.4.6.2). This mouse has been an extremely useful tool to understand the role of the primary cilium in musculoskeletal development, abolishing cilia expression in cells to 6% and providing mouse chondrocyte cell lines that provide a tractable way of investigating the role of IFT88 *in vitro*. This mouse does have some disadvantages as this mutation is ubiquitous, it is homozygous lethal and appears to still have some function as IFT88 deletion models manifest different phenotypes to the ORPK (McGlashan et al., 2007).

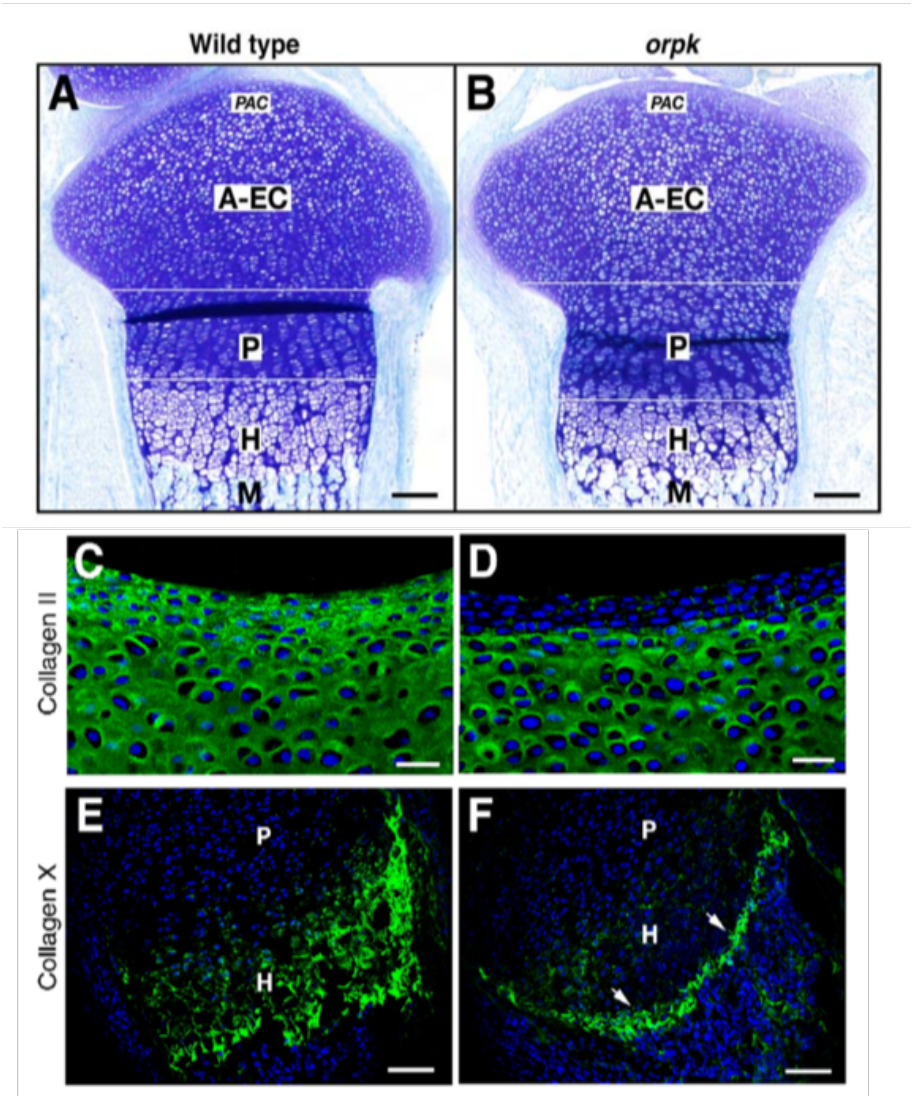


Figure 1.4.6.2: Disruption of IFT88 results in changes to cartilage deposition and joint formation
WT (A) and ORPK (B) limbs from E15 embryos reveal shortened growth plates. Type II collagen (collagen II) staining of articular cartilage in WT (C) and ORPK (D) sections. Type X collagen (collagen X) staining of growth plate cartilage in WT (C) and ORPK (D) sections. Figure adapted from McGlashan et al. 2007.

To further understand the role of the primary cilium in musculoskeletal tissues, genetic mouse models were created to target critical proteins to the cilia structure specifically within cartilage or to the musculoskeletal system. Using the *CreLoxP* system to target IFT88, *Prx1Cre*, was used to target IFT88 in the

limb bud mesenchyme (*Prx1Cre;IFT88*). This deletion resulted in limb bud patterning defects, leading to extensive polydactyly, and defects in endochondral bone formation (Fig. 1.4.6.3) (Haycraft et al., 2007a). The authors found this to be due to aberrant Ihh signalling within the growth plate resulting in its reduced length, documenting loss of Ptch1 and Gli1 expression. They also found accelerated hypertrophy, poor mineralisation, and delayed vascularisation. IFT88 loss in mouse models appears to mimic some animal models in which Ihh signalling is lost (Fig. 1.4.6.1).

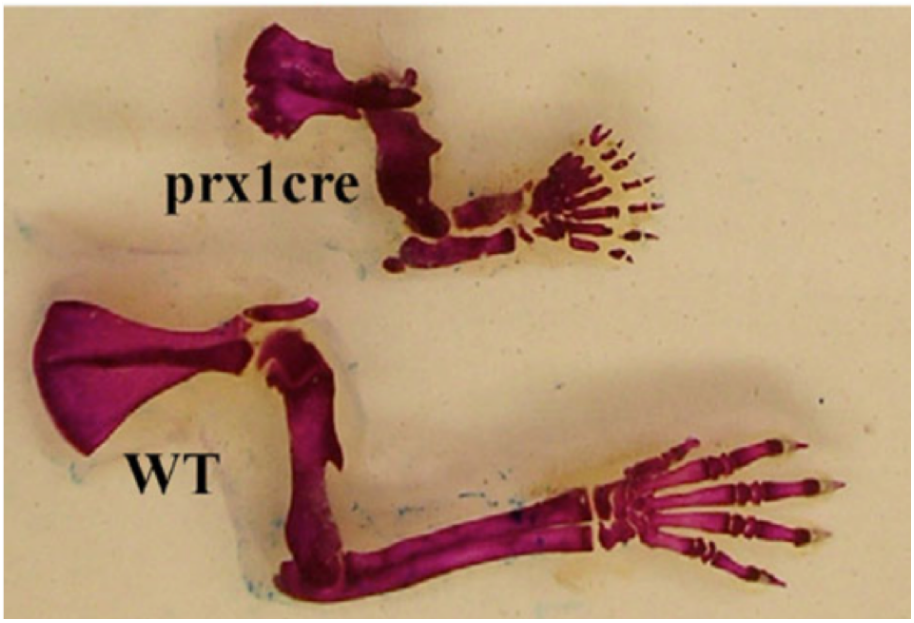


Figure 1.4.6.3: Deletion of IFT88 in the limb bud mesenchyme.
Alizarin red staining of Prx1Cre;IFT88 and WT controls.

Cartilage specific deletions of IFT88 have employed the type II collagen promoter, characteristically expressed by chondrocytes (*Col2a1Cre;IFT88*). This mouse model (Fig. 1.4.6.4) resulted in cilia loss on chondrocytes, severe joint malformation (Fig. 1.4.6.4 A &

B), loss of the growth plate and an apparent increase in articular cartilage thickness (Fig. 1.4.6.4 C & D), within which they found upregulated expression of osteoarthritis associated genes (MMP-13 and ADAMTS-5) (Chang et al., 2012). Additionally, they found upregulation of Hh signalling components, Ptch1 and Gli1 and reduced Gli3 repressor to activator ratio. They proposed this activation of OA related genes was due to reduced Hh repression by Gli3.

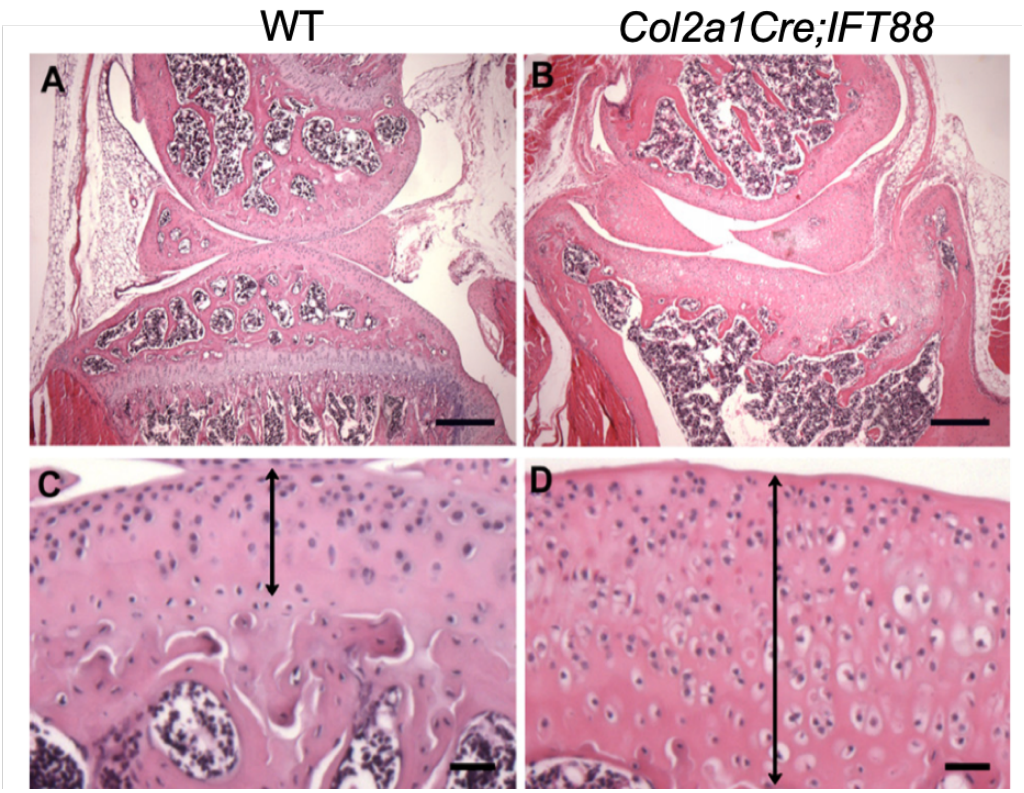


Figure 1.4.6.4: Cartilage specific deletion of IFT88.
Histological sections of knees from WT (A) and IFT88 null mice (B). Histological sections of articular cartilage beneath shows increased articular cartilage thickness in IFT88 null (D) mice in comparison to WT (C). Figure adapted from Chang et al. 2012.

Cartilage specific deletions of kinesin 3 (Kif3a) (Fig. 1.4.6.5), a motor protein involved in anterograde transport and thus carries

IFT88, results in loss of the growth plate (A&C), dwarfism (E), and altered production of the ECM protein aggrecan (F&G) when compared to controls (Song et al., 2007). Additionally, the authors compared cartilage specific deletions of IFT88 with Kif3a knockouts. They had independent phenotypes despite affecting the same anterograde system, hypothesised to be owing to Kif3a mutants maintenance of constitutively phosphorylated dishevelled 3, which is downstream of Wnt ligand binding (Corbit et al., 2008). Subsequently, it has been proposed that targeting of IFT88 is the best way to investigate the role of the primary cilium in cartilaginous tissues (Moore and Jacobs, 2018).

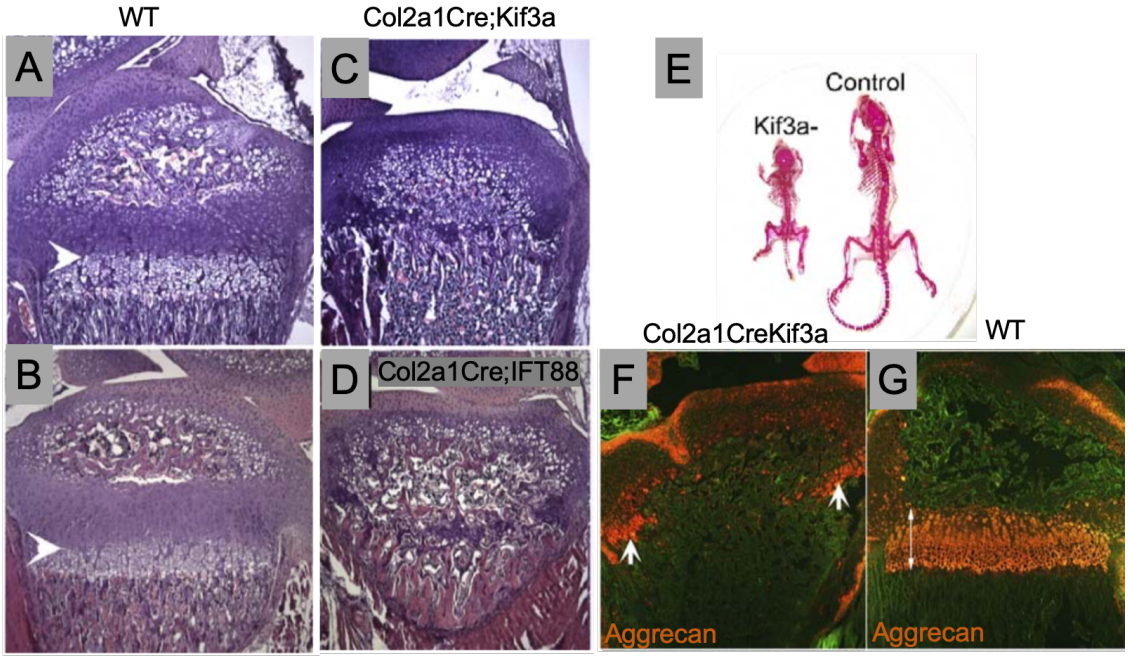


Figure 1.4.6.5: Cartilage specific deletion of Kif3a.
P15 WT joints of controls (A&B) for Col2a1Cre;Kif3a (C) and Col2a1Cre;IFT88 (D) respectively. Alizarin red staining of P30 WT and Kif3a-/- animals (E). Aggrecan expression in Col2a1Cre;Kif3a and WT joints (F and G). Figure adapted from Song et al. 2007.

Bardet Biedl syndrome (BBS) is a human ciliopathy that presents with MSK phenotypes including polydactyly. This syndrome arises from mutations to the basal body, a protein complex localised to the base of the primary cilium consisting of 7 BBS proteins. Mouse models have been primarily created to understand the role of the BBS proteins in the other phenotypes that present in this disease, such as obesity, diabetes and retinopathy. However, mutations to Bbs6 (Fig. 1.4.6.6 D), Bbs2 (Fig. 1.4.6.6 C) and Bbs1 (Fig. 1.4.6.6 B) each lead to thinner articular cartilage by 10 months of age in comparison with WT (Fig. 1.4.6.6 A) and loss of primary cilia expression in chondrocytes (Kaushik et al., 2009).

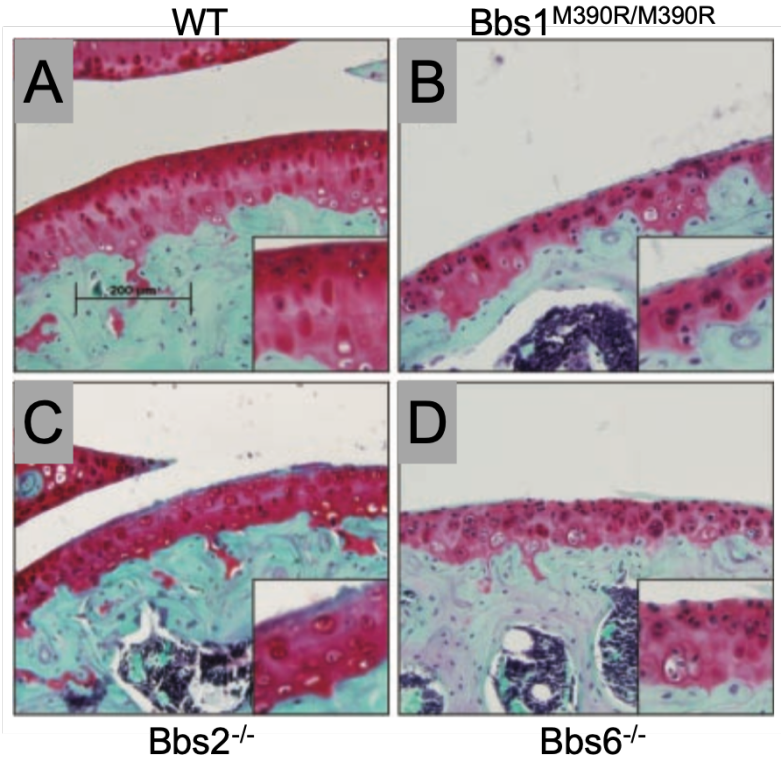


Figure 1.4.6.6: Deletion of BBS proteins in mice.
Histological staining of knee articular cartilage in BBS mutant mice revealed thinner cartilage in Bbs1M390R/M390R (B), Bbs2-/- (C) and Bbs6-/- (D) mice in comparison with control (A). Figure adapted from Kaushik et al. 2009.

A model to investigate the role of IFTs specifically in post-developmental cartilage was created, focussing on another IFT-B complex protein, IFT80. Using the *Col2CreER^{T2};IFT80*, IFT80 was deleted in the first two-weeks of life specifically within cartilage (Yuan and Yang, 2015a). Animals presented with dwarfism (Fig. 1.4.6.7 A), shortened growth plates (B), shortened long bones, thicker articular cartilage (C) and impaired Hh signalling. To date, there are no post-developmental knockout models of cilia proteins induced after 4-weeks of age in the mouse and hence the role of IFTs in adolescent and adult cartilage homeostasis is yet to be assessed.

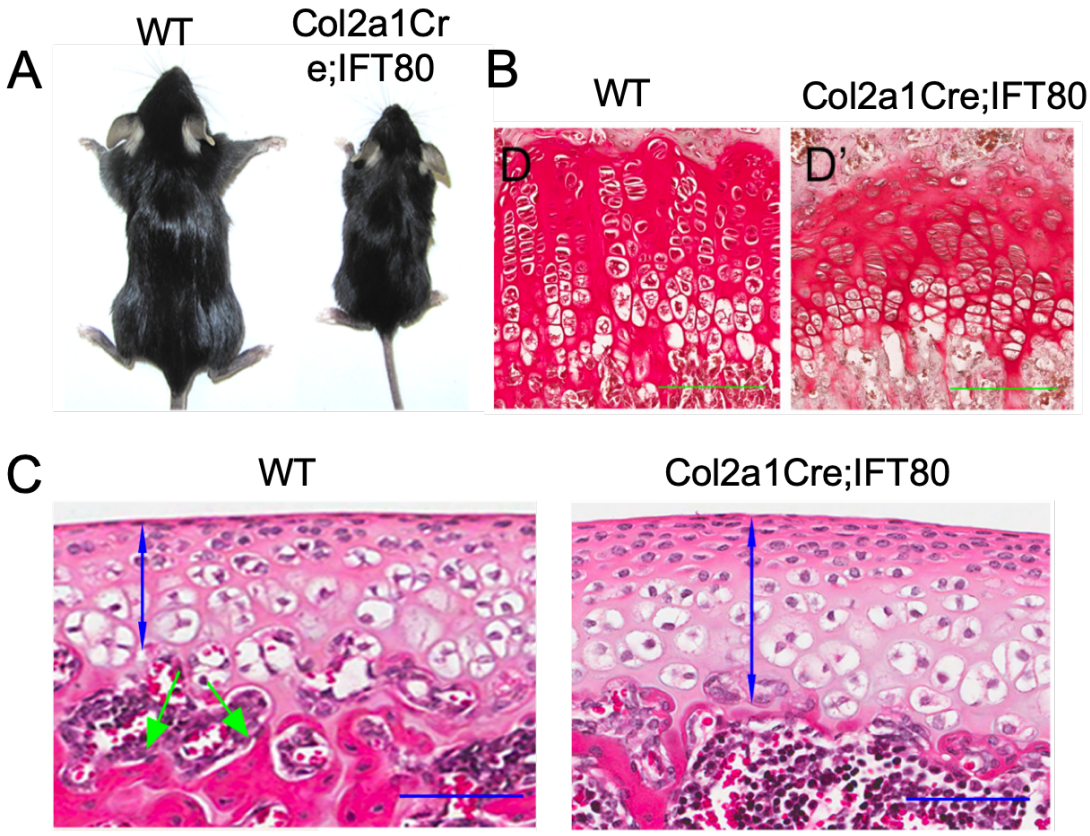


Figure 1.4.6.7: Cartilage specific post-natal deletion of IFT80.
WT and IFT80 null mice (A). Histological staining of growth plates revealed shorter growth plate in IFT80 null mice in comparison with WT (B). Histological staining of articular cartilage revealed thicker articular cartilage in IFT80 null mice in comparison with WT (C). Figure adapted from Yuan et al. 2015.

1.4.7 Summary of mouse model phenotypes

Table 1.1: Table summary of mouse model phenotypes.

Mouse model	Genetic mouse	Phenotype	Reference
Cartilage specific deletion of Indian hedgehog	Col2a1Cre;Ihh	Shortened limbs, accelerated hypertrophic differentiation, and loss of growth plate structure	Maeda et al. 2007
Cartilage specific deletion of Patched-1	Col2a1Cre;Ptch1	Increased articular cartilage thickness	Mak et al. 2008
Cartilage specific deletion of Smoothened	Col2a1Cre;Smo	Development: shortened long bones. Adult: Reduced articular cartilage thickness	Mak et al. 2008
Early limb bud mesenchyme	Prx1Cre;IFT88	Polydactyly, shortened long bones, accelerated hypertrophic differentiation, and shortened growth plates	Haycraft et al. 2007
Cartilage specific deletion of IFT88	Col2a1Cre;IFT88	Severely shortened limbs, accelerated hypertrophic differentiation, primary and secondary ossifcaiton centres merge, and loss of growth plate structure	Song et al. 2007
Hypormorphic mutation to IFT88 mouse model	ORPK	Malformation of tibia, altered matrix deposition in articular cartilage, disroganisation and alterred morphology of growth plate chondrocytes	McGlashan et al. 2007

Table 1.1: Table summary of mouse model phenotypes.

Cartilage specific deletion of kinesin 3a	Col2a1Cre;Kif3a	Dwarfism, disorganisation of growth plate, accelrated hypertrophic differentitation and reduced proliferation	Song et al. 2007
Cartilage specific deletion of IFT80	Col2a1Cre;IFT80	Post natal: Shortened limbs, chondrocyte disorganisation in the growth plate, and thicker articular cartilage	Yuan et al. 2015
Knock in mutation to Bardet beidl syndrome protein-1	Bbs-1 M390R/M390R	Thinner adult articular cartilage and loss of primary cilia	Kaushik et al. 2009
Deletion of Bardet beidl syndrome protein-2	Bbs-2 null	Thinner adult articular cartilage and loss of primary cilia	Kaushik et al. 2009
Deletion of Bardet beidl syndrome protein-6	Bbs-6 null	Thinner adult articular cartilage and loss of primary cilia	Kaushik et al. 2009

1.4.8 Mechanotransduction in musculoskeletal tissues

Mesenchymal stem cells (MSCs) are required for the homeostasis and repair of skeletal tissues. To do this, MSCs rely on bio-physico chemical cues in order to differentiate into the correct cell lineage. In the bone, MSCs rely on numerous signals for differentiation including Runx2, Osterix and, importantly, mechanics (Claes and Heigele, 1999; Nagel and Kelly, 2010). Recent research has shown that the mechanosensitive ion channel, TRPV4, is required for MSC mechanotransduction, mediating fluid shear stress induced calcium

signalling. Additionally, they demonstrated the importance of the ciliary localisation of TRPV4, observing that defective primary cilia were unable to initiate an osteogenic response to TRPV4 activation (Corrigan et al., 2018).

As previously stated, the primary cilium assembles on the majority of cell types, including that of bone cells such as osteocytes. Osteocytes are found in the lacunae of bone, where fluid moves through the material as a result of compressive strain impacted on the bone. This fluid flow through the lacunae is proposed to bend osteocyte cilia transmitting signals for bone remodelling (Leucht et al., 2013; Malone et al., 2007). They are thought to be acting through TRPV4 and PC1 channels (Hou et al., 2002; Masuyama et al., 2008).

In the cartilage matrix, ECM binding proteins and integrins localise to the primary cilia (Jensen et al., 2004). ECM components, more specifically collagen, associate with and bind to the primary cilium. The primary cilium then is proposed to bend in response to force transmitted through the ECM. Integrins are mechanosensitive proteins (Alenghat et al., 2009; Meyer et al., 2000), implying that cilia could be sensing compressive deformation of the surrounding ECM (McGlashan et al., 2006). Interestingly, the ORPK mutation leads to changes to the chondrocyte cytoskeleton, implicated in regulating cellular strain (Wang et al., 2016), and more specifically

in F-actin networks leading to failed hypertrophic reprogramming of chondrocytes (McGlashan et al., 2007). This interaction between the ECM and cilia has also been found in another MSK tissue, tendons, where orientation and position of the primary cilium is thought to be directed by the orientation of fibres (Donnelly et al., 2010).

The primary cilium disassembles in response to mechanical stimulation including loading of chondrocytes (Thompson et al., 2014a; Wann et al., 2012). When bovine chondrocytes are loaded, they release ATP which, in turn, upregulates the production of proteoglycan downstream to intracellular calcium signalling (Wann et al., 2012). Whilst culturing WT chondrocytes and those harbouring a hypomorphic mutation of IFT88 (ORPK), that both had and lacked a primary cilium, respectively, in an agarose gel, the ATP and calcium responses to mechanical loading were measured (Wann et al., 2012). This study demonstrated that chondrocyte primary cilia are not the initial mechanoreceptors, as the ATP response was unaffected between WT and ORPK chondrocytes. However, ORPK cells did not initiate a Ca^{2+} response to ATP despite the equal expression of purinergic receptors by WT and OPRK chondrocytes, suggesting cilia are required for transducing downstream ATP-Calcium signalling. Furthermore, ORPK cells were unable to upregulate aggrecan expression and sulphated

proteoglycan secretion. Indeed, ORPK chondrocytes exhibited reduced baseline proteoglycan production despite an apparently elevated aggrecan mRNA level. This study demonstrated that primary cilia are required for cartilage mechanotransduction

1.4.9 *In vivo* targeting of chondrocytes

To target cartilaginous tissues the two common promoters used with the *CreLoxP* system (detailed description in Methods) are type II collagen (Col2) and aggrecan (ACAN). These two proteins are expressed by chondrocytes. However, their efficacy/efficiency as promoters for inducible deletions of a target protein can be variable depending on the age of induction. Chondrocytes in an inducible *Col2Cre* mouse line crossed to a reporter (TdTomato) mouse line, will activate the reporter signal when tamoxifen is administered. In one study, the authors found that different chondrocyte populations were activated with tamoxifen during the first two-weeks of life in comparison with those at three or four-weeks of age (Nagao et al., 2016). They also showed that Col2 expression decreased with age.

Genes expressed by mature chondrocytes, if deleted embryonically, can be embryonic lethal. Therefore, to understand their role in the cartilage in adulthood, their deletion must be induced later in life. As such, these models usually employ an inducible Cre, activated by injections of tamoxifen. To target genes in the adult in aggrecan

expressing cells, there have been two inducible models created. Both models show activation of aggrecan on administration of tamoxifen when crossed to a reporter mouse model. They have also shown activation well into adulthood (up to 6 months) (Henry et al., 2009; Lo Cascio et al., 2014).

1.5 Aims

Main Aims

1. Validate a means by which to delete IFT88 in post-natal cartilage *in vivo*
2. Describe cartilage dynamics during mouse adolescence
3. Investigate the effect of deleting IFT88 in post-natal growth plate
4. Investigate the effect of deleting IFT88 in post-natal articular cartilage

Sub Aim

1. Investigate the role of IFT88 in aggrecan catabolism *in vitro*

2

Materials and Methods

I was taught that the way of progress was neither swift nor easy- Marie Curie
But still try. For who knows what is possible- Michael Faraday
Contents

2.1 Experimental animals 56
2.2 Surgical procedures 66
2.3 Tissue collection 70
2.4 Gene expression analysis 73
2.5 Micro-computed tomography (MicroCT) imaging and radiography 77
2.6 Histological and histomorphometric analyses 82
2.7 Western blotting 92
2.8 Cell Culture and Experiments 99
2.9 Data presentation and statistics 104

2.1 Experimental animals

All mice were housed in the biomedical services unit (BSU) at the Kennedy Institute, within the University of Oxford. Mice were housed 4–7 per standard individually ventilated cages and maintained under 12-h light/12-h dark conditions at an ambient

temperature of 21°C. Animals were fed a normal chow diet and water ad libitum.

2.1.1 Home Office Licence

All experiments were carried our on Professor Tonia Vincent's project licence (PPL: P7E1A3608) and under my personal licence which covers PIL A, B and C (PIL: ID62145EB).

2.1.2 Ethical consideration of animal use

Presently, animal models are widely used in research, with an exponential increase in publications using animals between the 1980s to present. As such, guidelines have been implemented accordingly throughout this period to improve both quality of life for the animals and to improve animal research reproducibility and reporting (Kilkenny et al. 2010). These guidelines encompassed within the Animal Research Reporting of In Vivo Experiments (ARRIVE) aim to increase the accuracy, transparency, and reproducibility and comprehensiveness of publications by providing a checklist to allow for a concise and logical approach to every manuscript. Osteoarthritis is also acknowledged by this group to be a multifactorial disease with many possible contributing factors, making it difficult to establish a 'gold standard' animal model (du Sert 2012). Global standards have therefore been recommended to limit variability and

irreproducibility across both laboratories and studies. The three 'Rs' (3Rs), reduction, refinement, and replacement, are considered to be the most important anchors within these ethical standards. Without underpowering a study, hence negating initial animal use, procedures and methods should be designed to reduce the number of animals used in a study. Procedures should also be refined to minimise suffering whilst maintaining the experimental output. If an alternative approach that does not require animals could be used, then this should be the first. Hence, careful planning of animal experiments such as power calculations to establish statistical significance, are required to comply with the 3Rs. A delicate balance must therefore be sought to ensure enough animals are being used to establish statistical significance, but not so many as to result in wasteful use of animals. Effect size (usually ≥ 0.5), power (usually $\geq 80\%$) and calculations of minimum sample size are required prior to any study. Avoiding bias within any study is also of great importance, and given that within this study outcomes could not be predicted, how to power the study was difficult. Every effort was taken to limit the number of animals used, and so animals used for the validation of this model, also provided knee joints to be used in the study. This ensured no data was wasted, despite the larger number of animals required to determine deletion of my protein within the cartilage. Throughout this thesis, I adhered to

the ARRIVE guidelines in all of my animal studies.

Power calculations

Power calculations are important in any study as they help to guide the researcher as to the minimum number of animals that will be required in a study, to see a true difference between groups, based on a pilot study. The pilot study is therefore required to determine the experimental sample size. Pilot data will yield two means which can be used to calculate the standardised effect size (signal/noise ratio) = (mean1-mean2)/SD. The signal to noise ratio generated can then be used to find 80-90% power assuming a 5% significance level and a two-sided test. More information about this table and calculations can be found here `http://www.3rs-reduction.co.uk/html/6_power_and_sample_size.html`.

2.1.3 Generation of mouse lines

A very common system for gene manipulation in animal models, including mice, is the Nobel prize winning Cre-Lox system, developed by Capecchi, Evans and Smithies (Capecchi, 2005). Briefly, LoxP sites are inserted either side of an exon of the gene of interest, thus creating a 'floxed' mouse (Fig. 2.1.3.1). Floxed mice can be mated (crossed) with Cre expressing transgenic mice. The LoxP sites are recognised by a Cre recombinase enzyme that cleaves the DNA. This enables Cre mediated removal of the floxed gene.

The Cre enzyme can also be controlled temporally or in a specific tissue manner. Expression of Cre can be engineered to be produced by select cell types expressing particular cartilage proteins such as type II collagen or aggrecan. To temporally control expression, an inducible feature can be added by inserting a modified estrogen receptor (ER) into the Cre promoter so that nuclear translocation can only occur upon administration of the drug tamoxifen which acting as an ER modulator or antagonist.

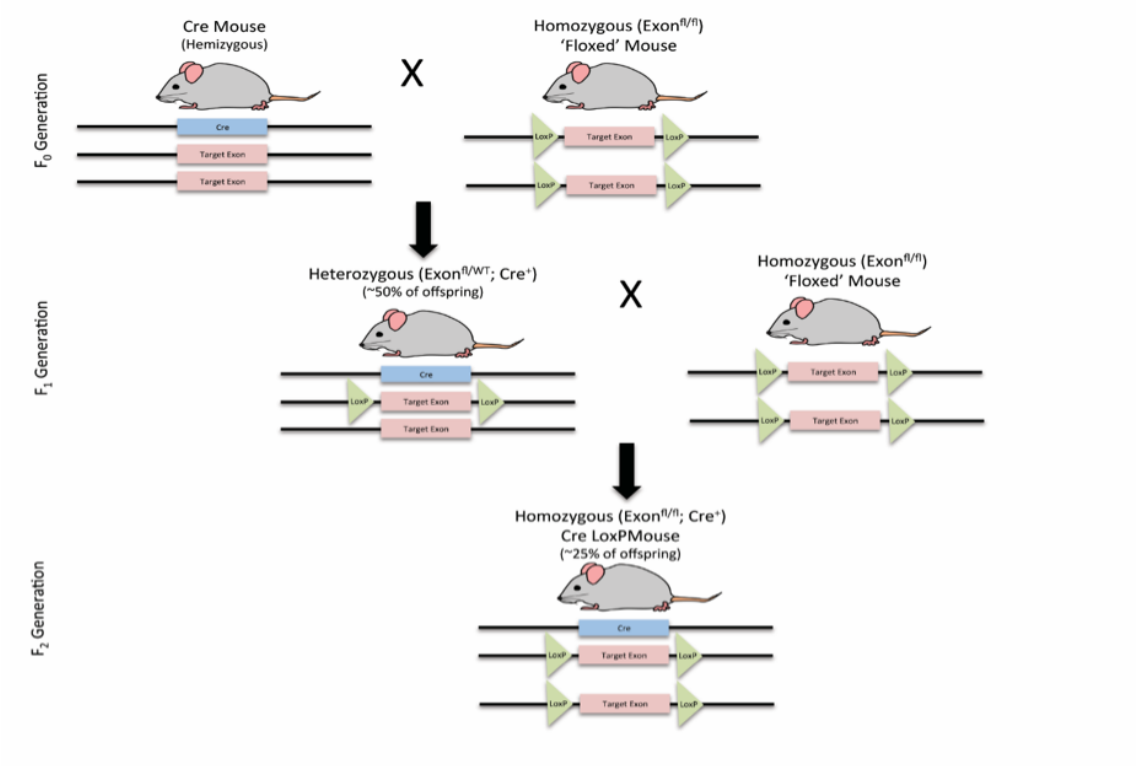


Figure 2.1.3.1: Generation of a conditional knockout mouse model using the Cre-LoxP system.
F0 generation: mating of hemizygous Cre with homozygous Exonfl/fl floxed allele mice generates progeny that are 50% heterozygous for the floxed allele (Exonfl/WT) and 50% hemizygous for the Cre transgene. F1 generation: Exonfl/WT Cre positive mice are crossed with homozygous Exonfl/fl mice to generate mixed litters of which approximately 25% will be homozygous for the floxed allele and also hemizygous for the Cre transgene. Reproduced from (Rheumatology (7 ed.) Ed. by M Hochberg, E Gravallese, A J Silman, J Smolen, M Weinblatt, and M Weisman. Animal Models of Osteoarthritis. Elsevier).

In this thesis, all mice were on a C57BL/6 background. *IFT88$^{fl/fl}$* mice were obtained from Jackson labs. Offspring were bred for 6 generations to establish colony (Jackson Laboratories: Stock No. 000664). *IFT88$^{fl/fl}$* mice were maintained as the control line, and in parallel offspring were crossed with the *AggrecanCreER^{T2}* mouse line, originally generated at the Kennedy Institute of Rheumatology (Lo Cascio et al., 2014). This mouse enables tamoxifen inducible Cre deletion, restricted to aggrecan expressing cells. Resultant cross generated *AggrecanCreER^{T2};IFT88$^{fl/fl}$* mice, henceforth in this thesis referred to as the cartilage knock out (cKO) mouse. Additionally, *IFT88$^{fl/fl}$* mice were crossed with ROSACreER^{T2} *(B6.Cg-Gt(ROSA)26Sor$^{tm1(cre\text{-}ER^{T2})Nat}$*/J), Jackson Laboratories: Stock No. 004847) mice to generate *ROSACreER^{T2};IFT88$^{fl/fl}$* mice, henceforth in this thesis referred to as the whole body knock out (WBKO) mouse.

2.1.4 Tomato Reporter mouse strain (B6.Cg-Gt(ROSA)26Sor$^{tm14(CAG\text{-}TdTomato)Hze}$/J)

The *B6.Cg-Gt(ROSA)26Sor$^{tm14(CAG\text{-}TdTomato)Hze}$*/J (Jackson Laboratories: Stock No. 007914) (TdTomato) was generated by, and originally procured from, the Jackson laboratory. They were a kind gift from Tal Arnon, based at the Kennedy Institute of Rheumatology. The *AggrecanCreER^{T2}* mouse was crossed with the TdTomato reporter

line to create the *AggrecanCreER^{T2}*;TdTomato mouse to understand activation of Cre in aggrecan expressing cells. Activation of the Cre enzyme results in the deletion of a STOP codon, releasing the inhibition on expression of TdTomato, resulting in the subsequent activation of red signal being emitted from cells.

2.1.5 DNA extraction and genotyping

Ear biopsies were obtained from mice and stored at -20°C for further analysis. DNA was extracted from ear samples and genotyped using the REDExtract-N-Amp Tissue PCR kit (Sigma Aldrich) according to manufacturer's instructions. Briefly, biopsies were thawed and 25 μl of tissue preparation solution was added to the sample. Subsequently 100μl extraction solution was added and samples were incubated for 10 minutes at room temperature. Samples were then heated using a heat block at 95°C for 3 minutes. Samples are briefly spun prior to addition of 100μl of neutralisation solution. Samples were vortexed well and spun. Supernatant can be removed to obtain DNA containing sample and stored at 4°C indefinitely. A Cre positive and heterozygous *IFT88$^{fl/fl}$* sample was used as a control. To genotype, 10μl of REDExtract-N-Amp PCR mix, 2μl of forward primer (10μM), 2μl of reverse primer (10μM), 2μl of diH2O and 4μl of DNA sample are mixed together in a PCR

tube and briefly spun. DNA was amplified using Bio-Rad C1000 touch thermocycler (Bio-Rad Laboratories, UK). For amplification of Cre, the following method was used:

o Step one: Temp: 94°C; Time: 3 minutes

o Step two: Temp: 94°C; Time: 30 Seconds

o Step three: Temp: 56°C; Time: 1 minute

o Step four: Temp: 72°C; Time: 1 minute

o Step five: (Press go to) Repeat Steps 2 - 4 x 34

o Step six: Temp: 74°C; Time: 2 minutes

o Step seven: Temp: 4°C; Time: infinity

For amplification of IFT88, the following method was used:

o Step one: Temp: 94°C; Time: 3 minutes

o Step two: Temp: 94°C; Time: 1 minute

o Step three: Temp: 53°C; Time: 1 minute

o Step four: Temp: 72°C; Time: 1 minute

o Step five: (Press go to) Repeat Steps 2 – 4 x 39

o Step six: Temp: 74°C; Time: 5 minutes

o Step seven: Temp: 12°C; Time: infinity

2.1.6 Primers for mouse genotyping

Table 2.1: Primers for mouse genotyping

Primer target	Primer sequence	Primer source
Cre recombinase	Forward: GCATTACCGGTCGATGCAACGAGTGATGAG Reverse: GAGTGAACGAACCTGGTCGAAATCAGTGCG	Jackson Laboratory, JAX®
Floxed IFT88	Forward: GACCACCTTTTTAGCCTCCTG Reverse: AGGGAAGGGACTTAGGAATGA	Jackson Laboratory, JAX®

To visualise results, gel electrophoresis of samples was used. Briefly, samples were loaded onto a 1.5% agarose gel containing 1:10000 SYBRsafe (Invitrogen). 15 μl of sample is loaded in to each well. 1μl 100BP ladder is added to lane 1. Cre samples are run for 50 minutes at 110V, 400 amps. IFT88 samples are run for 110minutes at 110V, 400amps. Cre positive samples will produce a band size of 34bp and a WT IFT88 band size is approximately 340bp. Homozygous flox positive IFT88 samples will have a larger band of 380bp. Heterozygous floxed mice will produce two bands, one of 380bp and one of 340bp.

2.1.7 Tamoxifen treatment

Tamoxifen was dissolved in 90% sunflower oil and 10% ethanol at a concentration of 20mg/ml by sonication on the day of first injection (fresh). Tamoxifen in solution was stored at 4°C between injections. Mice were injected on three consecutive days with a single dose, via intraperitoneal (IP) injection, according to weight. If below 20g mice received 1mg per tamoxifen per dose; between 20-25g 2mg per dose; and above 25g 3mg per dose. Mice were closely monitored and weighed throughout the tamoxifen administration period. Mice were collected by Schedule 1, 14 days after first injection.

2.2 Surgical procedures

2.2.1 Anaesthesia

At 10 weeks of age, mice were anaesthetised by inhalation of isofluorane (Vetpharma, Leeds, UK) at 4% for induction and 2% for maintenance with continuous 1.5-2 L/min oxygen flow. Once anaesthesia levels were achieved and before surgery, animals were injected subcutaneously with 0.3 mg/mL buprenorphine (Vetergesic Alstoe Animal Health, UK). Post-surgery, animals were placed in an incubator of ambient temperature at 30°C and recovered within five-ten minutes. Once fully recovered, animals were transferred to their cages with the environment-enhancing balcony removed.

2.2.2 Destabilisation of the medial meniscus (DMM)

Destabilisation of the medial meniscus (DMM) was performed by Jadwiga Zarebska as previously described (Glasson et al., 2005b) (Fig. 2.2.2.1). The right hindlimb was always operated on (ipsilateral). On achievement of anaesthesia the right hindlimb was shaved. The animal was then transferred to a dissection microscope for surgery. All subsequent procedures were conducted under sterile conditions. Iodine was applied to the surgical site before an incision of 5-8mm was made using a size 15 sterile blade (Swann-

Morten, Sheffield, UK) on the midline starting at the superior end of the patella. Using a 3mm size 15 ophthalmic scalpel (MSP, Puerto Rico), a medial para-patellar incision was made to cut through the fascia protecting the joint capsule. Mild bleeding may occur at this point which can be stemmed by applying pressure on the wound using sterile cotton swabs. The meniscotibial ligament, connecting the meniscus to the tibial plateau, was visually identified and cut using the same scalpel. Successful transection of the meniscotibial ligament was confirmed visually, before closing the joint capsule using absorbable 6/0 Vicryl sutures (Ethicon, Belgium). The wound was subsequently closed using two to three stitches of 5/0 Ethilon sutures (Ethicon, Belgium). Sham surgeries follow the same procedure up until visualisation of the meniscotibial ligament, where upon the wound was closed using above suturing method.

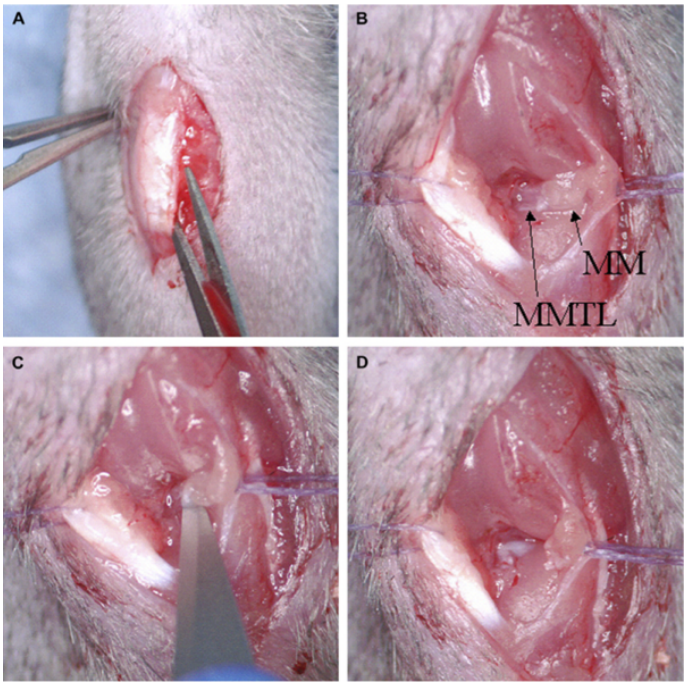


Figure 2.2.2.1: The destabilisation of the medial meniscus surgery.
(A) Opening of the joint capsule. (B) Identification of medial meniscus (MM) and meniscotibial ligament (MMTL). (C) Transection of the meniscotibial ligament. (D) Visual confirmation of transection. Reproduced from (Glasson et al., 2007).

2.2.3 Double neurectomy model (DN)

The double neurectomy surgery was performed by Jadwiga Zarebska. One or two days prior to surgery, mice are transferred to cages containing soft bedding. Briefly, animals were prepared for surgery in terms of anaesthesia and analgesia as described above, with the adjustment of shaving, where the right hind limb was shaved from the knee up to the hip and in the groin. Fur on the back just above the right limb is also shaved to expose the area from the spine to the flank on the right-hand side.

Using a 3mm size 15 ophthalmic scalpel (MSP, Puerto Rico), a longitudinal incision is made from the right knee joint up towards

the hip and inwards towards the groin. Fine-toothed forceps were used to separate the overlying skin to reveal the muscle, femoral artery and the femoral nerve running in very close proximity. Using curved forceps, the femoral nerve is separated from its soft tissue attachments underneath. The femoral nerve is carefully transected using micro-dissecting scissors and a 0.5cm section is removed. The wound was closed using the above suturing method with additional sutures added as required. The mouse is turned on to its front and the right hindlimb is stretched out. Using a 3mm size 15 ophthalmic scalpel (MSP, Puerto Rico), an incision of approximately 2cm is made from the spine outwards. Using curved forceps, the overlying skin is separated to reveal the muscle and the sciatic nerve. The curved forceps are inserted under the sciatic nerve to separate it from the surrounding tissue. A 1 cm region of the sciatic nerve is removed. Following this, the wound was sutured using the above described method with additional sutures added as required.

Mice were transferred to a recovery chamber as described above and recovered within 10 minutes of anaesthetic withdrawal. Successful operations will result in the loss of function of the right hind limb, leading it to be dragged by animals. Mice were subsequently housed in soft bedding without environment-enhancing balconies or tubes to prevent aggravation of exposed skin. Animals were

disturbed as little as possible. Sudocrem was applied to the skin of the foot if aggravated.

2.3 Tissue collection

2.3.1 Sacrifice- Schedule 1

At the point of sacrifice, mice were culled using a Schedule 1 method. In this case, increasing doses of carbon dioxide to induce asphyxiation was used, followed by cervical dislocation to confirm death.

2.3.2 Collection of whole knee joints

Following sacrifice, the skin surrounding the hindlimbs was removed to expose the knee joint. Surrounding muscle, ligaments and tendons were removed. Knee joints were removed by incising the femur above and tibia below the joint in the middle of the long bones. Joints were transferred to 10% formalin ready for histological processing.

2.3.3 Hip avulsion

Two weeks post-administration of tamoxifen, mice were sacrificed. Hindlimbs were exposed by removing the skin and surrounding tissue was removed from the bone. Subsequently, the femur was pulled away from the midline and pushed ventrally to dislocate it,

revealing the head of the femur with cartilage attached. The femur head was avulsed (removing cartilage) using forceps by gently applying pressure to the base of the hip cartilage and twisting. Hip cartilage was transferred to RNAlater (Invitrogen) and transferred to dry ice and stored at -80°C until further analysis.

2.3.4 Kidney and liver harvest

Two weeks post-administration of tamoxifen, mice were sacrificed using Schedule 1. After applying ethanol to the torso and stomach the skin was cut and removed without disturbing the fascia retaining the organs. The fascia is cut to expose the internal organ cavity and the kidney located behind the lower intestinal organs and isolated. The liver was also extracted by gently removing the organs under the diaphragm to expose the tissue. Samples were subsequently transferred to RNAlater and stored at -80°C until further analysis.

2.3.5 Isolation of costal cartilage

Mice were sacrificed by Schedule 1 between 4-6 weeks of age. The following was conducted in a fume hood. Mice were laid on their backs and the skin removed. 70% ethanol was used to sterilise and wet the area. Thoracic muscles were then removed and an incision made into the fascia from the naval to the sternum and then along the rib cage using fine forceps and scissors. The fascia

connecting the rib cage to the diaphragm and internal organs were gently removed. As much soft tissue as possible was also removed from the ribs prior to extraction. Both rib cages per mouse were isolated and placed in serum free DMEM. Soft tissues were removed using a scalpel and then discarded from the bone. All samples were kept on ice and then transferred to a cell/tissue culture hood where all subsequent procedures were conducted under sterile conditions. Tissues in between the ribs were removed carefully and translucent parts of the rib cage were kept. Samples were then washed with 1 x PBS whilst removing this intercostal material. Samples were rinsed twice with PBS. Samples were incubated whilst agitated at 37°C for 45minutes with 2.5ml of 3 $mgml^{-1}$ digestion medium. Digestion medium: 15ml of 20μm filtered digestion solution comprised of 75mg of collagenase type II (Worthington Biochemical Product Corporation: Cat. LS004177) dissolved in 25ml of serum free DMEM, giving a final concentration of 3 $mgml^{-1}$.

After 45 minutes, an additional 12.5ml of serum free medium was added to the solution to reach a final concentration of 0.5mg ml^{-1}. Samples were left overnight with 0.5 $mgml^{-1}$ digestion medium at 37°C whilst being agitated.

Aggregates were dispersed within the solution and passed through a 48μm filter into a falcon tube washing with 10 ml serum containing medium. Samples were centrifuged at

400g for 10 minutes at 37°C. The pellet was washed once with serum containing DMEM and re-centrifuged. Cells were resuspended in 10-20 ml of culture medium and counted using a haemocytometer. Chondrocytes were seeded according to experimental requirements, taking up to 5 days to adhere to cell culture surfaces.

2.4 Gene expression analysis

2.4.1 Extraction of RNA from liver and kidney

Liver and kidney samples were stored at -80°C in RNAlater. Approximately a third of liver or half of kidney samples were transferred to individual Eppendorf tubes containing 1ml Trizol (Invitrogen) before being vortexed for 5-10 minutes at 4°C. The supernatant was transferred to a fresh tube and 100μL 1-bromo-3-chloropropane (Sigma Aldrich, Germany) was added. The sample was then vortexed until appeared a milky pink and then incubated 5 minutes at room temperature. Subsequently, the mixture was centrifuged at 13,000rpm for 20 minutes at 4°C, to achieve separation of the organic and the aqueous phases. Without disturbing the organic phase below, the upper aqueous phase was transferred to a new tube and equal volume of 70% ethanol was added per tube. The samples were then passed through QIAGEN spin columns and washed with RNA extraction buffers according to

the manufacturer's instructions (RNeasy mini kit, Qiagen, Hilden, Germany). At the end, the RNA was eluted in 40μL of nuclease-free water and stored at -80 until further use.

2.4.2 Extraction of RNA from hip cartilage

The following procedure uses reagents from the RNeasy micro kit (Qiagen, Germany). For each sample (n), six hips were pooled in to one Eppendorf tube at the point of harvest. RNAlater was removed from cartilage once defrosted on ice. 150ul of RLT buffer was added to each sample and using a disposable size 22 scalpel, hip cartilage samples were pulverised. Samples were centrifuged at 13,000 rpm for 30 seconds at 4°C. 295μL of RNase-free water and subsequently 5μL of proteinase K (Qiagen, Germany) was added to the sample. Samples were mixed thoroughly by pipetting. Samples were incubated at 55°C for 10 minutes and centrifuged for 3 minutes at 11,500 rpm at room temperature. Supernatant was added to a new Eppendorf without disturbing pellet, and 100% ethanol was added. The sample was then transferred to a QIAmp spin column and processed according to the manufacturer's instructions (RNeasy micro kit, Qiagen, Germany) using Qiagen RNA extraction buffers. At the end, RNA was eluted in 14μL of nuclease-free water and stored at -80°C until further analysis.

2.4.3 RNA quality

A Nanodrop spectrophotometer ND-1000 (Thermo Fisher Scientific, UK) was used to assess the quality and quantity of the RNA extraction. An A260/280 ratio between 1.8-2.1 is required for RNA to be suitable for qPCR analysis. If sample values were outside these values, they were discarded from further analysis.

2.4.4 Reverse transcription

A high capacity RNA to cDNA kit (Applied Biosystems, CA, USA) was used to create complementary DNA (cDNA) from RNA. One hundred nanograms of RNA was used to synthesize cDNA per reaction mixture and volume was subtracted from nuclease free water required for reaction. Each reaction mixture contained 2μL 10X RT Buffer, 0.8μL dNTPs, 2μL 10X random primers, 1μL reverse transcription enzyme, 1μL RNAse inhibitor and 13.2μL nuclease-free water- sample volume to obtain a final reaction of 20μL. Tubes were briefly centrifuged before being put in a Bio-Rad C1000 touch thermocycler (Bio-Rad Laboratories, UK) for the reverse transcription process. The cycles followed the protocol of ten minutes at 25°C, two-hours at 37°C, five minutes at 85°C, and indefinite storage at 4°C. Samples were subsequently stored at -20°C.

2.4.5 Real-time polymerase chain reaction

Real-time RT-PCR was performed using TaqMan (FAM dye) Universal Master Mix II (Thermo Fisher Scientific). Each reaction consisted of 0.5μL cDNA template, 5μL Master Mix, 0.5μL primer, (0.5μL RNAse inhibitor in hip cartilage samples) and 4μL nuclease-free water. Samples were loaded in a 384-well plate and thermocycling was performed on a ViiA7 Real-Time RT-PCR System (Thermo Fisher Scientific) using the following protocol: hold 2 min at 50°C; hold 10 min at 95°C; 40 cycles: 15 s at 95°C, 1 min at 60°C; hold at 4°C. Data were captured and primary analysis was performed using Expression Suite Software (v.1.1; Applied Biosystems, Foster City, CA, USA) using the $\delta\delta$Ct method using 18S as a normalizing gene. TaqMan assays and primers (Table 2.2) were purchased from Thermo Fisher Scientific.

Table 2.2: Taqman primers for mouse tissues.

Abbreviations	Genes	Taqman primer probe set
18S	Eukaryotic rRNA 18S	Mm02601776_g1
IFT88	Ift88	Mm00493664_m1

2.4.6 Relative gene expression calculation

A threshold cycle (Ct) was determined by the software. The Ct value of the housekeeping gene, 18S, was subtracted from the Ct value from the gene of interest, to generate a δCt value. A $\delta\delta$Ct

value was calculated by subtracting the δCt of the control group from the δCt of the sample. In a final step, the formula ($2^{-}Ct$) was applied to the $\delta\delta$Ct value to calculate the fold change of the gene of interest from the control.

2.5 Micro-computed tomography (MicroCT) imaging and radiography

2.5.1 MicroCT analysis

Mice were sacrificed by a Schedule 1 method and knee joints were harvested as described above. Knee joints post-formalin fixation were transferred to 70% ethanol ready for MicroCT scanning using SkyScan1172 X-ray microtomograph (Brucker, Antwerp, Belgium). All scans were taken at the maximum resolution, at 10μm/pixel. Files were saved as DICOM files for analysis by ImageJ and CTan.

2.5.2 Growth plate measurements

Image sequences were opened in ImageJ. Using the femoral growth plates as an anatomical reference, knee joints were orientated and resliced to produce coronal sections throughout the whole joint. These newly orientated image sequences were saved. An anatomical reference was found, defined as when the lateral meniscus just disappeared from view at the distal end of the joint. Once this section had been found, the sequence was scaled (Fig.

2.5.2.1 A) to allow for measurements to be taken. Using the measurement tool in ImageJ, 8 measurements across the growth plate were taken and averaged to give average growth plate length (Fig. 2.5.2.1 B). In some animals, an elongated growth plate was observed bilaterally. Again, eight measurements were taken across the growth plate to include these regions and averaged across the total length of the growth plate (Fig. 2.5.2.1 C).

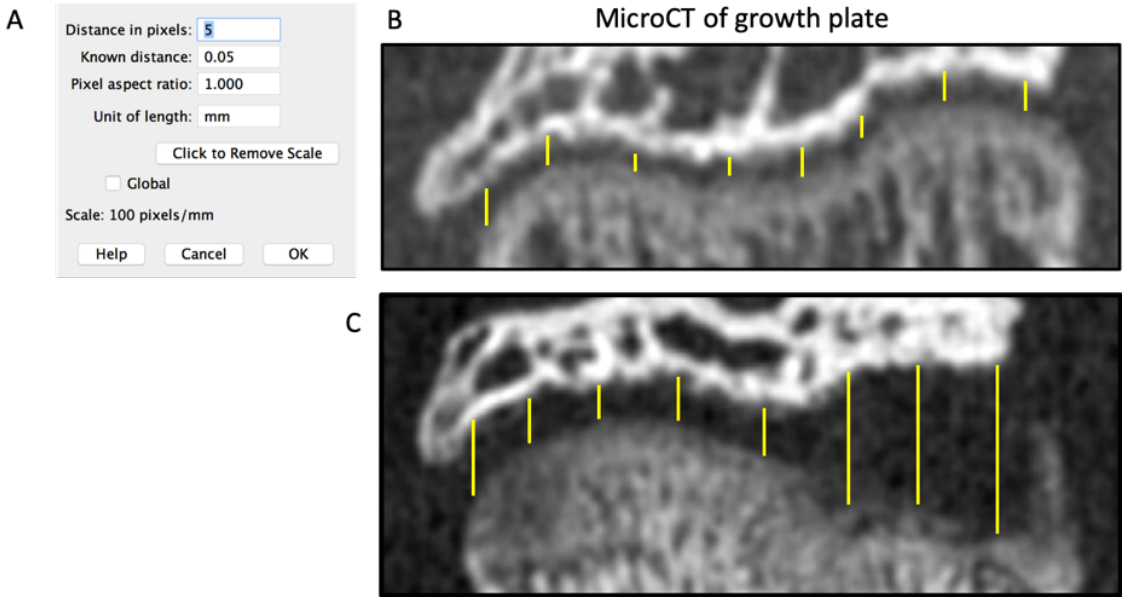


Figure 2.5.2.1: MicroCT growthplate measurements.
A) Calibration of image sequence in ImageJ. B) Measurements taken at 8 points across the growth plate and averaged. C) Example of eight measurements taken across the growth plate in the case of an extreme phenotype. These were averaged to find the mean growth plate length for these samples.

2.5.3 Thresholded MicroCT

Post-measurements of growth plate, the threshold function was used within ImageJ. Parameters for thresholding used were 128 and 255 as shown in A. This thresholding function removed regions of the growth plate that were not definitely bone, but perhaps

calcified cartilage, resulting in loss of grey areas (Fig. 2.5.3.1 B). Eight measurements were taken across the joint and averaged to find growth plate length for the knee joint. Phenotypes varied and large bilateral holes were also measured in thresholded sections (Fig. 2.5.3.1 C).

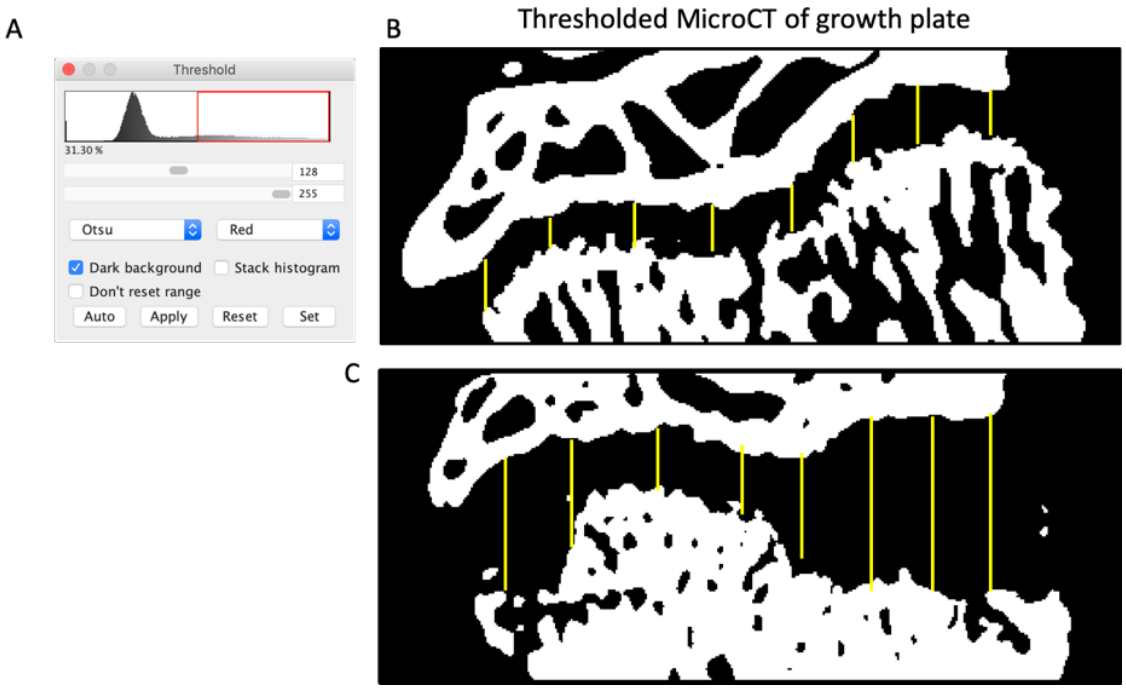


Figure 2.5.3.1: Thresholded MicroCT growthplate measurements.
Images were calibrated as shown in Fig. 2.5.2.1 A) Threshold range used in ImageJ B) Measurements taken at 8 points across the growth plate and averaged to find thresholded growth plate length. C) Example of eight measurements taken across the growth plate in the case of an extreme phenotype. These were averaged to find thresholded growth plate length for these samples.

2.5.4 Epiphysis and epiphyseal plate analysis

Joints were collected and fixed as described. They were subsequently transferred to 70% ethanol and scanned prior to histological assessment. Knee joints were imaged using a MicroCT scanner (SkyScan1172 X-ray microtomograph, Antwerp, Belgium)

within 70% ethanol (10μm/pixel, 3 minutes of acquisition time) (Blease et al., 2018).

Using the CTan (Brucker Belgium) programme, saved image sequences were opened in the software to conduct 3D parameter analysis. Using this software, the regions of interest could be selected and separated from the rest of the joint. The epiphysis was isolated away from the rest of the joint (Fig. 2.5.4.1 A) by drawing around each slice (Fig. 2.5.4.1 B) to isolate the plate as shown in 3D. The software processes this region of interest to calculate the bone volume (BV), total volume (TV), ratio of BV to TV (BV/TV), trabecular number (Tb.N), and trabecular spacing (Tb.Sp, mm). The epiphyseal plate, defined as the bone beneath the growth plate, was found from the bottom of the growth plate and to approximately 8mm down the bone. The software processed this region of interest to calculate the bone volume (BV), total volume (TV), ratio of BV to TV (BV/TV), trabecular number (Tb.N), and trabecular spacing (Tb.Sp, mm).

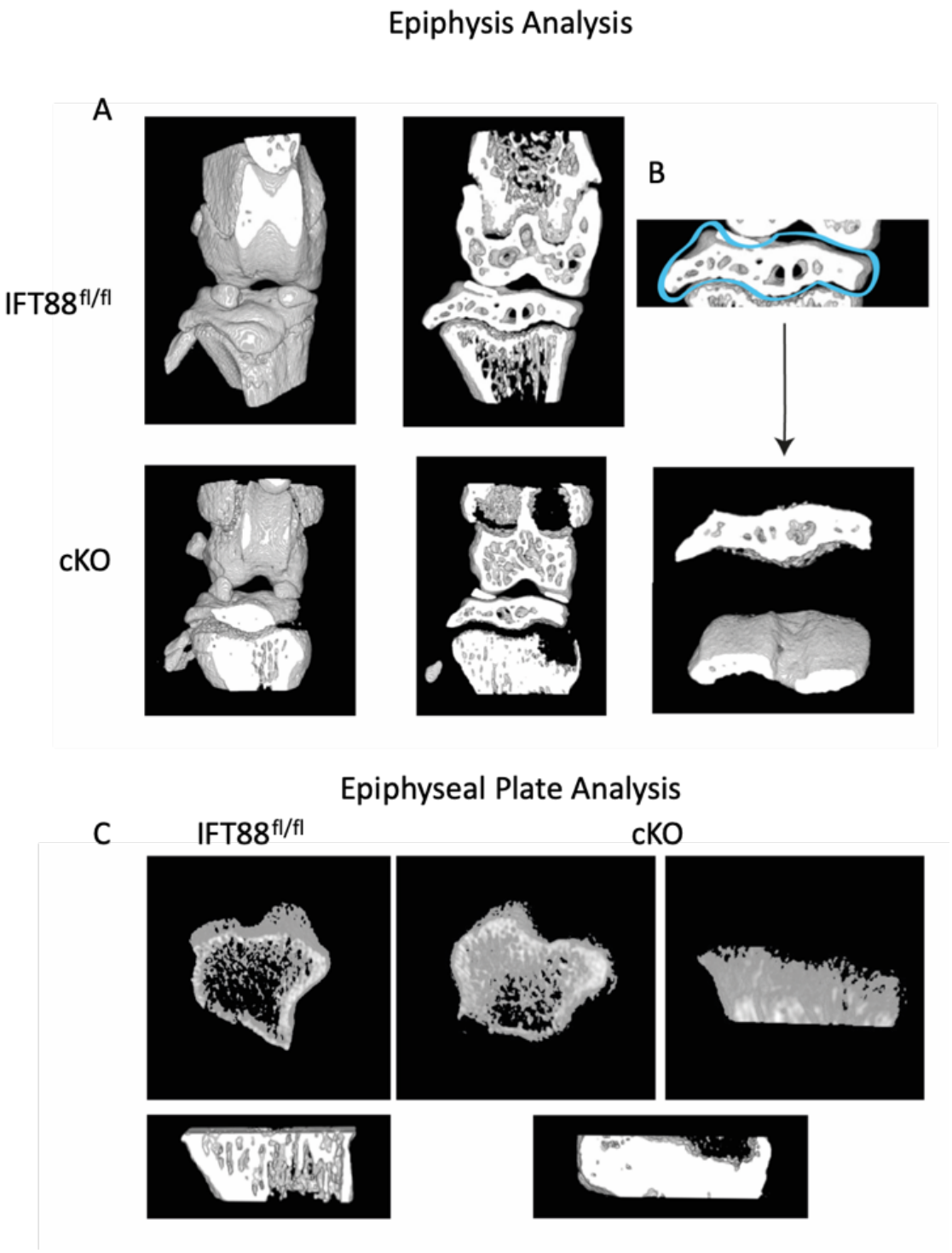


Figure 2.5.4.1: Analysis of epiphysis and epiphyseal plate.
Images were calibrated as shown in Fig. 2.5.2. A) Threshold range used in ImageJ B) Measurements taken at 8 points across the growth plate and averaged to find thresholded growth plate length. C) Example of eight measurements taken across the growth plate in the case of an extreme phenotype. These were averaged to find thresholded growth plate length for these samples.

2.6 Histological and histomorphometric analyses

2.6.1 Cryosectioning

Knees are collected as described in 2% paraformaldehyde (low % of PFA concentration used to prevent quenching of TdTomato signal) and stored at 4°C overnight. Samples are then washed with PBS before being transferred to a solution of 30% sucrose for 4-hours at 4°C. Samples were loaded into OCT directly within the cryostat machine, set at -16°C (machine details) with the patella facing upwards. OCT medium took a few minutes to freeze. Samples were trimmed by removing and discarding sections until the middle of the joint could be seen. Using Kawamoto's film method (http://www.section-lab.jp/index.html), film tape was cut to size, and sections were collected using forceps and transferred onto glass slides with the sample facing up. Samples were counterstained with 1:5000 DAPI for one minute before two times wash with PBS and mounted using Prolong Gold (Thermo Fisher Scientific).

2.6.2 Embedding knees in paraffin

Histology was performed by the histological team of the Kennedy Institute of Rheumatology (Bryony Stott, Ida Parisi, Marcia Curtinha, Claudia dos Santos Duarte). Mouse knees were collected by incising the muscle and bone at the proximal femur and distal

tibia, either side of the joint. Without disturbing the joint, the muscles were carefully removed. Samples were subsequently fixed in 10% neutral buffered formalin (CellPath, Newtown, UK) for 24-48 hours. 0.5M EDTA was used to decalcify joints for 7 days. Joints were processed using a Tissue-Tek VIP (Sakura, Torrance, Ca, USA and processed as follows; 1 formalin change, 70% alcohol, 5 changes of 100% alcohol, 3 changes of xylene, and finally 4 changes of molten paraffin wax. After processing, knees were embedded in paraffin wax, placing the patella at the bottom of the mould. 4μm coronal sections were cut using an Accu-Cut SRM 200 microtome (Sakura, Torrance, USA), at 80μm intervals, before staining with Safranin-O producing 10 or 15 slices through the middle or throughout the joint respectively.

2.6.3 Safranin-O and fast green staining

Tissue staining was also performed by the histological team of the Kennedy Institute of Rheumatology (Bryony Stott, Ida Parisi, Marcia Curtinha, Claudia dos Santos Duarte). The Tissue-Tek DRS 2000 autostainer and the Glas g2 coverslipper (Sakura, Torrance, USA), were used to stain slides with Safranin-O. Sections were warmed to 60°C overnight before staining, then dewaxed using 3 changes of xylene and 3 changes of 100% alcohol before washing in tap water. Slides were immersed in Heamotoxylin for 5 minutes

to stain nuclei, before washing in 1% acid alcohol (acetic acid) and tap water. Ammoniated water (1% NH3 in tap water) was used to 'blue' the sections for 2 minutes, before washing again in tap water. Sections were then stained with Safranin-O (1% Safranin dye in 1% acetic acid) for 10 minutes and washed with tap water. Slides were counterstained in 1% Fast green for 5 minutes. Finally, the sections were dehydrated using 3 changes of alcohol, each change lasting 1 minute, and then cleared in 2 changes of xylene before cover slipping using a DPX mountant (Sigma-Aldrich).

2.6.4 Articular cartilage thickness measurements

Safranin-O stained images were photographed using an Olympus Osteometric microscope using a 10x lens. Quantification of cartilage width was conducted with Image J (NIH, Bethesda, MD, USA). Images were opened in ImageJ. The middle of the joint was localised using the medial meniscus as an anatomical reference. When the middle of the joint is reached the medial meniscus will appear as a small triangle (Fig. 2.6.4.1 A). Histological sections were scaled using the scale bar automatically added by the microscopes software on taking of the image (Fig. 2.6.4.1 B).

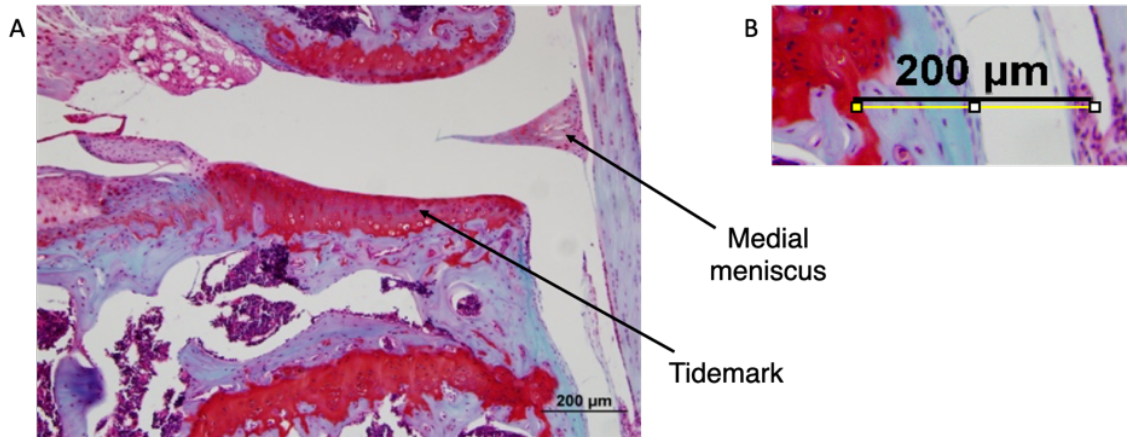


Figure 2.6.4.1: Representation of histological sections for analysis.
A) Coronal histological image of medial compartment showing the medial meniscus and its use as an anatomical reference to find the middle of the joint. The tidemark where uncalcified (above) and calcified (below) cartilage meet is also shown. B) Scale bar was used to calibrate measurements taken.

To assess cartilage thickness in the joint, one section either side of the middle was taken on both the lateral and medial sides, hence three slides for each side. In total this means there will be 6 images to analyse per joint. Using the measurement tool in ImageJ the middle of the cartilage can be located (Fig. 2.6.4.2 A). Measurements were taken perpendicular to the cartilage from the surface to the subchondral bone to find length of the middle. Measurements either side of the middle were taken (Fig. 2.6.4.2 B) to give three measurements for one side of the joint for thickness. This was repeated on all 6 images and averaged to give the total average width of cartilage. Where total length measurements were taken, measurements of the uncalcified region demarcated by the tidemark (Fig. 2.6.4.1 A) using Safranin-O staining were taken and subtracted from total length measurements

to give calcified measurements (Fig. 2.6.4.2 C). Articular cartilage thickness measurements were not conducted under double blind conditions.

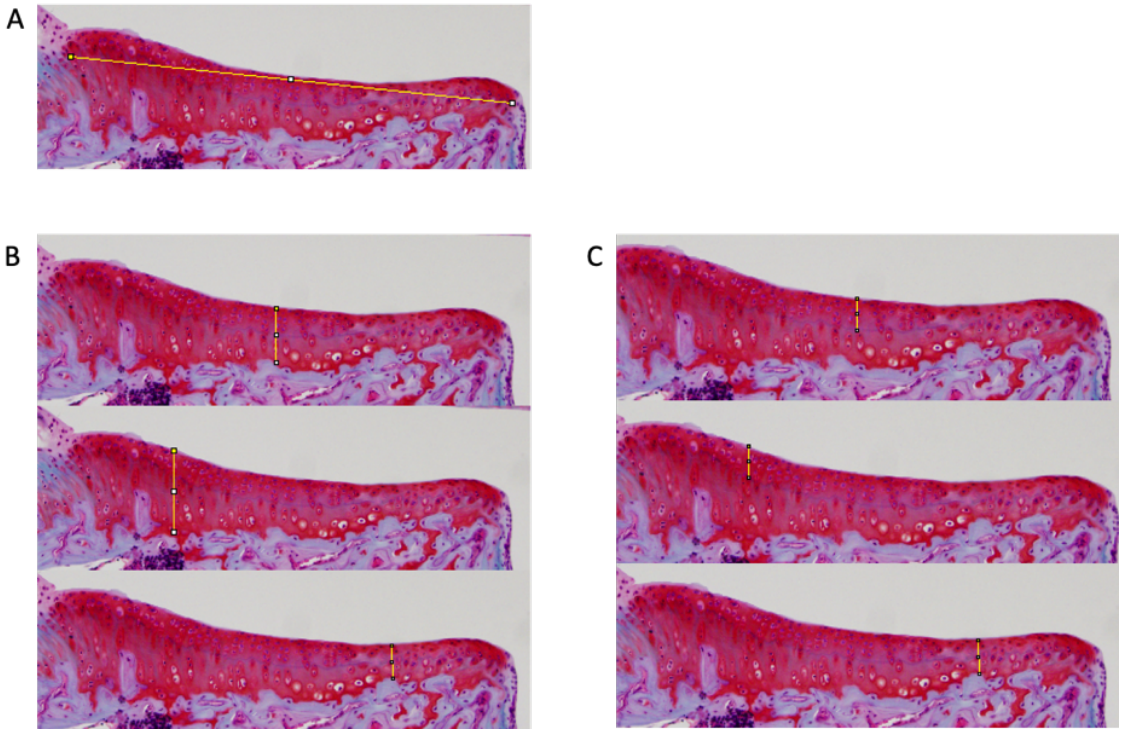


Figure 2.6.4.2: Histological sections illustrating method for articular cartilage measurements.
A) Line tool used in ImageJ identifies the middle of the joint. B) Representations of where measurements were taken within the articular cartilage using the middle generated by the line tool in A, as a guide. C) Representations of where measurements were taken of uncalcified cartilage (above tidemark).

2.6.5 Growth plate cartilage measurements: hypertrophic and proliferative regions

Images of histology were taken using an Olympus Osteometric microscope using a 10x lens. Quantification of cartilage length as conducted with Image J (NIH, Bethesda, MD, USA). Images were opened in ImageJ. The middle of the joint was localised using the medial meniscus as an anatomical reference. Measurements were

taken from two images, from beneath the lateral plateau and the medial plateau. Measurements were taken from the top of the growth plate to the trabecular bone (Fig. 2.6.5.1 A) at three points across each slide, resulting in 6 measurements per slice. This was repeated for the slice prior to and after the middle slice, to give measurements for three sections per joint. Total number of measurements for each joint should total 18.

Measurements were taken of the hypertrophic region (Fig. 2.6.5.1 B) across the joint in the same ways as above. Average length of hypertrophic region was taken from mean total growth plate length to give average length of proliferative region.

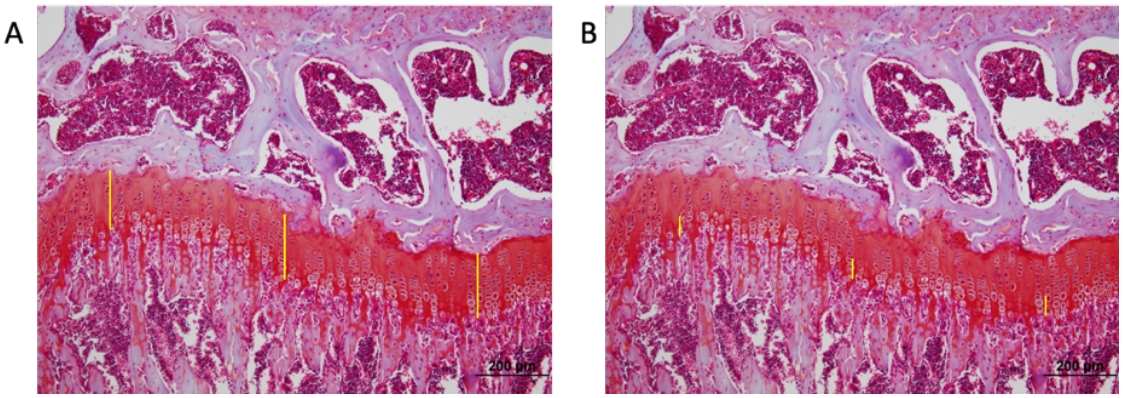


Figure 2.6.5.1: Histological sections illustrating method for growth plate cartilage measurements.
A) Representations of where measurements were taken within the growth plate cartilage. Three measurements taken across each 10x section (2 sections per slice and, 3 slices per joint and hence 6 sections per joint) B) Representations of where measurements were taken of hypertrophic cartilage.

2.6.6 Histological assessment of disease by OARSI scoring

Histological scoring followed the well established OARSI (Osteoarthritis Research Society International) guidelines (Glasson et al., 2010) and was performed by myself and Victoria Batchelor, who was blinded throughout the scoring process. For every joint, at least eight sections were assessed in the medial and lateral compartments including both the tibial and femoral surface. This results in four scores per section. The sum of these scores determined the score for that section. The top three scores were summed to generate the final score for each joint. Scores were averaged between the scorers for each joint to give an average OARSI score. If scores between assessors differed drastically, they warranted discussion, and a third independent blinded assessor was then included if a consensus was not reached. Representative images shown in Fig. 2.6.6.1 and scores shown in Table 2.3.

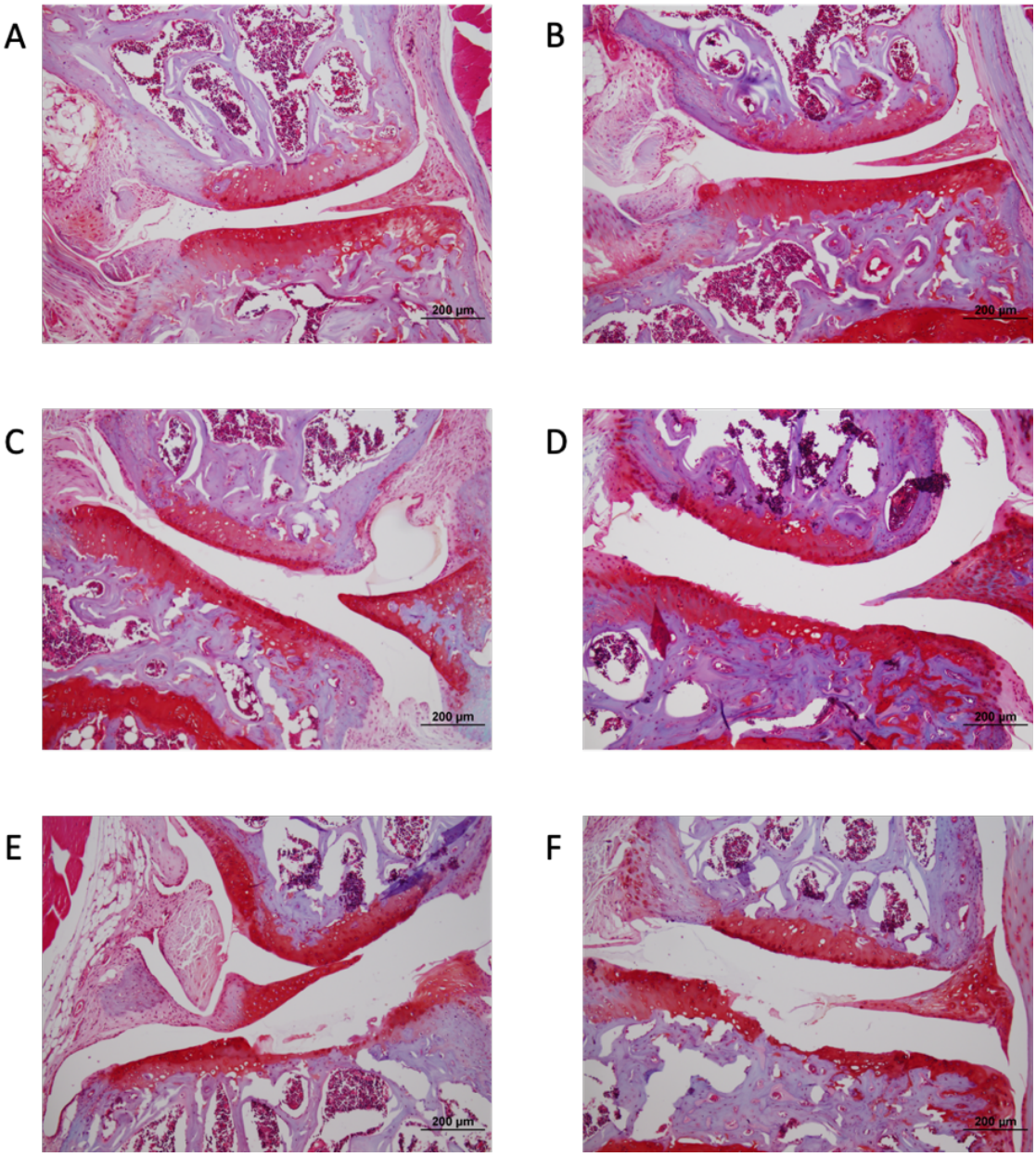


Figure 2.6.6.1: Representative images of 6 osteoarthritis histological scores taken from the medial compartment:
(A) 0, (B) 1, (C) 2, (D) 3 (E) 5, (F) 6 (scores for the tibial epiphysis).

Table 2.3: OARSI guidelines for histological scoring

	OARSI Score
0	Normal
0.5	Loss of Safranin-O staining without structural changes
1	Cartilage fibrillation without loss of cartilage
2	Erosion of cartilage and vertical clefts in the superficial layer with some loss of the surface lamina
3	Erosion of uncalcified cartilage to the calcified cartilage (tidemark)
5	Erosion of uncalcified cartilage to the calcified cartilage tidemark beyond the tidemark
6	Erosion of uncalcified cartilage to the calcified cartilage tidemark beyond the tidemark and down to the bone

2.6.7 Immunohistochemistry

Immunohistochemistry (IHC) was used to identify disrupted proteins of interest within the articular cartilage and growth plate. Knee joints were fixed and sliced as previously described to produce unstained paraffin coronal sections of knee joints. All washes are 2 minutes unless stated otherwise. These experiments were performed by myself or two undergraduate FHS students Emer Chang and Elinor McSorley.

Deparaffinisation: Slides were deparaffinised and rehydrated using 2 x 20min xylene washes, 1x 15min 100% ethanol wash 15min, 2 x 15min 96% ethanol wash, 10min 80% ethanol wash, 60min 70% ethanol wash, 10min 50% ethanol wash followed by 4 x PBS wash. Samples were quenched using 0.3M glycine for 40 min followed by 4 x PBS wash. Antigen retrieval: Antigen retrieval was performed via Proteinase K treatment in a pre-warmed humidified chamber at 37°C for 30 minutes. This was followed by treatment with 0.1U Chondroitinase ABC (MilliporeSigma) in 1 x 50mM Tris-HCl pH7.5, 50mM sodium acetate, 10mM EDTA buffer for 30mins. Slides were then permeabilised with 0.2% Triton-X (Sigma) for 15 min. All incubations were carried out in a humidified chamber. Blocking: Slides were blocked in 5% goat serum and 10% bovine serum albumin (Sigma) (blocking buffer) in PBS for

1 hr at room temperature. Primary Antibody: Samples were washed 4 x 1xPBST (PBS 0.1% Tween). Primary antibodies were made to appropriate concentrations as described. (ColX 1 in 50) made up in blocking buffer. Controls used either no primary or appropriate species IgG isotype control at 1:200. Samples were then incubated overnight at 4°C. Secondary Antibody: Samples were washed 4 x 1xPBST. Alexafluor anti-rabbit conjugate 555 (Invitrogen) or Anti-mouse conjugate 488 (Invitrogen) secondary antibodies were made up at 1:500 in blocking buffer depending on experimental requirements. Samples were washed 4 x 1xPBST. Slides were subsequently counter-stained with the nuclear stain DAPI (Thermo Fisher Scientific) at 1:5000. Samples were washed 1 x 1xPBS and residue removed. Coverslips were mounted onto slides using Prolong Gold (Thermo Fisher Scientific), sealed and imaged. Image analysis was conducted in ImageJ, using mean intensity in control slides to subtract from experimental images to find true staining intensity.

2.7 Western blotting

2.7.1 Cell lysate preparation

Prior to cell lysis, media was removed quickly and cells washed with cold PBS. Cells were lysed using 120μl of lysis buffer containing sodium orthovanadate (Sigma), Roche protease inhibitor

tablets (Sigma) all dissolved in NP-40 buffer. and Cells were incubated on ice for 5 minutes with lysis buffer. Wells were thoroughly scraped and left for another 5 minutes on ice. The sample was collected and put into a microcentrifuge tube that was then spun at 10,000rpm for 15 mins at 4°C to collect the supernatant. The supernatant was transferred to a clean tube, and assessed for protein concentration using the Pierce BCA protein quantification assay (Thermo Fisher Scientific). Subsequently samples were either stored at -20°C or boiled for 5 minutes at 100°C post-addition of Laemmli (Bio-Rad) and 1% β-mercaptoethanol.

2.7.2 SDS-PAGE

Cell lysate samples were resolved by sodiumdodecyl sulfate polyacrylamide gel electrophoresis (SDS-PAGE) on precast 4-12% or 8% polyacrylamide BisTris gels (Thermo Fisher Scientific), depending on requirements of the experiment. All LRP-1α (heavy chain) western blot analysis were run on denatured TCA gels (Thermo Fisher Scientific). The Chameleon® Duo Pre-stained Protein Ladder (LI-COR) for SDS PAGE, which includes 11 protein bands from 8- to 260-kDa, was used in experiments using LI-COR secondaries. In other experiments, NovexTM Sharp Pre-stained Protein Standard ladder (Life Technologies) was used, which includes 12 bands from 3.5- to 260 kDa. Gels were loaded

with 15-50μl of sample depending on experiment and were run for 110V for 5 minutes and then 160V for 60minutes.

2.7.3 Immunoblotting and band quantification

Following electrophoresis, samples were transferred on to a polyvinylidenefluoride (PVDF) membrane using a wet method, using a transfer buffer containing 20mM Tris, 120mM glycine and 10% methanol. Proteins were transferred at 100V for 90minutes at 4°C. Membranes were subsequently cut to size and blocked in 5% milk in TBS (3% milk in the case of FLAG-TS-5 experiments) for 1 hr at room temperature. Membranes were subsequently incubated with primary antibodies (table) in 5% BSA, 5% milk, or 3% milk in the case of FLAG-TS-5 experiments) overnight at 4°C. Membranes were washed 3 x 5minutes in TBS containing 0.1% Tween 20 (TBST). Membranes were subsequently incubated with appropriate species-specific infra-red secondary antibodies (LI-COR) in 5% (3% milk in the case of FLAG-TS-5 experiments). This was followed by 2 x 5 min washes in TBST and a single, final wash in TBS. Membranes were imaged using the Licor Odyssey infra-red scanner. Western blots were quantified in ImageJ. In the case of neoepitope, shed LRP-1 and sheddase (ADAM-17 and MMP-14) expression, horseradish peroxidase secondary antibodies were used at 1:1000 in addition to Enhanced ChemiLuminescence (ECL)

Plus detection (Thermo Fisher Scientific) and visualised using the Syngene G:Box imager (Fredrick, MD, USA).

2.7.4 Protein expression of IFT88 in hip cartilage

Hip cartilage was isolated from 10-week old mice, 2 weeks post-tamoxifen administration from *IFT88*$^{fl/fl}$ and cKO mice. The hip joint was avulsed using the same method used to isolate the hip cartilage for RNA extraction. Hip cartilage of 2 animals (4 hips) was pooled and protein was extracted using RIPA buffer and vortexing. Samples were separated using gel electrophoresis, transferred to a PVDF membrane and the membrane was probed for IFT88. IFT88 relative to actin showed no reduction in protein in comparison to the control. This is potentially owing to low abundance of sample.

2.7.5 Table of primary antibodies used in this thesis

Table 2.4: Table of primary antibodies used in this thesis. IHC: Immunohistochemistry, IF: immunofluorescence, WB: western blotting

Target	Abbreviation	Species	Supplier & category number	Use	Dilution
Aggrecan (6-B-4)	ACAN	Rabbit	Abcam, Cambridge, MA, USA, ab3778	WB	1/1000
ARGXX (BC-3)	ARGS	Rabbit	Abcam, Cambridge, MA, USA, ab3773	WB	1/50
Beta-actin	β-actin	Mouse	Cell Signaling Technology, Danvers, MA, USA, 3700	WB	1/1000
FLAG mouse	FLAG- M2	Mouse	MilliporeSigma, Burlington, MA, USA, F1804	WB	1/400
Acetylated α-tubulin (6-11B-1)	AcαTUB	Mouse	MilliporeSigma, Burlington, MA, USA	WB, IF	1/2000
LRP-1β-light chain	LRP-1β	Rabbit	Abcam, Cambridge, MA, USA, ab92544	WB, IF	1/1250
LRP-1α -heavy chain (8G1)	LRP-1α	Rabbit	Abcam, Cambridge, MA, USA, ab20384	WB	1/500
A disintegrin and metalloproteinase	ADAM-17	Rabbit	Abcam, Cambridge, MA, USA, ab2051	WB	1/1000

Table 2.4: Table of primary antibodies used in this thesis. IHC: Immunohistochemistry, IF: immunofluorescence, WB: western blotting

MMP14 (anti-catalytic domain EP1264Y)	MMP-14	Mouse	Abcam, Cambridge, MA, USA, ab51074	WB	1/2000
Arl13b	Arl13b	Rabbit	ProteinTech, Rosemont, IL, USA, 17711-1-AP	WB, IF	1/1000
Anti-AGEG	AGEG	Rabbit	a kind gift from Hideaki Nagase (University of Oxford)	WB, IHC	1/2000
Anti-type X collagen polyclonal	ColX	Rabbit	Abcam, Cambridge, MA, USA, ab58632	IHC	1/500
Tissue inhibitor of metalloproteinase 3	TIMP-3	Rabbit	Abcam, Cambridge, MA, USA, ab6000	WB	1/1000

2.7.6 Table of secondary antibodies used in this thesis

Table 2.5: Table of secondary antibodies used in this thesis. IHC: Immunohistochemistry, IF: immunofluorescence, WB: western blotting.

Target	**Supplier & category number**	**Use**	**Dilution**
AlexaFluor488-conjugated goat anti-mouse secondary	Invitrogen, A32723	IF or IHC	1/500
AlexaFluor555conjugated goat anti-rabbit secondary	Invitrogen, A32732	IF or IHC	1/500
IRDye® 800CW, Donkey anti-rabbit	Licor, Cambridge, UK, 926-32213	WB	1/7,500
IRDye® 680LT, Goat anti-mouse	Licor, Cambridge, UK, 926-68020	WB	1/7,500

2.8 Cell Culture and Experiments

2.8.1 Mouse chondrocyte cell line

In this thesis, an immortal mouse chondrocyte cell line previously generated from Tg737ORPK (ORPK) mice was used. Briefly, heterozygous Tg737ORPK (ORPK) mutant mouse lines were generated as previously described and crossed with a heterozygous Immortomouse (H-2Kb-tsA58) that harbour a temperature sensitive SV40 large T-antigen transgene under the control of an interferon inducible H-2Kb promoter to produce ORPK/Immortomouse compound heterozygous mice. Chondrocytes were isolated from these mice and were cultured in low glucose Dulbecco's Modified Eagles Medium (DMEM) (Sigma) containing 10% FBS (Sigma), 1% Penicillin/Streptomycin (Sigma) and 10ng/ml INF-$\gamma$and 2.5mM l-glutamine. ORPK mouse chondrocyte cell line and WT cell lines were cultured individually. Immortalised cells were cultured in 5% CO2 at 33°C with 10nM INF-γ, then cultured in non-permissive conditions at 37°C (without INF-γ) for 3 days before experiments are conducted. Methods previously described (Wann et al., 2012).

2.8.2 Human Articular Chondrocytes

Tissue samples and/or data obtained was collected with informed donor consent in full compliance with national and institutional

ethical requirements, the UK Human Tissue Act, and the Declaration of Helsinki (HTA Licence 12217 and REC 07/H0706/81). The research was supported by the National Institute for Health Research (NIHR) Oxford Biomedical Research Centre (BRC). Disclaimer: The views expressed are those of the author(s) and not necessarily those of the NHS, the NIHR or the Department of Health. This work has been supported by the Centre for Osteoarthritis Pathogenesis Versus Arthritis (Grant 20205 and 21621)

Human Articular Chondrocytes (HACs) were isolated from human cartilage patient samples. Patient samples were of varying ages and different stages of disease, but all required either whole joint of partial joint replacement treatment. All patients provided written and informed consent. Joints were washed on arrival in Dulbecco's modified Eagle's medium (DMEM) and trimmed to remove all excess fat or bone hanging off the joint. The joint was washed again in DMEM and transferred to a new container where cartilage was cut off the bone whilst submerged in DMEM (37°C). Cartilage fragments were transferred to another container containing DMEM. 1mg/ml of collagenase A (Roche) was made up fresh in DMEM. Collagenase was filter sterilised using a 0.2μm filter. Collagenase was made up for 3.5ml of medium per gram of cartilage and gently shaken at 55-100rpm at 37°C overnight (approximately 15-

20-hours). The following day the suspension was passed through a 70μm cell strainer (BD Falcon). Cells were centrifuged at 180g for 5 mins. The pellet was washed in 5ml of culture medium (DMEM with 10% FBS, 1000IU/ml of penicillin and 100μg/ml streptomycin, Sigma) and centrifuged as before. The pellet was suspended again in 10 ml culture medium and counted using a cell counter. Cells were plated in a T75 flask at 2-4x104 cells/cm^{-2}.

2.8.3 Transfections

siRNAs were rehydrated using siRNA buffer (Dharmacon) as per the manufacturer's instructions and kept at 10 or 200μM stocks. Cells were passaged and seeded for transfection. Cells were seeded into wells at 40-50,000cm^{-2} (HACs) or 200,000cm^{-2} (WT or ORPK chondrocytes) with culture medium and transfected 4-hours later. Media was removed from cells and OptiMEm was warmed to 37°C and 600μl was added to the wells (6-well plate). 50nM of non-targeting (NT) siRNA and 50nM of siRNA targeting IFT88 was prepared in OptiMEm along with equal volumes of OptiMEm with 4μl of lipofectamine 2000 reagent (lifetechnologies) (for a 6-well plate). The two solutions were combined, mixed and incubated for 5 minutes at room temperature. 400μl of this mixture was then added to each well in order to make up total volumes in the well to 1ml. After 90 minutes, 1ml of cell culture medium was added to

the well to dilute out the transfection reagents.

2.8.4 Aggrecan Overlay

Cell culture media was removed from cells and washed briefly with sterile PBS. Cells were serum starved for 1-hour to remove serum and subsequently, 1ml serum free DMEM containing 50μg/ml of aggrecan was added to cells (6 well plate) and left for 24-hours. Media was collected and cells disposed of. Deglycosylation 0.001U/μg of aggrecan required 0.01U of Chondroitinase ABC (MilliporeSigma) and 0.015U of β-galactosidase (Sigma) and dissolved in buffer (50mM Tris-HCl pH7.5, 50mM sodium acetate, 10mM EDTA). 50μl of this enzyme solution was added to each sample and incubated overnight at 37°C. Samples were then acetone precipitated by adding 1ml of ice-cold acetone to the sample, vortexing and incubating at -20°C in a freezer for 1-hour. Samples were then spun at 13,000g for 10minutes at 4°C. The supernatant was discarded carefully and the pellet was kept and air-dried. After 1-hour samples were dry and re-suspended in 50μl of loading buffer containing Laemmli loading buffer (Bio-Rad) and β-mercaptoethanol (1 in 10). The entire sample was loaded onto gel for western blot analysis. No loading control was used owing to the sample being loaded directly into Laemmli loading buffer. This is typical for this assay (Ismail et al., 2015a).

2.8.5 Endocytosis uptake assays

WT and ORPK chondrocytes were cultured as described. After culturing for 72-hours, cells were washed with PBS and cultured in serum free medium for 24-hours. Subsequently, medium was replaced with serum free medium containing 20 nM FLAG-tagged-ADAMTS-5. When experiment required cells were also cultured with a final concentration of 500 nM RAP (inhibitor of LRP-1 mediated endocytosis) for 20 min before the addition of ligands. Medium samples were collected straight into Laemmli loading buffer (Bio-Rad), boiled for 5 minutes, and frozen.

2.8.6 Immunofluorescence

Cells were cultured to confluence on 1.9cm^{-2} glass coverslips. For total cell staining, coverslip cultures were fixed using 4% para- formaldehyde at 37°C for 7 min, (except for LRP-1 cell surface staining, where incubation only occurred for 1 minute) followed by permeabilization with 0.5% Triton X-100 (this step was skipped for LRP-1 staining), and were blocked with 5% goat serum. Coverslips were incubated overnight at 4°C with primary Abs, depending on the protein of interest: acetylated a-tubulin (1:2000), arl13b (1:1000), LRP-1 (1:1000), FLAG-TS-5 (1:500), and EEA-1 (1:500). Coverslips were washed and incubated for 45 min in the dark at 25°C with Alexa Fluor 488 anti-mouse conjugate

(Invitrogen) and Alexa Fluor 555 anti-rabbit conjugate (Invitrogen) before mounting with DAPI (1:5000) counterstain (Thermo Fisher Scientific). For surface staining, coverslip cultures were only fixed for 1 min and no permeabilization was conducted before blocking with 5% goat serum. Samples were then treated the same as previously described. Coverslips were mounted onto slides using Prolong Gold (Thermo Fisher Scientific) and sealed. Images were acquired using an Olympus FluoView FV1000 Confocal Microscope (Olympus, Tokyo, Japan) with an oil immersion 363 objective to produce confocal serial sections for maximum-intensity z-stack reconstruction of monolayer fields with laser voltage, offset and gain held constant. The microscope so that the optical resolution in the XY plane was 0.188μm. Cilia length was measured using a medial line that was defined along the centre of the cilium using ImageJ. This image analysis was conducted by Megan McFie and Isabella Collins.

2.9 Data presentation and statistics

Graphs were generated in Prism 6. All data analyses were performed in GraphPad Prism 8.0 (GraphPad Software, CA, USA). Parametric and nonparametric tests were chosen after D'Agostino-Pearson omnibus normality tests. Statistical tests were used as described in Results.

3

The role of IFT88 in the regulation of matrix turnover *in vitro*

Man was made for Joy and Woe- William Blake

Contents

3.1 Introduction 105
3.2 Aims 110
3.3 Results 110
3.4 Discussion 131
3.5 Conclusion 139

3.1 Introduction

Tissue patterning and homeostatic processes require the tight regulation of cellular activities. In addition to managing their transcription, expression and secretion, the removal of extracellular proteins, such as enzymes, by receptor mediated endocytosis, is crucial to controlling their activity. In the extracellular matrix (ECM) of cartilage, the balance of anabolic and catabolic activity is controlled by chondrocytes. One mechanism for control over the potent enzymes responsible for the cleavage of matrix proteins is

their rapid removal from the extracellular space. This prevents uncompensated matrix destruction, as seen in musculoskeletal diseases such as OA (Glyn-Jones et al., 2015).

The unique composition of the articular cartilage ECM enables smooth articulation and the absorption of mechanical forces. The principal sulfated proteoglycan, aggrecan, provides a fixed density of anionic sidechains which promotes water retention, and hence is crucial to cartilages resistance to compression and load bearing properties. The activity of aggrecanases, a group of proteins from the A Disintegrin and Metalloproteinase with ThromboSpondin motifs (ADAMTS) family, which degrade aggrecan, is critically important to cartilage homeostasis. These enzymes are thought to play a central role in OA (Glasson et al., 2005b; Little et al., 2009), with the loss of aggrecan considered to be a key event of early arthritis, initially affecting the superficial zone and progressing to the deep zone. Degradation of collagen fibrils follows resulting in mechanical failure of the tissue. Additionally, elevated expression of MMPs has been found in cartilage and synovial tissues in patients suffering from OA (Tetlow et al., 2001; Struglics et al., 2006).

Aggrecan is formed of three globular-domains with glycosaminoglycan (GAG) side chains that extend from the core aggrecan protein (Fig. 3.1.0.1) and are cleaved by ADAMTS-5. Degradation of aggrecan by proteases such as ADAMTS-5 results in the formation of neoepitope

containing fragments. AGEG (Mr ;130 kd) and ARGS (Mr; 250, 180, and 70 kd) are both neoepitopes on fragments generated through the catabolic destruction of aggrecan (Fig. 3.1.0.1) (Ismail et al., 2015a).

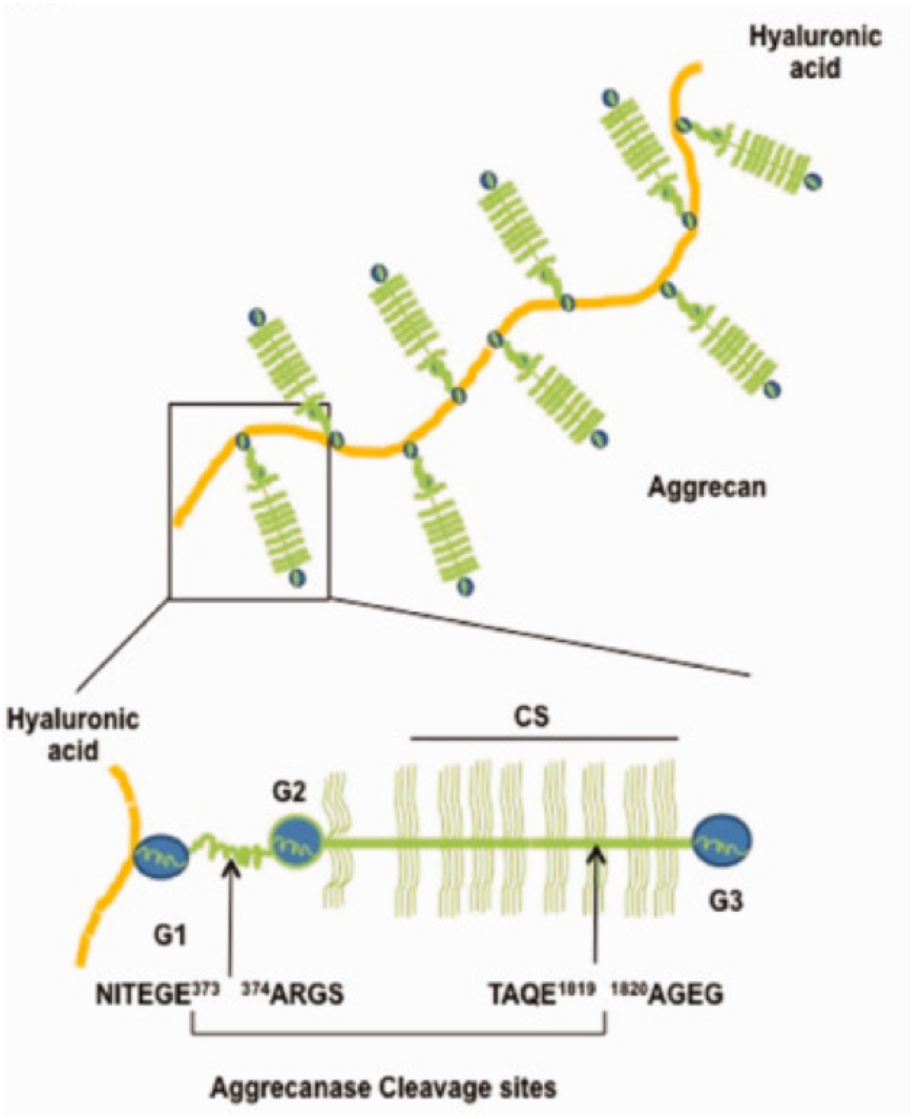


Figure 3.1.0.1: A schematic representation of aggrecan monomers forming a larger proteoglycan aggregate with hyaluronic acid.
A simplified schematic illustrating aggrecan monomers forming a proteoglycan aggregate by binding to hyaluronic acid. Enlargement of boxed area indicates location of the major aggrecanase cleavages sites immediately before Ala374 (ARGS) and Ala182 (AGEG). Arrows indicate aggrecanase-specific cleavages that generate ARGS and AGEG fragments. Figure reproduced from Ismail et al. 2015 (Ismail et al., 2015a).

Interleukin-1 (IL-1) has previously been demonstrated to stimulate

cartilage catabolism through the activities of ADAMTS-5 (Ismail et al., 2015b). IL-1 stimulation of chondrocytes results in resorption of articular cartilage (Rowan et al., 2003). Additionally, upstream pathways, including JNK and NFκB (Kobayashi et al., 2013), have been implicated in the regulation of ADAMTS-5 transcription.

Despite the link between aggrecanases and OA, mRNA levels of these proteases do not always correlate with destruction (Ismail et al., 2015a). Post-translational mechanisms for the regulation of cellular processes are important for the cell's ability to rapidly respond to a dynamic environment. Hence, many proteins are highly regulated, by inhibitors, through conformational change and, in the case of proteases, endocytosis (Hartmann et al., 2013). Endocytosis has been particularly implicated in the regulation of ADAMTS-5 (Yamamoto et al., 2016). Recent research has demonstrated the role of the low density lipoprotein receptor related protein-1 (LRP-1) in the endocytosis of aggrecanases, hence providing a post-translational mechanism for the regulation of aggrecanolysis (Yamamoto et al., 2016). A reduction in the rate of LRP-1 mediated endocytosis clearance of proteases has been documented in OA chondrocytes. Additionally, increased shedding of the LRP-1 extracellular α-heavy-chain required for ligand binding has also been found in OA chondrocytes. Disruption of LRP-1 mediated endocytosis is hypothesised to underlie increased

protease activity (Yamamoto et al., 2017).

Ciliary assembly and function both require IntraFlagellar Transport (IFT). The ciliary axoneme can either protrude out into the extracellular space, for example in kidney epithelial cells, or it is found invaginated, most typically in fibroblasts and chondrocytes, in a pit in the cell membrane called the ciliary pocket. The primary cilium and its pocket have been associated with vesicular trafficking activity (Molla-Herman et al., 2010) including within joint tissues such as cartilage (Rich and Clark, 2012). Interestingly, in trypanosomes, the analogous flagellar pocket is the only known site of endocytosis (Absalon et al., 2008). At present, it is unclear whether, in mammalian cells, the ciliary pocket is also a site of endocytosis and as crucial to the endocytosis process as it is in trypanosomes.

Crucial to IFT is the intraflagellar transport protein 88 (IFT88). Previous research in mouse models has shown that mutations to IFT88 result in disruption to cartilaginous tissue, resulting in matrix deposition, abnormal joint development and phenotypes similar to those seen in arthritic disease (Chang et al., 2012; McGlashan et al., 2007). Most of these phenotypes can largely be attributed to disrupted Hedgehog (Hh) signalling, a pathway that is heavily dependent on the primary cilium and IFT88 (Clement et al., 2009b). Whilst some studies have implicated Hh in OA (Lin et al.,

2009), other recent work has suggested a hedgehog-independent mechanism for matrix destruction (Thompson et al., 2015a).

In this Chapter, I set out to address whether IFT88 directly regulates matrix turnover in a manner independent of transducing pathophysiological stimuli. This Chapter addresses a putative role for ciliary IFT88 in matrix turnover, complementing previous *in vitro* studies addressing anabolic roles and serving as a hypothesis platform for future *in vivo* studies.

3.2 Aims

1. To use a mouse chondrocyte cell line harbouring a hypomorphic (loss of function) mutation to IFT88 and its wild-type (WT) counterpart to investigate the role of IFT88 in matrix turnover.
2. To explore the role of IFT88 in HACs in matrix turnover.

3.3 Results

3.3.1 Aggrecanolytic activity

In order to investigate the role of IFT88 in ECM degradation, the aggrecan overlay assay developed at the Kennedy Institute of Rheumatology by Heba Ismail was used (Ismail et al., 2015a). Briefly, cell cultures were incubated with medium containing bovine aggrecan over a time course. The conditioned medium was

then harvested after a specified time point, deglycosylated, acetone precipitated, and directly loaded into laemmli buffer. There are therefore no loading controls used in these studies. However, recent technologies have started to enable others in the laboratory to now use quantifiable techniques to assess quantitatively the amount of protein loaded in each experiment.

Here, a mouse chondrocyte cell line was co-cultured with aggrecan and media collected for western blot analysis. This chondrocyte line, (see Methods), was originally isolated from the Oak Ridge Polycystic Kidney (ORPK) mouse model. ORPK cells harbour a hypomorphic loss of function mutation to IFT88, resulting in reduced ciliogenesis. Proteolytic activity of the cells was analysed by western blot analysis; the more aggrecan fragments produced the more proteolytically active the cells. The cells have undetectable levels of intrinsic aggrecan neoeptiope production, requiring the addition of bovine aggrecan to the experiment. Media containing bovine aggrecan was incubated with WT and ORPK chondrocytes over a time-course of 6-, 12-, 18- and 24-hours. Co-cultured media was then acetone precipitated and deglycosylated prior to western blot analysis using an aggrecan antibody targeting the immunoglobulin-domain of aggrecan (6-B-4). However, for the majority of studies, an anti-AGEG and an anti-ARGS antibody (previously validated aggrecanolysis neoepitopes) were used. IL-1

stimulation of WT chondrocytes was used as a positive control, as it stimulates protease led aggrecan degradation (Ismail et al., 2015a).

3.3.1.1 Analysis of aggrecan degradation using the interglobulin-domain aggrecan antibody

Initial analysis using the interglobulin domain (IGD) antibody showed production of a 30kDa band in response to IL-1β in WT chondrocytes after 24-hours (Fig. 3.3.1.1 lane 2). The 30kDa fragment was observed after 6-hours of co-culture with bovine aggrecan. Running ORPK conditioned media resulted in a higher intensity band at 30kDa at every time-point in comparison with WT media. However, this antibody has previously been reported to bind many different sized fragments of aggrecan resulting in a protein smear when analysed by western blot, indicating non-specific cleavage of full length aggrecan (Fosang et al., 1992; Handley et al., 2001). Due to these factors, an antibody targeting a different portion of aggrecan was used in future experiments.

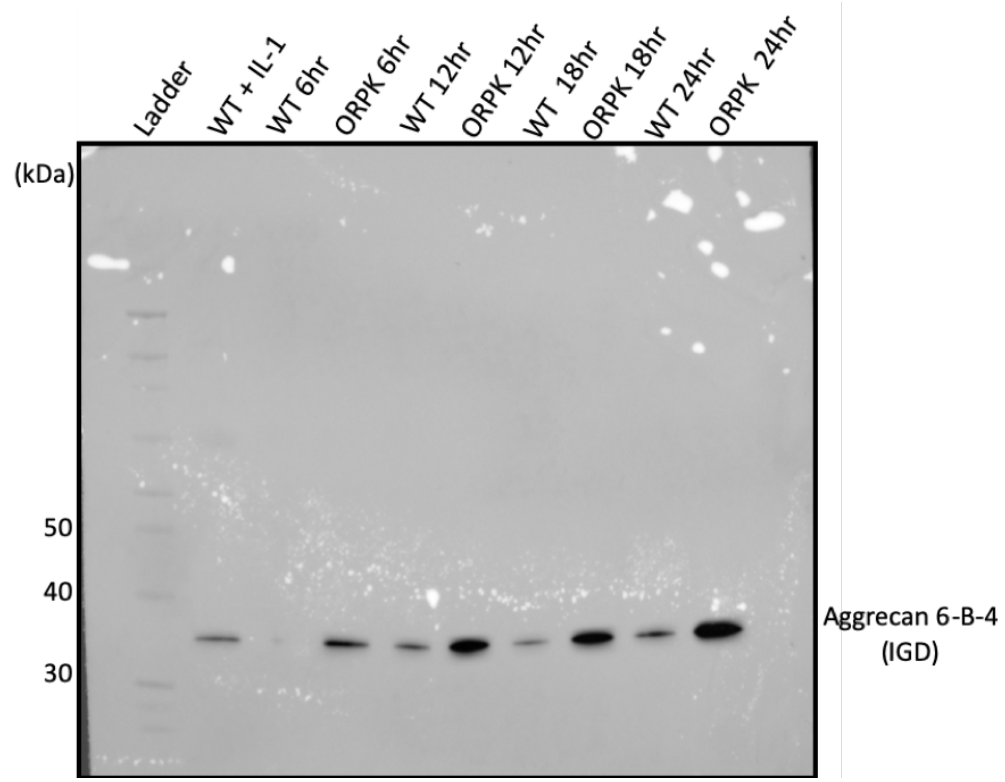


Figure 3.3.1.1: Western blot analysis of aggrecan degradation over a time-course. Media containing aggrecan was co-cultured with ORPK and WT cells over a time-course (6-, 12-, 18-, and 24-hours) (IGD: immunoglobulin domain). (Ismail et al., 2015a).

3.3.1.2 Validation of anti-AGEG antibody in human articular chondrocytes

Degradation of aggrecan by human articular chondrocytes (HACs) following stimulation with IL-1 has previously been documented (Ismail et al., 2015a). Hence, to establish this assay for my thesis, HACs isolated from an OA patient sample were co-cultured with aggrecan, or co-cultured with aggrecan and stimulated with IL-1 50ng/ml for 24-hours. IL-1 stimulation resulted in elevated production of the aggrecan neoepitope AGEG (130kDa) compared with unstimulated samples. However, this difference was only striking in one stimulated sample (Fig. 3.3.1.2). These results confirmed successful sample preparation for aggrecanolysis studies

supporting this assay for use in future experiments.

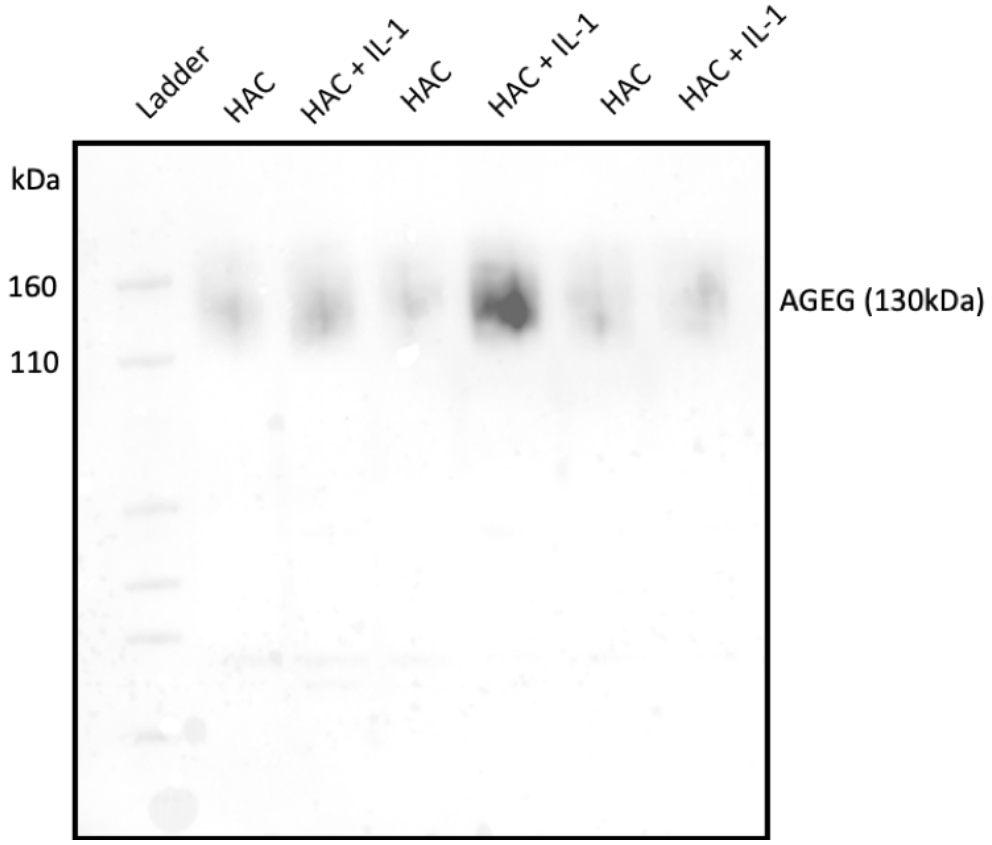


Figure 3.3.1.2: Validation of anti-AGEG antibody in human articular chondrocytes. HACs co-cultured with bovine aggrecan and stimulated with IL-1.

3.3.1.3 Validation of AGEG/ARGS in primary human chondrocytes over a time-course

HACs were co-cultured with aggrecan for either 8- or 24-hours. IL-1 stimulated samples were used as a control. Production of the AGEG fragment was higher when aggrecan-containing media was co-cultured with cells for 24-hours compared with 8-hours (Fig. 3.3.1.3 A). The same samples were also probed for ARGS, a neoepitope of aggrecan that is formed later during the time-course (Fig. 3.3.1.3 B). HACs produced higher levels of ARGS post 24-hour

incubation than 8-hours. As expected ARGS production was much lower 8-hours post-incubation than AGEG at the same time-point, as AGEG is cleaved first and is thought to be indicative of early aggrecan degradation (Fig. 3.1.01) (Tortorella et al., 2000).

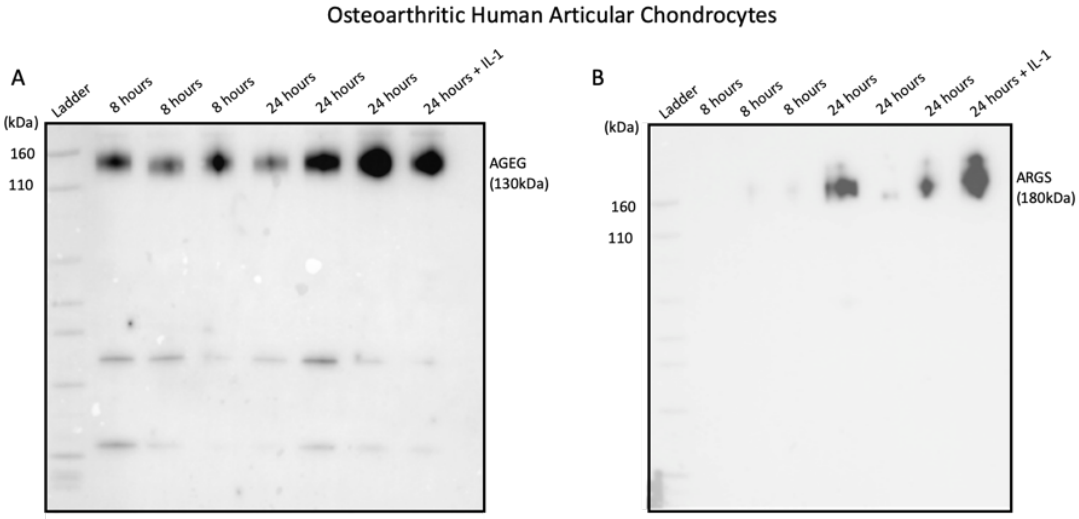


Figure 3.3.1.3: AGEG and ARGS production by Osteoarthritic (OA) HACs over a time-course.
A) Western blot analysis of AGEG production in OA HACs from the same patient when co-cultured with bovine aggrecan for 8- or 24- hours. Cells were also treated with IL-1 when co-cultured with aggrecan as a control. B) The same samples were also analysed by western blot for ARGS production.

3.3.1.4 Overlay assay in chondrocyte cell line

Having established a protocol, aggrecaneolytic activity was characterised in WT and ORPK samples. Production of AGEG in HACs and WT cells stimulated with IL-1 were compared with WT and ORPK unstimulated chondrocytes. WT samples stimulated with IL-1 showed higher levels of AGEG production than unstimulated WT cells (Fig. 3.3.1.4). ORPK samples showed much higher levels of AGEG production than WT samples and

similar to that of HACs stimulated with IL-1. This experiment demonstrated that ORPK cells exhibit qualitatively higher levels of aggrecan degradation than WT cells and at the level of pathogenic osteoarthritic HACs but without stimulation.

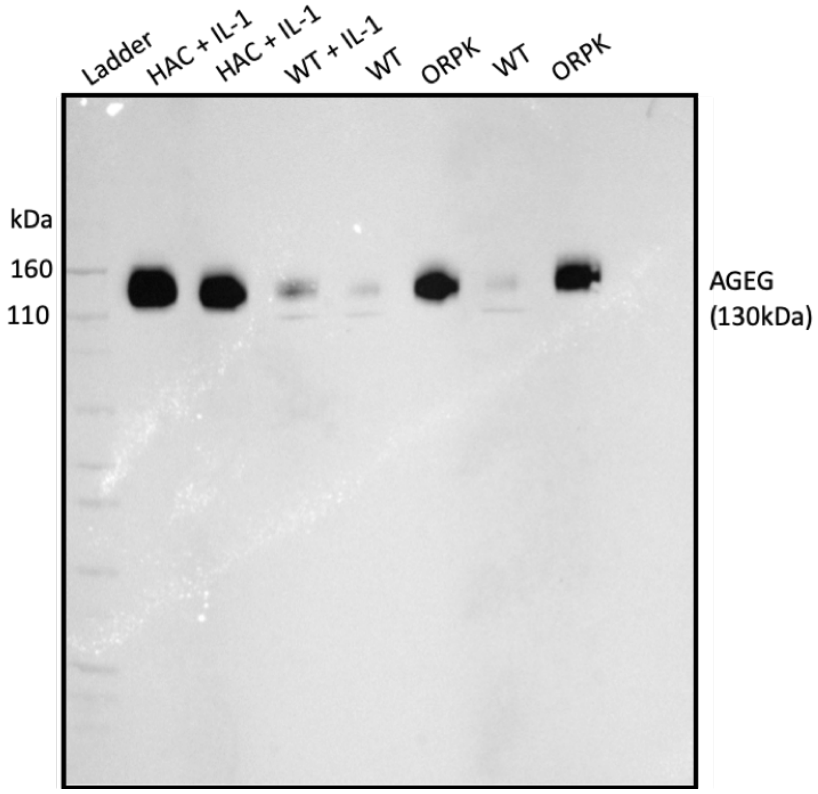


Figure 3.3.1.4: Overlay assay in chondrocyte cell line.
IL-1 stimulated HACs and WT samples were compared with WT and ORPK cells in terms of their AGEG production.

3.3.1.5 SiRNA targeting of IFT88 in primary human articular chondrocytes and its effects on cilia

HACs stimulated with IL-1 exhibited high levels of aggrecan neoepitope production compared with similarly treated WT chondrocytes and at the level of chondrocytes harbouring a mutation to IFT88. Hence, the effects of IFT88 deletion was

investigated in HACs, by siRNA targeting of IFT88 (siIFT88) using the transfection agent Lipofectamine. Non-targeting siRNA (siNTRNA) was used as a control. Cilia prevalence and length data was taken to assess the impact of IFT88 deletion on cilia of HACs. Western blot analysis of HAC lysates showed depleted levels of IFT88 in siIFT88 targeted cells in compared with siNTRNA transfected cells. These were also compared with lysates from cells that were not transfected to control for the potential effects of Lipofectamine and Opti-Mem on IFT88 protein expression (Fig. 3.3.1.5 A). HACs were also cultured and transfected on glass. Primary cilia were visualised using immunofluorescence (IF) staining with antibodies targeting acetylated-α-tubulin and Arl13b, and the nuclear counterstain DAPI (Fig. 3.3.1.5 B). Using three fields of view within each sample, cilia length was measured and classified into bin centres to visually represent distribution of cilia length within a cell population. HACs targeted with siIFT88 had a higher prevalence of shorter cilia than siNTRNA targeted HACs (Fig. 3.3.1.5 C). There was also a small but statistically significant reduction in the number of ciliated HACs in siIFT88 targeted cells in comparison with siNTRNA HACs (Fig. 3.3.1.5 D).

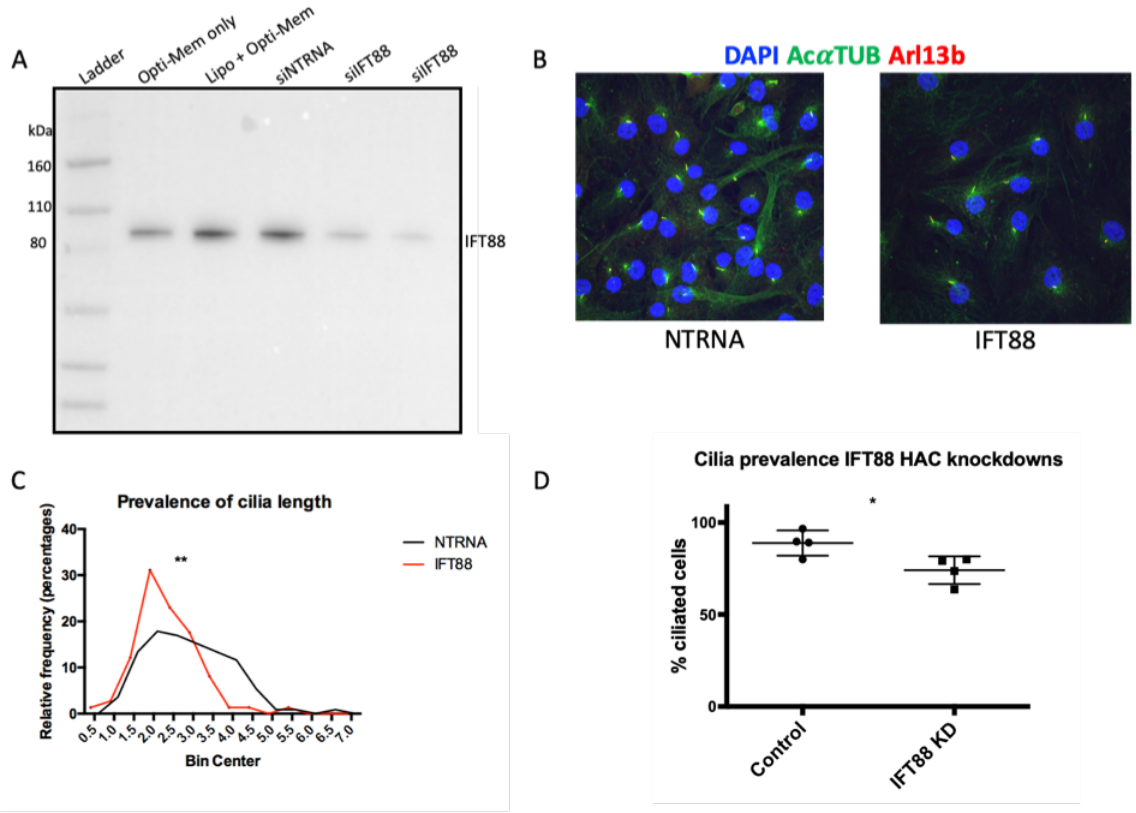


Figure 3.3.1.5: siRNA targeting of IFT88 in primary human articular chondrocytes and its effects on cilia.
A) IFT88 deletion in HACs analysed by western blot. B) IF images of HACs transfected with non-targeting siRNA (siNTRNA) and siRNA targeting IFT88. C) Cilia length prevalence, between siNTRNA and siIFT88 targeted HACs. D) Cilia % prevalence between control (NTRNA) and IFT88 KD (siRNA IFT88). Data represents the mean ± SD. Statistical difference is from a χ^2 analysis where *p<0.05, **p<0.01.

3.3.1.6 IFT88 deletion in HACs and its effects on AGEG neoepitope production

As chondrocytes harbouring the ORPK mutation demonstrated higher production of AGEG (Fig. 3.3.1.6) compared with WT chondrocytes, it was hypothesised that deletion of IFT88 in HACs could result in higher levels of AGEG production. In order to investigate this hypothesis, non-transfected and transfected HACs were co-cultured with aggrecan for 24-hours. However, as shown

below, preliminary results were variable, with siNTRNA showing elevated AGEG production in two of the three replicates analysed, thus indicating that siNTRNA could elevate AGEG production in comparison with siIFT88 transfected HACs. This suggested that the transfection protocol itself could elevate production of AGEG. Due to this result, HACs were not used further to explore the role of IFT88 in aggrecan degradation and the WT and ORPK cell lines were used.

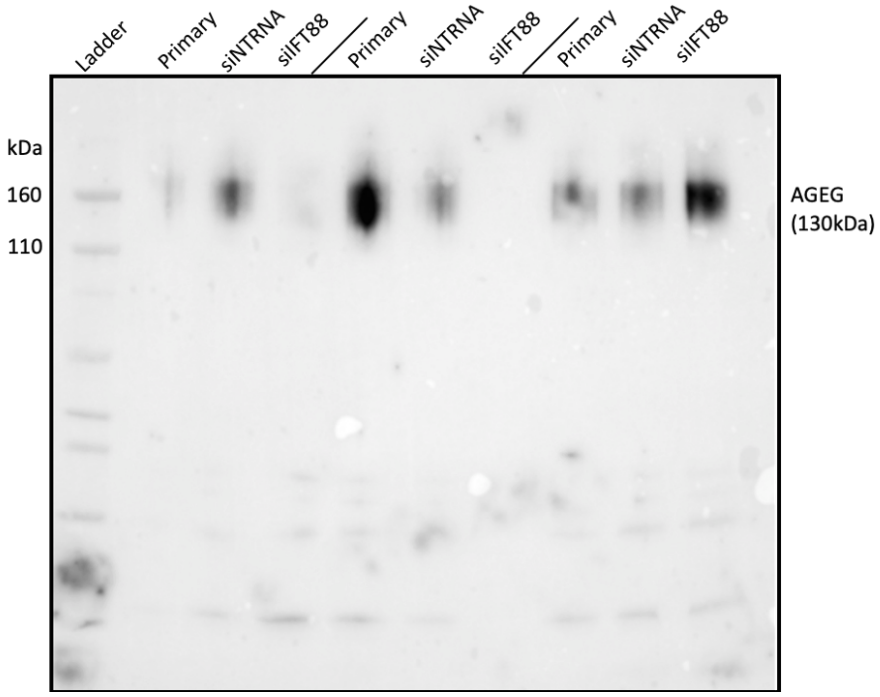


Figure 3.3.1.6: IFT88 deletion in HACs and its effects on AGEG neoepitope production.
Western blot analysis of AGEG production in untreated primary, siNTRNA transfected, and siIFT88 transfected HACs.

3.3.1.7 Aggrecanolytic activity in ORPK chondrocyte cell line

In order to investigate the role of IFT88 in aggrecanolytic activity, WT and OPRK chondrocytes were co-cultured with bovine

aggrecan over a time-course of 6, 12, 18 and 24-hours. AGEG production was analysed by western blot. WT cells produced consistently less AGEG at every time-point, in comparison to ORPK chondrocytes, which produced qualitatively more AGEG over the time-course. An IL-1 stimulated WT control showed much higher levels of AGEG produced than WT chondrocytes co-cultured with aggrecan after 24-hours (Fig. 3.3.1.7).

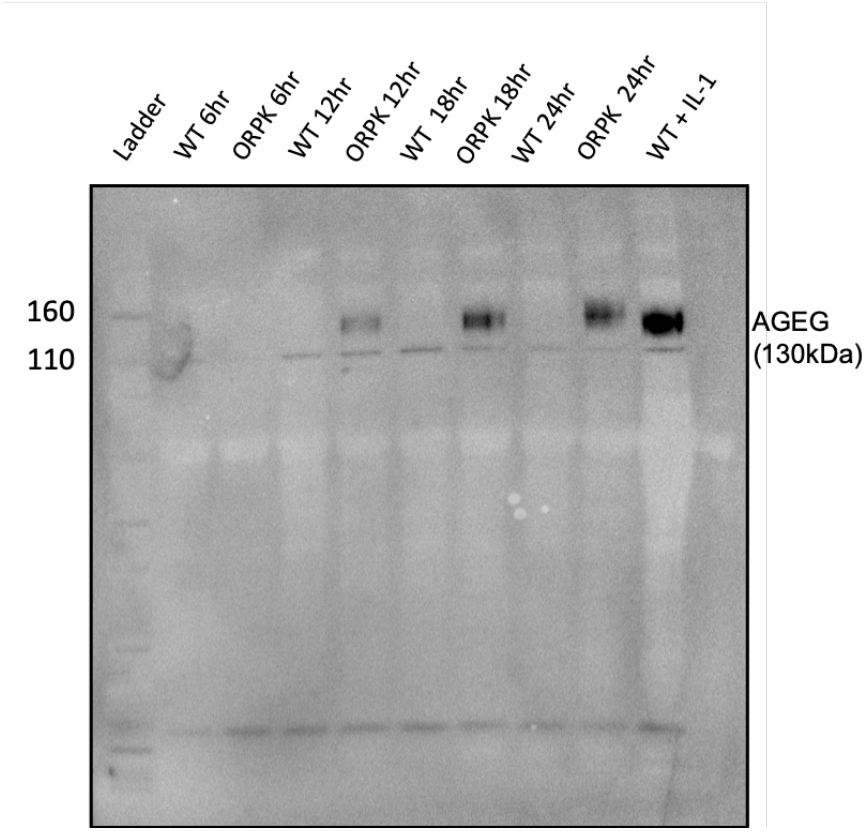


Figure 3.3.1.7: WT and ORPK AGEG production over a time-course
Western blot analysis of AGEG production in WT and ORPK chondrocyte conditioned media over a time-course of 6, 12, 18 and 24-hours.

3.3.2 Analysis of the regulation of protease clearance by endocytosis

Previous work in the laboratory had demonstrated that increased aggrecanolytic activity indicated by the production of AGEG neoepitope, could not be associated with transcriptional regulation of aggrecanases or higher activation of the JNK pathway (Coveney et al., 2018), a pathway known to elevate AGEG production (Ismail et al., 2015b; Ismail et al., 2015a). Previous and ongoing work within the Versus Arthritis OA Centre for Pathogenesis at the Kennedy Institute, had established a link between the ADAMTS-5 activity and its rate of clearance mediated by the cell surface receptor LRP-1. They demonstrated that OA samples presenting with elevated aggrecanase activity had impaired LRP-1 mediated endocytosis of ADAMTS-5 (Yamamoto et al., 2013b). In light of these results, WT and ORPK chondrocytes were cultured with FLAG-tagged ADAMTS-5 (TS-5-FLAG) and the rate of TS-5-3-FLAG clearance from the media was measured over a time-course from 20- to 80-minutes at 20-minute intervals. Repeat experiments were analysed by western blot (Fig. 3.3.2.1 A), quantified in ImageJ, and linear regression analysis was used to determine half-life of TS-5-FLAG clearance (Fig. 3.3.2.1 B). The LRP-1 antagonist, RAP, was added to WT cultures to confirm that uptake was occurring through the LRP-1 receptor. WT+RAP showed inhibited

clearance of TS-5-FLAG from the media with an average (mean) half-life of over 60-minutes in contrast with WT cells, which had a half-life of approximately 40-minutes (Fig. 3.3.2.1.1 B). The average extracellular half-life of TS-5-FLAG in ORPK cultures was approximately 35-minutes longer than that of WT chondrocytes (Fig. 3.3.2.1 C). This half-life was similar to that achieved by RAP inhibition in WT cultures. Despite repeating this experiment six times independently in triplicate, there is still high variability within the results as indicated by the large size of the SD error bars. However, there is a modest, reproducible reduction in the rate of TS-5-FLAG clearance in the ORPK chondrocytes compared with WT chondrocytes.

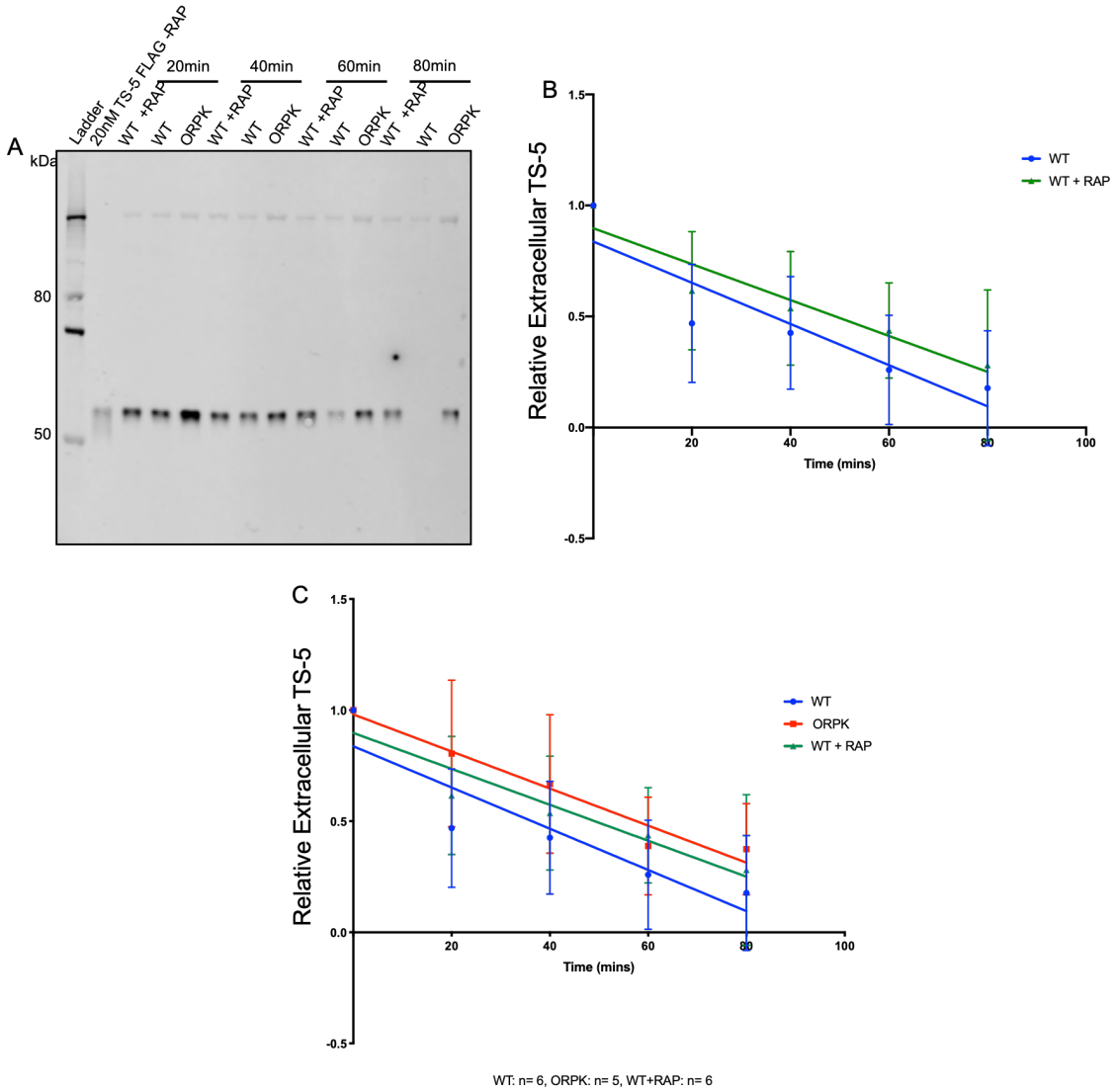


Figure 3.3.2.1: ORPK chondrocytes have reduced rate of clearance of TS-5-FLAG from the media than WT chondrocytes.
A) Western blot analysis of FLAG tagged TS-5 over a time-course (20, 40, 60, and 80 mins). B) Linear regression analysis of rate of clearance between WT chondrocytes and WT chondrocytes cultured with RAP with standard deviation. (WT: n=6, WT+RAP: n =6). C) Linear regression analysis of rate of clearance between WT and ORPK chondrocytes and WT chondrocytes cultured with RAP with standard deviation. (WT: n=6, ORPK: n=5, WT+RAP: n =6). Points on graphs represent the average 5/6 experiments repeated in triplicate. Data represents the mean ± SD.

3.3.3 Low-density lipoprotein receptor related protein-1β (LRP-1β) protein expression

The LRP-1 receptor has a transmembrane β-domain and an extracellular α-domain, the latter of which can be shed through the activity of membrane bound sheddases. Hence, to assess LRP-1 expression within cell lysates, the LRP-1β-domain is more representative of the total receptor expression than the LRP-1α-domain. Therefore, LRP-1β protein expression in WT and ORPK cell lysates was assessed by western blot analysis (Fig. 3.3.3.1 A). There was no qualitative difference in total LRP-1β levels observed between WT and ORPK chondrocyte lysates (Fig. 3.3.3.1 A). There was also no difference in total LRP-1β expression between WT and ORPK chondrocytes when normalised to actin (Fig. 3.3.3.1 B).

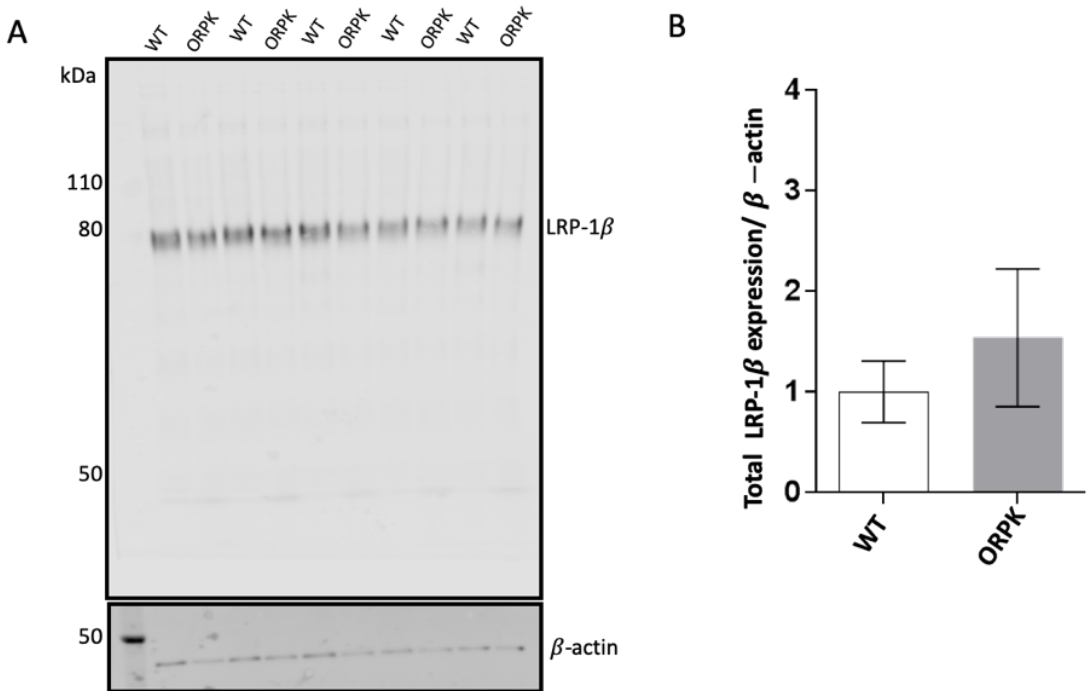


Figure 3.3.3.1: Total LRP-1 protein expression is not affected by ORPK mutation.
A) LRP-1β expression analysed by western blot analysis between WT and ORPK lysates. B) Total LRP-1 expression normalised to actin. WT n =5, ORPK n= 5. Data represents the mean ± SD.

3.3.4 Low-density lipoprotein receptor related protein-1β (LRP-1β) distribution

Previously, we have shown that IF-visualised, internalised TS-5-FLAG had polarised localisation in WT chondrocytes, a phenomenon absent in ORPK chondrocytes lacking cilia (Coveney et al., 2018). As there is no difference in the protein expression of LRP-1β between WT and ORPK cells, but there is a difference in its apparent function as measured by the endocytosis assay, it was hypothesised that there may be a difference in the distribution of the receptor alongside observed TS-5-FLAG localisation. IF staining

of LRP-1β revealed a punctate distribution of the receptor with the majority of the receptor localising to one side of the cell in the WT chondrocytes. Conversely, in ORPK chondrocytes, this localisation was altered, apparently more homogeneous in distribution (Fig. 3.3.4.1).

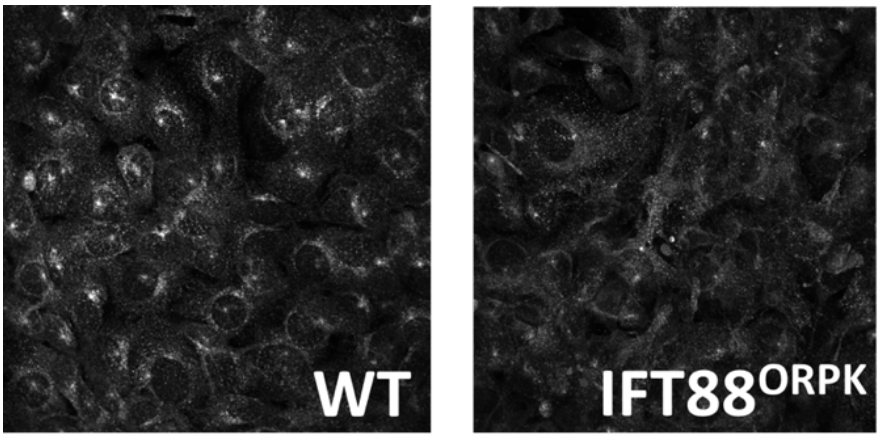


Figure 3.3.4.1: Distribution of LRP-1 receptor is qualitatively altered in ORPK cell line.
IF representative images of LRP- 1β in WT and ORPK cell line.

3.3.4.1 Subcellular localisation of low-density lipoprotein receptor related protein-1β (LRP-1β)

LRP-1β localises to the side of the cell presenting with a primary cilium, but it also localises focally to the base of the structure in WT murine articular chondrocytes (Fig. 3.3.4.2 A). This spatial relationship is also present in primary rib chondrocytes isolated from mice, as seen in both wide field view and in a close up of one cell (Fig. 3.3.4.2 B). Again, this same spatial relationship between the LRP-1β and the primary cilium was also observed in HACs (Fig. 3.3.4.2 C).

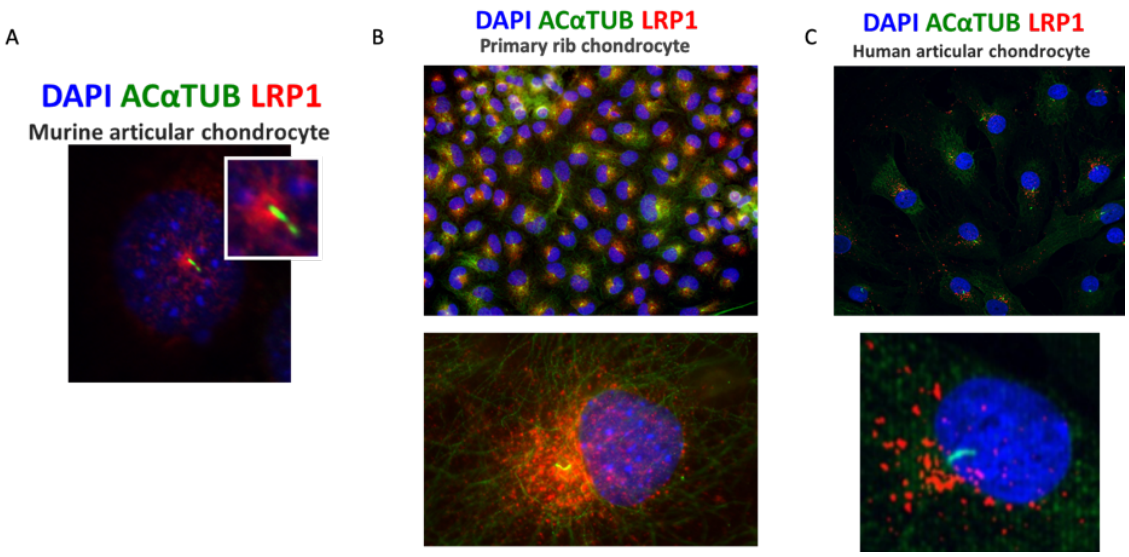


Figure 3.3.4.2: LRP-1β localises to the base of the primary cilium/ periciliary region in cell line, primary mouse chondrocytes and human articular chondrocytes.
All images were stained with acetylated alpha tubulin (ACαTUB), LRP-1 (LRP1) and counterstained with DAPI. A) A single murine articular chondrocyte. B) Wide field view of cultured primary rib chondrocytes isolated from mouse. Single chondrocyte shown beneath. C) Wide field view of human articular chondrocytes. Single chondrocyte shown beneath. Some images adapted from Coveney et al. 2018.

3.3.5 Low-density lipoprotein receptor related protein-1α (LRP-1α) chain shedding from the cell surface

LRP-1 consists of a large 515-kDa extracellular membrane α-chain and a smaller 85-kDa β-chain consisting of an extracellular, transmembrane, and cytoplasmic-domain. The α-chain contains ligand binding-domains that are responsible for binding to ADAMTS-5 (Yamamoto et al., 2013b). LRP-1 is cleaved by enzymes such as ADAM17 and MMP-14, a transmembrane enzyme, to release LRP-1 consisting of the entire α-chain and a portion of the β-chain. Both MMP-14 and ADAM17 sheddases have been associated with OA (Yamamoto et al., 2017). As shown in Fig. 3.3.3.1, there

was no difference in total LRP-1 β protein expression between WT and ORPK chondrocytes, however, there was an observed difference in the rate of endocytosis of TS-5-FLAG in ORPK chondrocytes than WT (Fig. 3.3.2.1 C). Observed increases in shedding in human OA samples with reduced endocytosis of TS-5-FLAG (Yamamoto et al., 2017), in conjunction with our comparable results (Fig. 3.3.3.1), led to the hypothesis that the LRP-1α chain could be shed more in ORPK than WT chondrocytes.

Conditioned media from both WT and ORPK chondrocytes was analysed by western blot for the shed LRP-1α chain. More LRP-1α chain was seen in the conditioned media from ORPK samples compared with WT (Fig. 3.3.5.1 A). In order to assess whether higher levels of shed LRP-1α was owing to increased presence of sheddases, cell lysates were analysed by western blot for ADAM17 and MMP-14. No significant difference in ADAM17 protein expression was observed between WT and ORPK samples when corrected for actin (Fig. 3.3.5.1 B). Conversely, western blot analysis of MMP-14 showed elevated protein expression in ORPK samples compared with WT (Fig. 3.3.5.1 C).

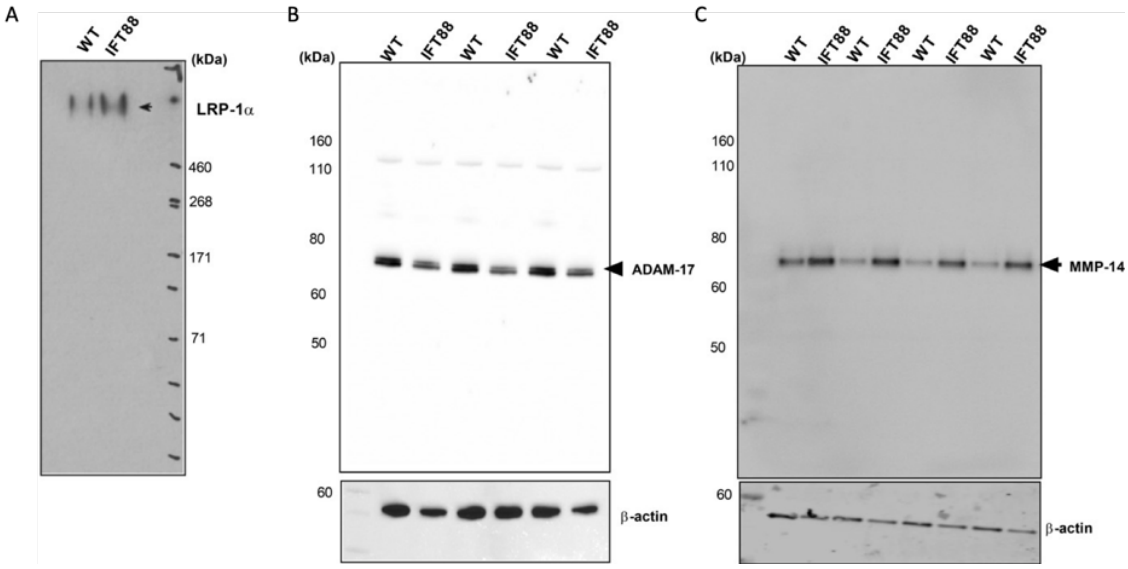


Figure 3.3.5.1: LRP-1α chain is shed more in ORPK chondrocytes and this is associated with higher presence of sheddase proteins.
Western blot analysis of A) Shed LRP-1α heavy chain cleaved by sheddases in the medium of WT and ORPK (IFT88) chondrocytes. B) ADAM17 sheddase with β-actin control from WT and ORPK (IFT88) chondrocyte lysates. C) MMP-14 sheddase with β-actin control from WT and ORPK (IFT88) chondrocyte lysates.

3.3.6 Schematic representation of proposed hypothesis

In this schematic (Fig. 3.3.6.1), both the WT and ORPK scenarios are presented. In the WT scenario (left), the primary cilium is located within the cilia pocket, hypothesised to be a site of endocytosis. ADAMTS-5 cleaves minimal aggrecan (process 1) as it is rapidly cleared from the ECM through binding to the LRP-1 receptor (process 2). In contrast, the ORPK scenario, where cells have either shortened or non-existent cilia have little or no pocket, has increased expression of the sheddase MMP-14, which cleaves the LRP-1 receptor (process 3), inhibiting ADAMTS-5 binding and removal from the ECM. Hence, higher levels of aggrecan degradation are observed in the ORPK scenario compared with WT.

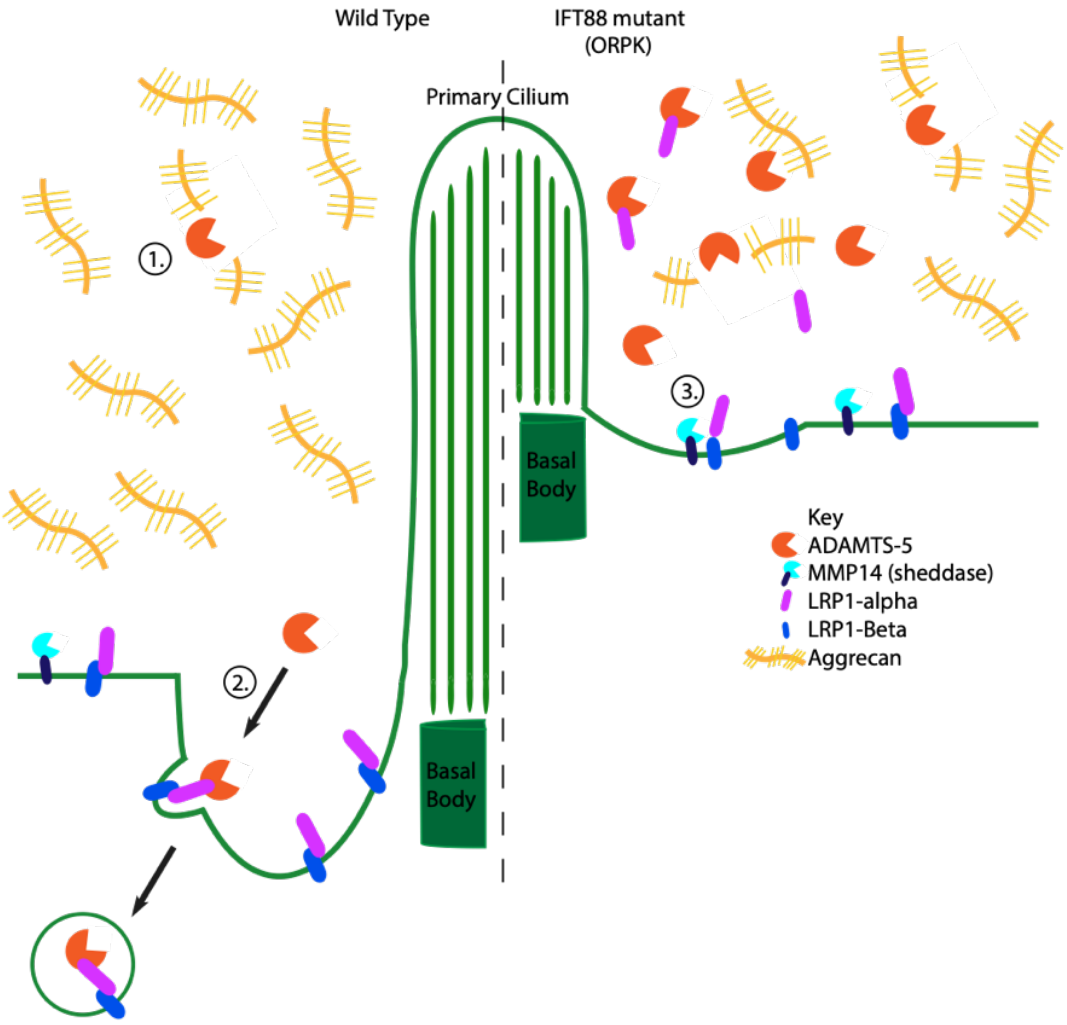


Figure 3.3.6.1: Schematic illustrating hypothesised mechanism behind elevated aggrecanase degradation observed in OPRK chondrocytes.
WT scenario on the left with the ORPK scenario on the right. 1. ADAMTS-5 cleaves aggrecan. 2. ADAMTS-5 binds to LRP-1 receptor and is endocytosed. 3. MMP-14 cleaves the LRP-1 receptor to release LRP-1α chain.

3.3.7 Summary

To summarise, this chapter describes elevated aggrecanolytic activity in chondrocytes with a hypomorphic mutation to IFT88. This mutation is associated with reduced endocytotic clearance of ADAMTS-5 by LRP-1, disrupted distribution of LRP-1 and increased LRP-1 shedding.

3.4 Discussion

The functions of both articular and growth plate cartilage are enabled by the composition, organisation and turnover of extracellular matrix. As such, skeletal development, joint health and disease are all defined by the regulation of matrix homeostasis; the careful balance of matrix anabolism and catabolism. The cilium/ciliary protein IFT88 has been previously associated with changes to cartilage development (Haycraft et al., 2007b; McGlashan et al., 2007) and homeostasis *in vivo* (Chang et al., 2012), and chondrocyte anabolism *in vitro* (Wann et al., 2012). In this chapter, I explored whether IFT88 regulates cartilage matrix catabolism *in vitro*.

The destruction of both aggrecan and collagen are observed in OA (Glasson et al., 2005b; Little et al., 2009). Previous work demonstrated that this mouse chondrocyte cell line had low collagenase and gelatinase activity. Hence, I focused on aggrecanolysis using an assay that was developed previously, known as the aggrecan overlay assay (Ismail et al., 2015b; Ismail et al., 2015a). Through use of an antibody targeting interglobular-domains of aggrecan, we were able to detect a very small fragment of aggrecan, which was elevated in ORPK cell conditioned media compared with WT. This was in contrast to the expected result of

many different sized fragments. However, this assay was originally developed to explore human chondrocyte aggrecanolytic activity and, in these experiments, mouse chondrocytes were used. The ability of mouse chondrocytes to degrade bovine aggrecan, which has a different amino acid sequence to mouse aggrecan, is not known. Hence, we analysed samples using antibodies that were previously used in this assay, rather than the 6-B-4 antibody which has not been validated/used in this experiment before. These antibodies targeted the AGEG and ARGS aggrecan neoepitopes.

OA HACs were transfected with siIFT88, with the aim of reducing IFT88 in cells, which resulted in a marked reduction in IFT88. However, this deletion of IFT88 failed to remove cilia, reducing prevalence only marginally, but did affect cilia length (Fig. 3.3.1.5). The aggrecan overlay assay was conducted in IFT88-deleted OA HACs cells alongside siRNA non-targeted controls. The preliminary results indicated that transfection alone resulted in elevated AGEG neoepitope production and hence OA HACs were no longer used. Additionally, healthy HACs are very difficult to obtain and whilst we are fortunate to received human OA samples, it is hard to establish a true control state. Another reason why I did not continue using the HACs was interpatient variability which may affect protease activity.

On probing mouse chondrocyte cell media for AGEG, I was

able to successfully observe production of a band recognised by the AGEG targeting antibody. However, we were unable to detect production of any ARGS fragment, suggesting that mouse chondrocytes are unable to degrade bovine aggrecan at the Ala374 site. This hypothesis was supported by the production of an ARGS fragment when bovine aggrecan was incubated with HACs, implying that the assay is functioning correctly. Potentially, an antibody developed to target bovine and human aggrecan was unable to detect an ARGS-reactive band as mouse aggrecan has a different amino acid sequence. In our experiments, ORPK chondrocytes displayed constitutively elevated aggrecanase activity, as indicated by elevated AGEG production, in comparison with the WT chondrocytes. This level of activity was comparable to that observed in OA HACs and WT chondrocytes stimulated with the inflammatory cytokine IL-1. A protease inhibitor could be used to confirm that the observed elevated aggrecanolytic activity defined by AGEG production was due to protease-mediated degradation of aggrecan. Work ongoing in the Wann laboratory has confirmed that treatment of cells with a protease inhibitor completely abolishes AGEG neoepitope production in WT, ORPK, and siRNA targeted cells. Ongoing work is confirming this activity is specifically ADAMTS-5 driven.

The WT and ORPK chondrocyte cell line allow us to easily and

tractably test the function of IFT88 in chondrocytes. The nature of this cell line (as described in methods) enables the temperature- and IFN-γ controlled immortalisation of chondrocytes, which in turn enables culturing and proliferation of chondrocytes providing a continuous source of cells for experiments. By removing IFN-γ and elevating the temperature, these cells can be transformed into primary-like chondrocytes, producing conditions closer to the physiological state. However, these chondrocytes have been documented to have altered cytoskeleton organisation and observed to divide more rapidly (McGlashan et al., 2007). Further, they appear to be qualitatively more fibroblastic than their WT counterparts. Additionally, differences are observed on comparing the phenotype of siRNA IFT88-deleted WT chondrocytes with ORPK chondrocytes between experiments, such as AGEG neoepitope production; the ORPK chondrocytes producing much more AGEG neoepitope in comparison with siRNA IFT88-deleted WT chondrocytes. Both within the literature and in the Wann laboratory it has been shown that the ORPK mutation does not result in ablation of the protein. Additionally, the ORPK mutation results in an approximate 85% reduction in cilia expression, but siRNA deletion of IFT88 results in a smaller reduction.

There are a number of possible explanations for observed

elevated aggrecanase activity seen, including alterations to the signalling pathways involved in the regulation of aggrecanase activity. Recently, OA protease activity has been linked to the JNK-2 pathway (Ismail et al., 2015a); however, qPCR analysis and subsequent pathway status assessments (phospho-blotting) within our group eliminated this as a possible factor as ORPK chondrocytes do not have constitutive JNK-2 activity (Coveney et al., 2018). Hence, we explored post-translational regulatory mechanisms for the regulation of enzymatic activity, including the removal of the proteases from the ECM by LRP-1 mediated endocytosis.

Previous work at the Kennedy Institute of Rheumatology established an endocytosis assay to measure endocytosis of TS-5-FLAG by human OA chondrocytes (Yamamoto et al., 2016). However, some optimisation was required in my hands as described. Interestingly, the zero-minute time-point where the sample had not come into contact with the cells in this experiment, appeared to always to be at a lower intensity than post 20-minute time-points. Uptake of TS-5-FLAG was very rapid and hence an appropriate time-course needed to be established to resolve differences, and blocking buffer, primary and secondary buffers and secondary antibody concentrations had to be optimised. Addition of RAP also appeared to increase the concentration of TS-5-FLAG

in comparison to non-treated WT samples at the 0-minute time-point. This was found to be due to TS-5-FLAG adhering to the tube surface, which was prevented by RAP. Hence, samples were immediately collected into denaturing loading buffer and boiled decreasing contact with plastic surfaces to which FLAG could bind. However, this would not completely prevent TS-5-FLAG sticking to the cell culture plate walls prior to denaturing. Five or six repeats of this experiment were conducted in triplicate due to this variability and quantification was averaged across the experiments. However, this experiment was repeated by others working in the laboratory and has continued to show consistently similar trends, with ORPK chondrocytes displaying reduced rate of uptake to a greater extent than those of RAP antagonised WT chondrocytes. As RAP inhibits LRP-1 mediated endocytosis and ORPK rates of uptake are lower than RAP treated WT cells, it suggests that there is a mechanism beyond LRP-1 influencing rate of clearance in OPRK chondrocytes (Coveney et al., 2018). TS-5 FLAG could be endocytosed by other cell surface receptors which are not blocked by the addition of RAP, but their function is impaired by the ORPK chondrocyte, perhaps due to loss of polarisation of cell surface receptors.

LRP-1 has been shown to be responsible for the endocytosis of many ligands including ADAMTS-5. In WT chondrocytes we found polarised surface LRP-1β signal on the side of the cell

presenting a primary cilium and at the cilia base. We found a similar polarisation of LRP-1β in cultured OA HACs and primary mouse rib chondrocytes (Fig. 3.3.4.2). This could indicate that one side of the cell is preferentially organised for endocytosis, a hypothesis now being directly tested in the group. Additionally, the ciliary pocket has been hypothesised to be a site of endocytosis (Rich and Clark, 2012). Assembly of a primary cilium could be important for organised/polarised endocytosis. On loss of the cilia structure perhaps polarised endocytosis is lost. This might explain why siIFT88 depleted chondrocytes, with little alteration in overall cilia prevalence, has limited effects on the rate of endocytosis and aggrecan degradation in comparison to siNTRNA chondrocytes. This work was conducted by Isabella Collins, another DPhil student in the Wann laboratory.

As described in this chapter and by others previously, LRP-1 is important for the clearance of aggrecanases including ADAMTS-5 (Yamamoto et al., 2016). However, the sheddase enzymes MMP-14 and ADAM17 cleave the LRP-1α receptor, releasing a soluble LRP-1 fragment and preventing endocytosis by reducing surface levels of LRP-1 (Yamamoto et al., 2017). ORPK chondrocytes were found to have elevated MMP-14 expression when compared with WT chondrocytes. Conversely, there was no qualitative difference in the expression of ADAM17 between WT and ORPK chondrocytes.

Tissue inhibitor of metalloproteinases (TIMP-3) is an endogenous inhibitor of collagenases and aggrecanases (Scilabra et al., 2013; Yamamoto et al., 2013b). We previously showed that TIMP-3 was not transcriptionally regulated in ORPK chondrocytes (Coveney et al., 2018). Western blot analysis of TIMP-3 in WT and ORPK cell lysates revealed that WT chondrocytes may express markedly more (cell associated) TIMP-3 protein than ORPK chondrocytes (Fig. 3.4.0.1). This stark difference in TIMP-3 protein expression could be evidence that it too is post-transcriptionally regulated and ORPK chondrocytes potentially release more TIMP-3 into the extracellular space, hence it is not observed in cell lysates. However, TIMP-3 can also bind to LRP-1. This would result in competitive inhibition of ADAMTS-5 and hence aggrecanase activity, contradictory to our results. Further studies will be required in order to investigate how the role of IFT88 and the primary cilium results in this altered activity displayed by MMP-14 and TIMP-3.

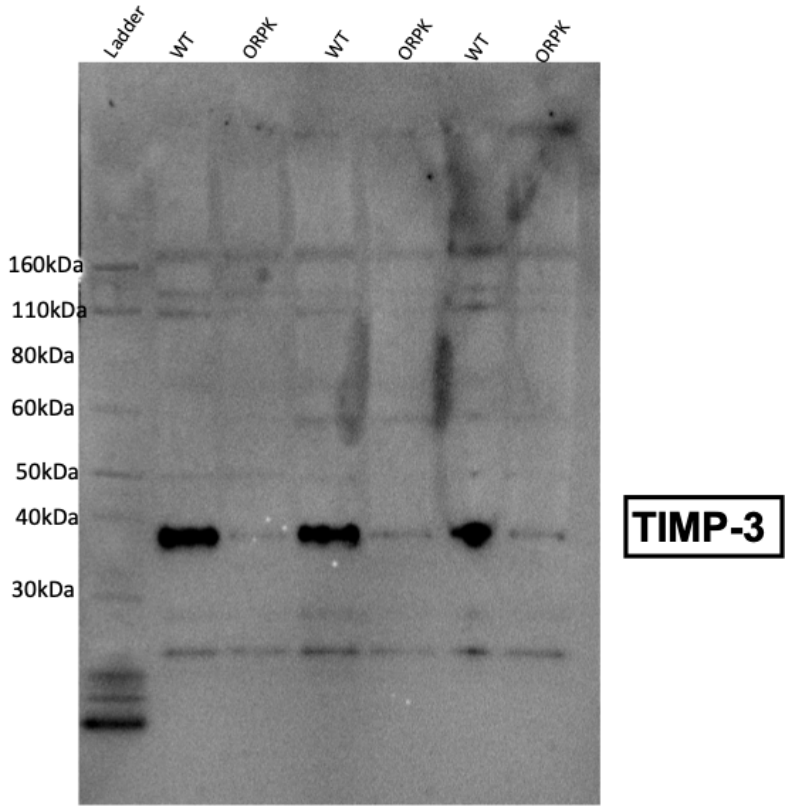


Figure 3.4.0.1: TIMP-3 protein expression is higher in WT than ORPK lysates. Western blot analysis of TIMP-3 in WT and ORPK chondrocyte lysates.

3.5 Conclusion

In conclusion, in this chapter, I have demonstrated preliminary data supporting a novel link between IFT88 and protease activity in chondrocytes. Additional work will be needed to explore the mechanisms behind this regulatory LRP-1 axis which has potential as a therapeutic target in OA.

4

Cartilage-specific inducible deletion of IFT88

I haven't failed. I've just found 10,000 ways that won't work- Thomas Edison

Contents

4.1 Introduction 140
4.2 Aims 146
4.3 Results 147
4.4 Protein 165
4.5 Histology of hip articular cartilage 168
4.6 AggrecanCreER^{T2};TdTomato reporter 170
4.7 *In vitro* deletion of IFT88 in primary rib chondrocytes 178
4.8 Discussion 183
4.9 Summary 194

4.1 Introduction

The only existing studies investigating the role of the primary cilium in post-natal development demonstrated that the organelle maintains influence in mouse cartilage tissues beyond embryogenesis.

Ciliary protein perturbation often leads to skeletal patterning abnormalities resulting in disturbed long bone elongation, often associated with shortening of the growth plate and thickening of the articular cartilage or changes to extracellular matrix composition (Haycraft and Serra, 2008; Yuan and Yang, 2015b). These developmental phenotypes have largely been attributed to disruption of ciliary regulated-Hh signalling (Clement et al., 2009b). However, the role of the primary cilium in musculoskeletal development beyond 4-weeks of age and in adult cartilage homeostasis is still unknown (Moore and Jacobs, 2018). Hence the ambitions of this chapter were to create an inducible cartilage specific deletion of IFT88 to explore its role in adolescent development, approaching skeletal maturity and adult homeostasis and disease.

The Cre-LoxP system is recognised as one of the most important technological discoveries enabling the study of gene function. In brief, flanking of a target gene by LoxP sites enables its deletion through the activity of the enzyme Cre recombinase (see methods x for more detail). Cre recombination takes place during interphase of cell division requiring the cells to be actively dividing in order to delete target genes. Placing the expression of Cre under desired promoters or enhancers can enable specific cell types or lineages to be targeted. Further, modifications to the

Cre enzyme itself by tagging an adapted estrogen receptor to the enzyme (*CreER*^{T2}) can enable for inducible targeting, through the administration of estrogen in the form of tamoxifen. Advantages include being able to control the timing of a deletion in a specific cell type, removing complications of potential developmental effects that could compromise the study. However, low levels of Cre recombination in inducible systems have been reported without the administration of tamoxifen and in undesired cell types, a phenomenon termed Cre 'leakiness.' To identify off target and unintended activity, reporter mice can also be combined with the temporal and inducible *CreER*^{T2} system, allowing for precise interrogation of lineage tracing. Incomplete recombination in all target cells has also been documented within these inducible mouse models (Stifter and Greter, 2020). Additionally, tamoxifen concentration required to activate Cre recombination can vary within mouse models, dependent on how the drug is administered (intraperitoneal injection or oral gavage) as this affects how the drug is metabolised and at what concentration it reaches target cell types. Some loxP genes are also recombined more easily dependent on their location within the genetic architecture of chromatin (Vooijs et al., 2001).

Within musculoskeletal tissue, many models have been generated in order to investigate the roles of genes in progenitor cells and

mature chondrocytes. Progenitor cells can be targeted using the following Cre drivers; *Prx1-Cre* (Logan et al., 2002), *Gdf-5-Cre* (Rountree et al., 2004), and *Sox-9-Cre* (Akiyama et al., 2005). To target mature chondrocytes, the most commonly used promoter is type II collagen (Col2), however, expression of Col2 in chondrocytes decreases spatially beyond 2-weeks of age (Nagao et al., 2016). As such, investigating the post-developmental roles of proteins in the cartilage has been difficult owing to inefficient recombination occurring in adult mouse chondrocytes using the promoter *Col2Cre* (Nakamura et al., 2006). In this study, the authors demonstrate that with age, Col2 expression decreases transcriptionally and dramatically changes where it is expressed, and it is no longer specific to chondrocyte cells (Nakamura et al., 2006). Another laboratory was able to demonstrate effective recombination using the *Col2Cre* promoter (Chen et al., 2007), but mice were given tamoxifen at 2-weeks of age, which is still early in post-natal development. Using the promoter of another characteristic chondrocyte protein, aggrecan, mouse models have been generated to target chondrocytes post-natally.

Aggrecan is a major proteoglycan of the ECM produced by chondrocytes of both the growth plate and articular cartilage. There are two mouse models that use the aggrecan gene to drive Cre expression. One model (Henry et al., 2009) was created by knocking

in the inducible recombinase construct *CreER^{T2}* downstream of the stop codon of the endogenous aggrecan gene (*Agc1$^{tm(IRES\text{-}creERT2)}$*). The other is used in this thesis and has been fully described in the next paragraph and in methods (Lo Cascio et al., 2014). However, these models using the aggrecan enhancer have not been used as widely as the Col2 enhancer models, with the majority of work focussed on developmental and hence embryonic cartilage, where Col2 expression is higher than aggrecan. Therefore, the aggrecan enhancer models are not as well characterised as relatively fewer studies have focussed on post-natal cartilage development.

In order to target mature adult chondrocytes, a mouse model generated at the Kennedy Institute of Rheumatology, utilising the aggrecan promoter was used (Lo Cascio et al., 2014). Four tandem repeats of the aggrecan enhancer from Henry et al 2009, were inserted upstream of the Col2a1 promoter, followed by insertion of *CreER^{T2}* between the regulatory elements, IRES and luciferase. Aggrecan is expressed in all cartilage rich tissues of the mouse, including the hip, knee, tail, xiphoid (unossified cartilaginous protrusion where the human sternum would be located), and paws as shown by the bioluminescent reporter (Fig. 4.1.0.1 B). This model is reported to have no off-target expression or effects (Lo Cascio et al., 2014). Aggrecan is expressed by chondrocytes during development and at skeletal maturity, hence, by using this

promoter, chondrocytes can be targeted in the post-natal and adult mouse (Lo Cascio et al., 2014). This mouse model is also an inducible system. The temporal control of deletion is important for the post-developmental deletion of genes. The *CreLoxP* system combined with the estrogen receptor has revolutionised conditional knockout mouse models. Cre recombinase is fused to a modified estrogen receptor, such that it does not bind to endogenous estrogen. This estrogen receptor also keeps the enzyme maintained in the cytoplasm. When tamoxifen (estrogen) is introduced, it binds to the estrogen receptor, enabling the Cre enzyme to translocate to the nucleus. All control animals $IFT88^{fl/fl}$ Cre negative mice also receive tamoxifen to mitigate for off-target effects of tamoxifen on bone (Zhong et al., 2015).

By crossing this inducible $AggrecanCreER^{T2}$ (Fig. 4.1.0.1 B) mouse with the $IFT88^{fl/fl}$ mouse (obtained from Jackson Laboratory) (Fig. 4.1.0.1 A), an inducible knockout model to delete IFT88 specifically in the cartilage was produced. The $IFT88^{fl/fl}$ mice (Cre negative) are the control mice in all experiments and receive tamoxifen at the same time-point as all $AggrecanCreER^{T2}$; $IFT88^{fl/fl}$ (cKO) mice. During this project, the $ROSA26CreER^{T2}$ mouse was also crossed with the $IFT88^{fl/fl}$ to create a whole body inducible knockout model, $ROSA26CreER^{T2}$; $IFT88^{fl/fl}$ (WBKO) (see methods for more details).

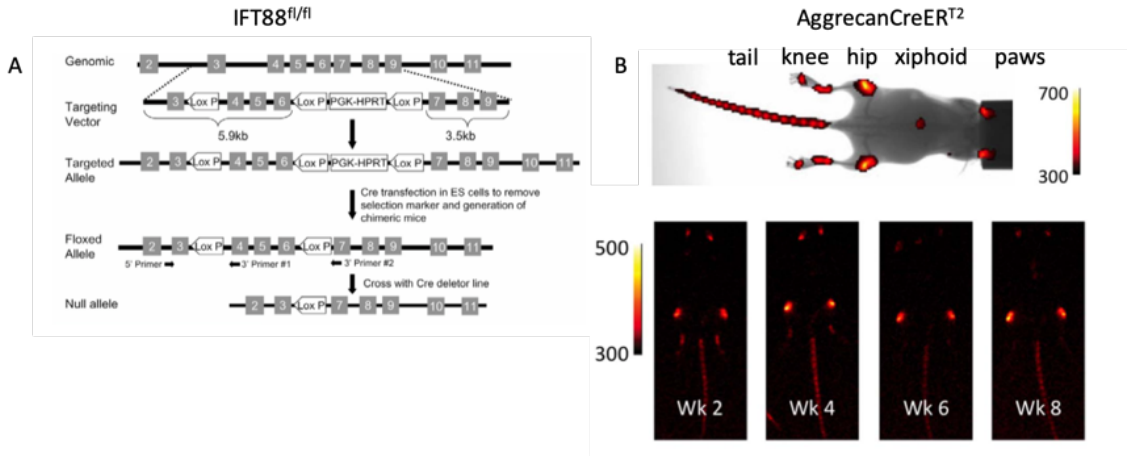


Figure 4.1.0.1: IFT88fl/fl and AggrecanCreER^{T2} mice.
A) Schematic illustrating flanking exon 4 and 6 in IFT88 gene. Figure reproduced from Jackson website. B) Aggrecan expression shown between 2- and 8-weeks of age in cartilaginous tissues including the knee, tail, hips, xiphoid and paws, using a bioluminescent reporter. Images adapted from (Lo Cascio et al., 2014).

4.2 Aims

1. To assess the *in vivo* inducible deletion of IFT88 using qPCR, western blot analysis and *in vitro* using RNA, isolated protein and immunofluorescence (IF).

2. To assess the localisation of Cre recombination as an indicator for deletion of IFT88 by crossing the AggrecanCreERT2 with a TdTomato reporter mouse line. Visualise through knee joint cryosections and IF.

4.3 Results

4.3.1 Genotyping

IFT88$^{fl/fl}$ mice were crossed with *AggrecanCreER*^{T2} mice. Genotyping was conducted on ear clips. DNA was extracted, amplified and analysed by gel electrophoresis. Floxed IFT88 produces a larger band size than un-floxed IFT88. Heterozygous (fl/WT) mice present with two bands (Fig. 4.3.1.1 A), in contrast to the single band produced by homozygous (fl/fl) animals. All animals in these results are homozygous (fl/fl). A sample known to be Cre positive was used as a control (Cre+ve). All animals in these results were found to be Cre positive (Fig. 4.3.1.1 B). Genotyping was conducted by myself periodically, however, mouse ear clippings were regularly sent to Jackson Laboratories for genotyping.

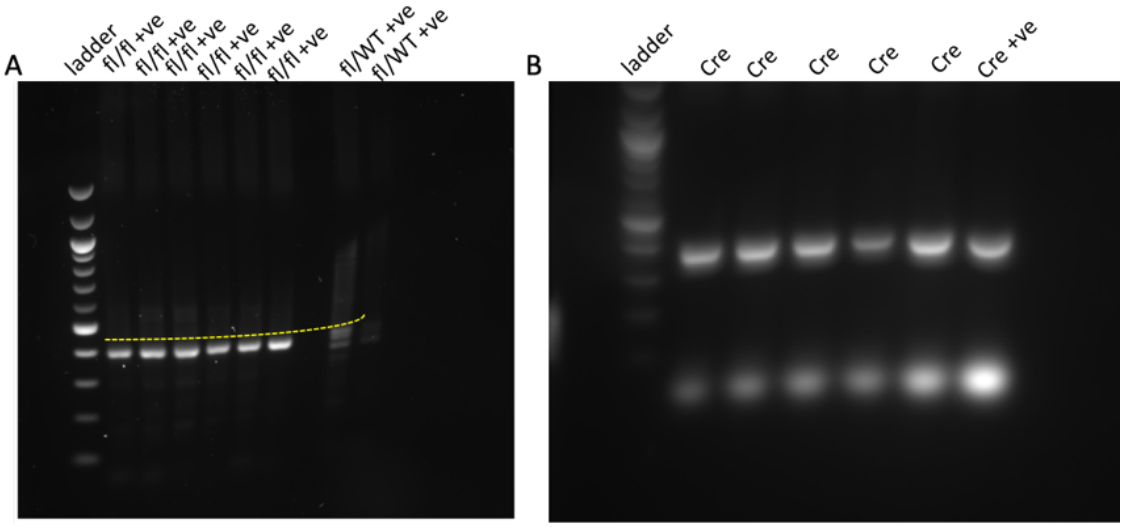


Figure 4.3.1.1: Cre and IFT88$^{fl/fl}$ identification of DNA isolated from mice.
A) Floxed IFT88 gene shown alongside heterozygous controls. A dotted line is used to show the floxed gene allele as the gel did not run straight. B) Cre positive DNA samples isolated from mice compared with Cre positive control.

4.3.1.1 Challenges of validation

It is important to understand the ability of the cKO mouse to delete IFT88 in cartilage tissue and ideally to be able to pair any phenotypic results to a deletion. Hence, a number of methods were used to fully understand and characterise the efficiency of the cKO mouse (Table 4.1).

Table 4.1: Challenges of validation and approach taken to understand the AggrecanCreER^{T2} system

	Challenges	**Experiment**
IFT88	Difficult to excise	Use a WBKO mouse to evaluate the efficiency of Cre mediated recombination and its capacity to delete IFT88.
	It is a low abundance protein	Compare expression of IFT88 between different tissues by qPCR
	Low turnover	Compare deletion of protein *in vivo* to that of *in vitro* systems
AggrecanCre	Not all cells express at any one time	Creation of a tomato reporter under the promoter of aggrecan. Cells expressing aggrecan shall activate reporter Cre recombination on administration of tamoxifen.
Cartilage	Low amounts found in the knee cartilage	Pool microdissected knee cartilage from 2-3 mice to analyse by qPCR.
	Hard to extract RNA from hip samples	Pool hip cartilage from 2-3 mice to analyse by qPCR.
	Hip ossifying	Histology of hip to assess phenotype of chondrocytes present within hip cartilage samples.

Table 4.1: Challenges of validation and approach taken to understand the AggrecanCreER^{T2} system

	Xiphoid	Isolate protein from cartilaginous rich sources.
	Ear	Potential for paired experiments with a cartilage rich source that could be analysed quickly by PCR.
	Tail	Potential for paired experiments with a cartilage rich source that could be analysed quickly by PCR.
Tamoxifen	Blood stream not delivering tamoxifen to all of the cartilage	Use tomato reporter to identify whether tamoxifen can penetrate to the deepest parts of the cartilage. Also isolate and culture chondrocytes from the rib cage to delete *in vitro* using tamoxifen. This will ensure delivery of the tamoxifen to all cells.

4.3.2 Expression of IFT88 in cartilaginous tissue: analysis of ear and tail DNA by PCR

Following administration of tamoxifen, *IFT88*$^{fl/fl}$ and cKO mice were sacrificed, and cartilage from the ear and tail was dissected. DNA was extracted from isolated cartilage, amplified and analysed by gel electrophoresis. No discernible reduction in IFT88 were observed in end-point PCR products from ear (E) or tail (T) samples from cKO mice when compared to control animals (Fig. 4.3.2.1). However, there is potential for contamination of cartilage samples by skin and bone. Due to this being end-point PCR, unless a very

robust deletion of IFT88 was achieved, small amounts of IFT88 DNA left would be amplified by the PCR protocol. Hence, this method was not used to validate the knockout of IFT88 in following experiments.

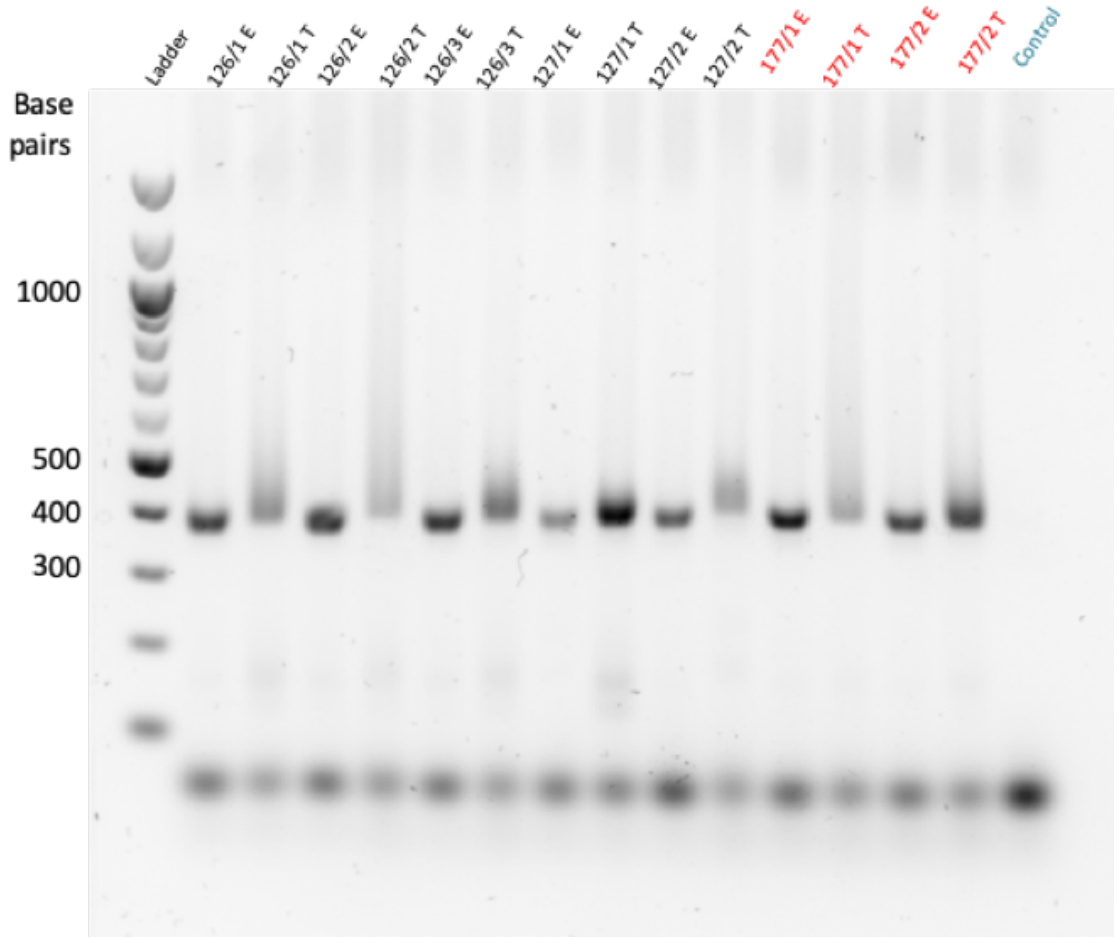


Figure 4.3.2.1: No reduction in IFT88 expression observed in cartilaginous tissues by end stage PCR.
Gel electrophoresis of ear (E) and tail (T) samples from cKO (black) and control ($IFT88^{fl/fl}$) (red) animals given tamoxifen. Water only control in blue.

4.3.3 Aggrecan expression profile

In humans, aggrecan is highly expressed in cartilage, but is also expressed in some soft tissues to include nerves (Fig. 4.3.3.1 A). In mice, aggrecan is also expressed in nervous tissue and other soft

tissues, though at lower levels than musculoskeletal and connective tissue (Fig. 4.3.3.1 B).

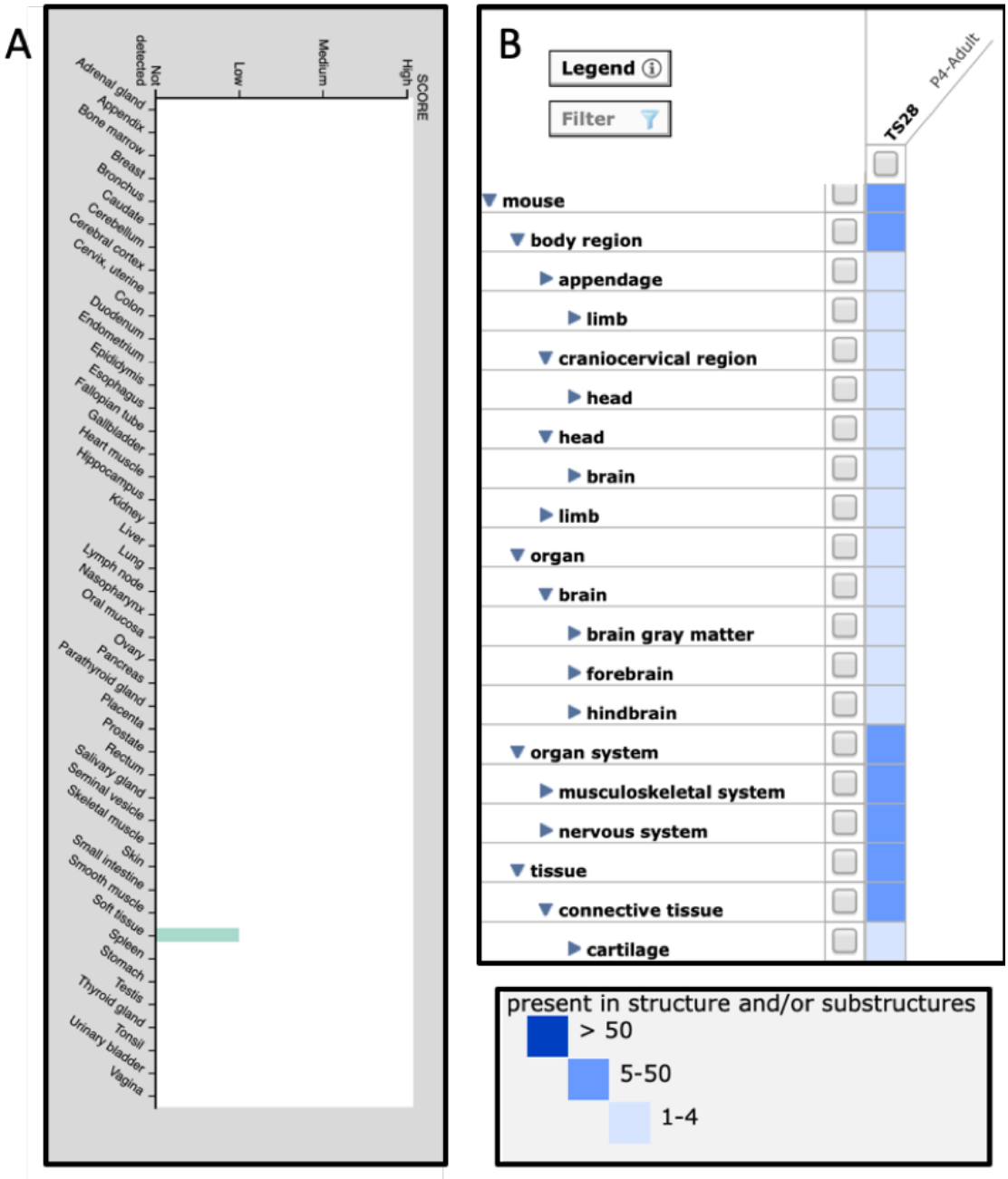


Figure 4.3.3.1: Aggrecan is expressed in cartilage and soft tissues in both humans and mice.
Table reproduced from Human Atlas (A) shows aggrecan is expressed at the level of RNA exclusively in soft tissues. Table (B) adapted from Mouse Genome Informatics (MGI) www.informatics.jax.org depicting RNA expression of aggrecan in mouse tissues.

4.3.4 IFT88 expression profile

Levels of IFT88 expression vary between tissues (Fig. 4.3.4.1), with the highest expression observed in the testis. The kidney and liver also have relatively high expression of IFT88 in comparison with other tissues with the kidney expressing higher amounts than the liver (Fig. 4.3.4.1 A). In mice, IFT88 is expressed through many of the organ systems similar to that seen in humans (Fig. 4.3.4.1 A) and also in connective tissue (Fig. 4.3.4.1 B).

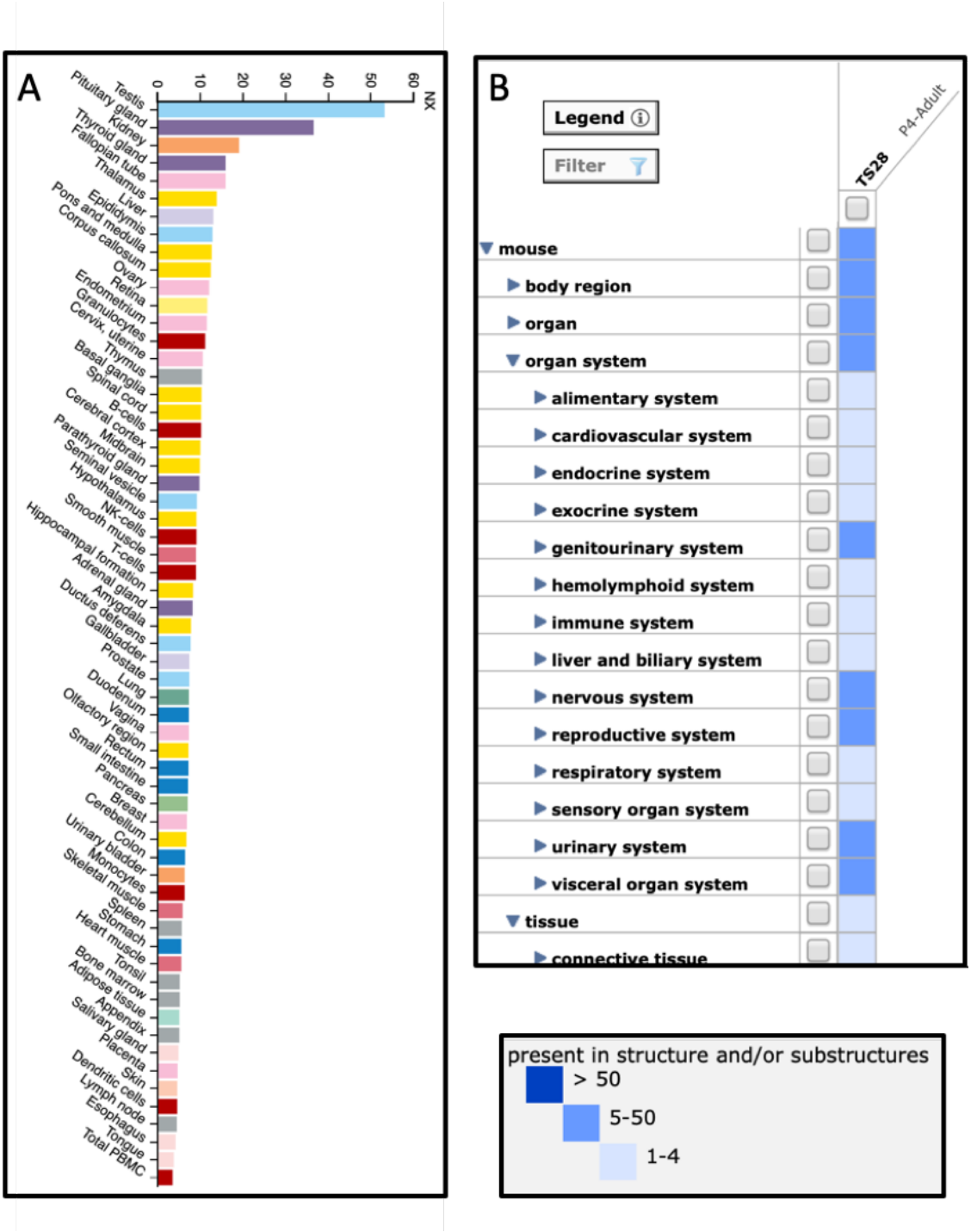


Figure 4.3.4.1: IFT88 is expressed across both human and mouse tissues.
Table reproduced from Human Atlas (A) shows IFT88 is expressed at the level of RNA across all tissues. Table (B) adapted from Mouse Genome Informatics (MGI) www.informatics.jax.org depicts RNA expression of IFT88 across all organ systems.

4.3.5 Relative expression of IFT88 in hip articular cartilage

RNA from hip cartilage, kidney, and liver samples at 10-weeks of age were compared for IFT88 expression in *IFT88*$^{fl/fl}$ mice. Relative IFT88 expression was similar between hip cartilage and liver samples (Fig. 4.3.5.1). In contrast, the kidney has approximately five-fold more expression of IFT88 than hip and liver samples in agreement with Human Atlas data.

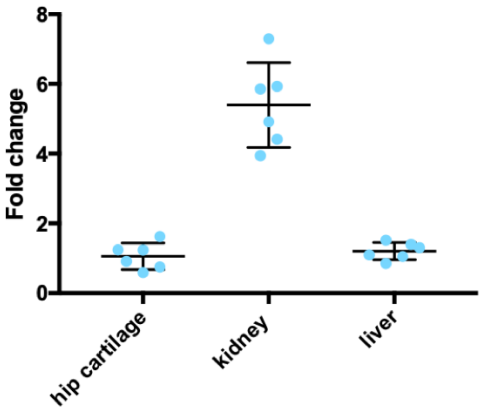


Figure 4.3.5.1: Relative expression of IFT88 across different tissues.
Expression of IFT88 in the kidney and liver was normalised to hip cartilage IFT88 expression at 10-weeks of age after normalisation to respective housekeeping gene 18S.

4.3.6 Relative hip cartilage expression of IFT88 with age

High 18S CT values were seen in all RNA samples isolated from the hip compared with liver and kidney samples, suggesting lower cell density in hip cartilage samples as the same 100ng of RNA was used for amplification across samples (Table 4.2). Even higher CT values for IFT88 were also observed, suggesting it is present in small amounts in these samples as demonstrated by the large

Delta CT. By comparing CT values between control animals at 6-weeks of age and 10-weeks of age, we can determine differences in IFT88 expression On comparing IFT88 expression in hip cartilage of 6- and 10-week old control mice, a three-fold decrease in IFT88 expression between these two time-points was observed. IFT88 expression between 6-and 10-weeks of age decreases and could increase the difficulty of identifying differences in IFT88 transcript expression between control and cKO samples especially at later time-points (Fig. 4.3.6.1).

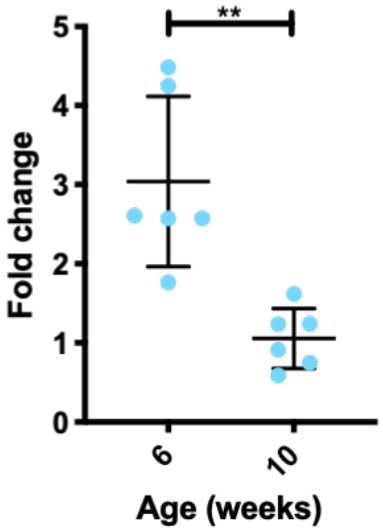


Figure 4.3.6.1: Hip cartilage IFT88 expression decreases between 6-and 10-weeks of age.
Fold change of IFT88 between 6- and 10-weeks of age. Data represents the mean ± SD (n=6). Statistical significance was determined using a Mann-Whitney U test where **p<0.01.

4.3.7 Assessment of IFT88 deletion in hip cartilage in cKO

4.3.7.1 Deletion at 4-weeks of age

The main aim of this thesis is to determine the role of IFT88 in mouse articular cartilage within the knee joint. However, with age, cartilage tissue volume decreases as it ossifies to form bone. Owing to this low abundance of tissue, at least 6 'knees' worth of cartilage would be required per n number. To reduce the number of animals required, hip articular cartilage was used as it has a larger surface area and is more abundant than knee cartilage.

Hip cartilage was removed from the hips by avulsion as at 6-weeks of age, 2-weeks post-administration of tamoxifen (4-weeks), to give a semi-sphere of cartilage shown in Fig. 4.3.7.1. Briefly, hips are dislocated from the hips socket and hip cartilage is gently squeezed and lifted off the femoral head using forceps. Six hip samples were pooled from 3 animals per n number. RNA was extracted from hip cartilage of cKO and control animals and was analysed by qPCR.



Figure 4.3.7.1: Hip articular cartilage.
Safranin-O staining of histological sections of avulsed hip cartilage. RNA is extracted from this piece of avulsed cartilage.

RTPCR analysis from hip cartilage at 6-weeks of age (tamoxifen treatment at 4-weeks of age)

RNA isolated from hip cartilage was revers transcribed to form complementary DNA (cDNA) prior to qPCR analysis. The 18S control genes produced average CT values of: IFT88$^{fl/fl}$= 24.62, and cKO = 21.50. The IFT88 control genes produced average CT values of: IFT88$^{fl/fl}$=29.41, and cKO = 28.78. The difference between the two CT values were calculated to find Delta CT. Average delta CT values of IFT88$^{fl/fl}$= 6.80 and cKO = 7.47 were found. The relative fold change in expression of IFT88 could then be calculated: IFT88$^{fl/fl}$= 1.05 cKO = 0.67. (IFT88$^{fl/fl}$: n=6 , cKO = 14).

Analysis of qPCR results showed that there was a difference in CT values between control and cKO samples, amounting to a reduction

in IFT88 equating to approximately 35%. CT values of 18S in cKO samples were lower than the *IFT88*$^{fl/fl}$ controls implying that cell density could have been higher in cKO samples than controls, given that 100ng of RNA was loaded per sample, perhaps indicating that it is not the most ideal control. CT values of IFT88 appeared to be lower in cKO than controls, but there was not as large a shift in 18S in the cKO (Fig. 4.3.7.2). As such, there was a larger shift in Delta CT values.

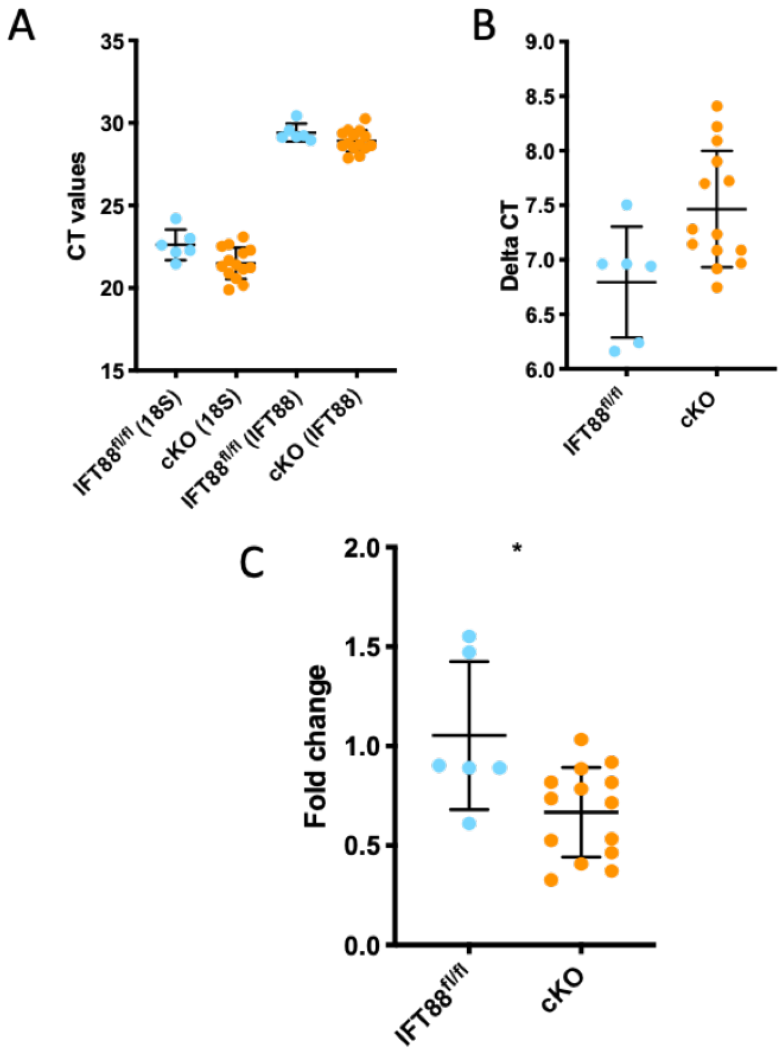


Figure 4.3.7.2: Tamoxifen induced a 35% knockdown of IFT88 in hip cartilage.
A) CT values of 18S and IFT88 in cKO and control animals. B) Delta CT values C) Fold change between control and cKO animals. Data represents the mean ± SD (n=6 controls, n= 14 cKO). Statistical significance was determined using a Mann-Whitney U test where *$p<0.05$.

4.3.7.2 Deletion at 8-weeks of age

By 8-weeks of age, skeletal growth in mice has slowed significantly, representing the earliest 'adult like' time-point. With age, articular cartilage ossifies and the growth plate thins increasing the risk of contamination and the difficulty of avulsion. Hip cartilage was avulsed from the hips at 10-weeks of age, 2-weeks post-administration of tamoxifen (8-weeks). Six hip samples were pooled from 3 animals per n. RNA was extracted from hip cartilage of cKO and control animals and was analysed by qPCR.

RNA isolated from hip cartilage was revers transcribed to form complementary DNA (cDNA) prior to qPCR analysis. CT values of 18S and IFT88 derived from qPCR data generated from RNA isolated from 8-week tamoxifen treated hips (A). The 18S control genes produced average CT values of: IFT88$^{fl/fl}$= 21.65, and cKO = 24.07. The IFT88 control genes produced average CT values of: IFT88$^{fl/fl}$=29.98, and CKO = 30.20. The difference between the two CT values were calculated to find Delta CT. Average Delta CT values of IFT88$^{fl/fl}$= 8.33 and cKO = 8.13 were found. The relative fold change in expression of IFT88 could then be calculated: IFT88$^{fl/fl}$= 1.03 cKO = 1.17. (IFT88$^{fl/fl}$: n=6, cKO = 5).

Analysis of qPCR results showed that there was very little difference in Delta CT values and hence no difference in fold change between

cKO and *IFT88*$^{fl/fl}$ values. Hence there was no detectable reduction in IFT88 expression in hip cartilage (Fig. 4.3.7.3). CT values of 18S in cKO samples were higher than the *IFT88*$^{fl/fl}$ controls implying that cell density was perhaps lower in the cKOs. CT values of IFT88 appeared to be no different between controls and cKOs.

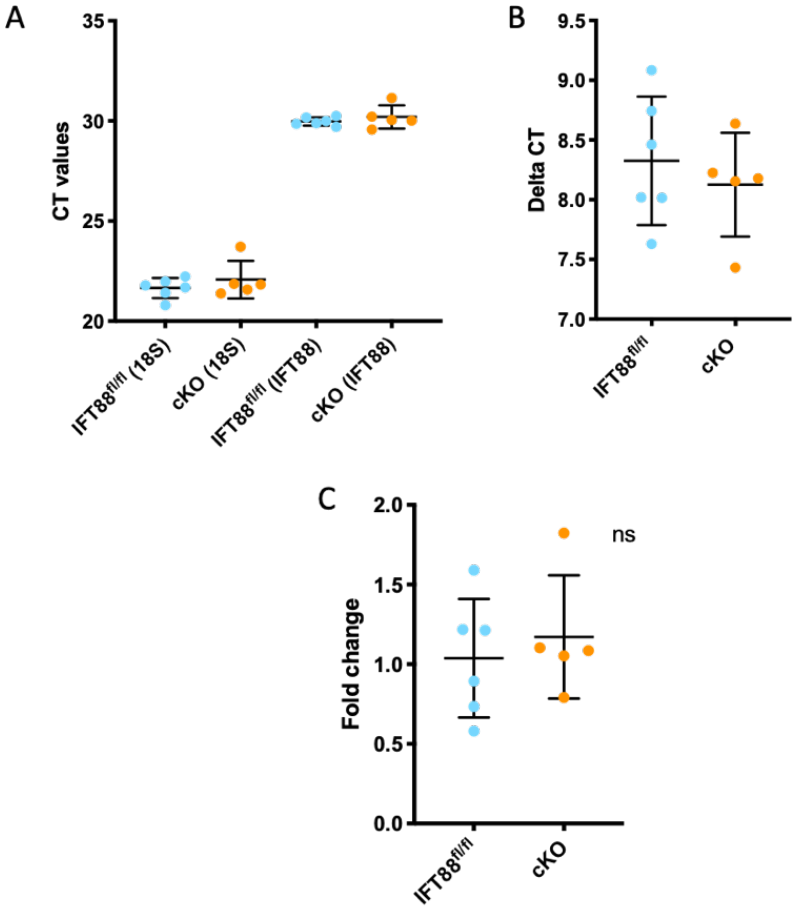


Figure 4.3.7.3: No measurable deletion of IFT88 observed in 10-week old mice.
A) CT values of 18S and IFT88 in cKO and control animals. B) Delta CT values C) Fold change between control and cKO animals. Data represents the mean ± SD (n=6 controls, n= 5 cKO). Statistical significance was determined using a Mann-Whitney U test.

4.3.8 Assessment of off-target deletion in non-cartilaginous tissues

A key aim of the approach was to specifically delete IFT88 in cartilage. To check for off-target deletion in the cKO mouse in other tissues, RNA from liver and kidney tissue was isolated from 10-week old mice to measure IFT88 expression 2-weeks post-deletion. Delta CT values and fold change were tabulated and compared between control and cKO samples (n=3). This confirmed that there was no off-target deletion observed in the cKO mouse post-administration of tamoxifen in liver and kidney tissues (Fig. 4.3.8.1).

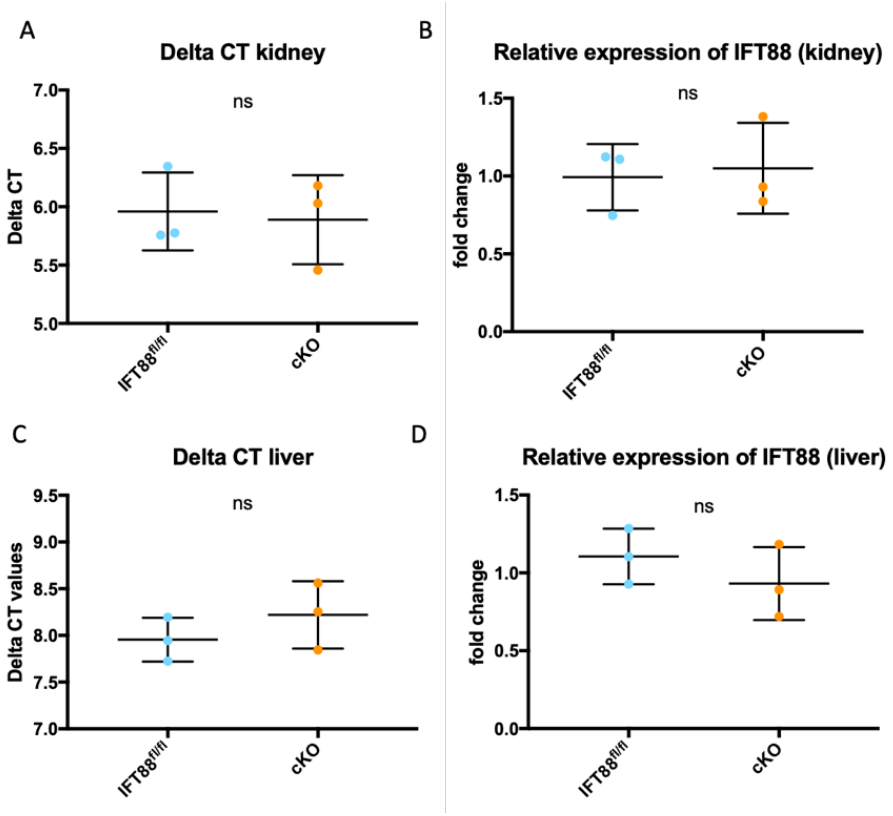


Figure 4.3.8.1: No off-target deletion of IFT88 in liver and kidney samples.
A) Delta CT values of IFT88 in control and cKO kidney samples. B) Fold change of IFT88 between control and cKO kidney samples. C) Delta CT values of IFT88 in control and cKO liver samples. D) Fold change of IFT88 between control and cKO liver samples. Data represents the mean ± SD (n=3 controls, n= 3 cKO). Statistical significance was determined using a Mann-Whitney U test.

4.3.9 Deletion of IFT88 using an inducible whole-body knockout Cre

Given our apparent inability to confirm reduction in expression of IFT88 in cartilage of adult mice and to establish the efficiency of recombination using flox alleles flanking IFT88, we made use of a pan-tissue or whole-body inducible knockout model (WBKO) targeting IFT88 with a Cre driven by the endogenous and ubiquitous mouse promotor ROSA26. This line was generated by crossing the *ROSACreER*^{T2} and the *IFT88*$^{fl/fl}$ mouse to create

ROSACreER^{T2};IFT88$^{fl/fl}$. RNA was isolated from liver and kidney samples from both control and WBKO mice 2-weeks post-tamoxifen administration at 6-weeks of age. All samples subsequently underwent RTPCR.

Administration of tamoxifen in WBKO mice resulted in a large shift in delta CT values in cKO samples compared with controls in liver samples (Fig. 4.3.9.1 A). Calculating fold change showed an approximate 75% decrease in IFT88 expression in the liver compared with the controls (Fig. 4.3.9.1 B). Administration of tamoxifen in WBKO mice resulted in a large shift in delta CT values in cKO samples compared with controls in kidney samples (Fig. 4.3.9.1 C). Calculating fold change showed an approximate 70% decrease in IFT88 expression in the kidney compared with the controls (Fig. 4.3.9.1 D).

These results suggest that the WBKO Cre is able to achieve a 70% reduction in IFT88, double that achieved by the cKO mouse (35% reduction) in cartilage samples. The use of the WBKO demonstrated that the Cre enzyme is able to succesfully access the genetic architecture where the floxed IFT88 gene is located to activate recombination. This diminishes the likelihood that the difficulty in deleting IFT88 is to do with its location within the chromatin. This also suggests there is no deficiency in the function of the floxed alleles in this mouse line. However, ROSA26 could be

more highly expressed than aggrecan, resulting in more successful recombination in the WBKO than the cKO.

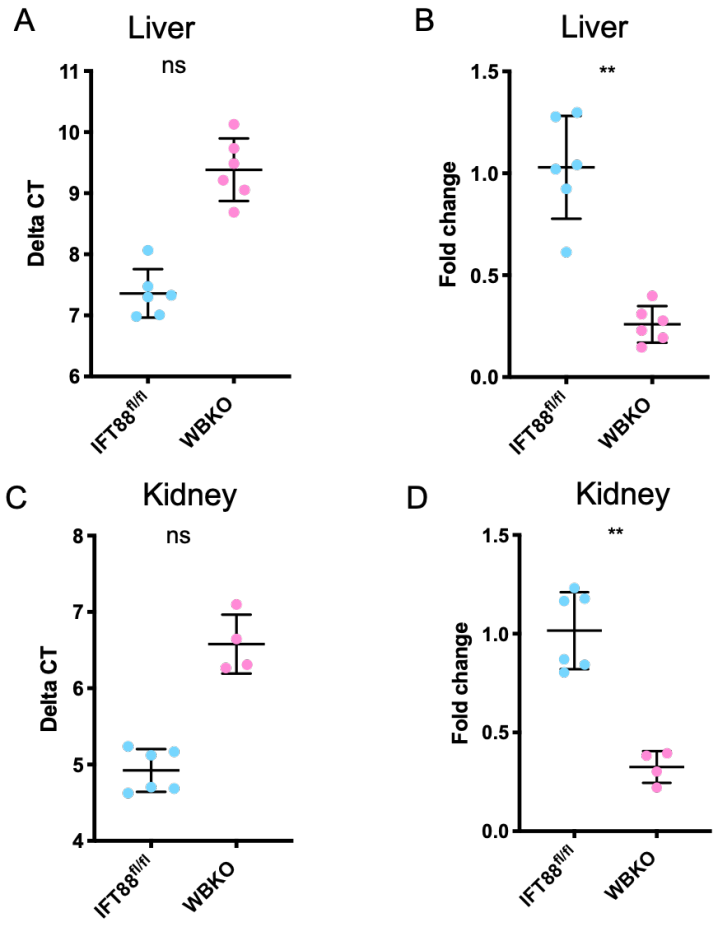


Figure 4.3.9.1: Deletion of IFT88 in liver and kidney samples.
A) Delta CT values of IFT88 in control and WBKO kidney samples (not significant). B) Fold change of IFT88 between control and WBKO kidney samples (not significant). C) Delta CT values of IFT88 in control and WBKO liver samples. D) Fold change of IFT88 between control and WBKO liver samples. Data represents the mean ± SD (liver samples: n=6 controls, n= 6 WBKO; kidney samples: n=6 controls, n= 5 WBKO). Statistical significance was determined using a Mann-Whitney U test where **p<0.01.

4.4 Protein

Results in section 4.3 illustrated the difficulty in achieving a reduction at the mRNA level of more than 35% in hip cartilage using the cKO. By using the WBKO, up to 75% of IFT88 could

be removed, demonstrating that the genetic architecture is not obstructing the deletion of IFT88 by the Cre enzyme. As many proteins are not solely regulated at the level of RNA, deletion of any gene, no matter how successful the recombination, is not always reflective of protein expression at tissue.

4.4.1 Assessment of IFT88 deletion at level of protein expression using xiphoid cartilage

Isolation of hip cartilage was predominantly used for analysis of deletion of IFT88 at the level of RNA, however, a larger source of tissue is required for quantification of protein via western blot analysis.

One of the most easily accessible sources of relatively large amounts of cartilage in the adult mouse is the xiphoid, a cartilaginous extension of the sternum usually ossified in humans. Xiphoid tissue was isolated from 6-week old cKO, *IFT88*$^{fl/fl}$ and 8-week old WBKO, mice 2-weeks after tamoxifen treatment.

Western blot analysis (Fig. 4.4.1.1 A) revealed an approximate 80% reduction in IFT88 in the cartilage of the WBKO in comparison with controls (Fig. 4.4.1.1 B). However, no statistically significant reduction in expression was observed in cKO cartilage in comparison with controls.

Establishing deletion of IFT88 in the WBKO demonstrated the

efficacy of the floxed IFT88 allele to significantly reduce IFT88 protein expression and that the Cre enzyme is able to access the floxed site within chromatin. However, this suggests that the cKO is not able to sufficiently delete IFT88 to observe a difference at the level of protein as is the WBKO.

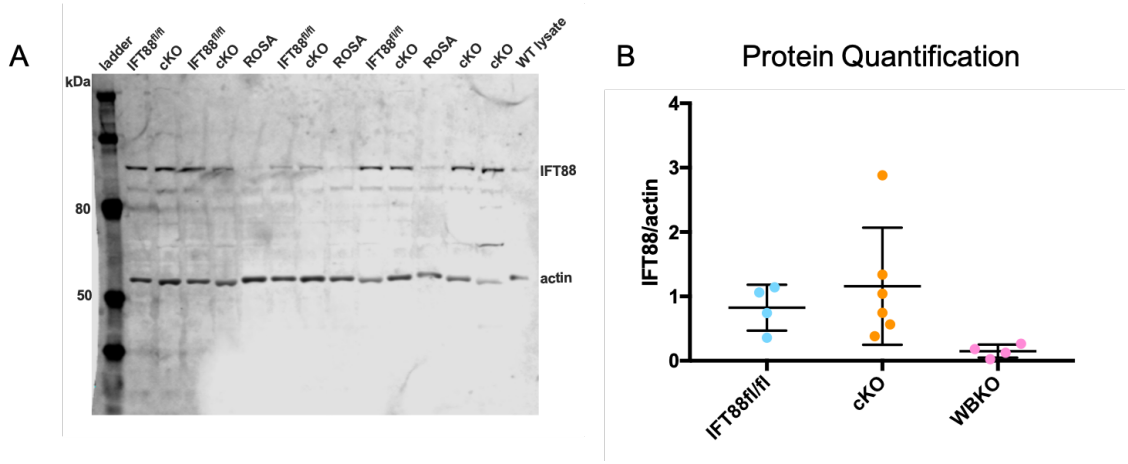


Figure 4.4.1.1: Deletion of IFT88 in xiphoid cartilage analysed by western blot.
A) Western blot analysis of IFT88 in cKO and WBKO xiphoid tissue 2-weeks post-deletion. B) Graphical representation of western blot analysis of IFT88/actin between control cKO and WBKO xiphoid tissue post-deletion. Data represents the mean ± SD ($IFT88^{fl/fl}$: n=4 animals, cKO = 6 animals, WBKO = 4 animals).

4.4.2 Protein expression of IFT88 in hip cartilage

Hip cartilage was isolated from 10-week old mice, 2-weeks post-tamoxifen administration from *IFT88*$^{fl/fl}$ and cKO mice. The hip joint was avulsed using the same method used to isolate the hip cartilage when isolating RNA. Hip cartilage of 2 animals (4 hips) was pooled and protein was extracted using RIPA buffer and vortexing to lyse the cells and extract protein. Samples were separated using gel electrophoresis, transferred to a PVDF membrane and the membrane was probed for IFT88. IFT88 relative

to actin showed no reduction in protein in comparison to the control (Fig. 4.4.2.1). Very low levels of IFT88 protein was seen in both control and cKO samples, suggesting that readily detectable levels of IFT88 protein could not be isolated from such a small cartilage sample.

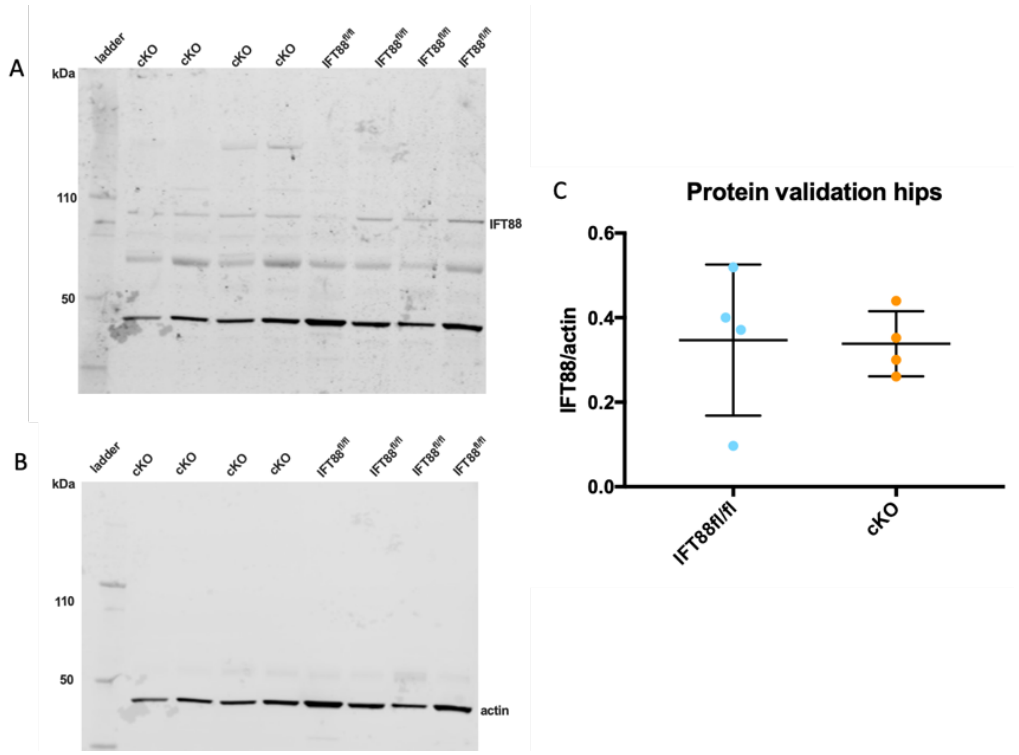


Figure 4.4.2.1: Deletion of IFT88 in hip articular cartilage analysed by western blot. A) Western blot analysis of IFT88 between control and cKO 2-weeks post-tamoxifen. B) Western blot analysis of actin between control and cKO 2-weeks post-tamoxifen. C) Graphical representation of western blot analysis of IFT88/actin between control and cKO samples post-tamoxifen. Data represents the mean ± SD (IFT88$^{fl/fl}$: n=4 animals, cKO = 4 animals).

4.5 Histology of hip articular cartilage

As the hip ossifies between 6-and 10-weeks of age introducing more bone and reducing the overall proportion of proliferating chondrocytes in the growth plate and superficial articular cartilage,

this could increase contamination of 10-week old samples with cells not expressing aggrecan. This contamination would decrease the chances of observing a deletion in the total sample by qPCR.

Using the cKO mouse line resulted in an approximate 35% reduction in IFT88 expression in hip articular cartilage between 4- and 6-weeks of age. We hypothesised that there could be cells within the articular cartilage that may not express aggrecan, such as hypertrophic chondrocytes. To assess populations of cells within the hip cartilage, whole hip joints and avulsed hip cartilage samples were harvested and prepared for histology (Fig. 4.5.0.1 A). Avulsed hip cartilage from mice aged 4- and 10-weeks was analysed by histology. At 4-weeks of age, there is a thin superficial layer of chondrocytes with a large hypertrophic region beneath. At 10-weeks of age, the superficial layer of chondrocytes appears to be qualitatively thinner than in 4-week old hip cartilage samples (Fig. 4.5.0.1 B and C). There is also a large region of hypertrophic chondrocytes that can be observed in 10-week old hip cartilage (Fig. 4.5.0.1 C). Hence, the limited reduction in IFT88 in these samples could be attributed to contaminating cells that do not express aggrecan at sufficiently high levels such as hypertrophic chondrocytes.

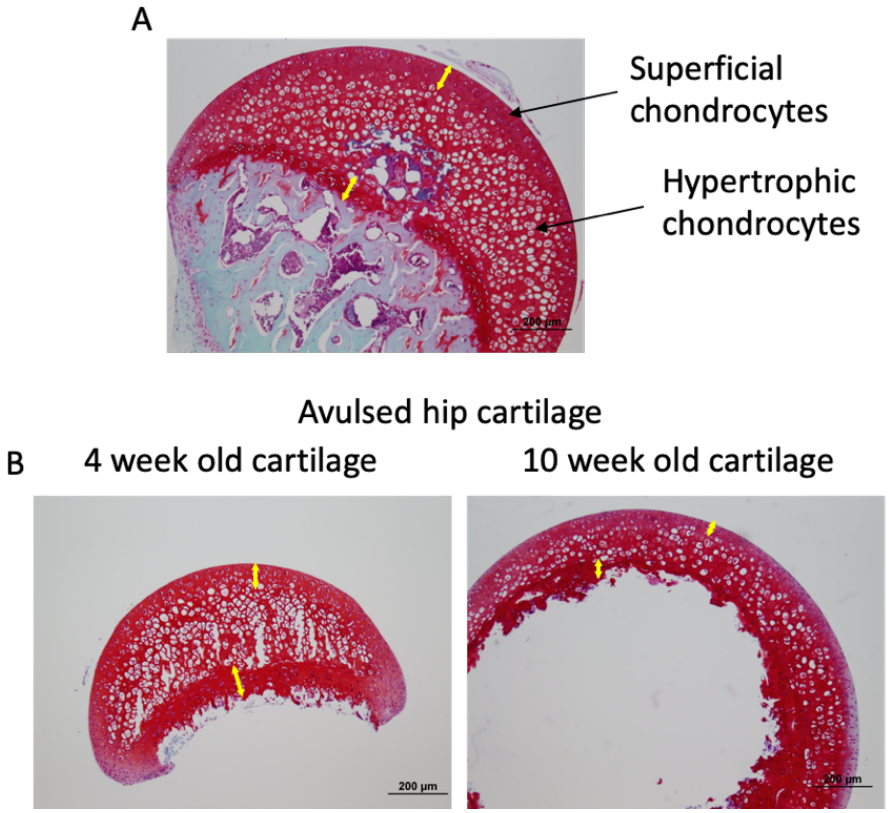


Figure 4.5.0.1: Histological sections of hip joints and hip articular cartilage.
A) Head of femur and hip cartilage from 10-week old mouse. B) Avulsed hip cartilage from 4- and 10-week old mice. Yellow arrows identify regions of superficial and hip growth plate chondrocytes most likely to express aggrecan.

4.6 AggrecanCreER^{T2};TdTomato reporter

4.6.1 Tamoxifen treatment (4-week) of AggrecanCreER^{T2};TdTomato

To understand the spatial activity of the *AggrecanCreER*^{T2} by visualising the location of chondrocytes that were undergoing recombination as a result of tamoxifen, the *AggrecanCreER*^{T2} was crossed with a tomato reporter mouse line to create *AggrecanCreER*^{T2};TdTomato. The administration of tamoxifen to the *AggrecanCreER*^{T2};TdTomato mouse activates the Cre enzyme to remove a floxed inhibitory STOP sequence within the TdTomato

gene in all aggrecan expressing cells resulting in expression of TdTomato.

Cre recombination at 6-weeks of age (2-weeks post-administration of tamoxifen at 4-weeks of age) was detected in the whole joint (Fig. 4.6.1.1 A), articular cartilage (Fig. 4.6.1.1 B), growth plate (Fig. 4.6.1.1 C), and hip cartilage (Fig. 4.6.1.1 D). Mice not treated with tamoxifen were used as a control. However, whilst there is Cre recombination within each of these cartilaginous populations, not every cell is demonstrating effective recombination. Knee and hip articular cartilage both show Cre recombination in a large majority of the chondrocytes. In knee cartilage, Cre recombination appeared to be consistent throughout the cartilage, driving in both superficial and deep zone chondrocytes (n=3) (Fig. 4.6.1.1 B). There is also no difference in Cre recombination between the lateral and medial plateaus. However, in hip cartilage, superficial chondrocytes demonstrate effective recombination whereas, deep zone or hypertrophic chondrocytes may not (Fig. 4.6.1.1 D). This could explain why RNA isolated from hip cartilage resulted in only a 35% reduction in IFT88. Within the growth plate, few columns of chondrocytes demonstrate Cre recombination (Fig. 4.6.1.1 C).

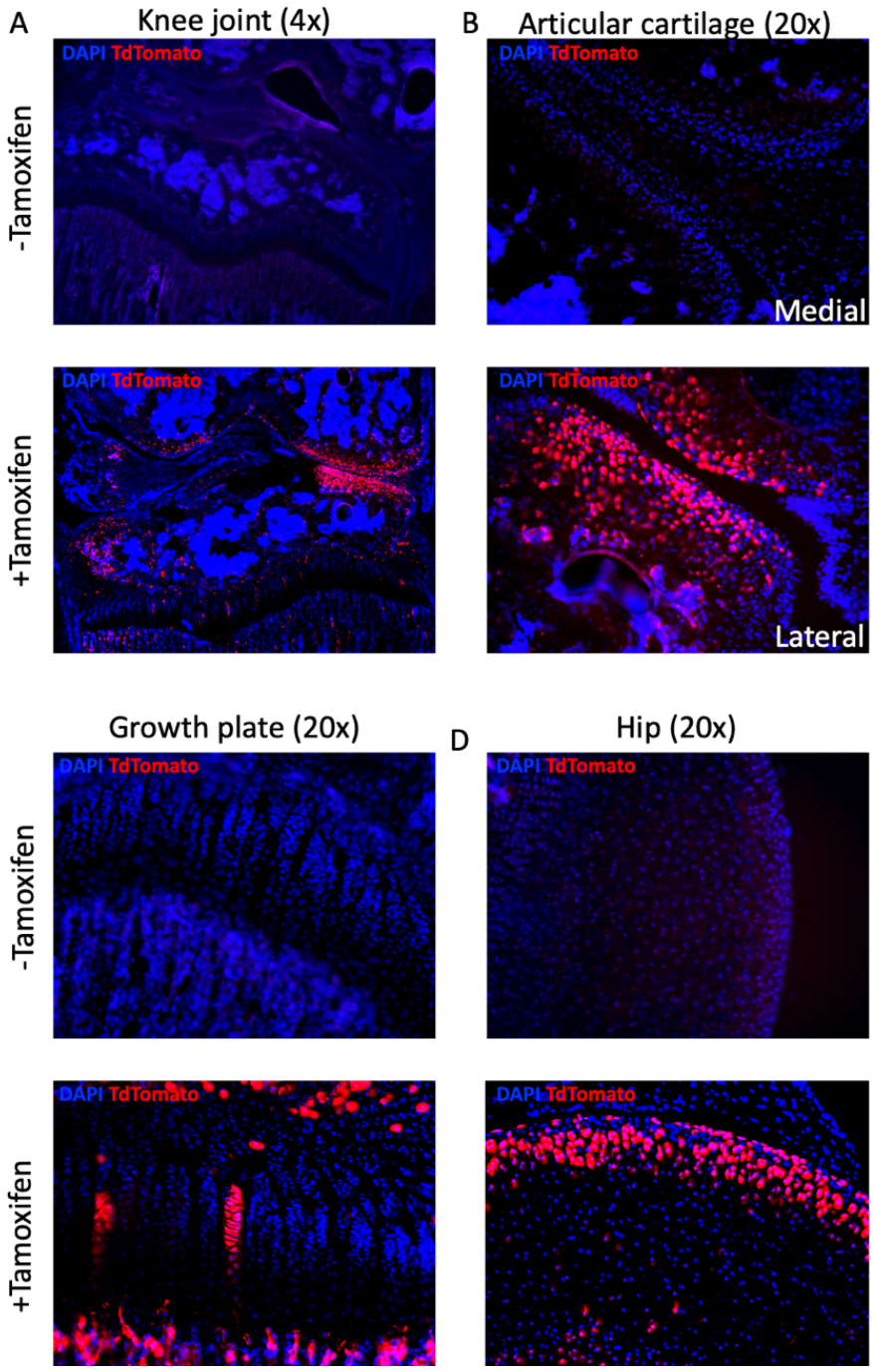


Figure 4.6.1.1: Cre recombination in cartilaginous tissue 2-weeks post-tamoxifen in AggrecanCreER^{T2};TdTomato reporter mice (6-weeks of age).
A) Whole joint sections (4x) from mice with and without tamoxifen treatment. B) Knee articular cartilage sections (20x) from mice with and without tamoxifen treatment. C) Growth plate cartilage sections (20x) from mice with and without tamoxifen treatment. D) Hip cartilage sections (20x) from mice with and without tamoxifen treatment. Sections were counterstained with the nuclear stain DAPI (1:5000) (n =3 with tamoxifen; n=3 without tamoxifen).

In order to confirm no off-target Cre recombination, kidney (Fig.

4.6.1.2 A) and liver (Fig. 4.6.1.2 B) tissues were also assessed. The tomato reporter confirmed that there was no Cre recombination in these tissues, further corroborating that there are no off-target effects in these animals.

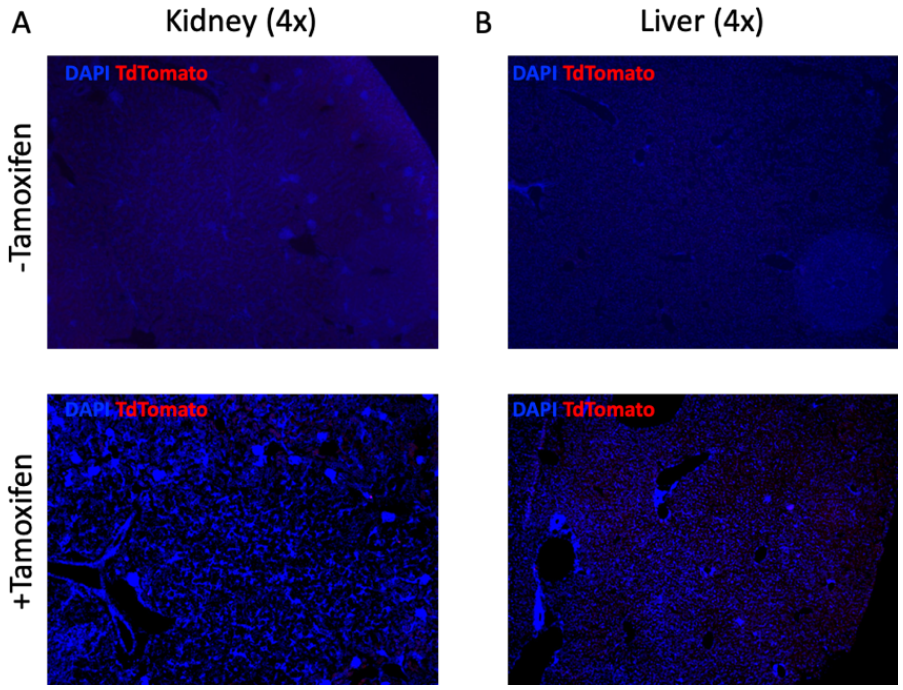


Figure 4.6.1.2: Cre recombination in kidney and liver 2-weeks post-tamoxifen in AggrecanCreER^{T2};TdTomato reporter mice (6-weeks of age).
A) Kidney samples (4x) from mice with and without tamoxifen treatment. B) Liver samples (4x) from mice with and without tamoxifen treatment. (n =3 with tamoxifen; n=3 without tamoxifen).

4.6.2 Tamoxifen treatment (8-weeks) of AggrecanCreER^{T2};TdTomato

Cre recombination at 10-weeks of age (2-weeks post-administration of tamoxifen at 8-weeks of age), was detected in the whole joint (Fig. 4.6.2.1 A), articular cartilage (Fig. 4.6.2.1 B), growth plate (Fig. 4.6.2.1 C), and hip cartilage (Fig. 4.6.2.1 D). Mice not treated with tamoxifen were used as a control. However, as seen at earlier time-points whilst there is Cre recombination within each of these cartilaginous populations, not every cell is demonstrating effective recombination. Knee and hip articular cartilage both show Cre recombination in a large majority of superficial chondrocytes. In knee cartilage, Cre recombination appeared to be consistent throughout the cartilage, driving in both superficial and deep zone chondrocytes (Fig. 4.6.2.1 B). There is also no difference in the ability of Cre to be activated between the lateral and medial plateaus. However, in hip cartilage, superficial chondrocytes demonstrate effective recombination whereas, hypertrophic chondrocytes do not (Fig. 4.6.2.1 D). As previously shown, there was no deletion or reduction in IFT88 observed at this time-point. Articular cartilage is an acellular tissue that ossifies and therefore could have been contaminated with hypertrophic chondrocytes or bone. Within the growth plate, few columns of chondrocytes demonstrate Cre recombination, but this Cre recombination was similar when compared with

4-week tamoxifen treatment (Fig. 4.6.2.1 C). Qualitatively, Cre recombination occurred at the superficial zone in articular cartilage, but this was observed in a thinner region of the cartilage in comparison with 4-week tamoxifen treatment.

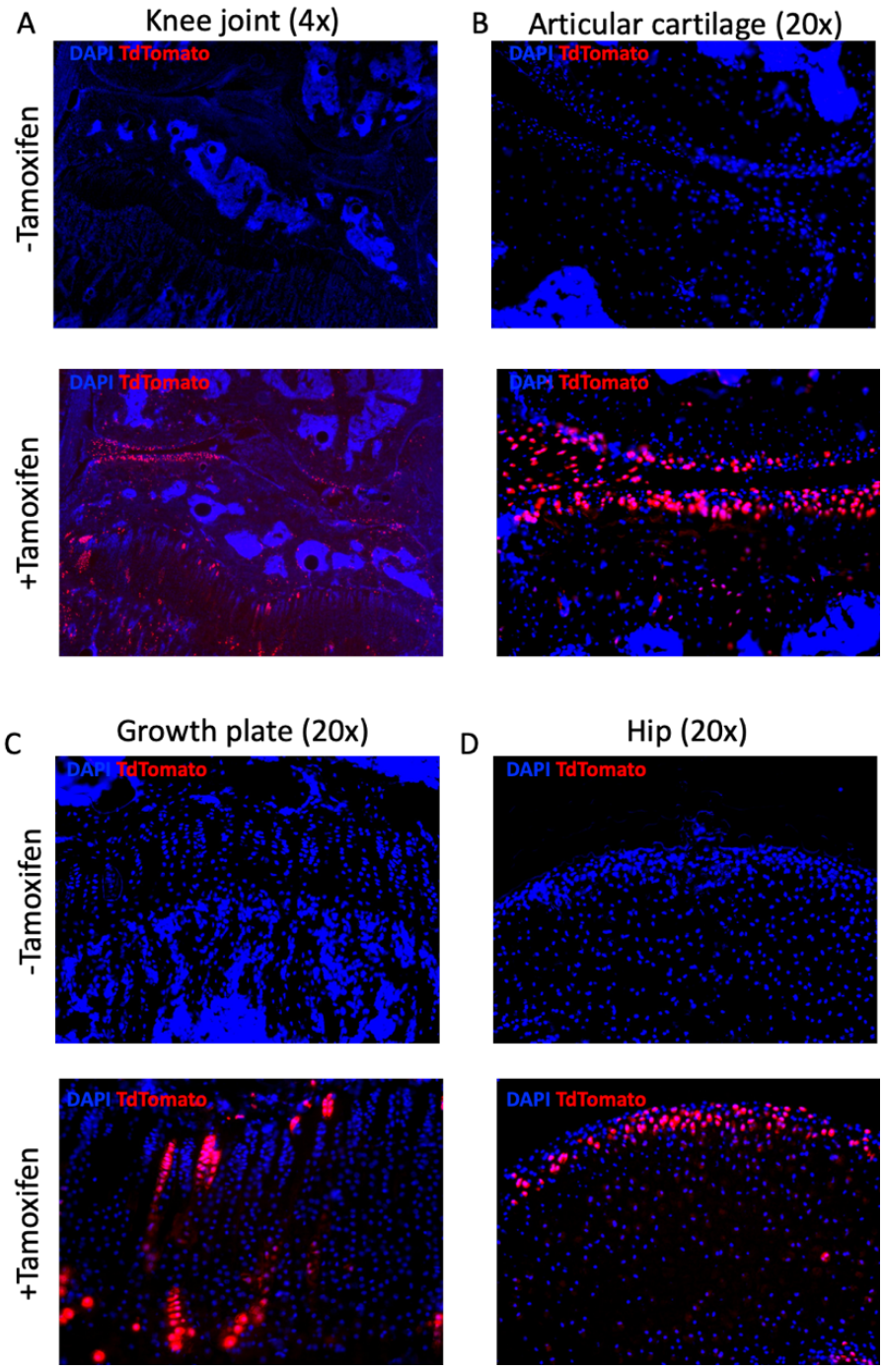


Figure 4.6.2.1: Activity of Cre in cartilaginous tissue 2-weeks post-tamoxifen in AggrecanCreER^{T2};TdTomato reporter mice (10-weeks of age).
A) Whole joint sections (4x) from mice with and without tamoxifen treatment. B) Knee articular cartilage sections (20x) from mice with and without tamoxifen treatment. C) Growth plate cartilage sections (20x) from mice with and without tamoxifen treatment. D) Hip cartilage sections (20x) from mice with and without tamoxifen treatment. (n =3 with tamoxifen; n=3 without tamoxifen).

Again, the tomato reporter confirmed that there was no Cre

recombination in kidney (Fig. 4.6.2.2 A) or liver (Fig. 4.6.2.2 B) tissues, further corroborating that there are no off-target effects in these animals.

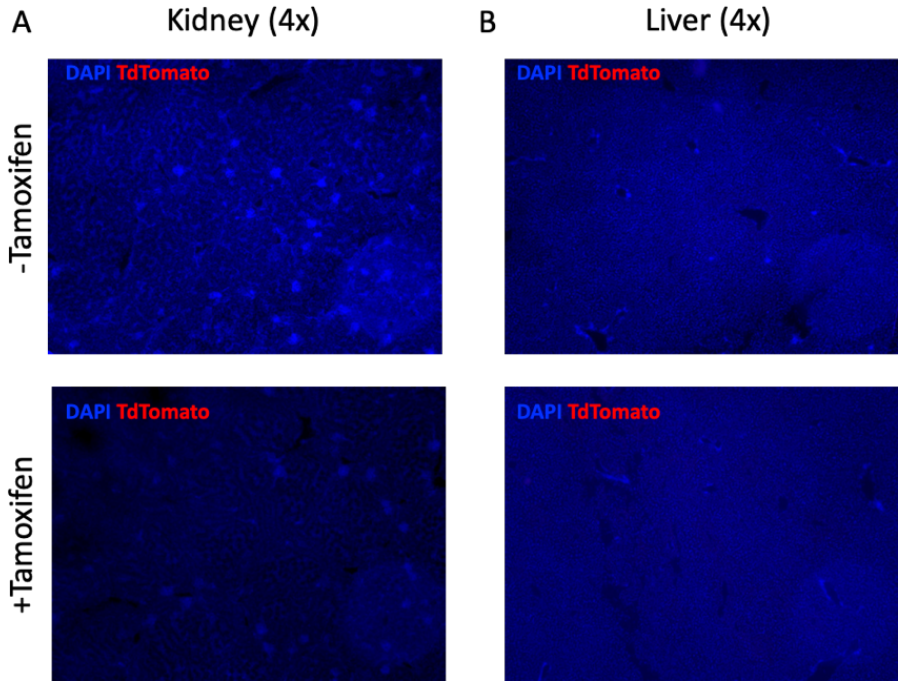


Figure 4.6.2.2: Activity of Cre in kidney and liver 2-weeks post-tamoxifen in AggrecanCreER^{T2};TdTomato reporter mice (10-weeks of age).
A) Kidney samples (4x) from mice with (below) and without (above) tamoxifen treatment. B) Liver samples (4x) from mice with (below)) and without (above) tamoxifen treatment. (n =3 with tamoxifen; n=3 without tamoxifen).

4.7 *In vitro* deletion of IFT88 in primary rib chondrocytes

4.7.1 RNA

In order to further characterise the deletion of IFT88 using the AggrecanCreER^{T2} mouse, chondrocytes were isolated from the rib cage of mice at 6-weeks of age. This aimed to remove the potential limitation of *in vivo* tamoxifen administration, and it not being able to penetrate the cartilage sufficiently to reach deep zone or growth plate chondrocytes. Chondrocytes were grown to confluence in conjunction with *in vitro* tamoxifen (4-OH) for 48-hours. RNA was then isolated from the samples for qPCR analysis. Results shown in Fig. 4.7.1.1 demonstrate an approximate 40% reduction in IFT88 (Fig. 4.7.1.1 C). This equates to a similar reduction seen in hip cartilage post-*in vivo* administration of tamoxifen (35%) .

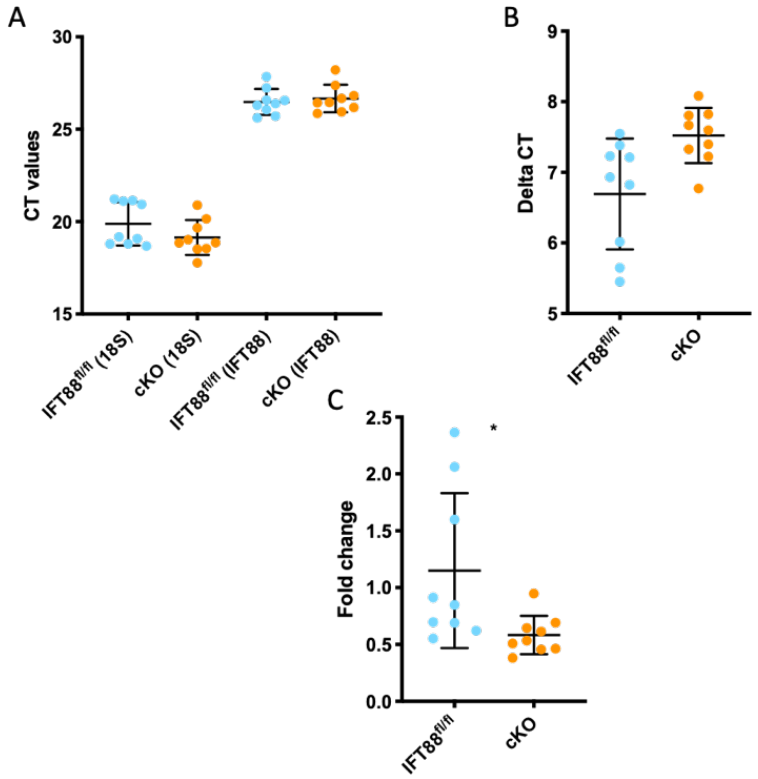


Figure 4.7.1.1: Deletion *in vitro* of IFT88 in rib chondrocytes analysed by qPCR. CT values of 18S and IFT88 derived from qPCR data (A). The 18S control genes produced average CT values of: IFT88$^{fl/fl}$= 19.88, and cKO = 19.14. The IFT88 control genes produced average CT values of: IFT88$^{fl/fl}$= 26.48, and cKO = 26.66. The difference between the two CT values were calculated to find Delta CT (B). Average delta CT values of IFT88$^{fl/fl}$= 6.69 and cKO = 7.52 were found. The relative fold change in expression of IFT88 could then be calculated: IFT88$^{fl/fl}$= 1.15 and cKO = 0.58. (IFT88$^{fl/fl}$: n=9 animals, cKO = 9 animals). These results demonstrate an approximate 40% deletion of IFT88 (C). Statistical significance was determined using a Mann-Whitney U test where *p<0.05.

4.7.2 Protein

Protein isolated from these same cells with a 40% mRNA reduction in IFT88 expression, did not show any depletion of IFT88 at the level of protein in comparison to controls by western blot analysis (Fig. 4.7.2.1).

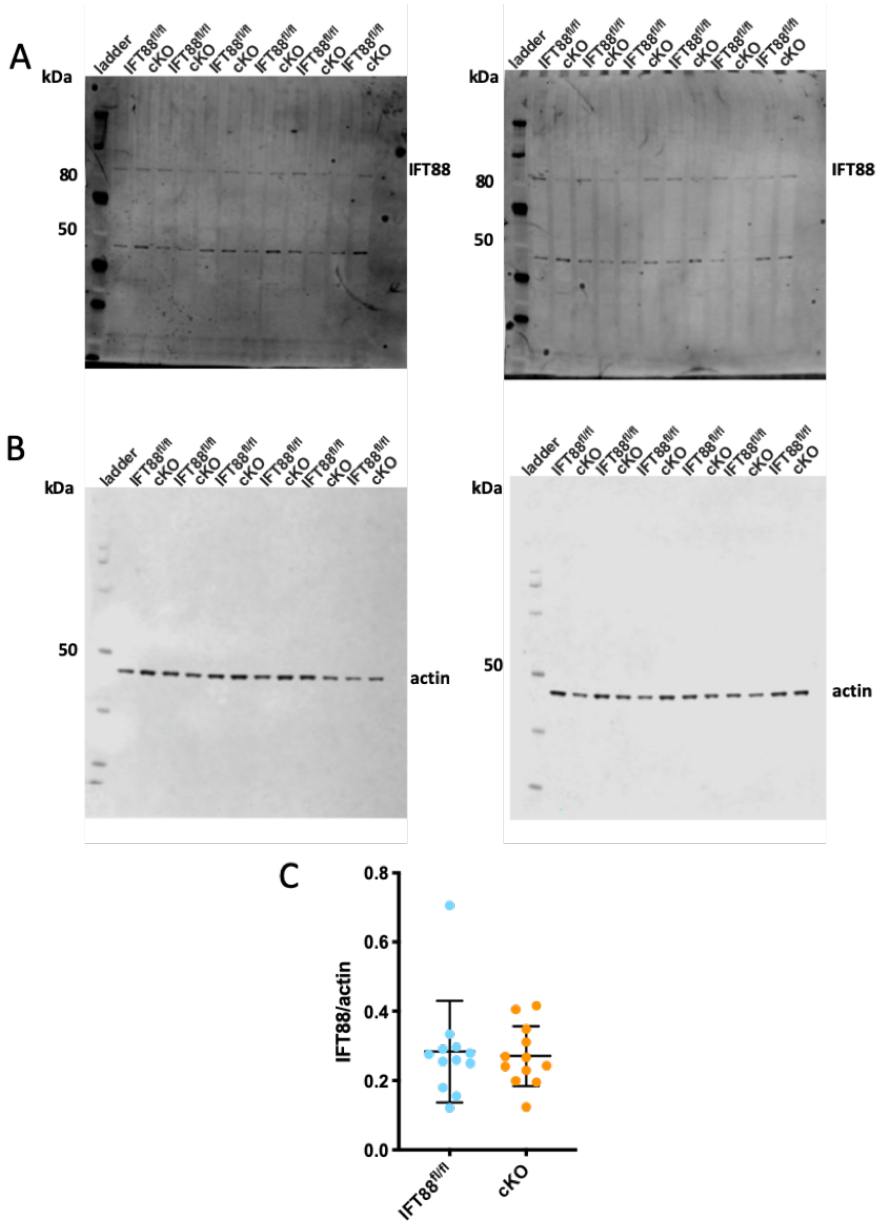


Figure 4.7.2.1: Deletion *in vitro* of IFT88 in rib chondrocytes analysed by western blot.
A) Western blot analysis of IFT88 between control and cKO chondrocytes post-deletion. B) Western blot analysis of actin between control and cKO chondrocytes post-deletion. C) Relative expression of IFT88 when adjusted to actin (not significant). Data represents the mean ± SD (IFT88$^{fl/fl}$: n=3 animals (4 replicates), cKO n = 3 animals (4 replicates)). Statistical significance was determined using a Mann-Whitney U test.

4.7.3 Immunofluorescence of rib chondrocyte primary cilia

In order to assess the effects of IFT88 deletion on the primary cilia structure, isolated rib chondrocytes were cultured, seeded, and

grown to confluence on glass and treated with *in vitro* tamoxifen. Cells were serum starved for 24 hours post-48-hour tamoxifen treatment. Serum starvation quiesces the cells and allows for cilium assembly. IF staining with AcαTub, Arl13b, and nuclear stain DAPI, marks the cilia structure and cell respectively (Fig. 4.7.3.1). There were no obvious qualitative cilia prevalence or length differences between control and cKO cells (n=3 animals). The morphology of the cells was qualitatively different between control and cKO chondrocytes, however, this could be attributed to differences in cell density. Chondrocytes isolated from the ribs of animals over 4-weeks old do not adhere to surfaces well.

Additionally, a 40% reduction in IFT88 at the mRNA level failed to remove protein as detected by western blot. This suggests that this level of deletion was not able to qualitatively alter cilia prevalence or appearance.

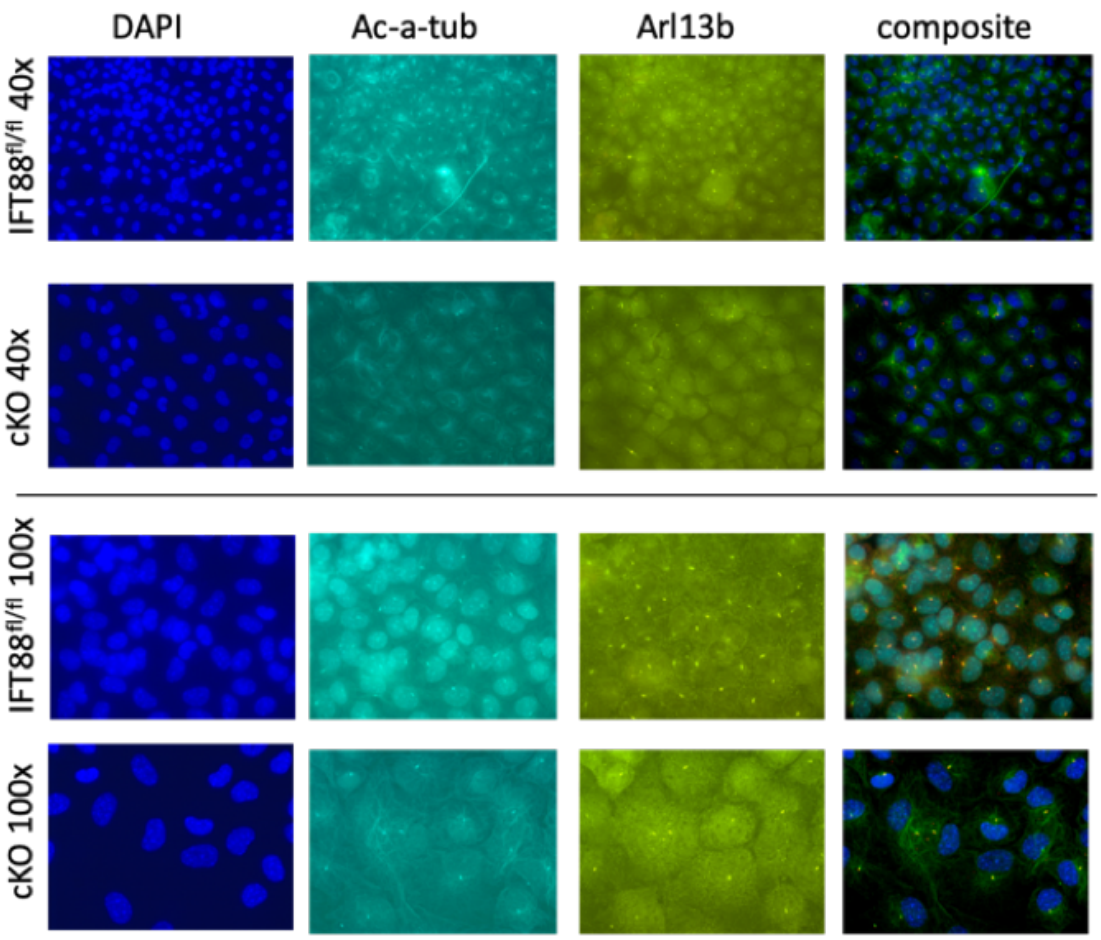


Figure 4.7.3.1: Immunofluorescent staining of rib chondrocytes.
Chondrocytes of control and cKO stained with AcαTub, Arl13b and nuclear stain DAPI at 40x and 100x. (n=3 animals for control and cKO).

4.8 Discussion

The purpose of this chapter was to describe the ability of the *AggrecanCreER^{T2}* driver to delete IFT88 in post-natal and adult cartilage.

There were some clear challenges I came across within this chapter:

1. Technical: Could I measure deletion of a low copy gene, in a subpopulation of chondrocytes within a small tissue sample without doing single cell analysis?
2. Biological: Could I discern the magnitude of the deletion, in what cell types, and in which locations?

I assessed the deletion of IFT88 both *in vitro* and *in vivo*. I successfully demonstrated an approximate 35% reduction in IFT88 by RTPCR in hip articular cartilage post-tamoxifen treatment at 4-weeks of age. This level of deletion was also observed by RTPCR in isolated rib chondrocytes treated with *in vitro* tamoxifen, but not at the level of protein. Cultured rib chondrocytes did not show obvious signs of disruption to the cilia structure post-reduction in IFT88. Additionally, I crossed the *AggrecanCreER^{T2}* with the TdTomato reporter mouse and identified disparate cartilaginous populations with activated Cre post-tamoxifen treatment at 4 and 8-weeks of age.

In theory, if aggrecan is expressed by all chondrocytes at the time that I administer tamoxifen, I should be able to isolate cartilage directly from cartilaginous regions dissected from the tail or ear to demonstrate a complete removal of IFT88. However, I was not able to show this with end-stage PCR, suggesting either incomplete recombination in all chondrocytes, or contamination of the sample by other tissues (Fig. 4.3.2.1).

On extraction of RNA from mouse kidney and liver samples, I found that the kidney had three-fold higher expression of IFT88 than liver samples, reflecting Human Atlas data (Fig. 4.3.4.1 A).

When validating the deletion of a gene in adult cartilage, many researchers at the Kennedy Institute of Rheumatology isolate hip cartilage rather than knee cartilage, as it is a more accessible, thicker and larger source of cartilage. Adult hip articular cartilage is an extremely acellular tissue that is difficult to avulse as the cartilage begins to ossify and integrates with the head of the femur. As seen by histology, 10-week old hip cartilage has a thin layer of superficial cartilage (Fig. 4.5.0.1) with aggrecan expressing chondrocytes seen in a small proportion of this layer as shown using the tomato reporter (Fig. 4.6.2.1). Thus, pure cartilage samples are difficult to obtain and the quantity and quality of RNA obtained can be low. Therefore, 6 hips from three animals were pooled. This could introduce some additional variability into the sample,

because if the deletion is not quite as efficient in one mouse than another, the deletion of IFT88 could be obscured. Interestingly, there is a three-fold decrease in IFT88 expression between 6-and 10-weeks of age, further increasing the difficulty of detecting a deletion of IFT88 in these older hip cartilage samples (Fig. 4.3.6.1).

Cartilage ossifies within the growth plate and the superficial articular cartilage thins with age, decreasing the amount of growth plate and superficial chondrocytes present in the hip sample, decreasing cartilage volume and increasing the difficulty of isolation. We hypothesise that owing to the high proportion of hypertrophic chondrocytes, and thus a lower proportion of aggrecan expressing cells, potential bone contamination, and pooling of hip samples resulted in an inability to detect a deletion in 8-week tamoxifen treated animals rather than a complete failure of the model at this time-point. However, by administrating tamoxifen at 4-weeks of age we did observe an approximate 35% reduction in IFT88 (Fig. 4.3.7.2). We hypothesise that in these samples there was a higher proportion of aggrecan expressing cells, fewer hypertrophic chondrocytes and it was more cellular than hip cartilage isolated at 10-weeks of age (Fig. 4.5.0.1).

As we had such difficulty validating this mouse model via RTPCR, and only observed a 35% deletion of IFT88 in cartilage samples, we hypothesised that potentially the IFT88 allele is

inherently difficult to delete owing to its location within the genetic architecture. Others have also commented, including Bradley Yoder and Courtney Haycraft, on the difficulty of deletion. We therefore tested this hypothesis by using a different Cre system by crossing the *IFT88*$^{fl/fl}$ with the whole body inducible *ROSACreER*^{T2} mouse line to generate *ROSACreER*^{T2};IFT88$^{fl/fl}$ (WBKO). The WBKO was able to achieve a 70% deletion of IFT88 within the kidney and 75% deletion in the liver (Fig. 4.3.9.1). We also established that the cKO exhibited no off-target deletion, with IFT88 mRNA levels unaffected by tamoxifen administration in kidney and liver samples (Fig. 4.3.8.1). These results confirmed that the *IFT88*$^{fl/fl}$ allele was working effectively. Of note, as the liver and kidney provide a source of cellular rich tissue, more RNA at a higher concentration and quality can be extracted in comparison to articular cartilage. Both RNA and protein expression of IFT88 are low, potentially impacting the ability to discern magnitude of IFT88 deletion. Interestingly, it also brought to attention the fact that a ubiquitous Cre driver, that is expressed in all tissues and by all cells, was only able to achieve a 75% maximum deletion. Hence, it might not be surprising that a much more specific Cre driver, such as the *AggrecanCreER*^{T2}, would not be able to achieve as measurable a deletion as a pan tissue knockout. Furthermore, the ROSA locus is highly expressed and could be expressed at a much higher level

than aggrecan, producing more Cre enzyme. This could result in higher levels of efficient recombination by the Cre enzyme in the WBKO than the cKO. The inability to produce a full deletion of IFT88 within cartilage tissue is a limitation of the cKO model.

Changes at the level of mRNA do not always correlate with that of protein. A large source of cartilage within the adult mouse is difficult to find and obtain. However, comparatively with the hip, the xiphoid is a large piece of tissue within the mouse that never ossifies and therefore remains cartilaginous throughout life. Xiphoid cartilage was isolated from 8-week old tamoxifen treated *IFT88*$^{fl/fl}$, cKO and WBKO mice, and were processed for analysis by western blot. The WBKO mouse was able to measurably reduce IFT88 protein in comparison to the control. However, the cKO animals were not able to affect any measurable level of deletion in comparison with the control (Fig. 4.4.1.1). Again, this potentially could be owing to heterogenous deletion within the xiphoid cartilage in comparison to the WBKO, which will delete ubiquitously. Indeed, on imaging the xiphoid of tamoxifen treated tomato reporter mice, we observed that some (yellow arrow), but not all cells were expressing aggrecan sufficiently to activate the tomato reporter, and there were contaminating cells (white arrows) (Fig. 4.8.0.1 below).

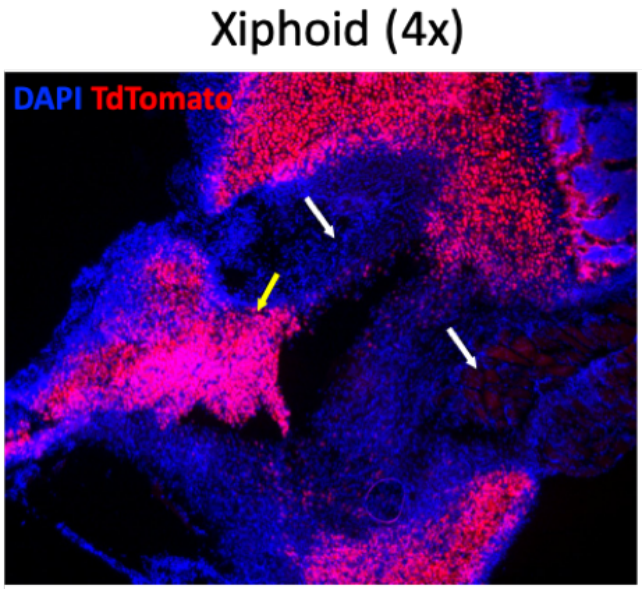


Figure 4.8.0.1: Aggrecan expression in xiphoid cartilage.
Cryosections of the xiphoid were imaged at 4x. Yellow arrow indicates aggrecan expressing cells glowing red. White arrows indicate chondrocytes not expressing aggrecan or other non-aggrecan expressing cell types.

In order to establish the deletion at the level of protein in articular cartilage, hip cartilage harvested from 8-week treated animals was processed ready for western blot analysis. Western blot analysis of IFT88 from hip cartilage samples showed no reduction in the levels of IFT88 when adjusted for actin (Fig. 4.4.2.1). However, at this time-point we were also unable to establish the deletion of IFT88 mRNA by RTPCR, so it is unsurprising we do not observe a deletion at the level of protein.

As I was unable to show a deletion at the level of both protein and RNA in hip cartilage, I looked at the histology of the hip cartilage (Fig 4.5.0.1). A large majority of the samples at both 4-weeks and 10-weeks of age contained hypertrophic chondrocytes.

Hypertrophic chondrocytes may not express aggrecan to the same extent as superficial chondrocytes and hence would not be able to delete IFT88, resulting in a potential masking of the deletion. I hence wanted to understand in which cells I was deleting in my samples to address this hypothesis. To understand this spatial activity of the *AggrecanCreER^{T2}*, I crossed this mouse line with the TdTomato reporter to generate *AggrecanCreER^{T2}*;TdTomato reporter mice. In this mouse line, the addition of the tamoxifen will activate the Cre enzyme, by allowing it to translocate from the cytoplasm to the nucleus. In aggrecan expressing cells of the *AggrecanCreER^{T2}*;TdTomato reporter mice, this can be used to remove the stop codon in front of the gene locus encoding TdTomato. Hence, if cells are glowing red, they are aggrecan expressing cells. This enabled us to understand what proportion of the chondrocytes were activating Cre post-tamoxifen administration and the location of these cells. This would test our hypothesis that we are only activating the Cre enzyme in a subset of chondrocytes.

When given tamoxifen at 4-weeks of age and harvested 2-weeks later, Cre recombination was found in superficial hip cartilage, knee articular cartilage, the medial meniscus, and growth plate cartilage (Fig. 4.6.1.1). However, not every chondrocyte within the articular cartilage of the knee or hip was TdTomato positive.

Within hip cartilage, hypertrophic chondrocytes did not exhibit Cre recombination, but deep zone knee articular cartilage chondrocytes were activated (Fig. 4.6.1.1 and Fig. 4.6.2.1). This mouse model also confirmed that injected tamoxifen was able to reach avascular articular cartilage. Additionally, only a few chondrocyte columns, presumably arising from daughter cells, within the growth plate exhibited Cre recombination. As so few columns are affected, it appears to be a relatively rare event. However, these sections are very thin and we are potentially missing the context of other columns being affected throughout the growth plate (Fig. 4.6.1.1 and Fig. 4.6.2.1).

Administration of tamoxifen at 8-weeks of age resulted in a qualitatively thinner population of the superficial cartilage expressing TdTomato in both the knee and hip in comparison with 4-week treated animals (Fig. 4.6.2.1 B and D). This could potentially reduce the population within these older samples of aggrecan expressing cells, reducing the ability to detect a deletion by qPCR. Growth plate chondrocytes were similarly activated in 8-week treated animals compared with 4-week treated animals. Tamoxifen administration did not result in any Cre recombination in liver or kidney tissues at either time-point, confirming there was no off-target Cre recombination, at least in these tissues (Fig. 4.6.1.2 and Fig. 4.6.2.2). Interestingly, some animals receiving

tamoxifen exhibited no Cre recombination at all, despite mice being homozygous positive for TdTomato and Cre (data not shown). This further highlights a limitation of this mouse model and could account for potential masking of deletion when samples are pooled. Additionally, this also suggests that aggrecan may not be expressed very highly within chondrocytes resulting in low levels of recombination and lower numbers of TdTomato expressing cells.

In hindsight, it would have been beneficial to cross the TdTomato with the *AggrecanCreER*^{T2};IFT88$^{fl/fl}$ mice as Cre recombination could have been matched with the level of deletion or phenotype and would have been able to confirm Cre recombination in specific animals. Additionally, animals expressing only AggrecanCre without a LoxP flanked target should be used as a control to account for toxicity or altered target gene expression resulting from LoxP insertion. To summarise, the reporter indicates that the Cre is showing recombination at 8-weeks but the population in which it activates in the hip, for example, is even smaller than at 4-weeks. The reporter additionally indicates that the efficiency of the Cre is not always consistent. Cre recombination requires cells to enter interphase in cell division. However, chondrocytes in adult tissues do not divide frequently and have a relatively low turnover, perhaps resulting in Cre recombination in a small proportion of cells. Collectively, this suggests mRNA analyses may be an underestimate

of the true efficiency of deletion in target cells.

The tomato reporter was very useful to understand in which cells and in what proportions Cre recombination was taking place. However, reporters do not necessarily represent accurate Cre recombinase activity as the efficiency of activating a reporter at one locus could have a very different efficiency at the target gene locus. The gold standard would be to isolate RNA from micro-dissected knee cartilage, which is underway, to investigate the deletion of IFT88 in this tissue. In order to understand the deletion on a single cell level, chondrocytes could have been isolated to enable reporter FACS sorting and subsequent deletion investigation, however, this requires extensive digestion steps to extract cells from the cartilage, compromising cell integrity and global gene expression. Further, the development of RNAScope technology which allows the visualisation of RNA expression at the level of the single cell within the tissue maintaining spatial resolution could have been used to confirm the deletion of IFT88 on a cell by cell basis. This would have been helpful to understand the proportion of cells that were undergoing Cre recombination and deleting the IFT88 gene.

Interestingly, a recent publication also described the limitations of using aggrecan as an inducible driver of Cre recombination within cartilaginous tissue of 5-week old mice. Whilst aggrecan

is very specific to chondrocytes, with very little off-target Cre recombination, it does not appear to be active throughout the tissue (Kitami et al., 2019). In this study they compared aggrecan, type II collagen (Col2) and Neuron glia antigen-2 (NG2) as drivers of Cre expression. NG2 encodes the ECM proteoglycan chondroitin sulfate. In comparison with the Col2a1CreER^{T2} and NG2CreER^{T2}, the *AggrecanCreER*^{T2} was active in very few cells. Additionally, we are able to replicate what has been observed by others about the *AggrecanCreER*^{T2} driver with our TdTomato reporter mouse, with only a small proportion of chondrocytes demonstrating Cre recombination. Whilst the authors focused on the temporomandibular joint (TMJ), this study supports the hypothesis this Cre may not be being activated in all chondrocytes within my mouse model.

Others have simply isolated chondrocytes to check deletion by *in vitro* methods. Here using articular rib chondrocytes, treated with tamoxifen, I observed an approximate 40% reduction in IFT88 by qPCR (Fig. 4.7.1.1). Despite this deletion, no difference was observed at the level of protein by western blot analysis (Fig. 4.7.2.1). We hypothesised that potentially a 40% reduction at the level of mRNA was not sufficient to reduce the levels of IFT88 to a discernible level for western blot analysis. As this level of deletion at the level of mRNA is similar to that observed in *in vivo*

tamoxifen treated hip cartilage isolated from the mice, it is evident that perhaps not all chondrocytes are expressing aggrecan at the time of deletion. Isolated rib chondrocytes were also cultured for easier imaging to visualise primary cilia. Primary cilia prevalence or length in cKO chondrocytes did not appear qualitatively different to control chondrocytes (Fig. 4.7.3.1). Work ongoing in the laboratory has demonstrated that a 90% siRNA deletion of IFT88 in the WT chondrocyte cell line results in an 80% reduction in cilia prevalence. This suggests that perhaps a 35% deletion of IFT88 is not sufficient to reduce cilia prevalence or length. This system, in future, could also be used to check cilia function by assessing the effects of IFT88 depletion on the Hh pathway.

4.9 Summary

The *AggrecanCreER^{T2}* mouse line is able to activate the Cre enzyme within articular cartilage within a subset of chondrocytes in both 4- and 8-week old mice, as shown by the TdTomato reporter mouse. Some populations within the medial meniscus and the growth plate are also targeted by *AggrecanCreER^{T2}*. The *AggrecanCreER^{T2}* is able to achieve an approximate 35% and 40% reduction in IFT88 in both *in vivo* and *in vitro* respectively. This appeared to have no discernible effects at the level of protein however, and did not appear to have a dramatic effect on cilia length and prevalence in

isolated primary chondrocytes. The challenges of validation and how they were addressed in this chapter are summarised in Table 4.8.

4.9.1 Summary of the challenges of validating this mouse model and how they were addressed

Table 4.2: Summary of the challenges of validating this mouse model and how they were addressed.

	Challenges	Experiment
IFT88	Difficult to excise	WBKO demonstrated that the Cre enzyme is able to excise the IFT88 gene.
	It is a low abundance protein	Not any lower than liver expression assessed by qPCR.
	Low turnover	Possibly low turnover *in vivo*, but siRNA deletion in an *in vitro* cell line of WT chondrocytes depleted 80% of protein within 48 hours.
AggrecanCre	Not all cells express at any one time	Tomato reporter showed limited number of cells within the cartilage showed recombination
Cartilage	Low amounts found in the knee cartilage	Microdissection of knee cartilage, pooled samples. Awaiting results.
	Hard to extract RNA from hip samples	Successfully isolated RNA from pooled hip samples from 2-3 mice.
	Hip ossifying	Hip ossifies in older mice. Hip cartilage isolated from older samples have far fewer aggrecan expressing superficial cartilage chondrocytes, potentially masking a deletion.

Table 4.2: Summary of the challenges of validating this mouse model and how they were addressed.

	Xiphoid	Potential contamination from other tissues, and not all sample expresses Cre to activate the TdTomato.
	Ear	Potential for contaminating tissues such as skin and hair. End point PCR amplifies any IFT88 present.
	Tail	Potential for contaminating tissues such as skin and hair. End point PCR amplifies any IFT88 present.
Tamoxifen	Blood stream not delivering tamoxifen to all of the cartilage	Tomato reporter doesn't discriminate between middle of the growth plate or the lateral sides. *In vitro* experiments conducted on rib chondrocytes showed tamoxifen was able to create a similar deletion to that seen *in vivo*.

5

The role of IFT88 in the adolescent growth plate and metaphysis

Everything has beauty, but not everyone can see- Confucius

Contents

5.1 Introduction 197
5.2 Aims 205
5.3 Results 206
5.4 Discussion 235
5.5 Summary 245

5.1 Introduction

As long bone elongation draws to a close during the adolescent phase of development, there is integration between two distinct, but overlapping processes; endochondral ossification and growth plate closure. Both of these processes are likely the result of the carefully timed integration of multiple signalling pathways and the organised differentiation of chondrocytes within the growth plate (Kronenberg, 2003).

In humans, the rate of growth plate closure varies throughout the

growth cycle. For example, during foetal development long bone growth rate is 100 cm per year which declines to less than 5 cm per year in childhood (Nilsson and Baron, 2004). This growth rate is briefly disrupted during adolescent growth spurts, before decelerating to a complete stop. As terminal length is reached at approximately 12-16 years of age in females and 16-19 in males, the growth plate fuses, ending bone elongation. This is not a trend found in other mammals where growth rate is more linear.

The growth plates are cartilaginous regions found at each end of the diaphysis that dynamically remodel to expand in length for the addition of bone and ultimate long bone extension. Growth plates achieve this through proliferation of chondrocytes at the end nearest to the epiphysis, and hypertrophic chondrocyte ossification nearest the diaphysis. As the long bone reaches its maximum length, proliferation of chondrocytes slows and halts, and the growth plate undergoes closure, narrowing until the epiphysis and diaphysis fuse (Fig. 5.1.0.1). However, in contrast with humans, this process is never fully completed in the mouse and a cartilaginous growth plate can still be seen by histology in mice at one year old.

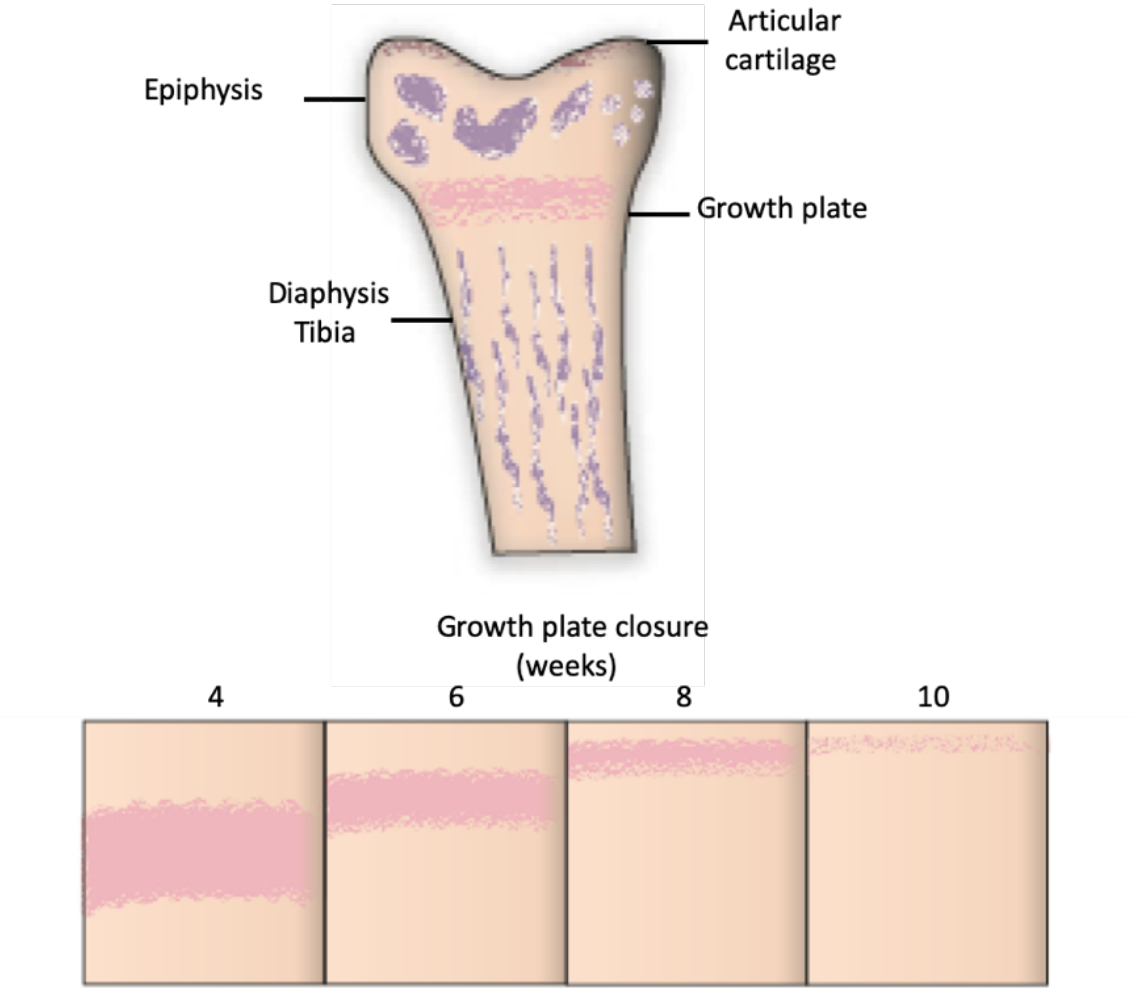


Figure 5.1.0.1: A schematic representation of tibial growth plate closure between 4-10-weeks of age. At the end of the tibial long bone, where it meets the femur at the knee joint, the epiphysis is lined with articular cartilage allowing for smooth articulation over the joints. The epiphysis sits on top of the growth plate. At the other end of the growth plate, is the diaphysis. The growth plate is responsible for elongation of the long bone, producing more template cartilage that can be ossified to bone. As terminal height is reached, production of this template slows whilst the remaining cartilage continues to ossify, resulting in narrowing of the growth plate, ultimately resulting in the diaphysis and epiphysis fusing. Here this schematic depicts growth plate closure in the mouse between 4-10 weeks of age.

The growth plate is made up of different chondrocyte populations that are responsible for the long bone elongation, hypertrophic, prehypertrophic, resting, and proliferative chondrocytes. Proliferative chondrocytes divide into strict columns at the edge of the epiphysis producing extracellular matrix and increasing growth

plate length. Simultaneously, columnar chondrocytes close to the diaphysis are becoming hypertrophic and laying down calcified matrix for subsequent ossification, and the invasion of osteoblasts and osteoclasts from the surrounding metaphyseal bone (Poole, 1991). These osteogenic cells undergo apoptosis, and the cartilage matrix is displaced with bone tissue by osteoblasts (Song et al., 2007). Recently, hypertrophic chondrocytes have been shown to transdifferentiate into osteocytes, in addition to undergoing apoptosis (Mizuhashi et al., 2018; Newton et al., 2019; Yang et al., 2014). This process maintains cartilage synthesis at one end of the growth plate, whilst enabling bone formation at the other end. This replacement of cartilage by bone depends on the cessation of matrix synthesis, the calcification of the cartilage by the surrounding hypertrophic chondrocytes and invasion of the vasculature from the metaphysis marrow (Kusumbe et al., 2014; Mackie et al., 2011) (Fig. 5.1.0.2). Whilst there is extensive literature on endochondral ossification and growth plate dynamics during embryonic and early development, comparatively little is known in the context of adolescent development and the final stages of growth plate closure.

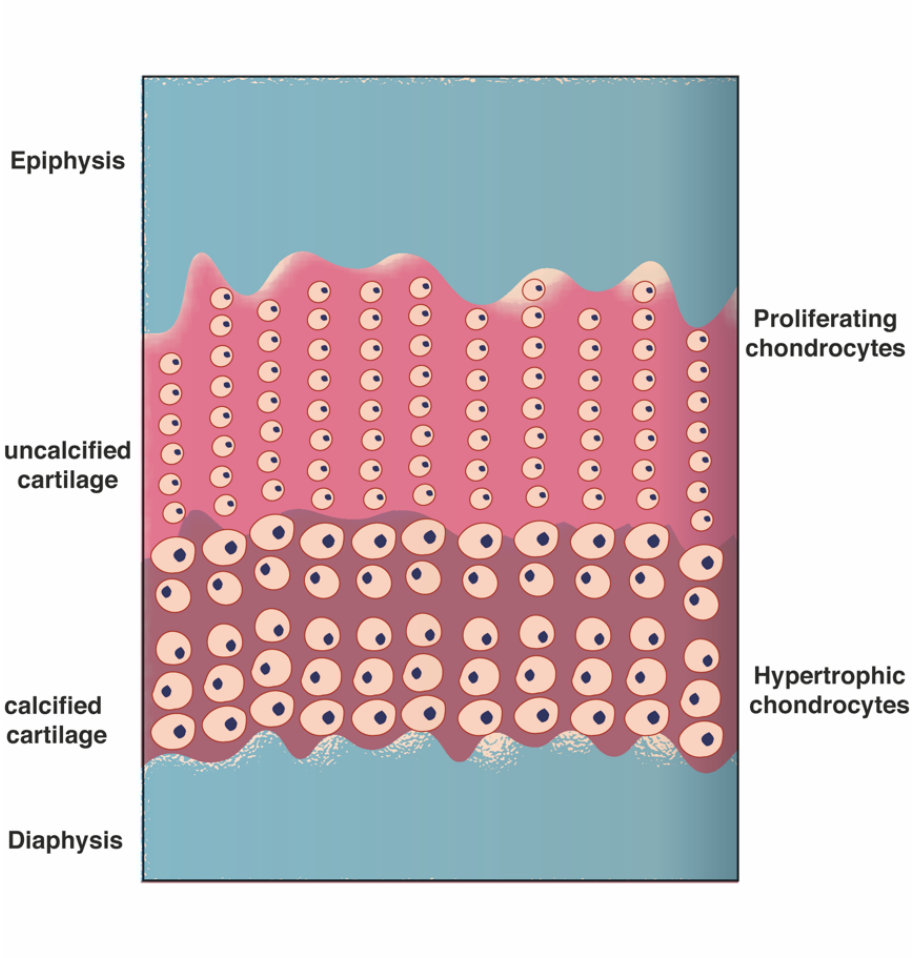


Figure 5.1.0.2: The growth plate. Schematic representation of the growth plate. Chondrocytes form long columns of cells. Proliferating chondrocytes close to the epiphysis elongate the growth plate. At the diaphysis, hypertrophic chondrocytes calcify their extracellular matrix in preparation for ossification and bone formation.

Research in embryonic development has demonstrated that growth plate dynamics are heavily reliant on the Parathyroid receptor related protein and Indian Hedgehog (PTHrP-Ihh) signalling axis, which is crucial to the organisation and differentiation of chondrocytes within the growth plate and their contribution to long bone growth (Racunica et al., 2007). The primary cilium is important for the regulation of Hedgehog signalling, and specifically Indian Hedgehog (Ihh) signalling within the growth

plate. Components of the Ihh pathway rely upon IFT88, hence removal of IFT88 may impact Ihh signalling and therefore growth plate development even during latter stages (Clement et al., 2009a; Haycraft et al., 2005).

There have been many models created to investigate the role of ciliary proteins and IFTs in embryonic development (Koyama et al., 2007; Maeda et al., 2007; McGlashan et al., 2007). Existing models, that have been used to remove IFT88 in cartilage, have been constitutive, thus affecting Ihh signalling during patterning of the embryo, significantly disrupting limb bud development (St-Jacques et al., 1999) and joint formation (Chang et al., 2012; Song et al., 2007). This confounds any interpretations pertaining to IFT88's role in adulthood. However, during embryonic development, limb bud specific Ihh deletion results in profound cartilaginous and subsequent skeletal phenotypes, including premature growth plate fusion and dwarfed long bones (Amano et al., 2016; Amano et al., 2015). Hence as Ihh has been shown to be important for growth plate dynamics and IFT88 has been shown to be important for Ihh signalling, we hypothesise that IFT88 will have a persisting role in the adolescent growth plate. These studies are crucial to our hypothesis.

Mechanical forces or loads resulting from weight bearing or muscle contraction have long been known to be important in

skeletal development and adult homeostasis. Additionally, the primary cilium in other cell types, including osteocytes and kidney epithelial cells, have long been thought to be 'mechanosensitive' organelles, bending in response to mechanical stimuli, such as fluid flow shear stress, to initiate intracellular calcium signalling (Delling et al., 2013b; Nguyen and Jacobs, 2013). Indeed, chondrocytes harbouring the ORPK hypomorphic mutation to IFT88, fail to induce matrix synthesis in response to mechanical load (Wann et al., 2012). *In vivo* studies on young chicks have established that increasing mechanical weight bearing load by 10% of body weight for 2-4 days using weighted bags, accelerates growth plate ossification and vascularisation (Reich et al., 2005). This group went on to show that mechanical loading alters the Ihh-PTHrP loop and affects subsequent proportions of hypertrophic and proliferating chondrocytes. Additionally, they also showed that mechanics also upregulates ciliary proteins IFT88 and KIF3A, coinciding with increased cilia prevalence in chondrocytes (Rais et al., 2015). Collectively, these studies raise the possibility that the primary cilium/IFT88 may play a role in growth plate chondrocyte mechanotransduction and thus growth plate dynamics.

Mechanical loads have also been shown to be very important in interzone cavitation and joint development (Murray and Drachman, 1969; Osborne et al., 2002; Pitsillides, 2006). Ihh

is also known to be mechanosensitive in chondrocytes, with Ihh being upregulated 18-fold in response to cyclic stretch culture in comparison with non-stretch cultures (Wu et al., 2001). Mechanics is also very important for the latter stages of skeletal development in adolescence. For example, this is observed in Osgood-Schlatters disease, where excessive high impact loading in teenagers results in painful swelling of growth plate cartilage (Ladenhauf et al., 2019), and associated with sub-patellar pain arising from an unfused bipartite patellar. However, very few studies investigate adolescent skeletal development. The only documented post-natal cartilage-specific deletion of an IFT, was conducted within the first 4-weeks of life and targeted IFT80, a protein, like IFT88, that is a component of the IFT-B complex in anterograde trafficking (Yuan and Yang, 2015b).

Understanding the normal physiology of this complex dynamic pathway in the final stages of endochondral ossification is insightful to our understanding of pathophysiology and physiological repair mechanisms. Growth plate cartilage is uniquely dynamic in its ability to remodel and regenerate. Research into pathways upregulated in wound healing processes has revealed evidence that matrix is repaired and the developmental pathways Ihh, Wnt and Notch were upregulated (Bielefeld et al., 2013). Interestingly, in human OA, the developmental pathway Ihh is also upregulated in

articular cartilage, a phenomenon also documented in the articular cartilage of mice 16-weeks post-surgical induction of OA (Lin et al., 2009). By understanding these processes and identifying new mechanistic targets, there is potential for new therapeutics to be discovered and used in the treatment of degenerative cartilage diseases such as OA.

In this results chapter, I aim to characterise the final stages of adolescent long bone elongation and the process of growth plate closure in the mouse, assessing the effect of IFT88 deletion in this context. I predominantly focussed on the tibial growth plate as its shape is less complex in comparison with the femoral growth plate. We hypothesise that IFT88 could be relevant to growth plate cartilage beyond natal and early life stages, potentially affecting Ihh regulated growth plate closure, transduction of mechanical cues or by affecting both of these pathways.

5.2 Aims

1. Characterise dynamic process of growth plate closure and endochondral ossification during the latter phases of adolescent development in the naïve wild type (WT) mouse.
2. Investigate whether the ciliary protein IFT88 is still crucial to growth plate cartilage development beyond 4-weeks of age.

5.3 Results

5.3.1 Characterisation of the tibial growth plate during the final weeks of mouse post-natal development

Before investigating the role of IFT88 in post-natal growth plate cartilage, characterisation of the naïve mouse growth plate was useful as there are limited descriptions after 4-weeks of age in the literature. MicroCT scans were taken of knee joints and the metaphysis, and by selecting one slice using an anatomical reference, the growth plate length was measured 8 times across the width of the growth plate and averaged (indicated in yellow in Fig. 5.3.1.1). By thresholding the MicroCT images, clear demarcation of the bone and the growth plate can be achieved. Thresholding MicroCT images increased the measurable length of the growth plate by removing 'grey' areas observed within the growth plate (Fig. 5.3.1.1). Thresholded MicroCT scans may remove partially calcified cartilage matrix associated with the hypertrophic region of the growth plate and therefore could give early insight as to the level of calcification within the tissue.

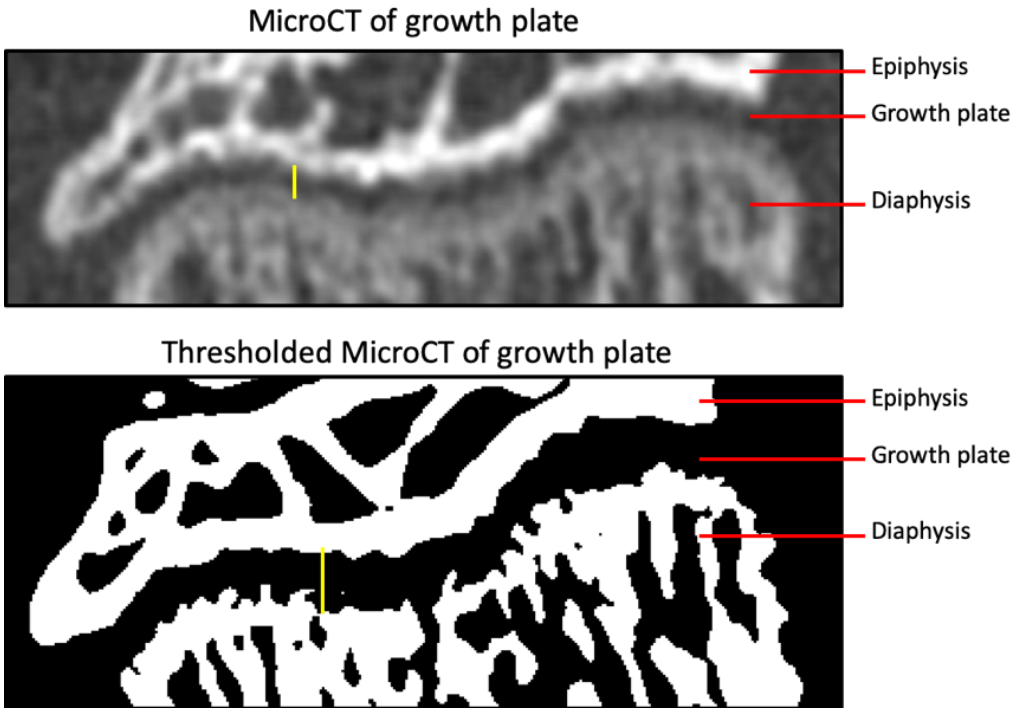


Figure 5.3.1.1: Raw (un-thresholded) and thresholded MicroCT images. Schematic defining methods of growth plate measurements taken between the eophysis and diaphysis (8 per joint). Yellow lines depict distance measured.

5.3.1.1 MicroCT analysis of growth plate closure

Growth plate length can be defined as the distance between the epiphysis and diaphysis parallel to the long bone. Using un-thresholded MicroCT images, growth plate length could be measured in naïve mice over time (Fig. 5.3.1.2 A). The growth plate shortens between 4-8-weeks of age from ~0.26mm to ~0.07mm. In the mouse, the growth plate never completely closes, but stable growth plate length is reached between 10-24-weeks of age.

Fig. 5.3.1.2 B is a reproduction of the characterisation of tibial elongation over one year (Beaucage et al., 2016). Previous work investigating the role of IFTs specifically in post-natal cartilage

studied IFT80 (Yuan and Yang, 2015b). Here, the authors deleted IFT80 between P4 and 2 weeks of age indicated by the black box shown on the graph (Fig. 5.3.1.2. B), which is during a period of rapid bone elongation and dynamic growth plate modelling. The red box highlights the time period in which I shall investigate the role of IFT88 in the growth plate.

Growth plate narrowing between weeks 4 and 10 is associated with the reduction in rate of tibia length increases (Fig. 5.3.1.2. B). There is rapid elongation of the tibia between 4-8-weeks of age at which point, it slows. Bone elongation does continue beyond this point, albeit 1mm between 8 and 52 weeks of age.

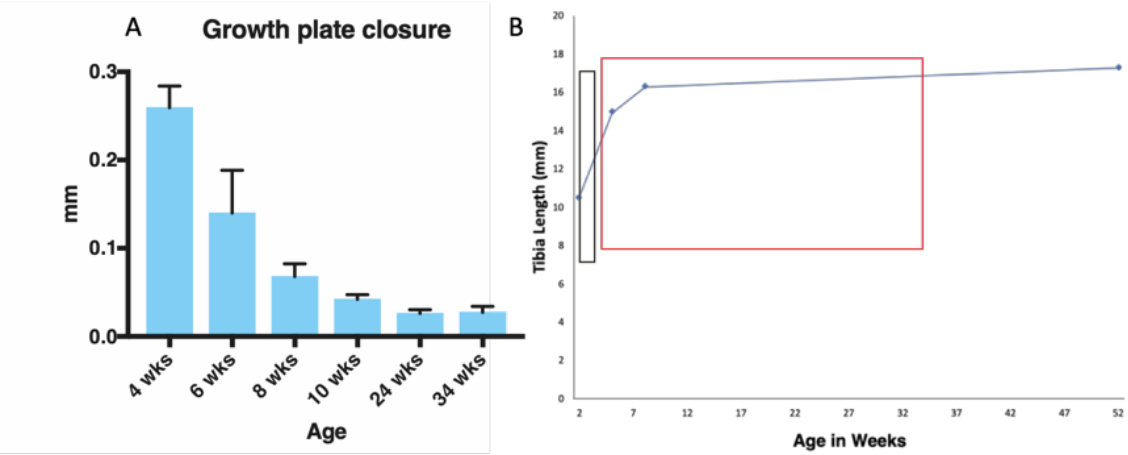


Figure 5.3.1.2: Tibial growth plate closure and tibial growth curves. A) Graph of growth plate measurements between 4 and 34-weeks of age. Error bars represent ±standard deviation. B) Tibia bone length between 2-52 weeks of age. Black box denotes time period previously studied for effect of IFTs, whereas the red box demonstrates time period of novel exploration conducted here.

5.3.1.2 Histological characterisation of growth plate morphology

To characterise growth plate cell populations, knee joints were coronally sliced stained and imaged for histological analysis. Safranin-O stains proteoglycan rich regions and therefore demarcates (in red) tibial growth plates and the articular surfaces (Fig. 5.3.1.3. A). Both 4x and 10x images, show a gradual narrowing of the growth plate between 6 to 10-weeks of age and visible shortening of cell columns through cell loss, within the growth plate (Fig. 5.3.1.3 A and B). Measurements of the total growth plate length (longest yellow line Fig. 5.3.1.3 B) were taken at each time point using 10x histology images and plotted (Fig. 5.3.1.3 C); average length reducing from ~260μm at 6-weeks of age to ~140μm by 10-weeks of age. Safranin-O staining enables separation of the hypertrophic region from the non-hypertrophic region of cartilage. Measurements were taken of the total growth plate length (yellow line) (Fig. 5.3.1.3 C), the hypertrophic (purple line) and proliferative regions (green line) (Fig. 5.3.1.3 D), (6x across growth plate width for 3 slices per mouse) and plotted respectively. There is a large decrease in the length of both of these regions between 6 and 8-weeks of age.

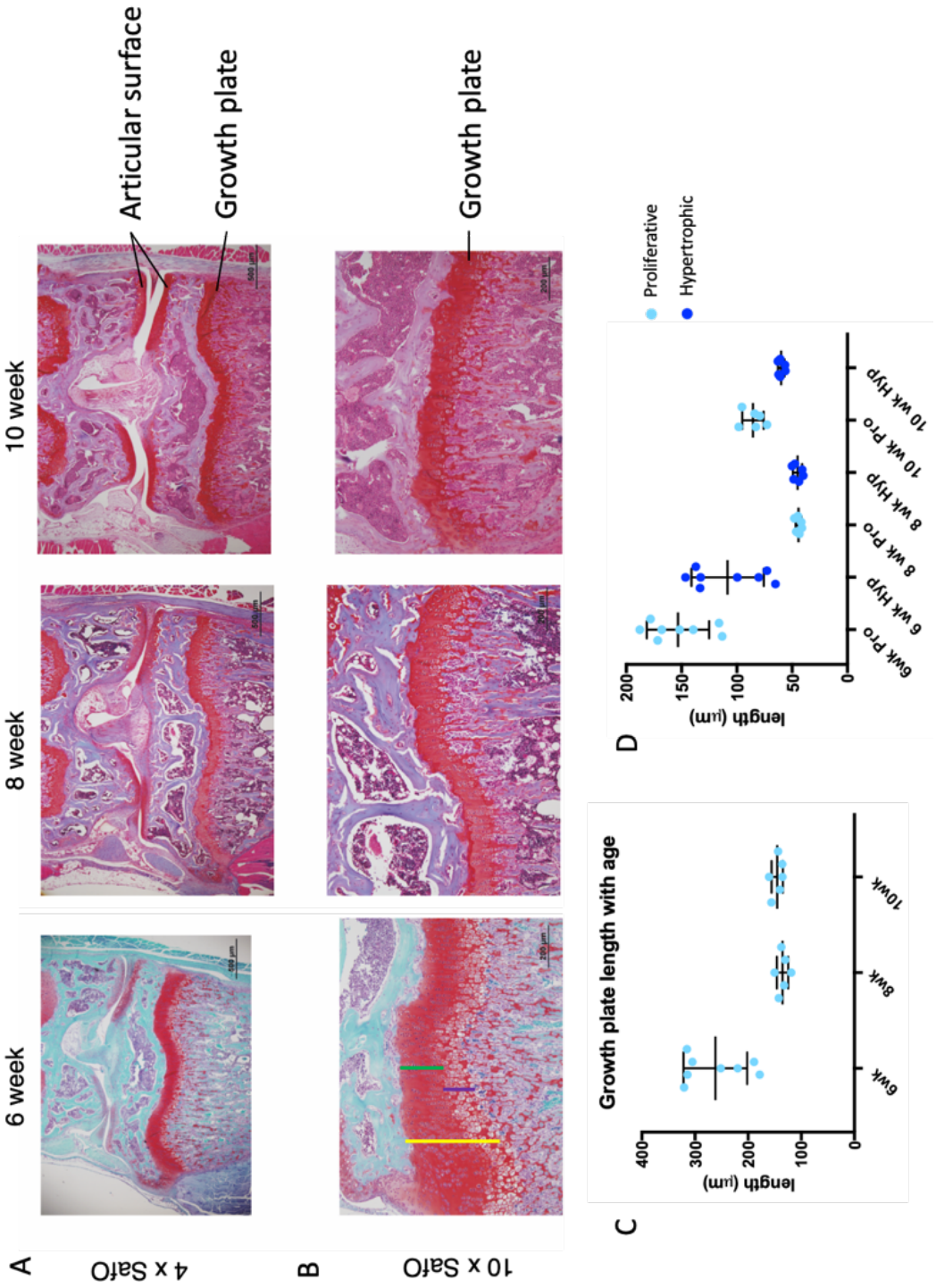


Figure 5.3.1.3: Characterisation of growth plate morphology: hypertrophic and proliferative chondrocyte populations. A) Histological 4x Safranin-O stained sections of knee joints at 6, 8 and 10-weeks of age. B) 10x Safranin-O images of their respective growth plates are shown, demarcating proliferative and hypertrophic regions (yellow lines depict total length, purple lines hypertrophic, and green proliferative measurements from the left). C) Total length of growth plate decreases with age from ~260μm at 6-weeks of age to ~140μm by 10-weeks of age. D) Lengths of proliferative and hypertrophic regions at each 6, 8 and 10-week timepoint. n=8, 5 and 6 respectively.

5.3.2 Correlation of MicroCT and histological measurements

To assess agreement between the two different methods of analysis, histological measurements were plotted alongside MicroCT measurements taken of knee joints. Fig. 5.3.2.1 A, demonstrates that un-thresholded MicroCT measurements are consistently lower than the histological measurements. However, when MicroCT measurements were taken from thresholded images of the joint (as described Fig. 5.3.1.1), this difference was largely lost in some of the samples (Fig. 5.3.2.1 B). Thresholding of images removed regions of the growth plate that had not registered as dense enough to be considered pure bone, and therefore likely calcified cartilage. Pairing of histological and un-thresholded MicroCT measurements, and histological and thresholded MicroCT measurements allowed a correlation graph to be plotted (Fig. 5.3.2.1 C and D respectively). Both correlation graphs produced a similar r^2 values of 0.6616 (Fig. 5.3.2.1 C) and 0.6739 (Fig. 5.3.2.1 D), however the coefficient of the slope differs between the graphs. The slope in graph C has a coefficient of 0.6136, whereas in graph D, the coefficient of the slope is 1.087. This demonstrates that the thresholded MicroCT measurements are more accurate at determining the full length of the cartilaginous growth plate. Moreover, the difference in thresholded and un-thresholded MicroCT measurements may give you a way to assess the length of the calcified region of growth plate

cartilage.

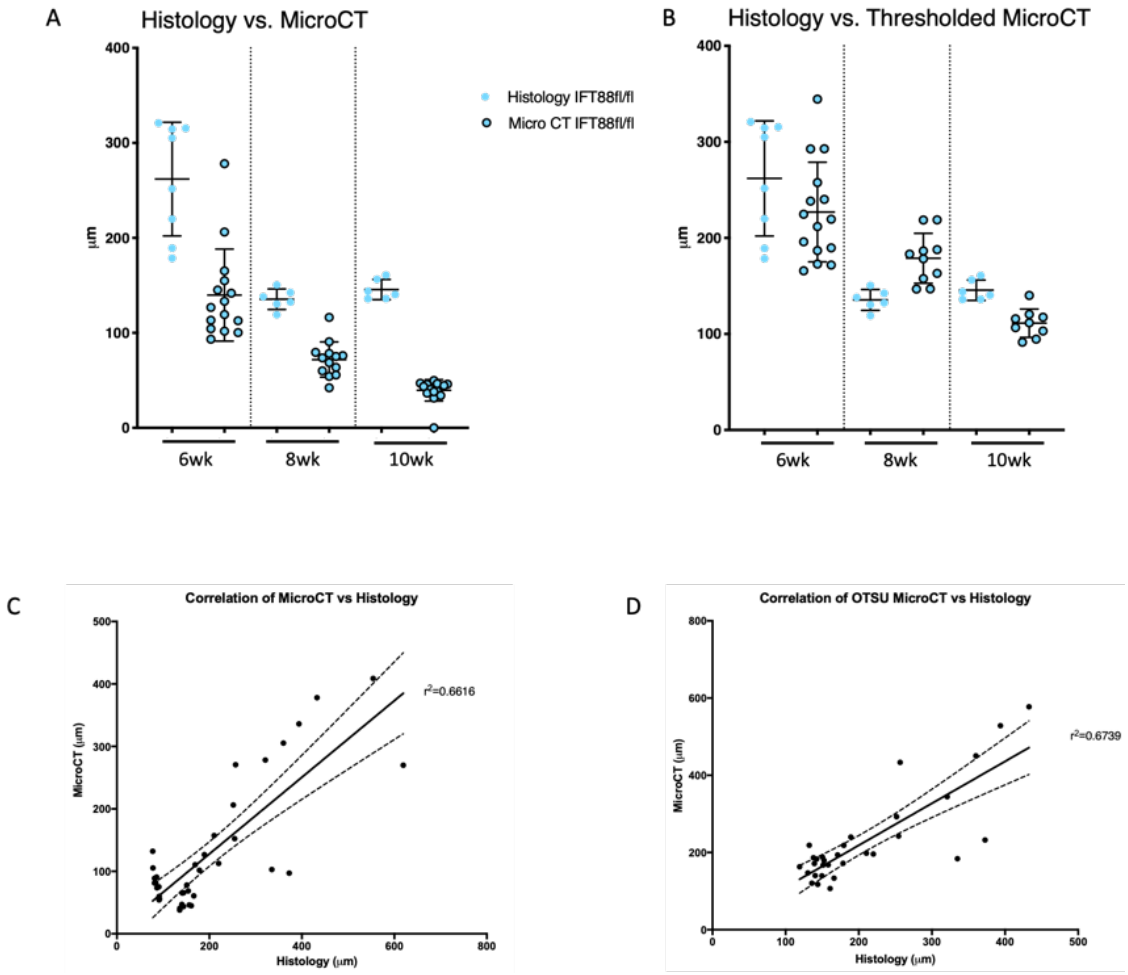


Figure 5.3.2.1: Histological measurements compared with MicroCT measurements. A) Histological measurements were compared with those taken from un-thresholded slices. B) MicroCT slices were thresholded, measured and compared with histological measurements. C) MicroCT and histology measurements were moderately correlated (r^2= 0.6616, F= 70.39, slope = 0.6136 ± 0.07314). D) Thresholded MicroCT and histology measurements were strongly correlated (r^2= 0.6739, F= 59.92, slope = 1.087 ± 0.1404). Data represents ±standard deviation and statistical significance was assessed using the non-parametric Mann-Whitney U test.

5.3.3 The effects of IFT88 deletion on the growth plate

5.3.3.1 Deletion of IFT88 results in qualitative morphological changes to the growth plate and bone

As aforementioned, previous work demonstrated that perturbation of IFT88 resulted in loss of the developmental growth plate (Chang

et al., 2012; Song et al., 2007; McGlashan et al., 2007). Having characterised the growth plate closure between 6-10-weeks of age, IFT88 was deleted specifically in the cartilage within this time period, using the *AggrecanCreER^{T2}*; *IFT88$^{fl/fl}$* (cKO) model as described in Chapter 4. The reporter mouse showed Cre recombination in some columns within the growth plate (Fig. 4.6.1.1 and Fig. 4.6.2.1). There appeared to be no regions of the growth plate affected more than others by the reporter, with columns activated across the entire width of the bone. All mice, including control animals, were given tamoxifen two weeks prior to sacrifice (Fig. 5.3.3.1).

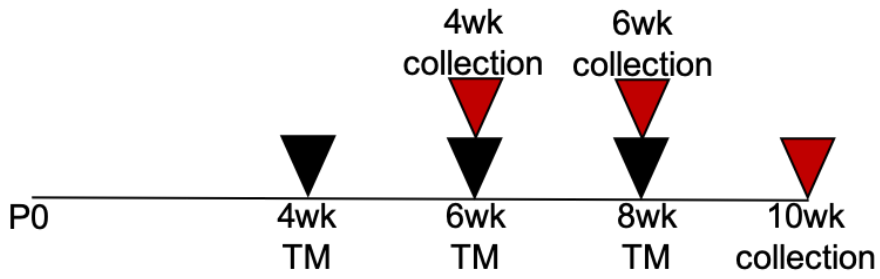


Figure 5.3.3.1: Experimental timeline. Schematic representation of experimental timeline. Animals are born (P0) and at either 4, 6, or 8-weeks of age given tamoxifen(TM) via I.P. injection (black arrows). Two-weeks post-tamoxifen, animals are collected. For example, mice receiving TM at 4-weeks of age are collected at 6-weeks of age.

Tamoxifen was administered at 4-weeks of age to control and cKO animals, and tissue was collected at 6-weeks of age. Raw, un-thresholded MicroCT images revealed deletion at 4-weeks of age resulted in a qualitatively longer femoral and tibial growth plates at 6-weeks of age, compared with controls (Fig. 5.3.3.2. Ai). A range

of phenotypes were observed in cKO animals including modest increases in growth plate length to, in extreme cases, large, often bilateral (apparently therefore uncalcified) holes that extended into the diaphysis (Fig. 5.3.3.2. Ai). MicroCT Slices were thresholded to create 3D cross sections (ii), which revealed the holes extend throughout the core of the bone but full 3D rendering (iii) shows the cortex was unaffected) (Fig. 5.3.3.2 Aii). Dramatic changes to the bone beneath the growth plate were also observed with a qualitative increase in bone density and loss of trabeculae seen in its control 3D rendering compared with controls (Fig. 5.3.3.2 Aiii). The 3D cross-sections accentuated what appeared to be marked increases in bone density in the epiphysis below the growth plate. Deletion at 6-weeks of age and collection at 8-weeks resulted in qualitatively longer growth plates than controls (Fig. 5.3.3.2 Bi). However, these differences were less obvious when compiled in to 3D cross sections or whole joint reconstruction in Fig. 5.3.3.2 Bii and Fig. 5.3.3.2 Biii respectively. As endochondral ossification comes to an end and growth plate closure rate decreases dramatically, it becomes much harder to distinguish obvious differences between control and cKO knee joints (Fig. 5.3.3.2 Ci). Deletion at 8-weeks and collection at 10-weeks revealed few qualitative morphological changes to the bone when compared with controls (Fig. 5.3.3.2 Cii). No obvious differences were qualitatively visible using the

3D whole joint reconstructions at this time point (Fig. 5.3.3.2 Ciii), perhaps owing to multiple slices blocking view.

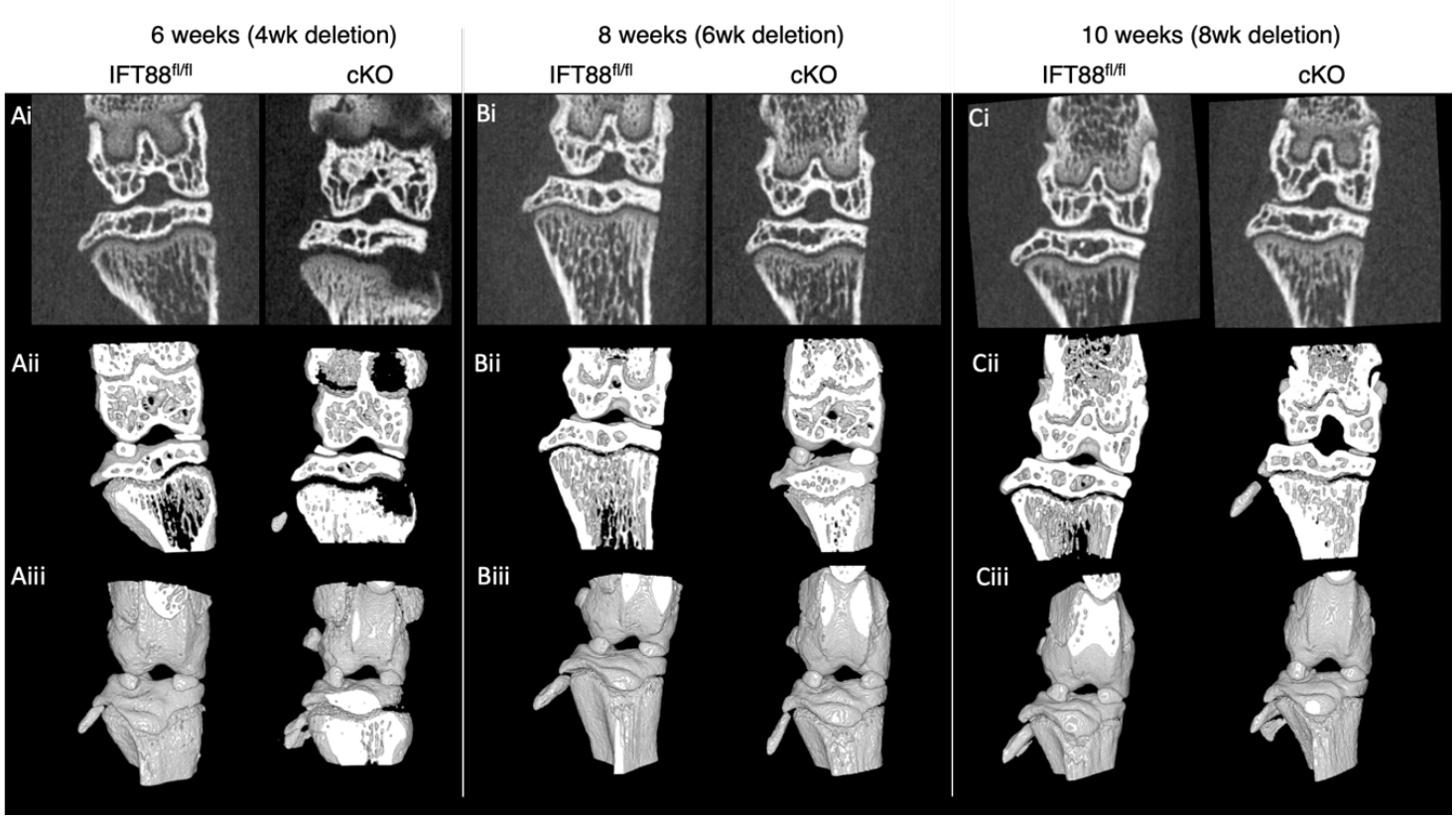


Figure 5.3.3.2: Deletion of IFT88 results in morphological changes to the growth plate. MicroCT slices were compared at anatomical reference points at each time point. cKO images were compared with their respective IFT88fl/fl controls at 6-, 8-and 10-weeks, deletion induced two weeks prior to collection at each time point (Ai, Bi, Ci). Representative knee joints were taken in all cases apart from in the 6-weeks (4-week deletion) (Ai) cKO animals where an extreme example was used. Using imageJ, 50 slices were thresholded and compiled to give a 3D cross section of each knee joint (Aii, Bii, Cii). C) All slices were thresholded and compiled to give a 3D model of the knee joint (Aiii, Biii, Ciii).

5.3.3.2 Deletion of IFT88 results in quantitative quantitative changes to growth plate length

Growth plate length was measured at 8 points across the width of the bone and averaged. Deletion of IFT88 at 4-weeks of age resulted in an increase of mean growth plate length from 0.14mm in controls to 0.23mm in cKO mice ($p<0.0001$, n=15 controls and n=27 cKO) (Fig. 5.3.3.3 A). Thus, mean growth plate length was approximately increased by 100% in cKO mice two weeks after tamoxifen. Some animals presented with much longer average growth plates owing to the lengths of bilateral holes. Within this data set, there also appears to be a split between the extremities of the phenotypes. Animals displaying much longer growth plates of 0.2mm were all from one cage, highlighting variability in phenotype perhaps based on genotype and efficacy of the Cre driver or owing to behavioural differences between cages. Deletion of IFT88 at 6-weeks of age also resulted in statistically significantly longer growth plates at 8-weeks of age, with a mean of 0.13mm compared with 0.07mm of controls ($p<0.0001$, n=12 controls and n=17 cKO). Deletion of IFT88 at 8-weeks of age also resulted in statistically significantly longer growth plates at 10 weeks of age, with a mean of 0.08 mm compared with 0.04mm in controls ($p<0.0001$, n=17 controls and n=22 cKO). This is, on average a doubling in growth plate length, but with one outlier (Fig. 5.3.3.3 C). In this case, perhaps

the median would be more appropriate as the distribution is not gaussian in this data. In all experiments, the control animals were treated with tamoxifen, controlling for its effects.

All growth plate lengths were plotted next to each other in time deletion order, including naïve joints at time of deletion of 4-weeks and at 10-weeks of age (Fig. 5.3.3.3 D). All cKO growth plate lengths at collection were not statistically significantly shorter than the growth plate lengths at the time they received tamoxifen (D), indicating a complete inhibition of growth plate closure over this period. This phenotype is in contrast to previous work that showed accelerated growth plate closure or narrower growth plates earlier in development (Haycraft and Serra, 2008; McGlashan et al., 2007; Yuan and Yang, 2015b).

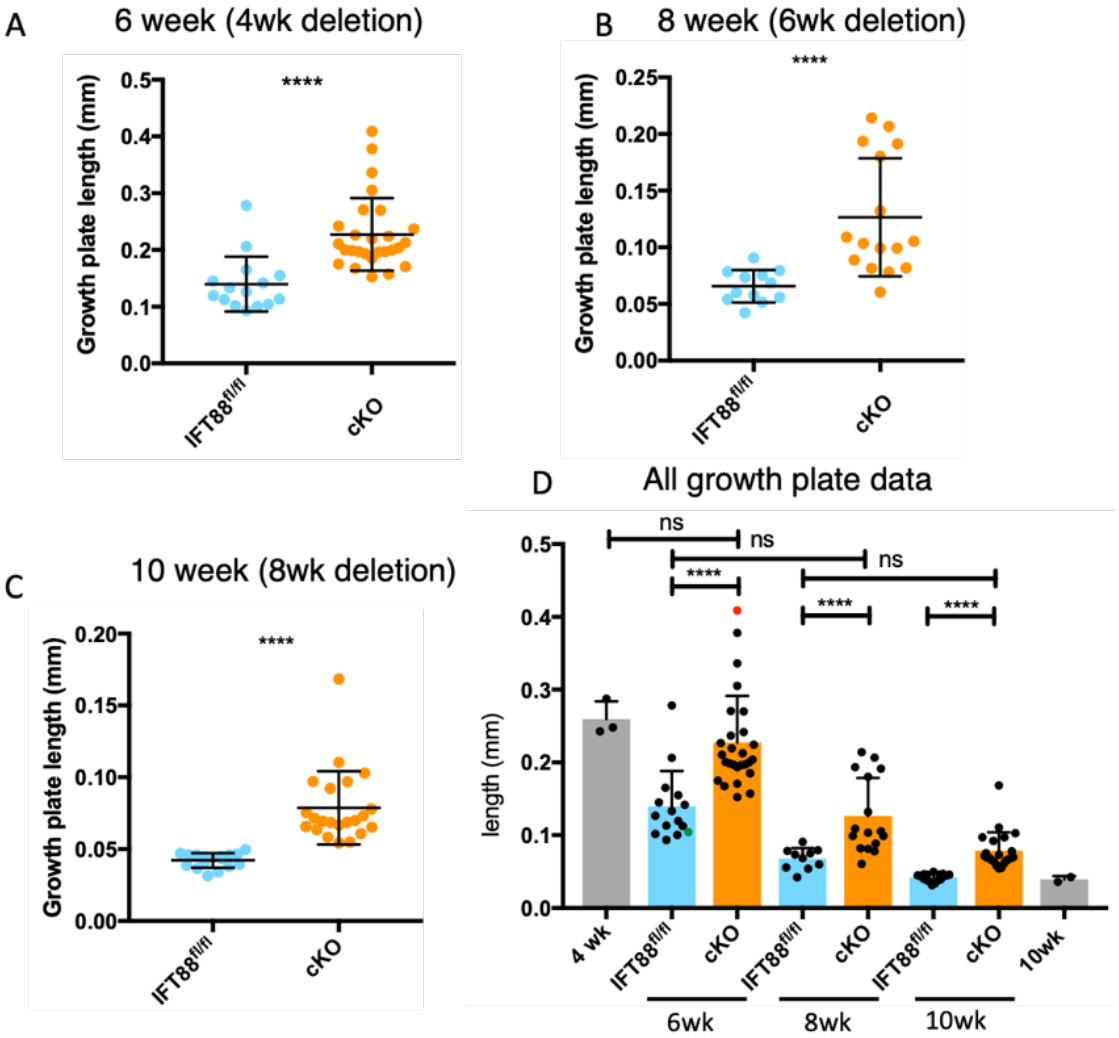


Figure 5.3.3.3: Effect of IFT88 deletion of growth plate length. Eight growth plate measurements were taken from MicroCT images across the width of the tibia from a MicroCT slice identified using an anatomical reference for consistency. A) Lengths of growth plate post 4-week deletion of IFT88 alongside controls ($p<0.0001$, n=15 controls and n=27 cKO). B) Lengths of growth plate post 6-week deletion of IFT88 alongside controls ($p<0.0001$, n=12 controls and n=17 cKO). C) Lengths of growth plate post 6-week deletion of IFT88 alongside control ($p<0.0001$, n=17 controls and n=22 cKO). D) All data from each time point was plotted against each other including growth plate length data taken from 4-week old mice at which tamoxifen was given, and at 10-weeks of age, the final collection time-point. Red (cKO) and green (IFT88fl/fl) dot measurements taken from MicroCT image shown in Fig. 5.3.3.1 Ai. All cKO growth plate lengths at collection were not statistically significantly shorter than the growth plate lengths at the time they received tamoxifen (D). Data represents ±standard deviation and statistical significance was assessed using the non-parametric Mann-Whitney U test where **** =$p<0.0001$

5.3.3.3 Histology reveals deletion of IFT88 results in morphological changes to the growth plate

Owing to striking differences observed in MicroCT images, histological sections of knee joints were made to investigate the morphology of the growth plate. Growth plate length was measured at 3 points across 6 10x histological images (medial and lateral images from consecutive slices) and averaged to give an averaged growth plate length from 18 measurements per mouse joint. These measurements were plotted in Fig. 5.3.3.4 D.

Measurements taken from histology of 6-week old (treated with tamoxifen at 4-weeks of age) control and cKO animals confirmed longer growth plates in cKO mice compared with controls (Fig. 5.3.3.4 D). This relationship was not as statistically strong as seen in the MicroCT, perhaps because far fewer n was used in this data set to analyse the growth plate by histology. The large bilateral holes, previously observed in the MicroCT images, were filled predominantly with hypertrophic chondrocytes (Fig. 5.3.3.4 A, circled in yellow). Deletion at 6-weeks in cKO animals revealed longer growth plates compared with controls two weeks later (Fig. 5.3.3.4 B). The same trends were seen at other timepoints, and in extreme cases, cKO animals exhibited wider growth plates particularly on medial and lateral sides (yellow circles), with the central section of the growth plate largely unaffected (Fig. 5.3.3.4 A

and Fig. 5.3.3.4 C).

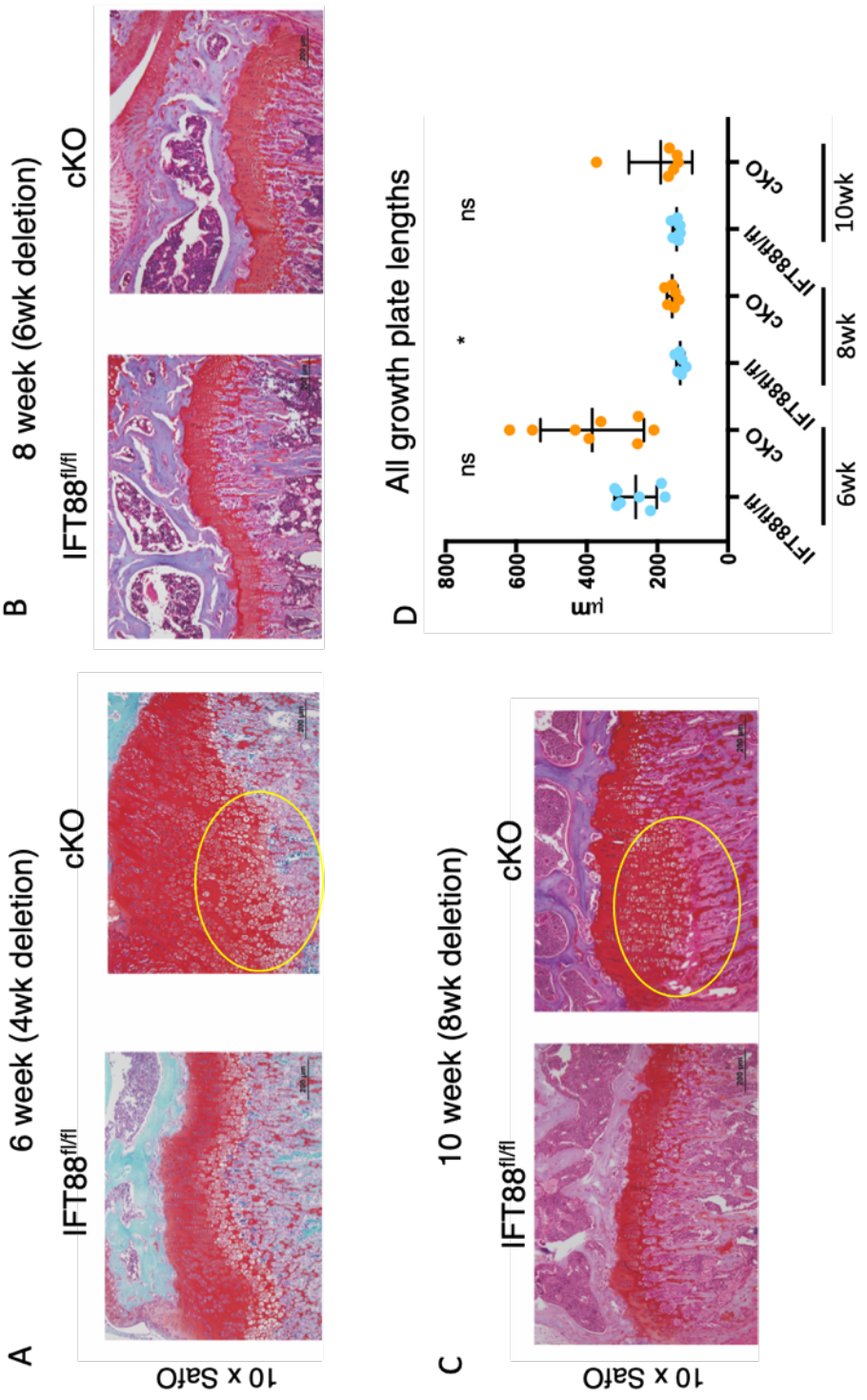


Figure 5.3.3.4: Deletion of IFT88 results in morphological changes to the growth plate. Histological 4x Safranin-O stained sections of knee joints at 6, 8 and 10-weeks of age (A, B and C). Beneath, 10x Safranin-O images of their respective growth plates are shown demarcating proliferative and hypertrophic regions. D) Total length of growth plates plotted at each time point of deletion. Yellow circle highlights hypertrophic chondrocytes in cartilaginous hole of growth plate. Data represents ±standard deviation and statistical significance was assessed using the non-parametric Mann-Whitney U test where *=$p<0.05$.

5.3.3.4 Hypertrophic and proliferative chondrocyte populations

As previously stated, the relationship between proliferative and hypertrophic chondrocytes is tightly regulated and controlled through a careful balance of relative Hh and PTHrP signalling. By deleting IFT88, chondrocytes may be unable to respond appropriately to Hh ligand. This could result in proliferative chondrocytes being unable to respond to Hh, subsequently not releasing PTHrP to continue proliferating. This prevents other chondrocytes from becoming pre-hypertrophic or hypertrophic chondrocytes, resulting in accelerated hypertrophy of the growth plate. Hypertrophic chondrocytes may also not be able to initiate downstream ossification programmes such as the upregulation of crucial transcription factors, Sox-9 and Runx2. This could result in failed calcification of the ECM surrounding the hypertrophic chondrocytes and ultimately failed ossification.

To understand what could be happening to these chondrocyte populations, measurements of each of these regions representing these populations were taken from 10x histological images. The 4-week deletion of IFT88 resulted in no-statistically significant changes to the proliferative and hypertrophic regions two weeks later, but there were qualitative differences. Again, too few n could be contributing to a lack of statistically significant difference. Hypertrophic region measurements in the cKO have high inter-

animal variation from less than 100μm to more than 300μm, highlighting the extremities in the phenotypes observed (Fig. 5.3.3.5 A). However, the 6-week deletion of IFT88 results in a statistically significantly longer proliferative region ($p<0.05$) in comparison with controls, but no statistically significant difference is seen in the hypertrophic region (Fig. 5.3.3.5 B). A similar trend was observed with the deletion at 10-weeks (Fig. 5.3.3.5 C). At all ages of deletion, some animals presented with more proliferative and hypertrophic chondrocytes than controls.

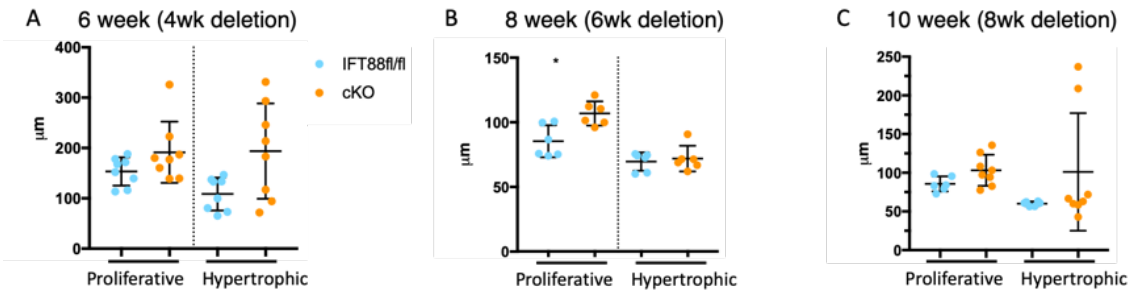


Figure 5.3.3.5: Histological measurements of hypertrophic and proliferative regions of the growth plate. A, B and C show proliferative and hypertrophic measurements between control and cKO animals at 4, 6, and 8-week deletion respectively. Data represents ±standard deviation and statistical significance was assessed using the non-parametric Mann-Whitney U test where *=$p<0.05$.

5.3.3.5 Insights gleaned from MicroCT and histological hypertrophic region measurements

Using these data found in Fig. 5.3.3.3 A and B, the difference between un-thresholded MicroCT values and thresholded MicroCT values were found. This revealed the length of the less defined grey strip sitting at the top of the diaphysis and bottom of the growth plate. This region was not defined by the MicroCT as bone, but could potentially be the calcified region of the cartilage, known as the chondro-osseous junction. Measurements of the hypertrophic region, derived from histological images (Fig. 5.3.3.4), were compared with that of the chondro-osseous measurements. Control thresholded MicroCT measurements were found to be similar with those found of the hypertrophic region. However, in some cKO samples (4- and 6-week deletion), thresholded MicroCT measurements were smaller than that of the hypertrophic region. This suggests that the hypertrophic region may have failed to calcify and hence was shorter in length. A linear regression analysis revealed that chondro-osseous measurements and histology measurements are weakly correlated (Fig. 5.3.3.6 D: r^2= 0.4268, slope = 0.4531). However, this difference may have only been discernible at these earlier time points, owing to the growth plate being larger and, hence, measurements taken from the MicroCT had a smaller potential for resolution error as the MicroCT

resolution is 10μm per pixel.

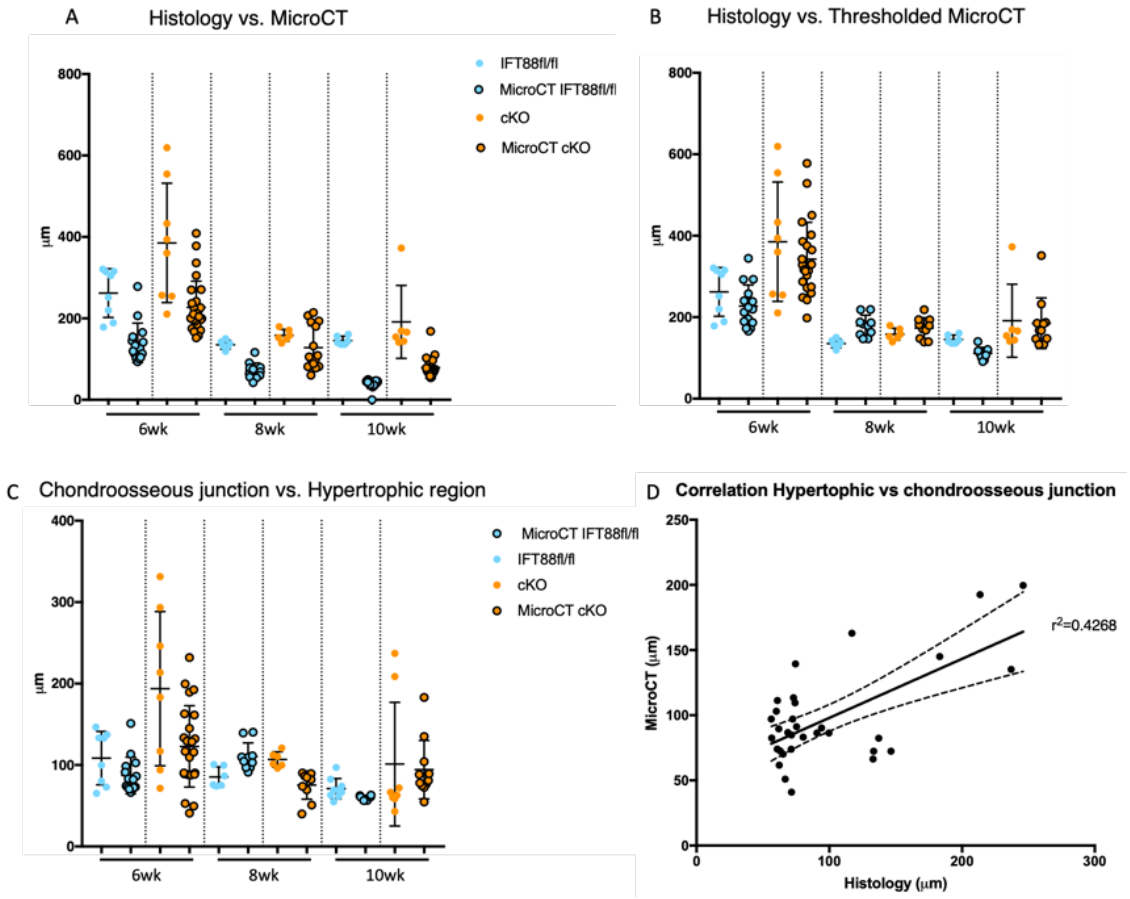


Figure 5.3.3.6: Effects of IFT88 deletion on the growth plate and hypertrophic chondrocyte regions. A) Histological measurements were compared with those taken from MicroCT slices in control and cKO animals. B) MicroCT slices were thresholded, measured and compared with histological measurements. in control and cKO animals. C) Thresholded MicroCT measurements and non-thresholded MicroCT measurements were used to find calcified regions of cartilage at the distal end of the growth plate. These measurements were compared to histological measurements of the hypertrophic region, a region of calcified cartilage. D) MicroCT measurements and histology measurements were weakly correlated (r^2= 0.4268, F= 22.34, slope = 0.4531 ± 0.09586). Data represents ±standard deviation.

5.3.4 Immunohistochemistry analysis of growth plates and the effects of IFT88 deletion on type X collagen expression

In Fig. 5.3.3.3 and Fig. 5.3.3.4, large cartilaginous bilateral holes were observed in the growth plate cartilage of cKO animals that appeared to be filled with chondrocytes morphologically resembling hypertrophic chondrocytes. In the previous section (Fig. 5.3.3.6), length of hypertrophic chondrocytes weakly correlated with the chondro-osseous junction. Measurements of the hypertrophic region from control animals appeared to coincide with measurements taken from their respective chondro-osseous junction measurements. Whereas, in 8-week cKO animals (Fig. 5.3.3.6 C), hypertrophic chondrocyte measurements greatly differed to that of respective cKO chondro-osseous measurements, suggestive that the matrix surrounding the hypertrophic chondrocytes might not be calcifying or that hypertrophic chondrocytes are not producing type X collagen (ColX), a phenotypic marker of 'true' hypertrophic chondrocytes.

In order to determine whether these hypertrophic chondrocytes had differentiated correctly, ColX immunohistochemistry was performed as ColX is used as a characteristic phenotypic marker of hypertrophic chondrocytes. To explore whether hypertrophic chondrocytes were expressing ColX at this chondro-osseous

junction, and particularly whether chondrocytes within extreme phenotypic cases with large bilateral holes had differentiated, coronal sections were immunofluorescently stained with both DAPI and ColX. This was performed at each time point of deletion for 4-, 6-, and 8-week animals (Fig. 5.3.4.1, 5.3.4.2, and 5.3.4.3). Safranin-O stained images from three different control mouse knee joints are shown with their paired DAPI and ColX IF stained images displayed below. At every time point, clear staining of ColX can be seen at the chondro-osseous junction. Type X collagen immunohistochemistry identified large numbers of ColX expressing hypertrophic chondrocytes in the growth plates of cKO animals at every experimental time point, indicating that hypertrophic differentiation is unaffected by lack of IFT88 (Fig. 5.3.4.1, 5.3.4.2, and 5.3.4.3). In cases where growth plates had large cartilaginous bi-lateral holes, this was found to be rich in ColX staining, suggesting these holes were filled with hypertrophic chondrocytes (Fig. 5.3.4.1). This region of hypertrophic chondrocytes could be seen in Safranin-O histological sections above each IF stained image.

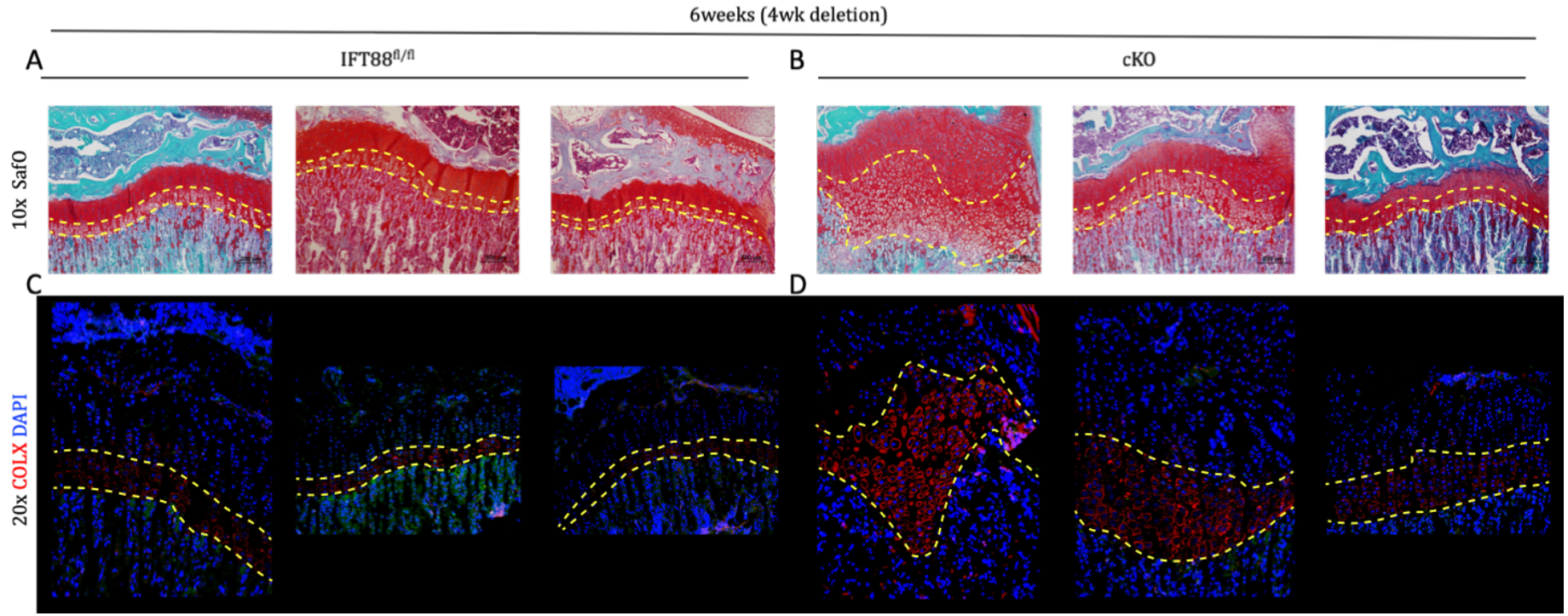


Figure 5.3.4.1: Histological coronal sections of 6-week old knee joints revealed longer growth plates in cKO animals. A) 10x Safranin-O stained histological sections of IFT88fl/fl mouse growth plates. Hypertrophic chondrocyte regions are marked by dashed yellow lines. Beneath, respective IF ColX stained sections (20x) showed expression in the growth plate nearest to the bone and localised to hypertrophic chondrocytes marked by dashed yellow lines (C). B) 10x Safranin-O stained sections of cKO mice knee joints. Hypertrophic chondrocyte regions are marked by dashed yellow lines. Beneath, respective IF ColX stained sections (20x) showed strong expression within hypertrophic chondrocytes, with an apparent larger band of ColX expression in the growth plate than in control mice. Large cartilaginous holes were confirmed to be filled with ColX expressing hypertrophic chondrocytes marked by dashed yellow lines (D). All IF sections were counterstained with the nuclear stain DAPI.

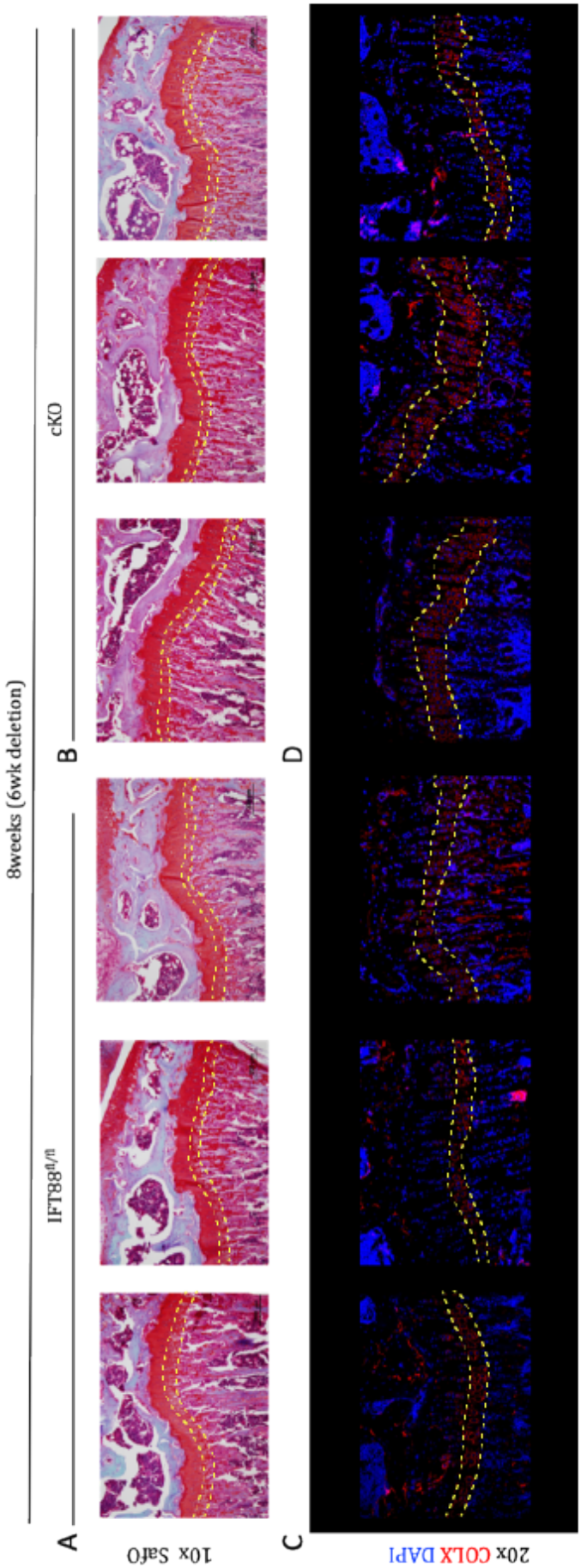


Figure 5.3.4.2: Longer growth plates in cKO animals associated with larger regions of col X staining. A) 10x Safranin-O stained histological sections of IFT88fl/fl mouse growth plates. Hypertrophic chondrocyte regions are marked by dashed yellow lines. Beneath, respective IF ColX stained sections (20x) showed expression in the growth plate nearest to the bone and localised to hypertrophic chondrocytes marked by dashed yellow lines (C). B) 10x Safranin-O stained sections of cKO mice knee joints. Hypertrophic chondrocyte regions are marked by dashed yellow lines. Beneath, respective IF ColX stained sections (20x) showed strong expression within hypertrophic chondrocytes, with an apparent larger band of ColX expression in the growth plate than in control mice marked by dashed yellow lines (D). All IF sections were counterstained with the nuclear stain DAPI.

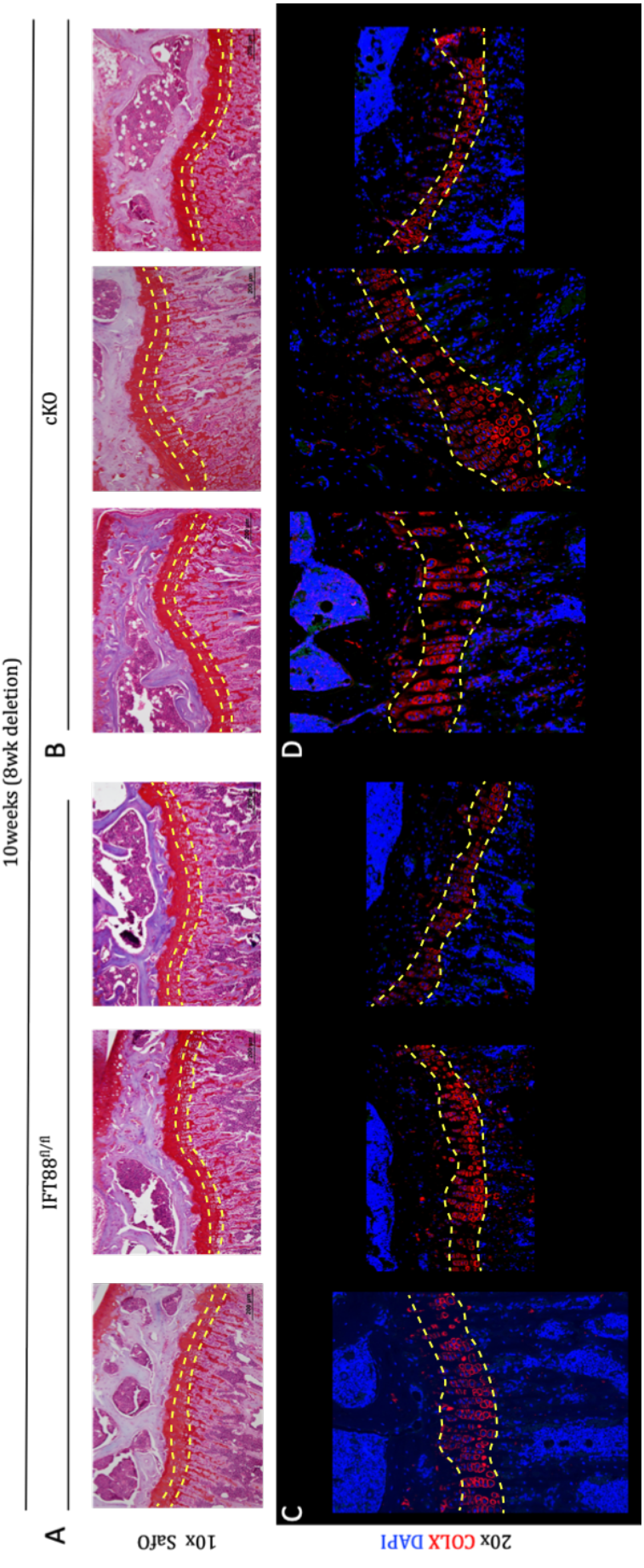


Figure 5.3.4.3: Histological coronal sections of 10-week old knee joints revealed growth plates filled with ColX expressing chondrocytes in both control and cKO animals. A) 10x Safranin-O stained sections of IFT88fl/fl mouse growth plates. Hypertrophic chondrocyte regions are marked by dashed yellow lines. Beneath, respective IF ColX stained sections (20x) showed expression in the growth plate nearest to the bone and localised to hypertrophic chondrocytes marked by dashed yellow lines (C). B) 10x Safranin-O stained sections of cKO mice knee joints. Hypertrophic chondrocyte regions are marked by dashed yellow lines. Beneath, respective IF ColX stained sections (20x) showed strong expression within hypertrophic chondrocytes, with an apparent larger band of ColX expression in the growth plate than in control mice marked by dashed yellow lines (D). All IF sections were counterstained with the nuclear stain DAPI.

5.3.5 Characterisation of bone morphology

5.3.5.1 Cartilage specific deletion of IFT88 results in changes to trabeculae immediately beneath growth plate, but has no effect on the epiphysis

It is well known that there is cross talk between the cartilage and the bone. Trabeculae differences were seen in the diaphysis directly beneath the growth plate (Fig. 5.3.3.1). It was also hypothesised that disturbances to the growth plate could be affecting the epiphysis. Changes observed in MicroCT slices and 3D reconstructions to the bone were investigated using CTan analysis software. Using the MicroCT files, a region of interest was selected throughout the joint, 3D compiled, and analysed for total volume (TV), bone volume (BV), bone volume/total volume (BV/TV), trabecular separation (Tb.SP), and trabecular number (Tb.N). These values are widely used to determine bone phenotypic differences in and between bone samples. The tibial epiphysis sits on top of the growth plate and beneath the articular cartilage. Analysis of the epiphysis in each of TV, BV, BV/TV, Tb.SP, and Tb.N two weeks post-deletion at 6, 8 and 10-weeks of age (Fig. 5.3.5.1 A) resulted in no statistically significant differences in any of these parameters, except in BV in the 8-week deleted group (Fig. 5.3.5.1) where a statistically significant decrease observed was observed in cKO ($p<0.05$). In contrast, the bone found just beneath the growth plate (epiphyseal plate) was much more affected. By 6

weeks of age, deletion of IFT88 resulted in a statistically significant total increase in BV ($p<0.05$), BV/TV ($p<0.05$), decreased Tb.SP ($p<0.0001$) and an increase in Tb.N ($p<0.0001$) when compared with controls (Fig. 5.3.5.1 B). Hence revealing that the removal of IFT88 increased the number of trabeculae, ultimately resulting in an increase in bone density (BV/TV). This pattern was seen less prominently when deleting IFT88 by 8 and 10-weeks of age (Fig. 5.3.5.1 D and F). In these two experiments, no statistically significant differences were observed in TV, BV or BV/TV. However, in both experiments there was a statistically significant decrease in Tb.SP coinciding with an increase in Tb.N. This could be as a result of a mechanoadaptation to the longer and more unstable growth plate, or reflective of making different bone in the first place as a result of altered cartilage produced in the growth plate.

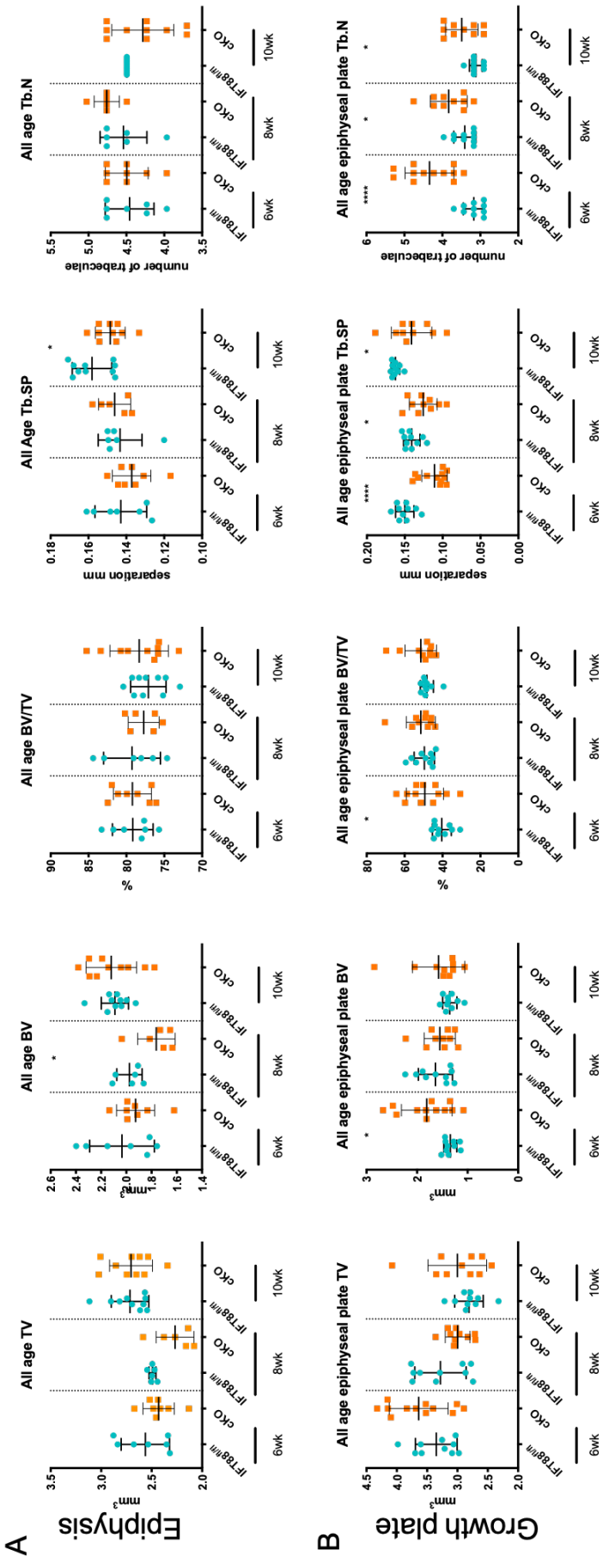


Figure 5.3.5.1: Deletion of IFT88 results in changes to the bone beneath the cartilage in the epiphysis and bone beneath growth plate. Graphs A and B summarise differences in CTan measurements taken from the epiphysis and epiphyseal bone (beneath the growth plate) as a result of IFT88 deletion at 4, 6, and 8-weeks respectively. Data represents ±standard deviation and statistical significance was assessed using the non-parametric Mann-Whitney U test where *=$p<0.05$ and ****=$p<0.0001$

5.4 Discussion

In this chapter, I have characterised the final stages of growth plate dynamics, and the impact that IFT88 deletion has on these processes. Deletion of IFT88 during adolescence inhibits growth plate closure, halting any narrowing of the growth plate over the two weeks post deletion (Fig. 5.3.3.1). This stalling of growth plate closure is characterised by the loss of ossification in the hypertrophic region of the growth plate, and alterations to trabeculae spacing and number (bone density) in the nearby regions of the diaphysis (Fig. 5.3.5.1). These results are in contrast with previous cartilage specific and constitutive deletions of IFT88, where growth plate closure was accelerated or the growth plate was abolished, potentially illuminating evolving roles for IFT88 and, by extension, the primary cilium at this later point in skeletal maturation.

The ciliary protein IFT88 has previously been implicated in endochondral bone formation (Song et al., 2007) and changes to articular and growth plate cartilage (McGlashan et al., 2007; Song et al., 2007). Removal of IFT88 in these studies resulted in shortened growth plates and shortened long bones. However, these studies looked much earlier in development than presented in this thesis. Herein, this study demonstrated that the removal of

IFT88 specifically in cartilage at 4, 6 and 8-weeks of age resulted in statistically significantly longer growth plates two weeks later, in contrast to previous work (Fig. 5.3.3.2). This was confirmed by both MicroCT and histology (Fig. 5.3.3.3 and Fig. 5.3.3.4).

Quantification of hypertrophic and proliferative regions of the growth plate revealed that there were no statistically significant changes seen between the control and cKO hypertrophic regions in the majority of cases. However, there were trends towards longer proliferative and hypertrophic zones at both 6- and 8-weeks of age in cKO animals compared with controls.

There was significant variation of phenotype observed within the cKO groups, with outliers seen in the growth plate at 8-week deletion of IFT88. We hypothesised that the variable efficacy of the Cre in this mouse, showing heterogeneous activation of chondrocytes within the growth plate cartilage and also only being able to achieve an ~35% deletion of IFT88 at the level of mRNA (Chapter 4), led to different proportions of chondrocytes being affected, leading to extremes of phenotypes.

Previous models targeting IFT88 during development in the cartilage (*Prx1Cre;IFT88*), have resulted in accelerated hypertrophic differentiation coupled with fewer proliferating chondrocytes and a shorter growth plate (Song et al., 2007). However, interestingly, the authors documented delayed vascularisation of the growth

plate cartilage in mutant mice and the persistence of hypertrophic chondrocytes, similar to what we observed in this chapter. A similar phenotype, of accelerated hypertrophic differentiation, as found in an inducible cartilage specific model targeting Ihh (*Col2Cre;Ihh*) and included a dramatic loss of type II collagen expressing proliferating chondrocytes (Maeda et al., 2007). The proliferative zone was documented to be unaffected in ORPK mutant mice at post-natal day 4 (McGlashan et al., 2007), which is in contrast to what we observe in this Chapter when deleting IFT88 at 4- and 6-weeks of age (Fig. 5.3.3.4). Hence, from the literature we may have predicted an increase in hypertrophic differentiation and a longer hypertrophic chondrocyte region of the growth plate. However, to our knowledge, assuming an IFT-Hh mechanism would be disturbed, we would not have predicted longer non-hypertrophic and proliferating regions of chondrocytes as we see in cKO animals.

Measurements taken from both MicroCT and histology revealed statistically significant differences at each time point between cKO and controls. However, MicroCT measurements were smaller than nearly all histological measurements taken (Fig. 5.3.3.6). However, when MicroCT images were thresholded, the coefficient of the correlation between MicroCT and histology measurements approached 1. This suggests that measurements taken from thresholded MicroCT images were much more accurate than

those taken without histology and closer to the true histological measurement value. There is also a possibility that by thresholding MicroCT images, the calcified region of the growth plate cartilage, normally associated with the hypertrophic region, could be removed. By plotting hypertrophic histological measurements next to those produced from the subtraction of MicroCT measurements from thresholded MicroCT measurements, otherwise referred to as the chondro-osseous junction, a weak correlation could be identified. Interestingly, when comparing the chondro-osseous junction with the hypertrophic region, in cKO animals, the measurements failed to match. This suggests that hypertrophic chondrocytes were not able to calcify the matrix around them inhibiting ossification at this junction, illustrated by the schematic Fig. 5.4.0.1.

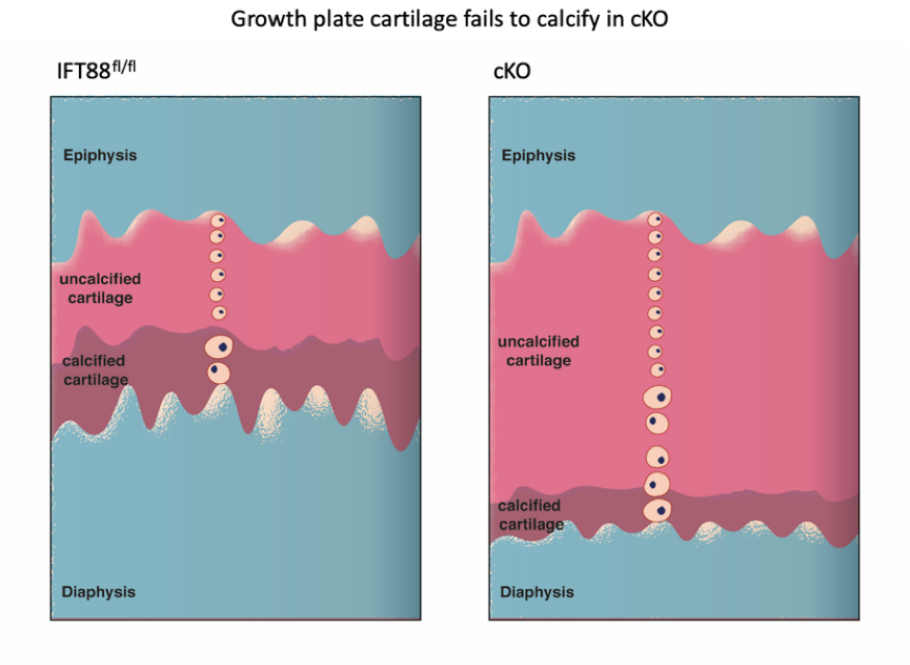


Figure 5.4.0.1: Growth plate cartilage fails to calcify in cKO. This schematic illustrates the hypothesis that IFT88 reduction results in failed calcification of the cartilage surrounding hypertrophic chondrocytes. In control mice, hypertrophic chondrocytes calcify their surrounding matrix to allow for subsequent downstream processes to ossify the matrix, and hence the formation of bone. In contrast, on deletion of IFT88 (cKO), whilst chondrocytes do undergo differentiation to become ColX expressing chondrocytes, they fail to calcify their surrounding matrix. Without this calcification, no ossification can occur and downstream processes to form bone are inhibited.

To explore possible reasons for this failure of growth plate closure, I stained histological sections with ColX. ColX is a marker of hypertrophic chondrocytes and is required for the transformation of the ECM at the interface between growth plate and bone. As shown in Fig. 5.3.4.1, Fig. 5.3.4.2 and Fig. 5.3.4.3, I found it to be both expressed and secreted by hypertrophic chondrocytes at every age of deletion. The phenotype, therefore, is not a failure of chondrocytes to differentiate into hypertrophic chondrocytes, but deletion of IFT88 could potentially affect subsequent ossification processes.

Potential theories explaining this observed phenotype include disruption to the PTHrP-Ihh axis, which is extremely important for the regulation of endochondral ossification and processes within the growth plate (St-Jacques et al., 1999). This axis involves hypertrophic chondrocytes producing Ihh, which stimulates the proliferative chondrocytes to produce PTHrP. PTHrP induces chondrocytes to proliferate, but also inhibits other chondrocytes within the proximity becoming hypertrophic chondrocytes. Ihh and PTHrP mutant mice result in shortened growth plates (Lanske et al., 1999b; Maeda et al., 2007). Ihh signalling is dependent on the primary cilium and IFT88 (Clement et al., 2009a). Hence, we might hypothesise that the removal of IFT88 alters Ihh signalling, perturbing this PTHrP-Ihh axis and therefore altering the length of both the proliferative and hypertrophic region. We hypothesised that if by deleting IFT88, ciliary Ihh signalling is altered, chondrocytes, whether resting, proliferative or hypertrophic, might have an altered response to Hh ligand. Our results showed that proliferative and hypertrophic chondrocytes were being maintained, suggesting that proliferative chondrocytes were still responding to Ihh signalling to proliferate and secrete PTHrP. Additionally, chondrocytes were transitioning to become hypertrophic chondrocytes that expressed ColX. We found that hypertrophic chondrocytes were perhaps failing to calcify their

matrix and this could potentially be owing to a failure to differentiate from this stage. This could be indicative of perturbed Ihh signalling in hypertrophic chondrocytes

Additionally, we hypothesised that removal of IFT88 alters the chondrocytes' ability to regulate Ihh signalling and also respond to mechanical weight bearing load, resulting in bilateral ectopic cartilage formation in the highest loaded regions of the joint seen in our 4- and 8-week deleted mice most prominently. Previous work has linked BMP signalling molecules (FGFs) and Wnt signalling to the mechanical regulation of joint formation in muscle-less mice (Rolfe et al., 2014). These pathways have also provisionally been linked to the primary cilium (Moore and Jacobs, 2018).

As previously mentioned, mechanics is extremely influential in growth plate dynamics, influencing matrix turnover and signalling, and has been characterised in the early post-natal development of chicks (Reich et al., 2005; Reich et al., 2010; Reich et al., 2008). In children, the role of mechanics in post-natal skeletal development has been well documented with limb length discrepancy arising from paralysis in one limb (Ratliff, 1959), the paralysed limb being shorter than the other. Similar clinical manifestations are observed in children with hemiplegic cerebral palsy (Walsh et al., 2000; Riad et al., 2010). Furthermore, murine growth plates have been shown to be regulated by mechanical forces during limb development, in

cases of space flight or unloading of joints by tail suspension (Park et al., 2012; Duke et al., 1985; Duke et al., 1990).

We hypothesise that the removal of IFT88 in a proportion of chondrocytes, would result in failed transduction of mechanical cues to the chondrocytes. This then affects the highly sensitive and dynamic signalling pathways within the growth plate, resulting in failed matrix calcification and formation of bilateral and ectopic cartilaginous holes. Nonetheless, questions remain to be answered as to how mechanical stimuli are transduced to intracellular signals and how this contributes to healthy joint development.

Although further investigation and characterisation is required, within these bilateral holes, there was an apparent loss of growth plate chondrocyte columnar organisation, most notably within the hypertrophic chondrocytes. Previous work has shown that IFT88 and by extension the primary cilium organises cell polarity in tenocytes (Donnelly et al., 2010). In addition, the removal of the ciliary associated kinesin, KIF3A, results in growth plate chondrocyte columnar disorganisation (Song et al., 2007).

Recently, research implicates the IFT80 in vascular invasion as a crucial part of fracture healing and is required for ossification (Liu et al., 2019). However, mechanisms by which vascular invasion occurs at the interface between hypertrophic chondrocytes and the bone, during growth plate closure and endochondral ossification,

remain not well understood. Cartilage is a highly avascular tissue, in contrast to bone which is one of the most highly vascularised tissues in the body, requiring a drastic change to its physiology. This transformation of the cartilage composition at the site of hypertrophic chondrocytes is vital for angiogenesis and hence bone formation (Vu et al., 1998). Angiogenesis requires the extracellular matrix to be proteolytically modified to allow the invasion of endothelial cells. This process also mobilises signalling molecules crucial to this process and is associated with the activity of MMPs (Birkedal-Hansen, 1993; Karelina et al., 1995). MMPs are also highly expressed in embryonic development where high levels of tissue remodelling occurs. Hence, future work might include staining for MMPs, such as MMP-9 and angiogenic factors such as VEGFR.

In Fig. 5.3.5.1., we investigated the impact of IFT88 deletion on the epiphysis and the diaphysis directly beneath the growth plate. We saw no changes to any classical bone measurements (including BV, TV, BV/TV, Tb.SP, and Tb.N.) within the epiphysis as a result of IFT88 deletion at any age. However, on analysis of the region beneath the growth plate we saw statistically significant changes to BV, TV, BV/TV, Tb.SP, and Tb.N. when deleting IFT88 at 6-weeks of age. This indicates substantial remodelling resulting in increased trabeculae density and therefore increased bone volume.

In Fig. 5.3.3.3, MicroCT images revealed apparent differences to the metaphyseal bone beneath the growth plate. These observed and quantified changes could be owing to impaired matrix synthesis by hypertrophic chondrocytes, leading to altered bone formation. Perhaps the loss of IFT88 results in loss of mechanically stimulated calcification of the growth plate cartilage of which mechanics is crucial to this process (Klein-Nulend et al., 1986). However, on deletion of IFT88 at 6 or 8-weeks of age, no statistically significant differences were observed in BV, TV or BV/TV, but statistically significant differences were found in Tb.SP and Tb.N. Again, an increase in Tb.N and decrease in Tb.SP, in comparison with controls, was recorded. This could again be reflective of reduced growth plate dynamics during this time period, resulting in a less prominent phenotype. Additionally, with age, there is a gradual trend towards increasing the distance between trabeculae (increased Tb.SP) resulting in fewer trabeculae (lower Tb.N). In cKO animals, this trend was absent resulting in unchanged trabeculae number and spacing. This could potentially explain this apparent delayed maturation of the bone beneath the growth plate.

Furthermore, Ihh is not only required for growth plate formation and for the stimulation of chondrocytes to undergo hypertrophy, but is also important for osteoblast differentiation (Hilton et al., 2005). PTHrP is also important for vascular invasion and bone

formation (Lanske et al., 1999b). Ihh is a mechanically regulated gene (Wu et al., 2001). If mechanically induced expression of Ihh is altered, PTHrP may not be stimulated properly resulting in accelerated differentiation of chondrocytes to a hypertrophic state, resulting in rapid closure of the growth plate or complete loss of the structure (Lanske et al., 1999b). Additionally, PTHrP-/- mice showed delayed vascular invasion and decreased trabecular bone formation (Lanske et al., 1999b). The heterogeneity of deletion may explain extremities of phenotypes, with some animals having more IFT88 as a result of lower recombination than others resulting in differences in signalling pathway disruption. Additionally, IFT88 requirements could be distinct at different stages of growth plate development between 4 and 10-weeks of age. Further investigation, for example using angiogenic markers and indices for vascular invasion in the context of this apparent failed growth plate closure phenotype downstream to IFT88 removal, would help to elucidate whether failed ossification of the growth plate was owing to failed vascularisation.

5.5 Summary

In summary, these results demonstrate that IFT88 maintains its influence in cartilage development beyond 4-weeks of age. Removal of IFT88 results in gross changes to the growth plate

and bone beneath during adolescent development, most notably when deleted at 4-weeks of age during a dynamic phase of growth. These results suggest that this could be owing to failed transduction of mechanical cues and/or Ihh signalling of hypertrophic chondrocytes to remodel and calcify their surrounding cartilage matrix and initiate ossification processes such as angiogenesis.

6

The role of IFT88 in post-natal articular cartilage

Do what you can, with what you have, where you are- Theodore Roosevelt

Contents

6.1 Introduction 247
6.2 Aims 252
6.3 Results 254
6.4 Discussion 285
6.5 Summary 291

6.1 Introduction

In the previous chapter, I showed that removal of IFT88 from chondrocytes affected growth plate cartilage during post-natal-weeks 4-10. More specifically, in cKO mice, calcification of the hypertrophic region of growth plate cartilage was inhibited, resulting in longer growth plates and a failure of growth plate closure. This is in contrast to Hh mutants and deletion of ciliary proteins at earlier timepoints in development, raising the possibility of an evolving role for ciliary IFT/the primary cilium in

post-natal cartilaginous tissues. The striking failure of ossification in the peripheral growth plate of cKO mice, in contrast to the growth plate in the centre of the tibia, also implicates a cell extrinsic factor, such as the response to mechanical forces, is relevant in the IFT88 cKO scenario. It is likely that Hh signalling was also being altered in this context either downstream to altered mechanotransduction and/or as a direct result of targeting IFT88.

Very little is known about the role of IFT88, or indeed other cilia proteins, in adult articular cartilage homeostasis and disease. Ligand-induced (thus ciliary regulated) Hh signalling has been proposed to play a role in osteoarthritic disease of the articular cartilage (Lin et al., 2009). In addition, *in vitro* studies implicate IFT88 in the articular chondrocyte response to compressive loading (Wann et al., 2012).

In contrast to dynamic growth plate cartilage, articular cartilage is often considered a nearly inert protective covering, created to bear loading at the joints through an adults lifetime (Fig. 6.1.0.1), with some of its extracellular matrix (ECM) components being turned over extremely slowly (Heinemeier et al., 2016). Other components of the ECM are turned over more frequently and this is important for the maintenance and health of the tissue. Loading of the joint is crucial for its development, maintenance, and health; pathology arises in part as a result of aberrant loading.

Association studies of gait analysis, kinematics, joint shape, and physical activity in both knee and hip osteoarthritis (OA), suggest the significance and importance of mechanical loading through weight and muscular contractions (DeFrate et al., 2019). However, investigations of the mechanosensitive nature of musculoskeletal tissues has predominantly focused on bone and muscle, as cartilage is comparatively very difficult to visualise (Galea et al., 2017; Ziaaldini et al., 2017).

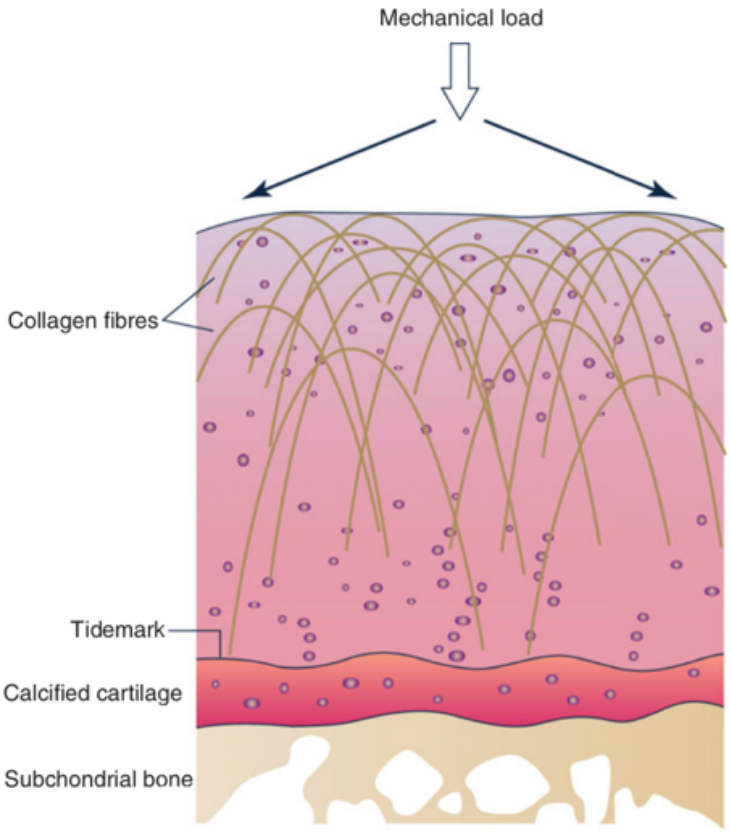


Figure 6.1.0.1: Articular cartilage dissipates mechanical load equally across the tissue. Mechanical load is dissipated throughout the articular cartilage tissue through the unique structure of collagen fibres and their interactions with ECM proteins. The articular cartilage meets the calcified cartilage at the tidemark which mediates the transition to the subchondral bone. Reproduced from (Vincent et al 2018).

Cartilage is a mechanosensitive tissue, with articular chondrocytes closely monitoring and remodelling their environment in response to mechanical loading by altering the synthesis and catabolism of the ECM (Grodzinsky et al., 2000; Palmoski and Brandt, 1984). Mechanically induced stress in chondrocytes results in Runx2, ADAMTS-5 and MMP-13 upregulation (Mitchell et al., 1996; Tetsunaga et al., 2011). Both ADAMTS-5 and MMP-13 have been linked to degradation of the cartilage leading to OA (Chen et al., 2012; Glasson et al., 2005b; Little et al., 2007). It is therefore well established that mechanical input is crucial in cartilage development and homeostasis, but also that pathophysiological loads can lead to OA (Vincent and Wann, 2018). To study the progression of OA in mouse models, the surgical destabilisation of the medial meniscus model is commonly used (Glasson et al., 2005b; Glasson et al., 2007). Cutting the medial meniscus results in joint destabilisation, leading to OA like changes, such as cartilage loss and osteophyte formation, as early as 4-weeks post-surgery, and fully developed OA by 16-weeks (Blease et al., 2018). Despite the wide acceptance that mechanics is central to cartilage health and disease (DeFrate et al., 2019; Sanchez-Adams et al., 2014; Vincent and Wann, 2018), it is still unknown which components of the joint are responsible for sensing these mechanical loads.

Articular chondrocytes express a singular immotile primary cilium

(Poole et al., 1997), which has previously been likened to a 'mechanosensor', most famously within the kidney (Nauli and Zhou, 2004; Praetorius and Spring, 2001; Praetorius and Spring, 2003). In chondrocytes, the primary cilium can either project into the ECM or be invaginated within the cell membrane, exposing only the tip of the structure (Poole et al., 1997). Within research exploring the role of the primary cilium in cartilage, previous *in vitro* work has implicated IFT88 to be crucial for the mechanically induced production of ECM proteins in chondrocytes (Wann et al., 2012). Furthermore, mechanical loading has also been shown to reduce cilia length and prevalence in bovine chondrocytes (McGlashan et al., 2010).

As outlined in the introduction to this thesis, ciliary IFT is also now associated with the regulation of a plethora of cell signalling pathways and behaviours including Hh, Wnt, TGF, IGF, autophagy, and cell differentiation (Christensen et al., 2012; Clement et al., 2013b; Gerdes et al., 2007; Joukov and De Nicolo, 2019). Many of these pathways are likely to be influential in adult articular cartilage. The aberrant activation of Hh signalling, itself mechanosensitive (Rolfe et al., 2014; Thompson et al., 2014a; Wu et al., 2001), has been identified in human OA (Lin et al., 2009), and its genetic and pharmacological inhibition rescues OA progression in the mouse. Prior to this, the regulation of the Hh pathway

in adult articular cartilage had been demonstrated to result in alterations to articular cartilage thickness, the regulation of which is poorly described and understood.

Matrix turnover, Hh signalling, and mechanics are all factors implicated in OA and cartilage homeostasis, and all have links specifically to IFT88 and therefore potentially, by extension, to the primary cilium. With this substantial evidence, we hypothesized that IFT88 and the cilium could be crucial to adult cartilage homeostasis and understanding more about its role could allow for its exploitation during targeted treatments to maintain cartilage health. I hence aimed to investigate whether IFT88 maintained influence beyond embryonic and early post-natal development in articular cartilage homeostasis in the mouse.

6.2 Aims

1. To characterise the naïve process of articular cartilage maturation during adolescent development and adult homeostasis up until 8 months of age in the mouse).
2. To investigate whether the ciliary protein IFT88 retains influence in the maturation and homeostasis of articular cartilage beyond 4-weeks of age. The effects of cartilage specific IFT88 deletion during adolescent development at 4, 6- and 8-weeks of age were characterised through use of

histological analysis and immunohistochemistry.

6.3 Results

6.3.1 The post-natal adaptation of mouse tibial articular cartilage

An abundance of literature can be found describing embryonic formation of articular cartilage. In contrast, there has been less characterisation of articular cartilage during adolescence and adulthood. Cartilage thickness measurements were taken from the mouse tibial plateau (Fig. 6.3.1.1 A, as described in Methods). After a relatively stable phase between 6- and 8-weeks, between 8- and 10-weeks of age, cartilage thickness increases by ~10%, increasing by ~9μm. Between 10- and 22-weeks of age the cartilage continues to thicken by ~5% or 5μm. Therefore between 8- and 22-weeks of age there is an increase of 15% in total thickness. By 8 months of age, a slight decrease in total articular cartilage thickness is observed (Fig. 6.3.1.1 B).

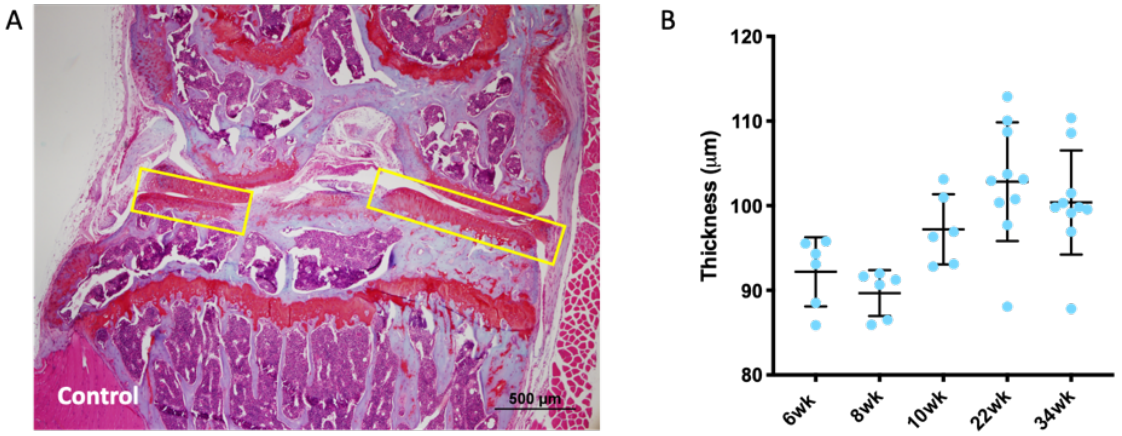


Figure 6.3.1.1: Tibial articular cartilage thickness. A) Histological coronal section of 10-week old knee joint. Yellow boxes demarcate tibial plateaus of which measurements were taken. Three measurements were taken from each plateau from three consecutive sections from the middle of the joint B) Articular cartilage thickness of the tibia plateau. Data represents ±standard deviation, n ≥ 6.

6.3.1.1 Analysis of medial and lateral articular cartilage thickness between 6- and 34-weeks

There is a difference in weight bearing between the medial and lateral plateaus; the highest pressure is exerted on exposed medial cartilage in the mouse, whilst in the human, the lateral meniscus takes the highest force (Blease et al., 2018). The menisci protect the articular cartilage by absorbing some of these axial mechanical forces, but the lateral meniscus is larger and covers more of the cartilage than the medial mensicus. Additionally, the medial plateau also experiences higher loads in humans (Liu et al., 2010). Owing to the differences in mechanical loading on both the lateral and medial plateaus and the mechanosensitive nature of cartilage (Racunica et al., 2007), measurements taken of the tibial plateau were split between the two plateaus. At each time point the medial

cartilage is thicker than the lateral, the medial cartilage continuing to thicken over time (8-22-weeks) (Fig. 6.3.1.2).

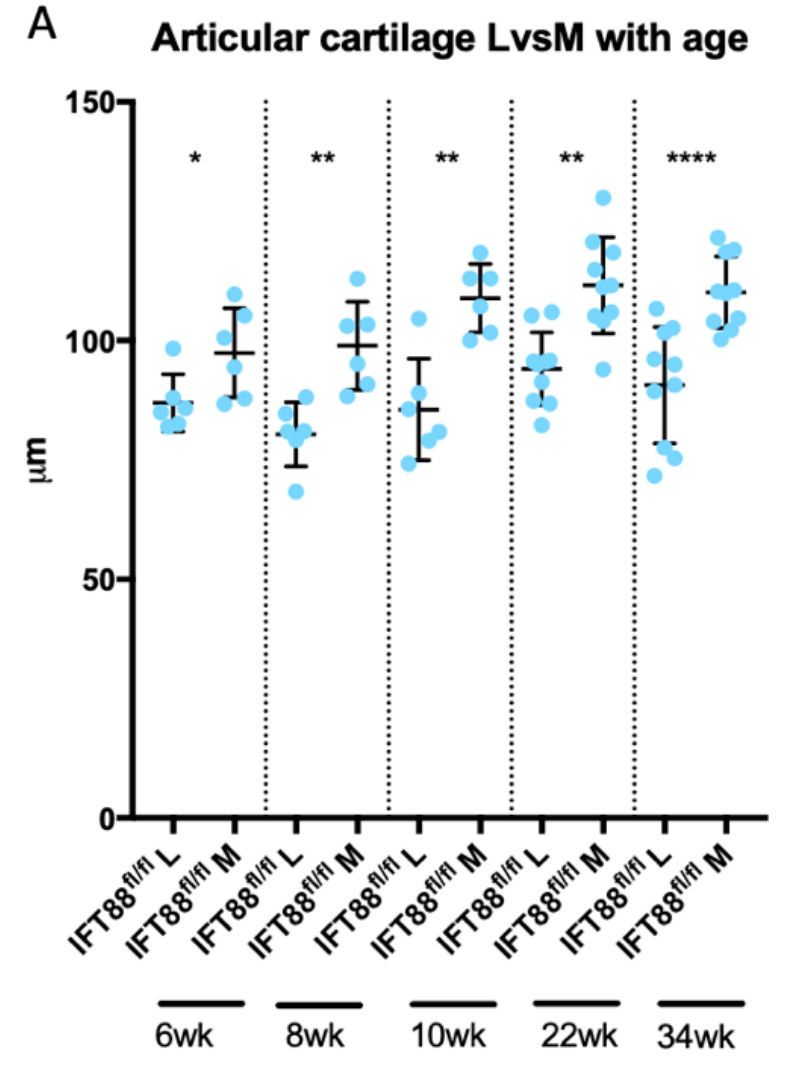


Figure 6.3.1.2: Articular cartilage is significantly thicker on the medial plateau at every age between 6- and 34-weeks. Thickness measurements were taken from control animals. A) Articular cartilage thickness measurements on the lateral (L) and medial (M) side at each age: 6-, 8-, 10-, 22-weeks and 34-weeks. Data represents ±standard deviation and statistical significance was assessed using the non-parametric Mann-Whitney U test where *p<0.05, ** p<0.01, and ****p<0.0001

6.3.1.2 Articular cartilage calcification

It has previously been documented that cartilage gradually calcifies with age in humans (Mitsuyama et al., 2007; Shitama, 1979).

To further characterise naïve articular cartilage in this mouse model, measurements were taken of the uncalcified and calcified regions of cartilage. These two regions are distinct and can be distinguished by Safranin-O staining, using the tidemark (See Methods Fig. 2.6.4.2 for a more detailed description of method). The uncalcified region of cartilage is more proteoglycan rich than the calcified cartilage beneath, and hence the regions are demarcated (Fig. 6.3.1.3 C). Graphs below display cartilage measurements of uncalcified and calcified cartilage (Fig. 6.3.1.3 A) and the respective ratios of each type of cartilage (Fig. 6.3.1.3 B) between 6-weeks and 8 months of age. At 6-weeks of age the articular cartilage consists of ~60% uncalcified cartilage and ~40% calcified cartilage (Fig. 6.3.1.3 B). At 8-weeks of age, there is equal representation of calcified and uncalcified cartilage, however, by 10-weeks of age, there is significantly more calcified cartilage than uncalcified. This disparity continues to widen with age until the cartilage consists of ~60% calcified cartilage and ~40% uncalcified by 22-weeks of age (Fig. 6.3.1.3 B).

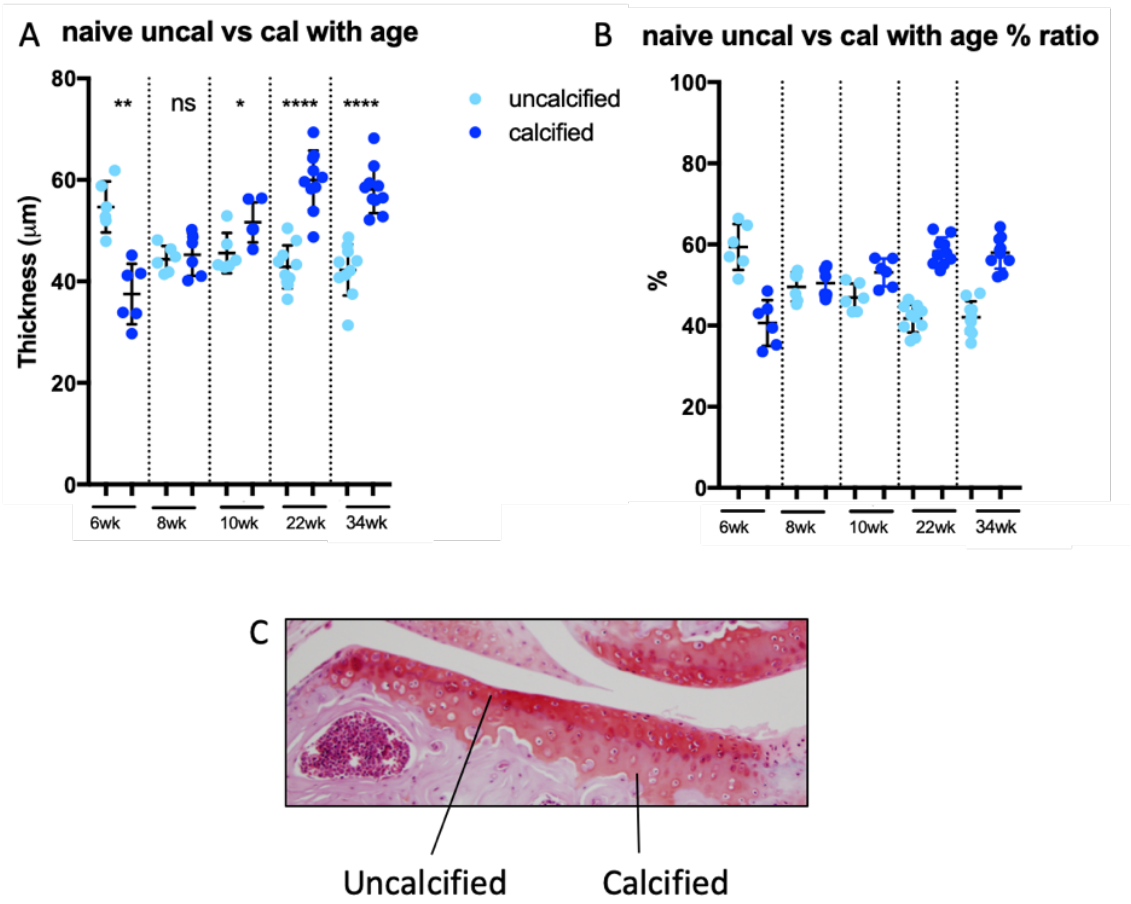


Figure 6.3.1.3: Articular cartilage calcifies with age. A) Uncalcified and calcified measurements of articular cartilage at each time point. B) Uncalcified and calcified cartilage measurements as a percentage ratio of total cartilage thickness. C) Histological section showing where calcified and uncalcified measurements were taken from. See Methods Fig. 2.6.4.2 for a more detailed description. Data represents ±standard deviation and statistical significance was assessed using the non-parametric Mann-Whitney U test.

When these changes in calcified and uncalcified cartilage were considered in parallel as depicted in Fig. 6.3.1.3 B, it becomes clear between 6-8-weeks of age, ~10% of uncalcified cartilage was lost and/or replaced with equal amounts of calcified cartilage. Between 8-10-weeks ~3% of uncalcified cartilage underwent calcification and by 5 months of age (22-weeks) this had widened to ~5% at which time, the tissue stabilises (Fig. 6.3.1.5 B). Therefore, calcified

cartilage increases its contribution to total cartilage thickness over time, as a result of losses to the uncalcified region. This process is illustrated schematically in Fig. 6.3.1.4 C.

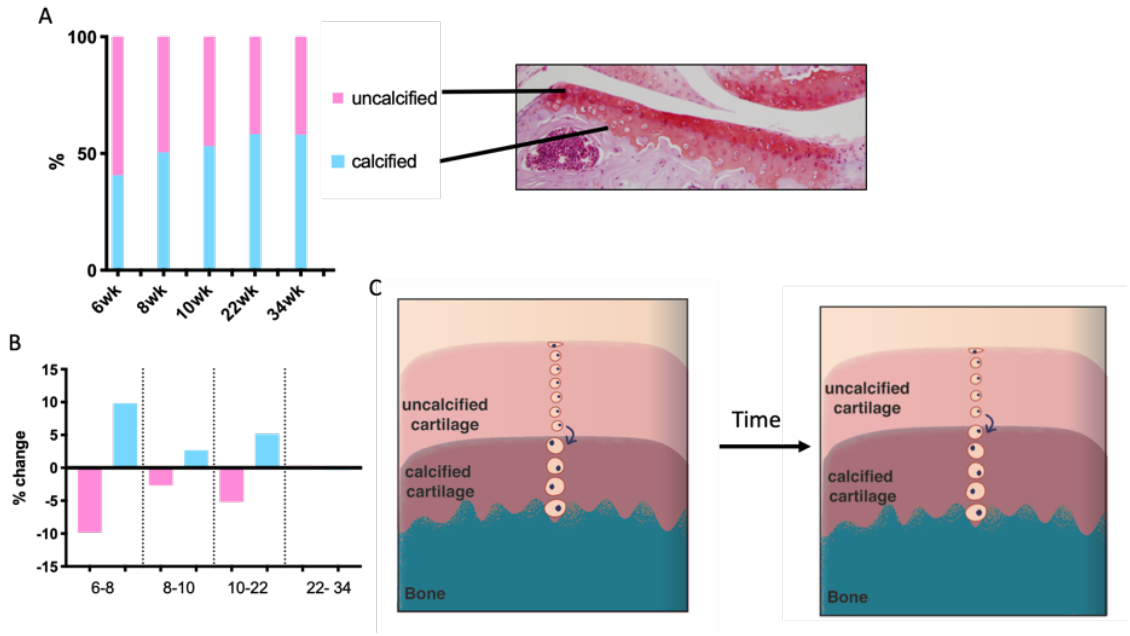


Figure 6.3.1.4: Articular cartilage calcifies with age, replacing uncalcified cartilage with calcified cartilage.
A) Uncalcified and calcified cartilage measurements as a percentage ratio of total cartilage thickness over time referencing histological section from where measurements were taken. B) Differences in uncalcified and calcified measurements between sequential age groups identifying loss of uncalcified cartilage is replaced by calcified cartilage. C) A schematic representation illustrating the loss of uncalcified cartilage to calcified cartilage over time.

Despite observed differences in total thickness of the calcified and uncalcified cartilage between lateral and medial plateaus (Fig. 6.3.1.5 A), when considering these measurements in relation to total length of cartilage, in percentage ratio terms, this difference is eradicated (Fig. 6.3.1.5 B). Hence, there is no difference in the composition of articular cartilage between lateral and medial plateaus and they consist of equal ratios of calcified and uncalcified

cartilage and both plateaus calcify at equal rates over time.

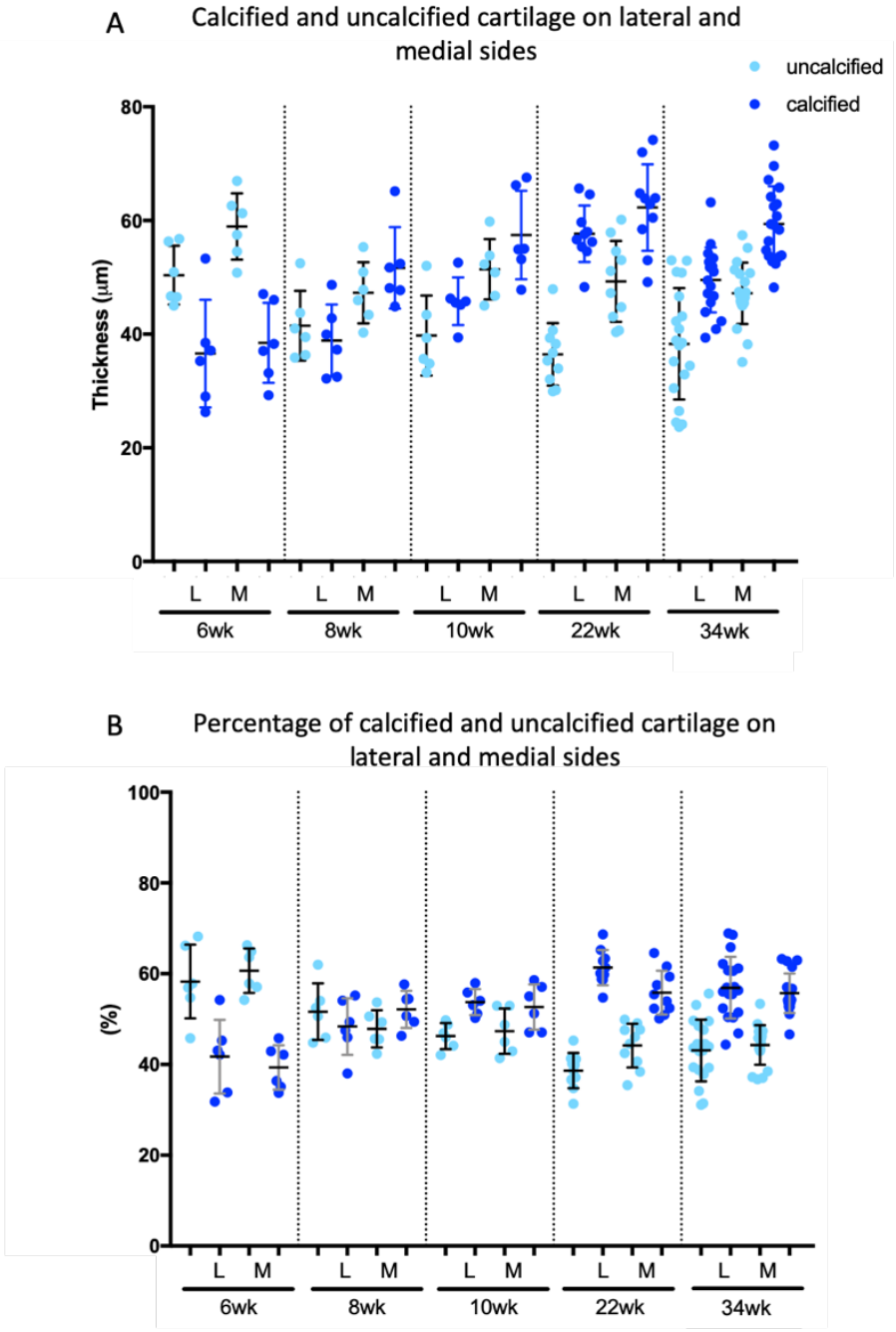


Figure 6.3.1.5: Calcified and uncalcified measurements differ between lateral and medial plateaus, but this difference is not reflected as a proportion of total cartilage thickness. A) Calcified and uncalcified measurements separated between lateral and medial plateaus. B) Uncalcified and calcified cartilage measurements separated by side and calculated as a percentage ratio of total cartilage thickness on respective side. Data represents ±standard deviation.

6.3.2 The role of IFT88 in adolescent articular cartilage homeostasis

6.3.2.1 Cartilage thickness

Between 6- and 10-weeks of age cartilage thickness increases by 10%, and shifts to more calcified cartilage in both the medial and lateral compartments. Previous models constitutively targeting IFT88 in developing cartilage observed increased articular cartilage thickness (Chang et al., 2012) and disorganisation of chondrocytes in presumptive articular chondrocytes (McGlashan et al., 2007). As observed in Chapter 5, a range of phenotypes were seen across cKO animals. Phenotypes ranged from very little changes to articular cartilage to those with very thin articular cartilage and meagre proteoglycan staining (Fig. 6.3.2.1 A). Tibial plateau cartilage thickness in both compartments was measured, averaged and compared with control counter-parts post-deletion of IFT88 at 4- and 6-weeks of age. Significantly thinner cartilage was seen two-weeks post-deletion at both time points (Fig. 6.3.2.1 B). Separation of measurements by medial and lateral plateau revealed statistically significant differences were only measured on the medial plateau at 8-weeks, two-weeks post-deletion at 6-weeks of age (Fig. 6.3.2.1 C). However, interpretations made at these time points would have to consider the potential destabilisation of the joint by large changes inflicted to the growth plate cartilage as

described in Chapter 5.

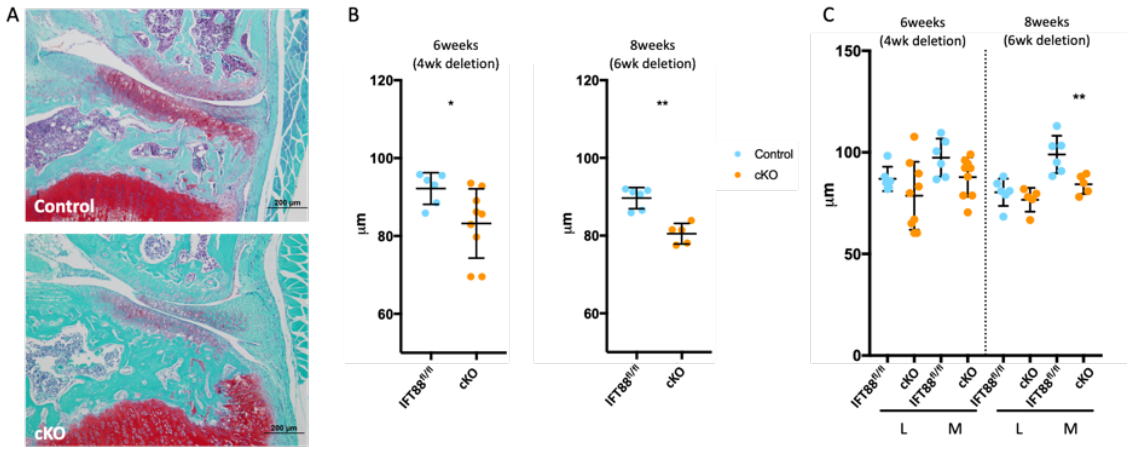


Figure 6.3.2.1: Effects of IFT88 deletion in articular cartilage. A) Control and cKO images representing cartilage thinning and loss of proteoglycan staining. B) Total cartilage thickness measurements from the articular cartilage of control and cKO animals two weeks post tamoxifen at 6 (left) or 8 (right) weeks of age. C) Cartilage thickness measurements taken from lateral (L) and medial (M) plateaus from control and cKO animals two weeks post tamoxifen at 6 (left) or 8 (right) weeks of age. Data represents ±standard deviation and statistical significance was assessed using the non-parametric Mann-Whitney U test where *p<0.05, and ** p<0.01

6.3.2.2 Cartilage calcification

To understand observed differences to cartilage thickness (Fig. 6.3.2.1 B), calcified and uncalcified cartilage measurements were taken, as described for naïve mice. Examination of cartilage thickness at 6-weeks of age revealed a significant decrease in calcified cartilage thickness on the lateral plateau, two-weeks after tamoxifen treatment at 4 weeks of age (Fig. 6.3.2.2 A). However, no other statistically significant changes were observed between uncalcified or calcified cartilage on either the lateral or medial plateaus.

At 8-weeks of age, a statistically significant decrease in calcified

cartilage was observed on the medial plateau two-weeks post-tamoxifen treatment in cKO (Fig. 6.3.2.2 B). This was in contrast to the observed decrease in calcified cartilage thickness on the lateral plateau at 6-weeks of age (Fig. 6.3.2.2 A). No other significant changes were observed between uncalcified or calcified cartilage on either the lateral or medial plateaus at 8-weeks of age.

Cartilage homeostasis and integrity is reliant on the composition of the ECM (Sanchez-Adams et al., 2014). In the literature (Mitsuyama et al., 2007) and within data sets above (Fig. 6.3.1.3) ~60% of articular cartilage is calcified and 40% uncalcified by adulthood. Within these data, (Fig. 6.3.2.2 C) earlier in development at 6-weeks of age, the uncalcified cartilage makes up a larger proportion of the cartilage, at 60% to 40% calcified cartilage. By 8-weeks of age (Fig. 6.3.2.2 D) the articular cartilage slowly transitions to 50% equal composition. Therefore, percentage ratios were calculated from measurements in Fig. 6.3.2.2 A and B and displayed in Fig. 6.3.2.2 C and D. Deletion of IFT88 at 4-weeks of age resulted in no significant changes to the uncalcified and calcified cartilage ratios in the articular cartilage (Fig. 6.3.2.2 C). However, two-weeks post-deletion at 6-weeks of age, there is a significant change to the ratio of uncalcified and calcified cartilage on the medial plateau bringing the articular cartilage to ~50% equal composition, potentially inhibiting a natural calcification process or reflecting a

substantial loss of calcified cartilage (Fig. 6.3.2.2 D).

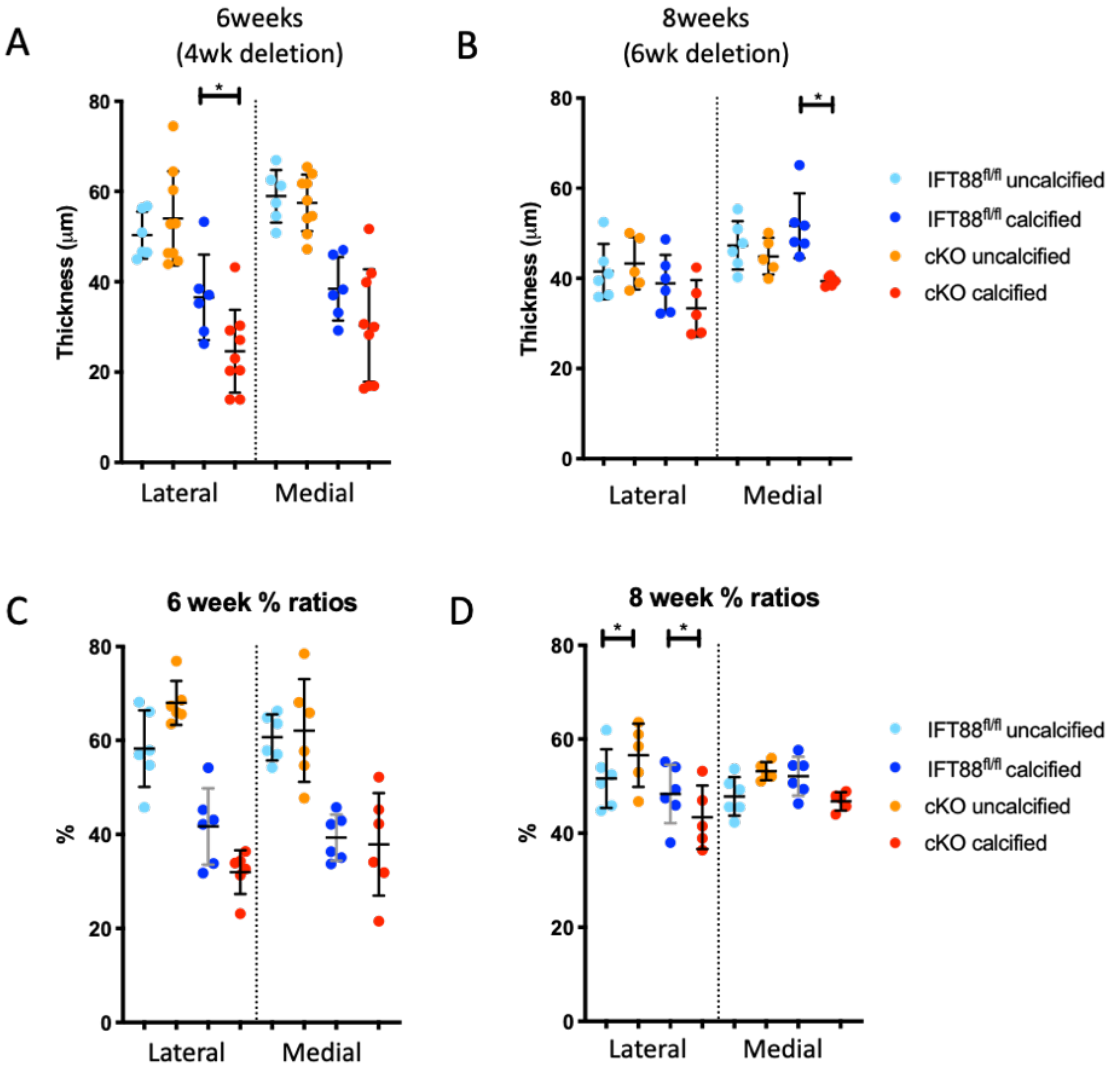


Figure 6.3.2.2: Removal of IFT88 results in decreased calcified cartilage thickness by 8-weeks. A) Measurements of calcified and uncalcified cartilage were split between lateral (L) and medial (M) at 6-weeks of age (4wk deletion). B) Measurements of calcified and uncalcified cartilage were split between lateral (L) and medial (M) at 8-weeks of age (6wk deletion). C) Percentage ratios of calcified and uncalcified cartilage were calculated for L and M sides in control and cKO animals at 6-weeks of age (4wk deletion). D) Percentage ratios of calcified and uncalcified cartilage were calculated for L and M sides in control and cKO animals at 8-weeks of age (6wk deletion). Data represents ±standard deviation and statistical significance was assessed using the non-parametric Mann-Whitney U test where *p<0.05.

6.3.3 The role of IFT88 in adult articular cartilage homeostasis

6.3.3.1 Deletion of IFT88 in adult articular cartilage

Previous data in this chapter revealed thinning of the articular cartilage post-deletion of IFT88 during adolescence (Fig. 6.3.2.1). Earlier in this chapter (Fig. 6.3.1.2) it was demonstrated that articular cartilage thickness increases after 8-weeks of age, increasing 10% between-weeks 8- and 10 and 15% between 8 and 22-weeks.

Mice were given tamoxifen via I.P injection at 8 weeks of age and collected at 10, 22 or 34 weeks of age as illustrated in the schematic below (Fig. 6.3.1.3).

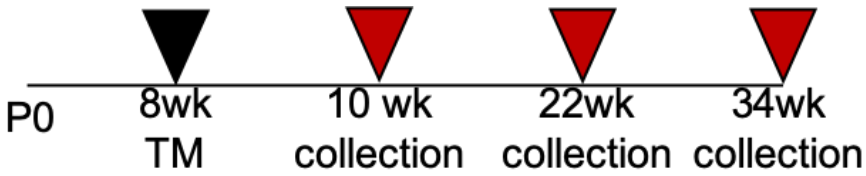


Figure 6.3.3.1: Experimental timeline. Schematic representation of experimental timeline. Animals are born (P0) and at 8-weeks of age given tamoxifen(TM) via I.P. injection (black arrows). Animals were collected at 10, 22 or 34-weeks of age.

When deletion was induced at 8-weeks of age, this 10% increase in thickness from ~89μm to ~97μm was inhibited in cKO mice, with 10-week old cKO thickness remaining at ~89um. The difference between control and cKO mice continued to increase between 10- and 22-weeks of age (14-weeks post-deletion) with controls measuring ~102μm, by which time cKO cartilage was on

average 20% thinner, at 82μm. The cartilage thickness of cKO animals at 22-weeks of age was 8% thinner than that of 8-week old controls, demonstrating that these animals never increased their cartilage thickness indicative of an inhibition of cartilage thickening followed by a thinning. By 6-months post-deletion (34-weeks of age), average articular cartilage thickness had not reduced any further but large changes were apparent in some animals as described in next section (Fig. 6.3.3.2).

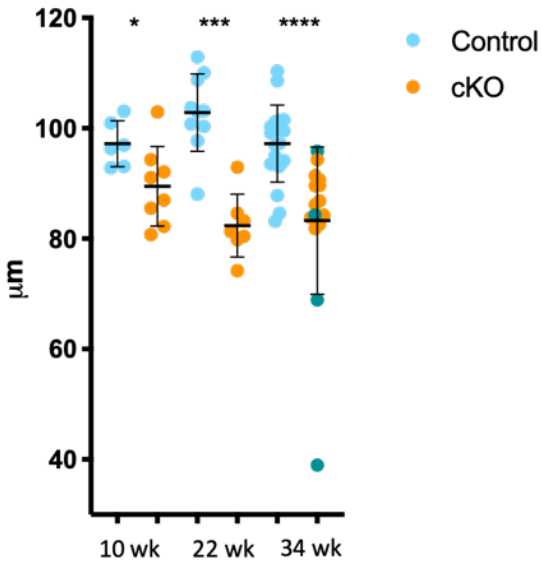


Figure 6.3.3.2: Deletion of IFT88 results in complete inhibition of cartilage thickening followed by progressive cartilage loss within two-weeks. Total cartilage thickness measurements at 10-weeks, 22-weeks and 34-weeks with deletion at 8-weeks of age. Green dots represent animals exhibiting total loss of medial cartilage and osteophyte development.

6.3.3.2 Deletion of IFT88 resulted in atrophy of articular cartilage followed by spontaneous disease by 34 weeks of age

By 34 weeks of age, deletion of IFT88 at 8-weeks of age resulted in spontaneous total loss of cartilage in five animals

presenting with osteophytes and high OARSI scores, disease progression reminiscent of other surgical or spontaneous models of osteoarthritis (Glasson et al., 2007; Staines et al., 2017b) (Fig. 6.3.3.3 A). Other animals in this experimental group did not have spontaneous disease, but did exhibit thinner articular cartilage reminiscent of atrophy. Interestingly, these changes were observed predominantly on the medial plateau, whereas the lateral plateau remained largely unaffected (Fig. 6.3.3.3 B).

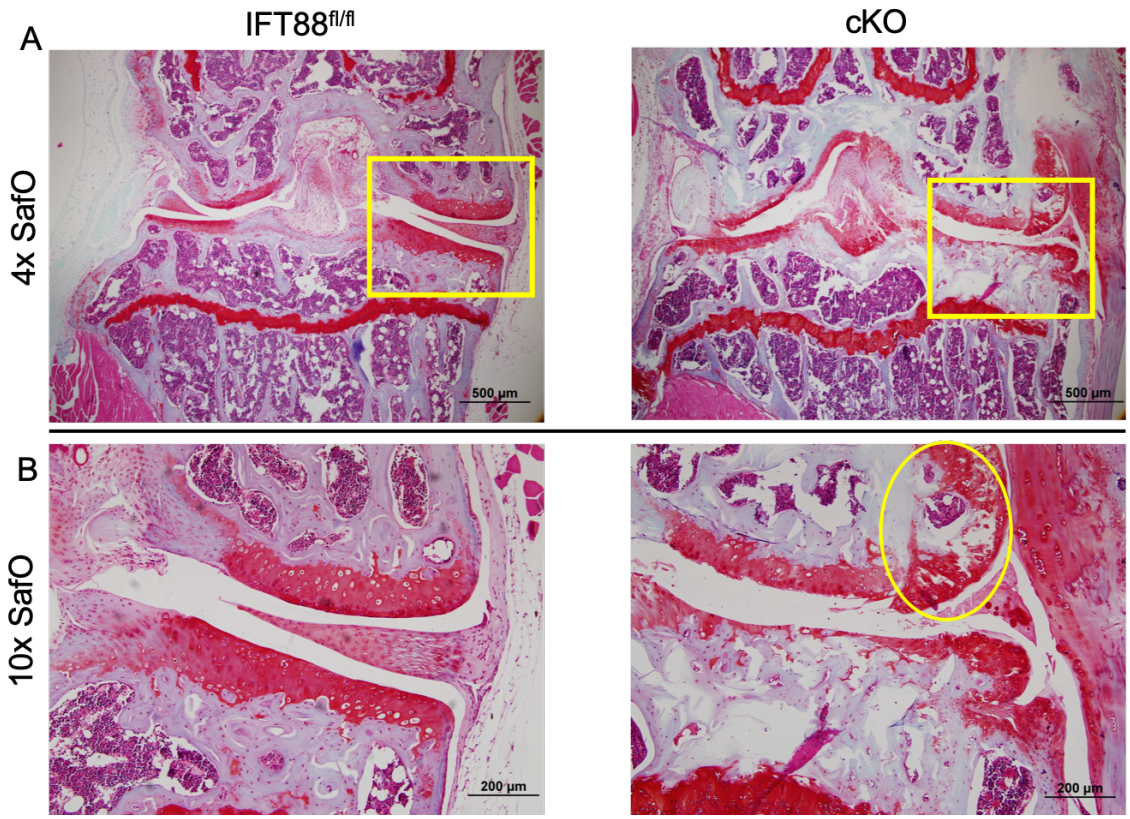


Figure 6.3.3.3: Spontaneous osteoarthritis observed 6 months post-deletion of IFT88 at 8-weeks of age. A) Whole joint Safranin-O stained images (4x) of control and cKO animals. B) 10x Safranin-O images of medial compartment from control and cKO animal sections in A. Osteophyte circled in cKO B.

6.3.3.3 Lateral and medial plateau articular cartilage thickness

In some circumstances (green points on Fig. 6.3.3.4 A), there was total loss of articular cartilage only observed on the medial plateau (Fig. 6.3.3.4). Indeed, the medial plateau was affected at all timepoints (Fig. 6.3.3.4 B). Separating medial and lateral measurements revealed that the medial plateau was at first failing to thicken to that of the controls by 22-weeks and then actively thinning between 22-and 34-weeks of age. This pattern was not observed on the lateral plateau (Fig. 6.3.3.4 A).

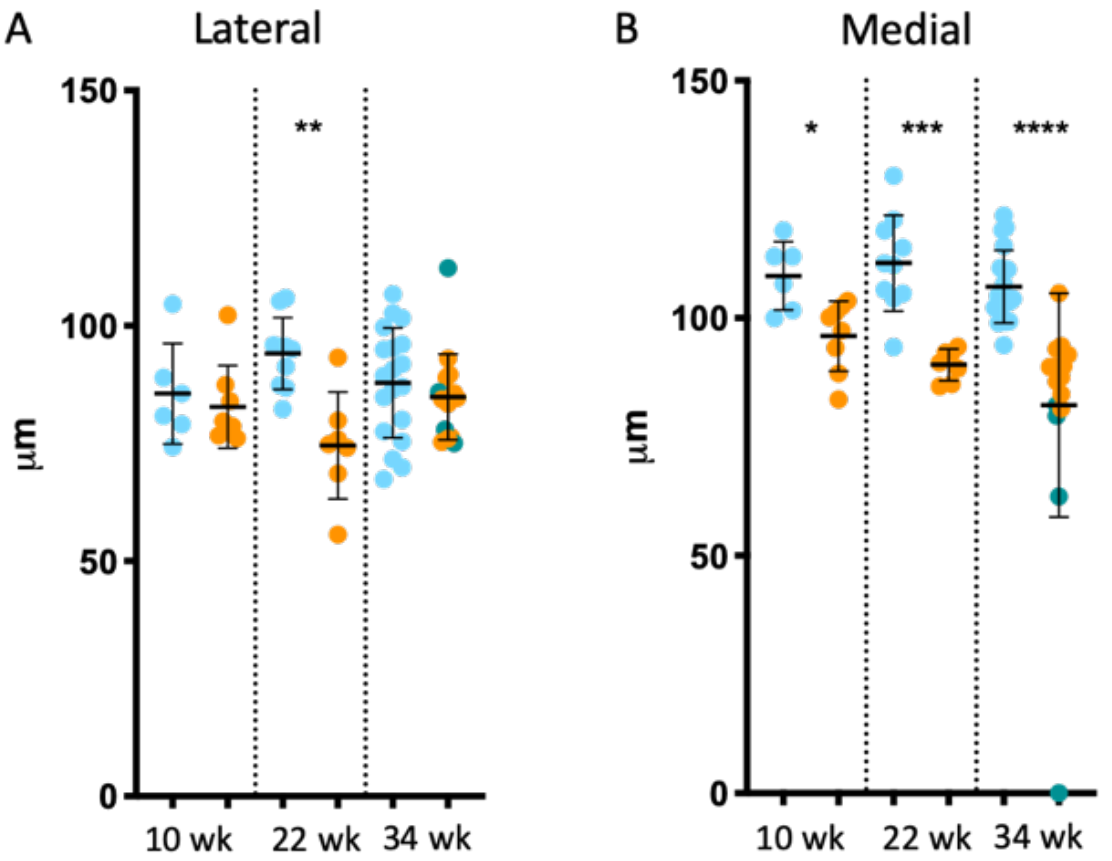


Figure 6.3.3.4: Deletion of IFT88 results in complete inhibition of cartilage thickening followed by progressive cartilage loss within two-weeks predominantly on the medial plateau. Lateral (A) and Medial (B) cartilage thickness measurements. Green dots represent measurements taken from sections with osteoarthritic disease as classed by OARSI score. Data represents ±standard deviation and statistical significance was assessed using the non-parametric Mann-Whitney U test where *p<0.05, ***p<0.001, ****p<0.0001.

6.3.3.4 Analysis of relative articular cartilage calcification

Between 8- and 22-weeks of age, the cartilage continues to calcify switching from a 50:50 ratio of uncalcified to calcified cartilage at 8-weeks, to 40:60 by 22-weeks (Fig. 6.3.3.4). Deletion of IFT88 at 8-weeks of age resulted in no changes in uncalcified articular cartilage thickness at any time point apart from on the medial plateau at 8 months of age, especially where spontaneous disease was observed

(indicated in green) (Fig. 6.3.3.5 A). Conversely, at every time point and all sides, the calcified region of cartilage was thinner post-deletion of IFT88 and was observed in both the medial and lateral compartments (Fig. 6.3.3.5 B).

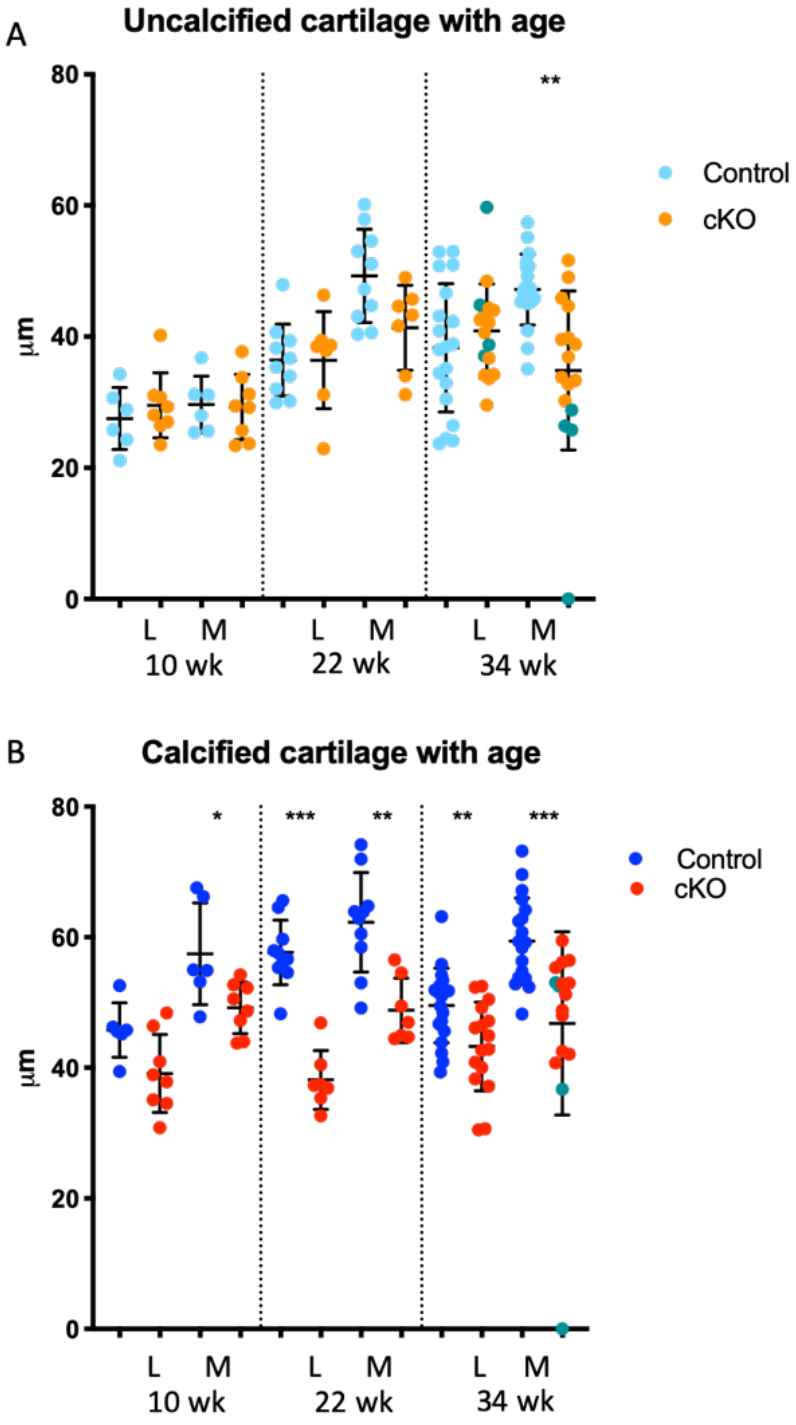


Figure 6.3.3.5: Removal of IFT88 results in significantly thinner calcified cartilage, prior to spontaneous disease. A) Uncalcified cartilage measurements 2-weeks, 14-weeks and 6 months post-deletion of IFT88. B) Calcified cartilage measurements 2-weeks, 14-weeks and 6 months post-deletion of IFT88. Green dots represent measurements taken from sections with osteoarthritic disease. Data represents ±standard deviation and statistical significance was assessed using the non-parametric Mann-Whitney U test where *p<0.05, **p<0.01, ***p<0.001.

6.3.3.5 Percentage ratios of uncalcified and calcified cartilage reveal changes in cartilage composition on the lateral and medial plateau

Measurements of calcified and uncalcified cartilage were calculated as percentage ratios of their respective total cartilage thickness and plotted against age for the lateral (Fig. 6.3.3.6 A) and medial (Fig. 6.3.3.6 B) side. On the lateral plateau in the controls, we can see a change in the ratio of uncalcified cartilage to calcified cartilage between 8- and 22-weeks of age from 60:40 to 40:60 respectively. This can also be seen on the medial plateau. There appears to be a crucial turning point between uncalcified and calcified cartilage ratios at 8-weeks of age where the ratios are equal on lateral and medial plateaus. IFT88 is being deleted at 8-weeks, just at the turning point, during this last maturation phase. In cKO animals on the lateral plateau, the ratio of calcified to uncalcified cartilage at 10-weeks of age is also 50:50 as in controls. However, by 22-weeks of age, these ratios remain at approximately 50:50, whilst in controls it moves to a 40:60 ratio of uncalcified to calcified cartilage. Uncalcified cartilage represents a larger percentage ratio in cKO than in controls. However, on the medial plateau there were no significant differences in ratios of uncalcified and calcified cartilage between cKO and control animals at 10 or 22-weeks of age, but by 34-weeks of age, ratios started to return to 50:50 ratios.

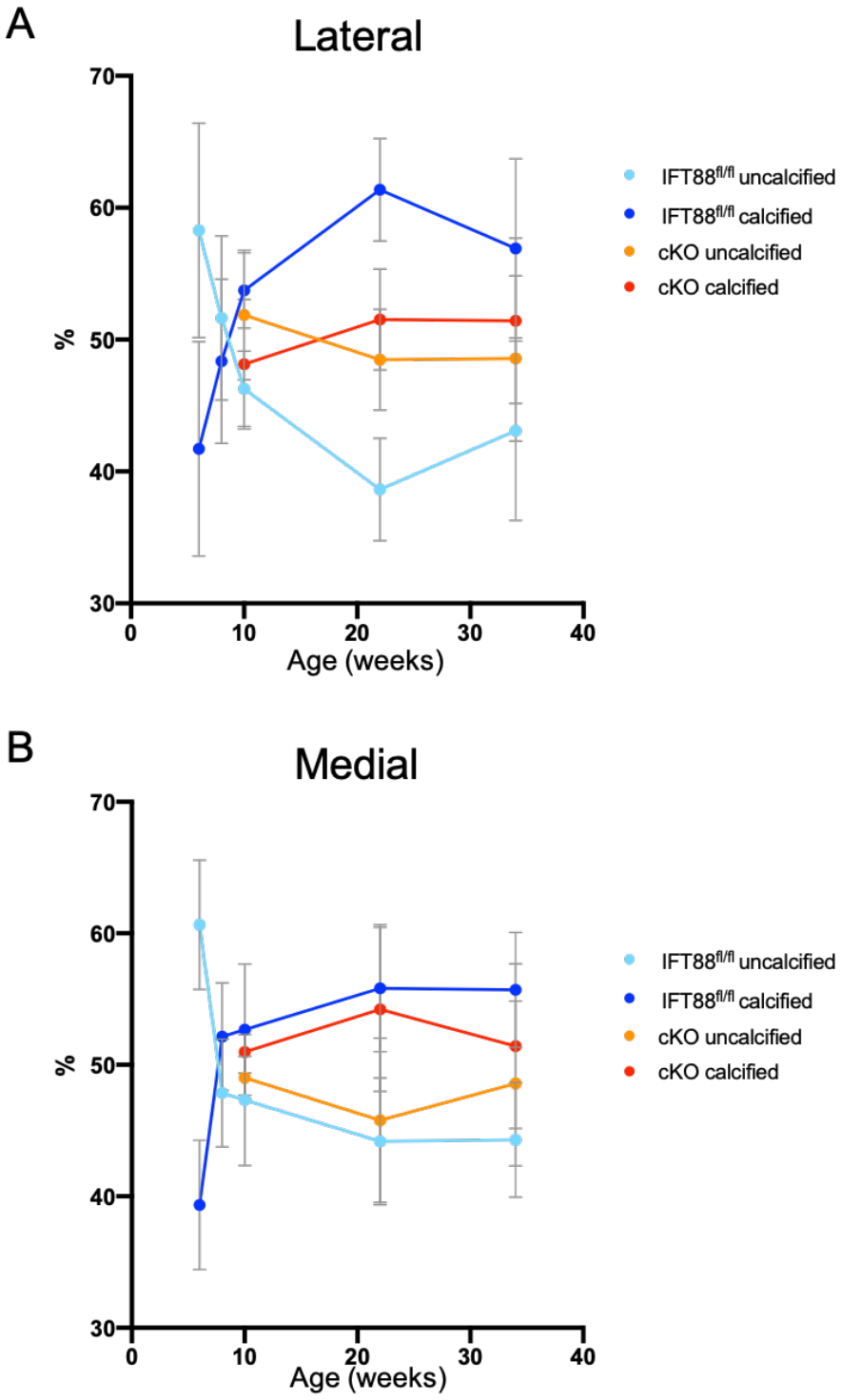


Figure 6.3.3.6: Percentage ratios of uncalcified and calcified cartilage reveal changes in cartilage composition on the lateral and medial plateau. Percentage ratios of uncalcified to calcified cartilage on the lateral (A), and medial (B) side between 8- and 34-weeks of age. Data represents ±standard deviation.

6.3.4 Type X Collagen

Hypertrophic chondrocytes are present in the calcified region of cartilage and are responsible for the adaptation of the cartilage to mediate the interface between the mechanically stiffer subchondral bone than the less stiff uncalcified articular cartilage. Changes to the thickness of the calcified cartilage were observed in Fig. 6.3.3.5. As demonstrated in the growth plate, the dysregulation of Hh signalling results in impaired hypertrophic differentiation, loss of type X collagen staining, and loss of the calcification of the hypertrophic chondrocytes surrounding matrix (Amano et al., 2016; Lin et al., 2009). Recently, the suppressor of calcification ecto-enzyme Enpp1 was found to be downregulated in OA in both human and mouse samples. Enpp1 deficiency leads to calcification of the joints, and is linked to increased Hh signalling in these Enpp1 null mice (Jin et al., 2018). As such, it was hypothesised that perturbation of IFT88 could be impairing the Hh signalling pathway in the calcified region of cartilage, resulting in failed hypertrophic differentiation and subsequent failed ECM calcification (Mak et al., 2006). Type X collagen (ColX) is a marker of hypertrophic differentiation, and its antibody was used to visualise ColX expression in control and cKO histological sections. Due to the variability and qualitative nature of IHC, changes in ColX expression were difficult to resolve. Ongoing studies are

following these results up with qPCR analysis of micro-dissected cartilage.

6.3.4.1 Type X Collagen staining in the articular surface on deletion of IFT88 at 4-weeks of age

On deletion of IFT88 at 4-weeks of age, there appeared to be no observed differences in immunohistochemical staining of ColX between control and cKO animals (n=6, with 3 shown in Fig. 6.3.4.1).

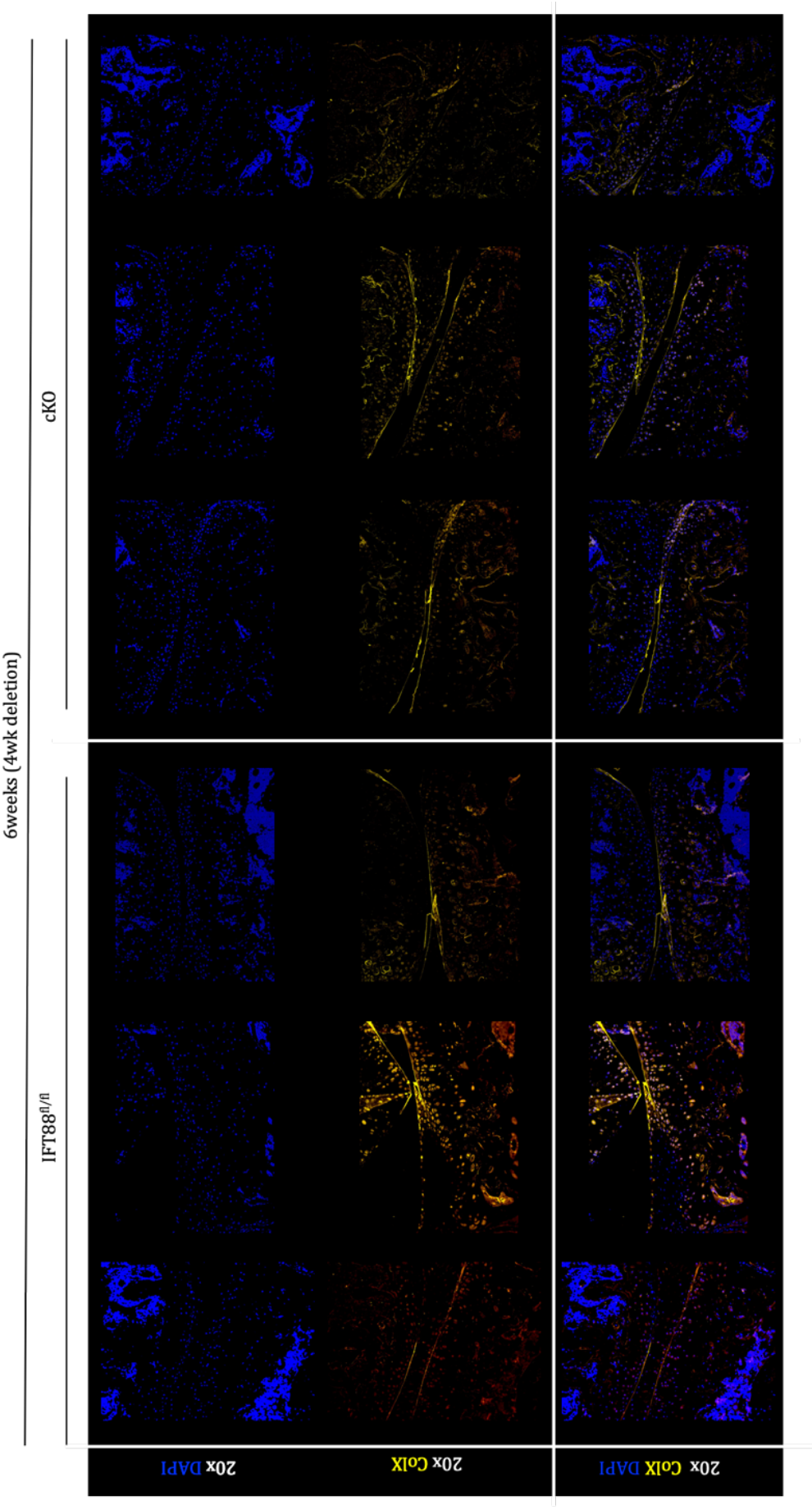


Figure 6.3.4.1: No observed differences in ColX staining on deletion of IFT88 at 4-weeks of age. 20x DAPI (blue), ColX (yellow), and merged images in both control and cKO animals at 6-weeks of age (deletion at 4-weeks)

6.3.4.2 Type X Collagen staining in the articular surface on deletion of IFT88 at 6-weeks of age

On deletion of IFT88 at 6-weeks of age, there appeared to be no observed differences in immunohistochemical staining of ColX between control and cKO animals (n=6, with 3 shown in Fig. 6.3.4.2).

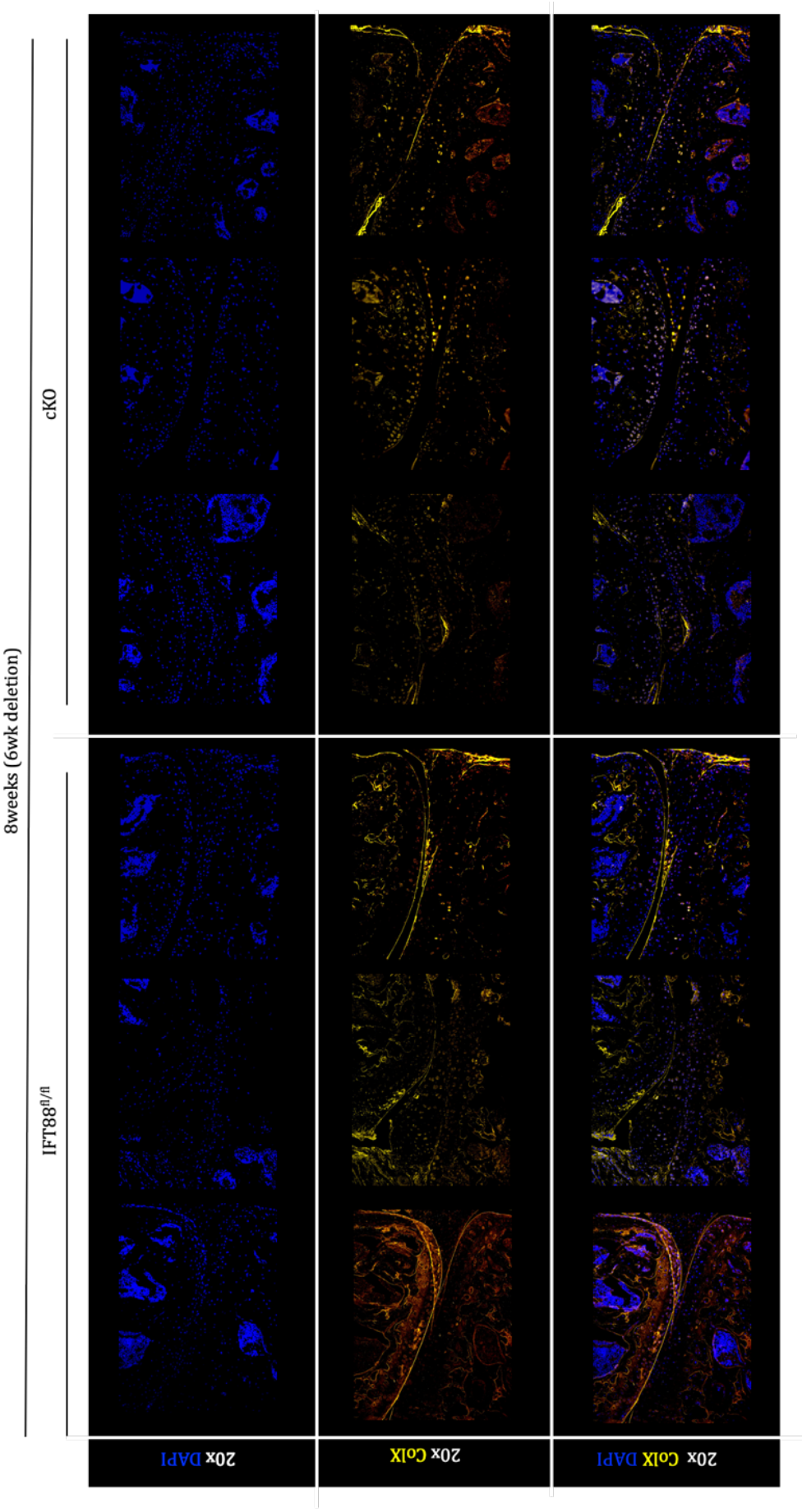


Figure 6.3.4.2: No observed differences in ColX staining on deletion of IFT88 at 6-weeks of age. Coronal sections of the knee joint showing the medial compartment (20x). On top are nuclear stained sections with DAPI (blue). In the middle ColX (yellow) staining. On the bottom are merged images of DAPI and ColX in both control and cKO animals at 8-weeks of age (deletion at 6-weeks).

6.3.4.3 Type X Collagen staining in the articular surface on deletion of IFT88 at 8-weeks of age

On deletion of IFT88 at 8-weeks of age, rapid thinning, particularly in calcified cartilage, was observed as shown in Fig. 6.3.3.4. Staining with ColX showed no differences between control and cKO animals in the calcified cartilage region (Fig. 6.3.4.3).

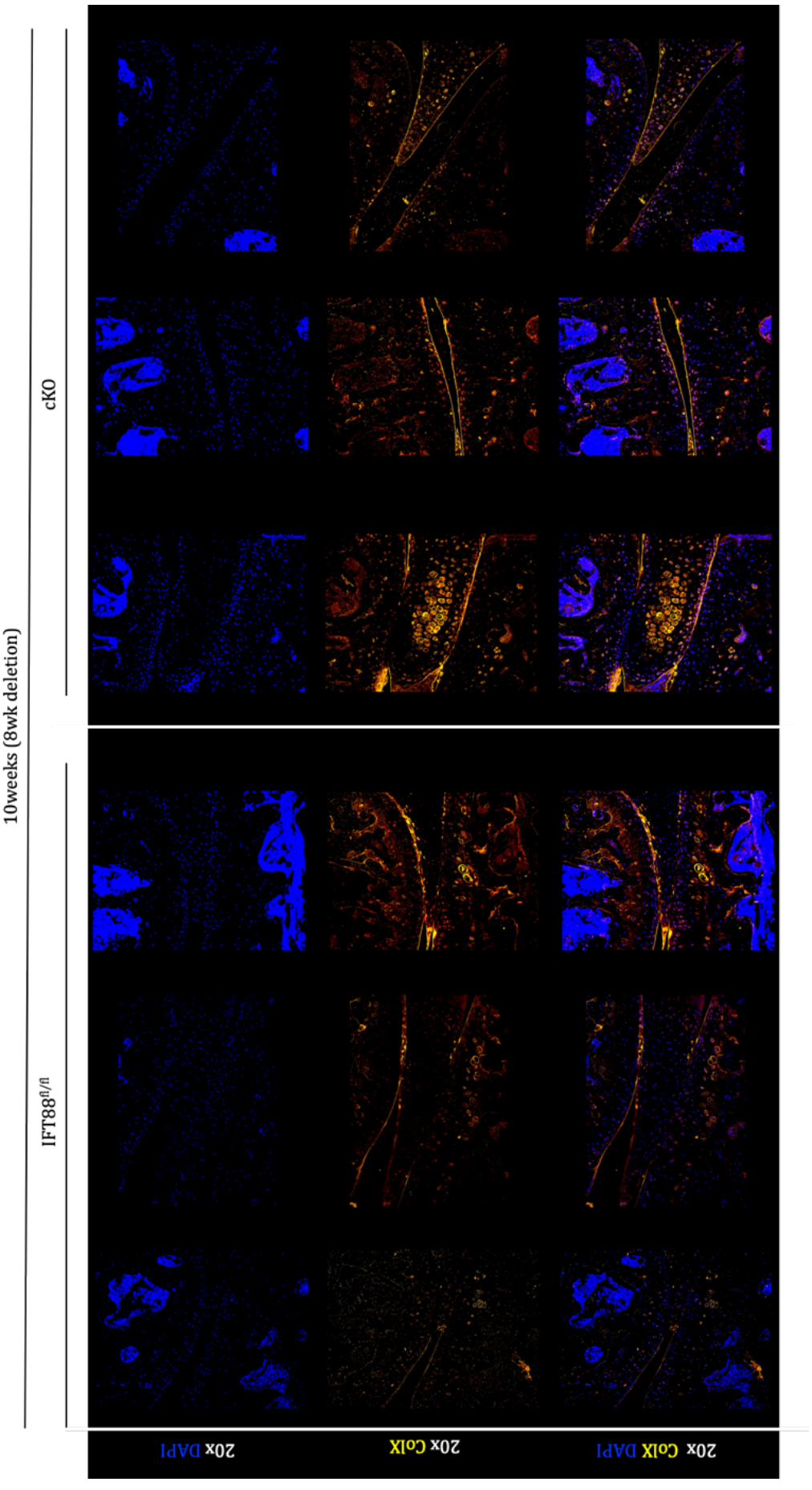


Figure 6.3.4.3: No observed differences in ColX staining on deletion of IFT88 at 8-weeks of age. Coronal sections of the knee joint showing the medial compartment (20x). On top are nuclear stained sections with DAPI (blue). In the middle ColX (yellow) staining. On the bottom are merged images of DAPI and ColX in both control and cKO animals at 10-weeks of age (deletion at 8-weeks).

6.3.4.4 Loss of calcified cartilage is not owing to elevated aggrecan degradation in cKO animals

As there was no difference in ColX staining, changes to cartilage thickness, in either the calcified or uncalcified layer, could be owing to increased matrix turnover and elevated degradation of the cartilage. Aggrecan is a major proteoglycan that makes up the articular cartilage. Aggrecan is degraded by aggrecanases including ADAMTS-5 to produce the neoepitope AGEG, and also the tissue bound fragment NITEGE (Sandy et al., 1992). Loss of this domain of aggrecan results in a loss of binding to hyaluronan, a crucial protein part of the ECM, affecting matrix composition and mechanical properties. Hence, elevated expression of aggrecanases have been associated with cartilage destruction and OA (Glasson et al., 2005b; Little et al., 2007).

To investigate whether observed loss of cartilage could be owing to elevated degradation of the ECM, immunohistochemistry for the tissue residing fragment, NITEGE, was performed on unstained histological sections from control and cKO animals (Fig. 6.3.4.4 and Fig. 6.3.4.5). At 10-and 22-weeks of age, post-deletion of IFT88 at 8-weeks of age, there appeared to be no difference in NITEGE staining between cKO animals in comparison with controls (Fig. 6.3.4.4 and Fig. 6.3.4.5). Hence, this potentially excludes a hypothesis involving higher turn-over of aggrecan as a result of IFT88 deletion,

however, this will have to be repeated (n=3 in each group).

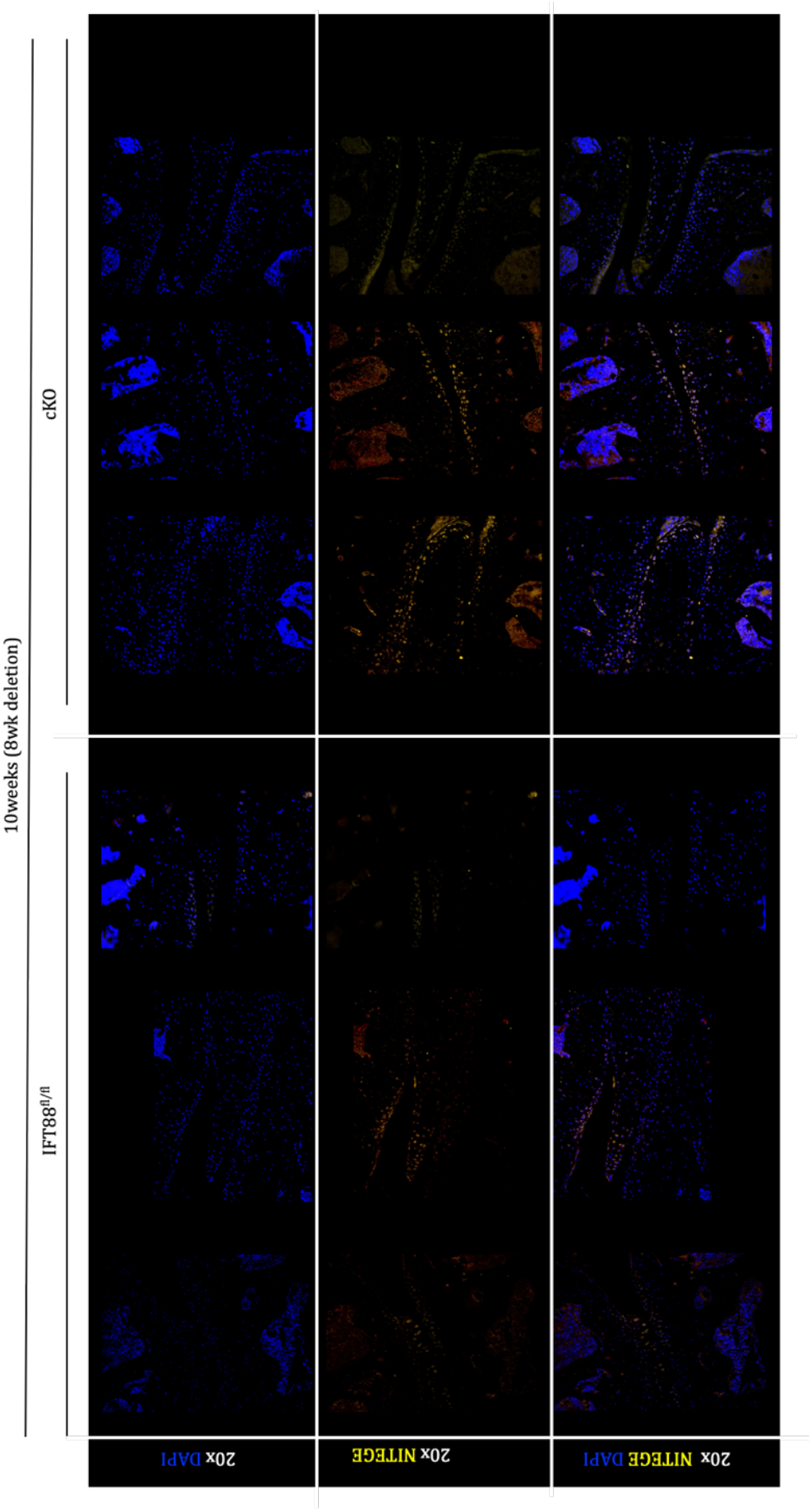


Figure 6.3.4.4: Neoepitope (NITEGE) staining in articular cartilage. Coronal sections of the knee joint showing the medial compartment (20x). On top are nuclear stained sections with DAPI (blue). In the middle NITEGE (yellow) staining. On the bottom are merged images of DAPI and NITEGE in both control and cKO animals at 10-weeks of age (deletion at 8-weeks).

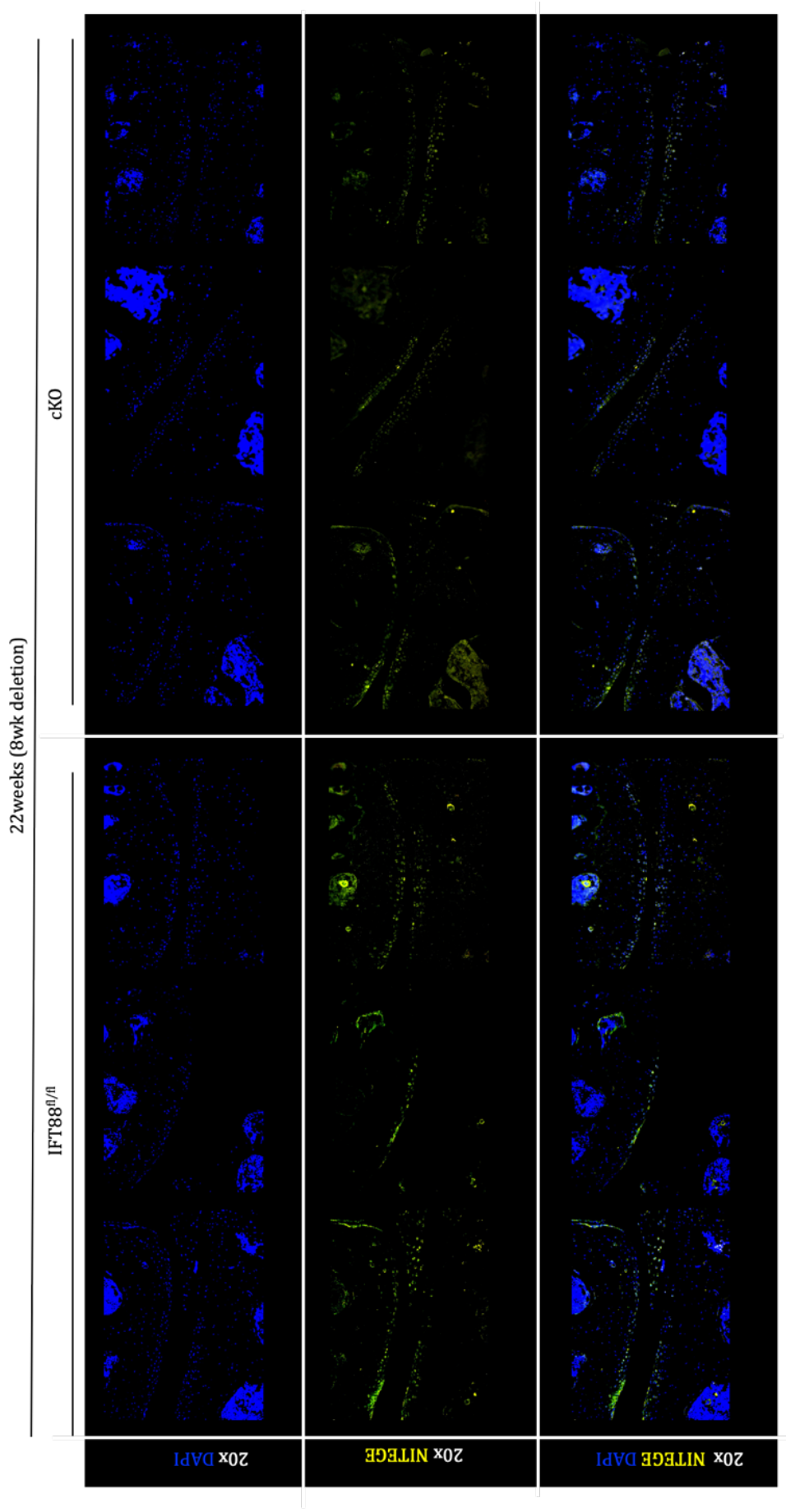


Figure 6.3.4.5: Neoepitope (NITEGE) staining in articular cartilage. Coronal sections of the knee joint showing the medial compartment (20x). On top are nuclear stained sections with DAPI (blue). In the middle NITEGE (yellow) staining. On the bottom are merged images of DAPI and NITEGE in both control and cKO animals at 22-weeks of age (deletion at 8-weeks).

6.4 Discussion

Previous work investigating the role of the primary cilium and IFT88 in articular cartilage has largely been conducted in early development. Very little is understood about the role of IFT in the articular cartilage beyond 4-weeks of age. In this chapter, I aimed to describe naïve maturing cartilage beyond 4-weeks of age during the latter stages of development, and to understand the potential role of IFT88 in these processes described. The data concentrated on cartilage thickness and the relative proportions of uncalcified and calcified regions within.

Between 6- and 8-weeks of age, there is change in articular cartilage thickness in control mice. However, at 8-weeks of age, the articular cartilage of cKO animals is thinner than that of controls, suggesting that cartilage has thinned. In contrast, after 8-weeks of age, there is a gradual thickening of articular cartilage on the tibial plateau up until 22-weeks of age from ~93 to 103μm (Fig. 6.3.1.2). This demonstrates that articular cartilage continues to remodel, to 'mature' beyond 8-weeks of age. The majority of this thickening in control animals between 8- and 22-weeks of age is attributed to the medial plateau of the articular cartilage, whereas lateral cartilage thickness increases are modest during this time period (Fig. 6.3.1.2). This difference in medial and

lateral thickness has been proposed to be owing to differences in mechanical loading between the plateaus. Human and mouse studies have demonstrated that the highest loads are often localised to the medial condyle, and hence medial cartilage could be adapted accordingly (Bruns et al., 1994).

With age, articular cartilage calcifies as a result of relative losses of uncalcified cartilage (Mitsuyama et al., 2007). By using Safranin-O staining to demarcate regions of uncalcified and calcified cartilage, I measured the thickness of each layer. Over the time period I studied, between 6-22-weeks of age, the composition of the cartilage changes, with calcified cartilage increasing in thickness over time, whilst uncalcified cartilage thickness decreases (Fig. 6.3.1.3 A). At 6-weeks of age, ~60% of cartilage is uncalcified which decreases to ~40% by 22-weeks of age. This change in composition perhaps is necessary for the maintenance of a chondro-osseous junction between the less stiff uncalcified cartilage and the much stiffer subchondral bone. Differences in cartilage thickness between each time point demonstrate a progressive loss of uncalcified cartilage, which is directly replaced by calcified cartilage in percentage terms (Fig. 6.3.1.4), a progressive relative 'calcification'. Separation of calcified and uncalcified cartilage by medial and lateral plateaus demonstrated that, in contrast to changes in thickness, which were most apparent on the medial

plateau, progressive 'calcification' was equal in both compartments (Fig. 6.3.1.5 B). These observed differences in composition could have significant implications for the mechanical properties of the articular cartilage. This in turn likely affects the mechanical strains transduced to the chondrocyte.

During the adolescent phase of development, deletion of IFT88 resulted in ~10% thinner articular cartilage overall at 6- and 8-weeks of age, 2-weeks post-deletion (Fig. 6.3.2.1 A). This demonstrated that IFT88 is crucial for this metric of cartilage maturation. There was also significant loss on the medial plateau two-weeks post-deletion at 6-weeks of age (Fig. 6.3.2.1 B). Between 6-8-weeks of age in naïve circumstances, there is a gradual calcification of cartilage altering the ratio of uncalcified cartilage to calcified cartilage from approximately 60:40 to approximately 50:50 respectively. Upon deletion of IFT88 there was a significant change to the ratio on the medial plateau, reflecting a potential inhibition of calcification. This follows a significant reduction of calcified cartilage on the medial plateau (Fig. 6.3.2.2). As the medial plateau experiences higher load, perhaps the removal of IFT88 has affected mechanically induced downstream signalling pathways that are important for the calcification of the articular cartilage. Alternatively, the removal of IFT88 could be inhibiting the maturation of the cartilage, perhaps by altering Hh signalling,

and transitioning from a predominantly uncalcified cartilage to calcified cartilage.

I also investigated the role of IFT88 beyond 8-weeks of age, characterising at 10, 22- and 34-weeks of age. Removal of IFT88 at 8-weeks of age resulted in an inhibition of thickening between 8- and 10-weeks of age (Fig. 6.3.3.2). This inhibition of thickening was largely observed on the medial plateau (Fig. 6.3.3.4) suggesting that removal of IFT88 inhibited a natural thickening process in medial articular cartilage, which could be important for its adaptation and in particular its mechanoadaptation to an increased loading environment. By 22 weeks of age, articular cartilage was thinner in cKO animals than control counterparts indicating atrophy. Thinner cartilage is associated with human OA disease in the clinic. Hence, atrophy of cartilage in cKO animals could predispose the cartilage to disease. Indeed, in some animals we observed severe spontaneous OA like disease by 34 weeks of age, only on the medial plateau.

As shown in Fig. 6.3.3.2 this is a still a relatively dynamic period, in which articular cartilage is maturing and transitioning to contain a higher percentage ratio of calcified cartilage. Deletion of IFT88 at 8-weeks of age also resulted in significantly thinner articular cartilage at 22-weeks and 34-weeks of age (Fig. 6.3.3.2), though the most dramatic loss occurred by 10-weeks. In some animals,

deletion of IFT88 resulted in spontaneous disease exclusively on the medial plateau at 34-weeks of age (Fig. 6.3.3.3). This prompted the separation of lateral and medial measurements. At every time point post-deletion at 8-weeks, significant articular cartilage thickness changes were observed on the medial plateau whereas the lateral plateau remained unaffected (Fig. 6.3.3.4). This was again shown to be affecting only *medial calcified cartilage* thickness by 10-weeks of age and then both lateral and medial calcified cartilage by 22-weeks and 34-weeks of age. This loss of calcified cartilage could reflect inhibited maturation of the calcified cartilage, or lack of expansion of calcified cartilage ECM by hypertrophic chondrocytes. Conversely, on analysis of ratios of calcified an uncalcified cartilage, the lateral plateaus showed the most prominent changes, altering the uncalcified to calcified 40:60 ratio to 50:50 at every time point (Fig. 6.3.3.5). How this impacts the mechanics of the tissue and whether this change could be chondroprotective, inhibiting thinning and disease, is yet to be investigated.

However, medial cartilage is exposed to higher load in regions unprotected by the medial meniscus than lateral cartilage (Bloecker et al., 2012). This suggests that rapid thinning on the medial plateau could be influenced by either failed or exacerbated mechanotransduction of signalling pathways potentially mediated by IFT88. The striking loss of calcified cartilage observed as early

as two-weeks post removal of IFT88 on the medial plateau suggests a failed mechanoadaptation of the cartilage resulting in subsequent spontaneous loss of cartilage and OA-like disease in some animals. Removal of IFT88 could perturb signalling and hence affect the chondrocyte's ability to transduce mechanical signals to the rest of the cell altering the mechanoadaptation of cartilage. However, in the growth plate, Hh signalling is required for chondrocytes to undergo hypertrophy, calcify their surrounding matrix to initiate osteogenesis (Amano et al., 2016; Amano et al., 2015). Type X collagen (ColX) is expressed by hypertrophic chondrocytes and can be used as a marker of chondrocyte differentiation. Histological sections from control and cKO knee joints were probed for ColX. No differences were observed in ColX staining in deep zone chondrocytes between control and cKO animals at 6-, 8- or 10-weeks of age (Fig. 6.3.4.1, Fig. 6.3.4.2, Fig. 6.3.4.3).

In order to understand whether loss of articular cartilage could be owing to increased degradation of aggrecan, we performed immunohistochemistry on unstained sections targeting the aggrecan neoepitope containing fragment NITEGE. However, we found no obvious qualitative difference in NITEGE staining, between control and cKO, and none in the calcified cartilage region where the greatest thinning was observed. Hence, this potentially excludes a hypothesis involving higher turn-over of aggrecan as a

result of IFT88 deletion, however, this will have to be repeated (n=3 in each group).

We cannot rule out the role that chondrocytes and the ECM could play in contributing to the thickness of the articular cartilage. During cartilage maturation, chondrocytes could increase the distance between each other by producing more ECM and hence increasing thickness of the cartilage. This could happen at a greater rate in the calcified region where chondrocytes have undergone hypertrophy and expanded. Conversely, the chondrocytes in the uncalcified layer could calcify the ECM around them, increasing the thickness of the calcified region and moving the tide mark. Perhaps cell density analysis would be able to address this question, however, the lack of regularly organised chondrocyte columns in mouse articular cartilage makes this difficult to interrogate.

6.5 Summary

In conclusion, in this chapter, I have shown that the articular cartilage continues to adapt into adulthood, thickening and calcifying over time. Deletion of IFT88 resulted in an inhibited thickening of articular cartilage, followed by atrophy predisposing the articular cartilage to spontaneous disease. These failed adaptations predominantly affected the medial plateau as seen by inhibited thickening and loss of calcified cartilage. This

demonstrates that IFT88 maintains influence in the adult joint and has a role in articular cartilage homeostasis. Next in this thesis and beyond, I will explore mechanistic possibilities to include the role of Hh signalling, mechanics or perhaps the interaction between these two pathways.

7

Is IFT88 a regulator of the cartilage response to loading

Not all those who wander are lost- J.R.R. Tolkein

Contents

7.1 Introduction 293
7.2 Aims 297
7.3 Results 297
7.4 Discussion 312
7.5 Summary 317

7.1 Introduction

In Chapter 5, I described how deletion of IFT88, during adolescence, resulted in inhibited growth plate maturation, specifically leading to a failure of ossification that was most pronounced in the lateral aspects of the tibial growth plate. These bilateral failures in growth plate dynamics, led us to consider whether changes in the growth plate response to mechanics might underlie the phenotype. Could ciliary IFT be part of the cartilaginous mechanostat of the growth plate?

In the previous chapter, the deletion of IFT88 resulted in the inhibition of articular cartilage thickening between 8- and 10-weeks of age. This was followed by thinning of articular cartilage in cKO animals between 10- and 22-weeks of age. We found this loss was predominantly on the medial side, which receives higher loads (Liu et al., 2010). By 34-weeks of age, in a sub set of animals, this thinning preceded total cartilage loss and bone remodelling, including osteophyte formation, resembling osteoarthritic disease and resulting in high disease (OARSI) scores. Previous animal studies, reducing mechanical loading in the joint, also observed losses in calcified cartilage thickness, indicative of its mechanosensitivity (Kiviranta et al., 1987; Palmoski et al., 1979).

Articular cartilage atrophy is molecularly and structurally distinct from cartilage loss observed in OA disease (Vincent and Wann, 2018). In OA, there is increased protease mediated matrix catabolism coupled with a failed anabolic response (Troeberg and Nagase, 2012). Increased pathological shear forces, introduced through the surgical destabilisation of the joint by cutting the medial meniscus (DMM model) (Glasson et al., 2007; Little and Hunter, 2013), is associated with OA-like disease (Brandt et al., 2009) and up-regulation of proteases *in vivo*. This upregulation of proteases can be abrogated by joint immobilisation (Burleigh et al., 2012) demonstrating a requirement for pathological loading

in the development of OA. DMM is a widely used model to study osteoarthritis, with animals developing early signs of OA by 8-weeks and full-blown OA by 16-weeks. This destabilisation of the joint results in pathological mechanical loading, and closely resembles post-traumatic OA (PTOA) (Ojanen et al., 2019), such as cruciate rupture during sport (Brown et al., 2006). OA starts with fibrillation of the superficial articular cartilage which spreads throughout the tissue and is associated with bone remodelling and osteophyte formation (Brown et al., 2006). In humans, pathological mechanics arising from abnormal shear stress, such as rapidly changing direction during a game of tennis, or, tendon injury resulting in destabilisation and introduction of non-axial mechanical forces can lead to disease pathogenesis (Guilak, 2011; Sanchez-Adams et al., 2014). Shear stresses have been shown to be detrimental to cartilage health resulting in accelerated loss of proteoglycan, whereas axial loading maintains and promotes proteoglycan production (McCulloch et al., 2018; Oka et al., 2019).

However, compressive loads are equally important to cartilage health and homeostasis. Without physiological compressive loading, in cases of paralysis, the cartilage atrophies and there is evident proteoglycan loss (Anderson and Breidahl, 1981; Leroux et al., 2001; Pool, 1974). Only in circumstances where biomechanics and gait are changed to minimise aberrant shear forces, can exercise

post-injury increase GAG production (Roos and Dahlberg, 2005).

In the previous chapter, changes to the articular cartilage as a result of IFT88 deletion, suggested that alterations to Hh signalling (indicated by lack of cartilage calcification, which has been previously shown to be Hh-dependent), and or mechanotransduction, could be mediating subsequent thinning. Both pathological mechanics (Burleigh et al., 2012) and aberrant Hh signalling (Lin et al., 2009) have been linked to cartilage, destruction, and the development of osteoarthritis. Additionally, Hh signalling is required for hypertrophic chondrocyte differentiation within the growth plate and articular cartilage (Lin et al., 2009), and also for the calcification of the articular cartilage during maturation (Jin et al., 2018). The role of the primary cilium and IFT88 is well known to be responsible for the tuning of hedgehog signalling (Clement et al., 2009a) and it has also been linked to mechanotransduction (Nauli et al., 2003; Thompson et al., 2014b).

Collectively, these data (Chapter 6) and previous research leads to the hypothesis that deletion of IFT88 might change how the cells within cartilage perceive mechanics, perhaps 'blinding' the chondrocyte to mechanical loads, making cartilage less mechanoresponsive. The primary cilium could be important for the chondrocyte's response to physiological compressive loads, and not to pathological shear forces. Hence, the introduction

of pathological shear mechanics by destabilisation (DMM), in conjunction with previously observed cartilage thinning in cKO animals, could result in exacerbated disease. Additionally, removal of physiological compressive loads, important for cartilage health, through an immobilisation model might lead to inhibited thickening and maturation of articular cartilage between 8- and 10-weeks of age.

7.2 Aims

To investigate whether IFT88 is important in mediating the cartilage response to changes in mechanical load:

1. Introducing shear mechanical forces through the destabilisation of the medial meniscus model in control and cKO mice.
2. Removing compressive load through the double neurectomy model (immobilisation), cutting the femoral and sciatic nerve in control and cKO mice.

7.3 Results

7.3.1 Joint Destabilisation

7.3.1.1 Destabilisation of the medial meniscus (DMM) model

Pathophysiological shear stress is associated with increased risk of OA development (Muthuri et al., 2011). Experimentally, OA can

be induced in small animal models through cutting of the medial meniscus, resulting in a destabilisation of the knee joint. To explore whether the deletion of IFT88 affected the joint's response to DMM, 8-week old mice were given tamoxifen and surgery was performed at 10-weeks of age (Fig. 7.3.1.1 A). Knee joints were collected 8- or 12-weeks post-surgery (Fig. 7.3.1.1 A). SHAM surgeries, in which the knee joint capsule was opened but the medial meniscus was not cut, were used as a control for each genotype. Harvested knees were processed for histochemical analysis. Histological sections were assessed for cartilage degradation using the OARSI scoring method, a well recognised method for quantifying severity of cartilage disease. Example images show medial compartments of cKO and control mice at both 8- and 12-weeks post-DMM (Fig. 7.3.1.1 B).

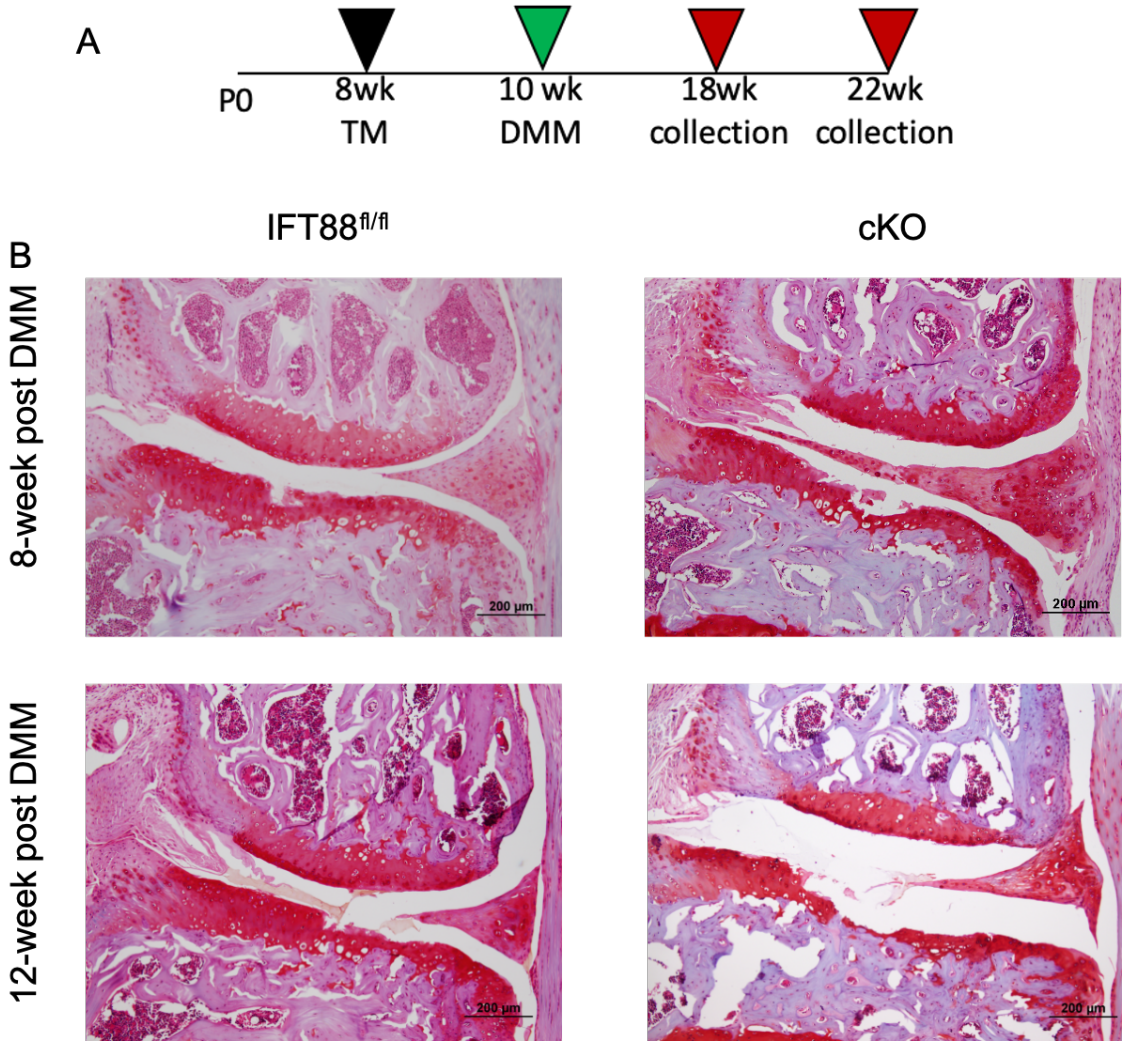


Figure 7.3.1.1: Representative histological sections of control and cKO medial compartments 8- and 12- week post DMM surgery. A) DMM surgery was performed on 10-week old mice (green arrow), two-weeks post tamoxifen (black arrow), and collected 8- or 12-weeks later (red arrows). B) Histological sections of cKO and control knee joints were stained with Safranin-O, and photographed at 10x to assess levels of articular cartilage degradation.

Both control and cKO animals exhibited increased disease scores in comparison with their respective SHAM controls at both 8- and 12-weeks post-surgery. There was no significant difference in OARSI scores between control and cKO animals at 8-weeks post-DMM surgery (Fig. 7.3.1.2 A). At 12-weeks post-DMM surgery cKO animals presented with statistically significantly higher disease scores in comparison with SHAM controls (Fig. 7.3.1.2 B).

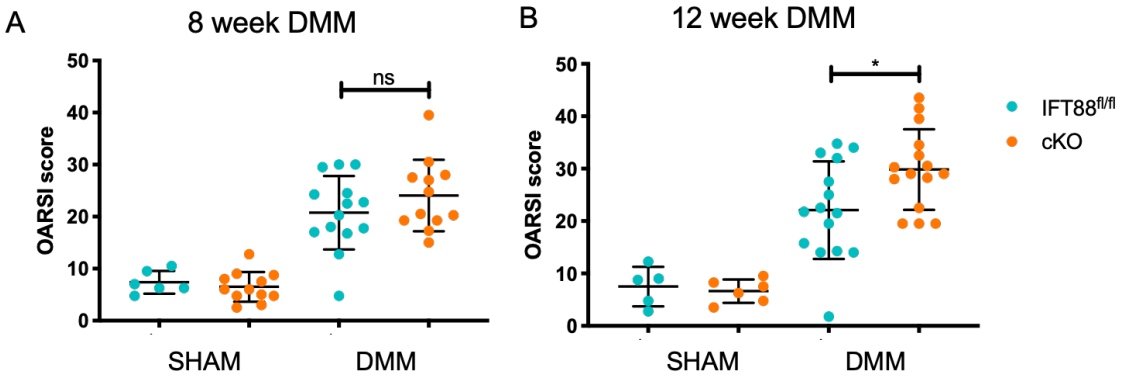


Figure 7.3.1.2: DMM surgery results in significantly higher OARSI scores 12-week post-surgery in cKO animals. Scores were generated by assessing the level to which articular cartilage was lost and the three highest summed scores per compartment were used to generate an OARSI score (see Methods). A) OARSI scores 8-weeks post-DMM and SHAM controls in cKO (orange) and control (turquoise) animals. B) OARSI scores 12-weeks post-DMM and SHAM controls in cKO (orange) and control (turquoise) animals. Data represents the mean ± SD (n=9 controls, n=11 cKO). Statistical significance was determined using a Mann-Whitney U test where *=$p<0.05$.

7.3.2 Unilateral joint immobilisation by double neurectomy

7.3.2.1 Growth plate

Mice were given tamoxifen at 8-weeks of age over three consecutive days, after which, they underwent surgery to remove 2-3mm of both the femoral and sciatic nerve in the right hindlimb (hereafter termed ipsilateral) (Fig. 7.3.2.1. A). This resulted in the mouse being unable to use the ipsilateral hindlimb, dragging it along the floor of the cage, resulting in reduced load bearing in this joint. The left (contralateral) hindlimb was therefore the dominant hindlimb, which is potentially sustaining a higher load compared with normal physiological loading. Histological analysis of coronal knee joint sections resulted in longer growth plates with cartilaginous bilateral holes in 50% of mice, in both control and cKO groups (Fig. 7.3.2.1. B). This phenomenon was only observed in the contralateral hindlimbs. All ipsilateral (reduced load bearing) hindlimb growth plates appeared unaffected.

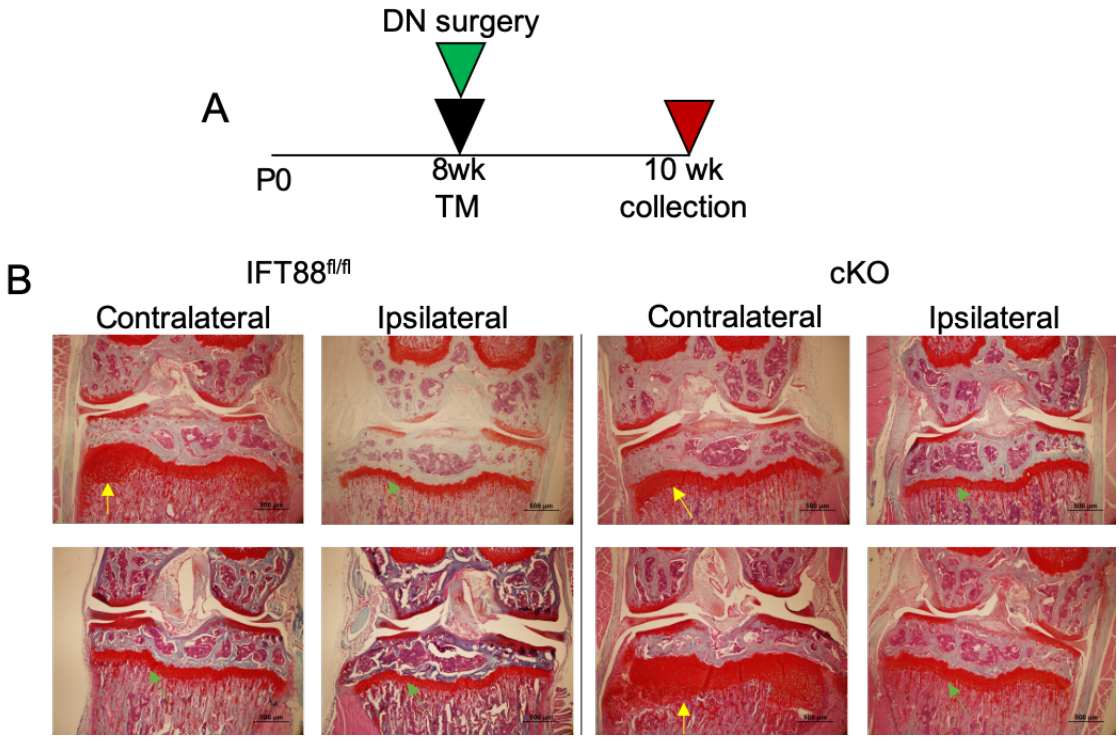


Figure 7.3.2.1: Histological staining of ipsilateral (immobilised) and contralateral joints. A) Double neurectomy (DN) surgery was performed at 8 weeks of age after tamoxifen (TM, black arrow) administration at 8 weeks of age. Animals were collected at 10 weeks of age (red arrow). B) Histological sections of cKO and control knee joints were stained with Safranin-O, and photographed at 4x. Yellow arrows point to longer abnormal growth plates or those exhibiting bilateral holes whereas green arrows point to growth plates that appear morphologically normal.

Growth plate lengths were measured across the width of the bone and averaged. In the ipsilateral hindlimbs, there was no difference observed between control and cKO growth plate lengths (Fig. 7.3.2.2). In the contralateral hindlimb, there were striking changes to growth plate length in a subset of animals. Although not statistically different overall, it was interesting that this growth plate phenotype observed in some of the hindlimbs was similar to that observed in non-operated (naïve) cKO mice (Chapter 5).

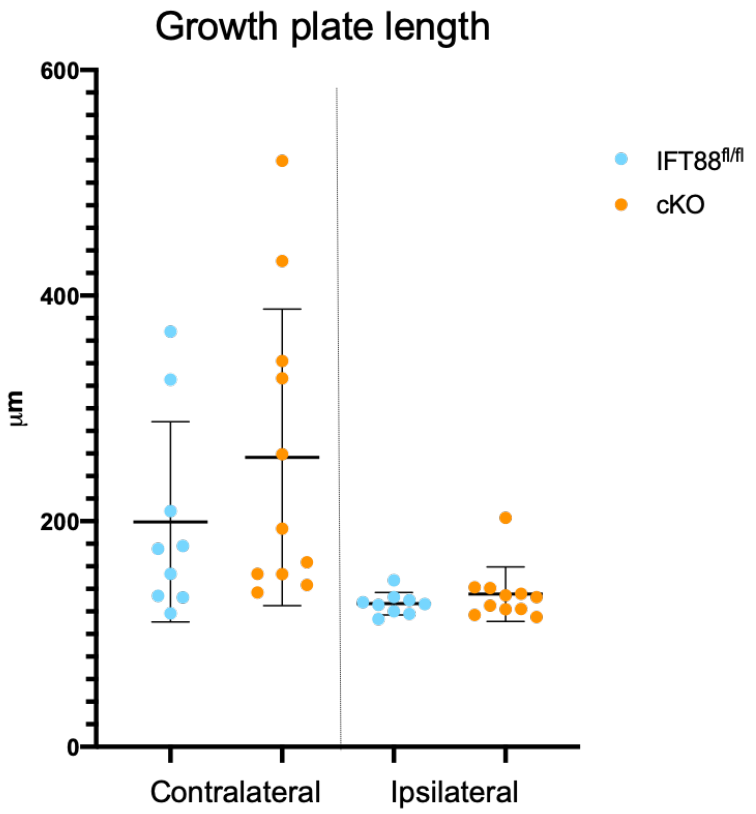


Figure 7.3.2.2: Contralateral and ipsilateral growth plate length measurements of cKO and control animals. Double neurectomy surgery was performed at 8 weeks of age, 3-days post tamoxifen administration, and legs were collected two weeks later. Histological measurements of contralateral and ipsilateral knee joint tibial growth plates were taken and plotted. Data represents the mean ± SD (n=9 controls, n=11 cKO). Statistical significance was determined using a Mann-Whitney U test.

7.3.2.2 Articular cartilage thickness

Articular cartilage of contralateral and ipsilateral joints from cKO and control animals was measured. As previously described in Chapter 6, cKO cartilage was ~10% thinner than that of controls, in both ipsilateral and contralateral joints. It was hypothesised that removal of compressive load would result in thinner articular cartilage. However, ipsilateral cartilage of control mice was not thinner than that of control contralateral cartilage (Fig. 7.3.2.3). As

the ipsilateral cartilage did not thin, it is difficult to make further interpretations about the role of mechanics in cartilage thickness changes.

A longer more cartilaginous growth plate could alter the mechanics of the joint above it and hence potentially affect articular cartilage thickness. In the contralateral joints, there was a larger spread of growth plate lengths than in the ipsilateral (Fig. 7.3.2.2). In order to investigate whether growth plate mechanics could have affected the cartilage thickness above it, articular cartilage measurements taken from animals presenting with bilateral growth plate holes were marked with crosses. There appeared to be no trend between longer growth plates and cartilage thickness, with measurements from these animals being equally dispersed throughout the data (Fig. 7.3.2.3). Hence, thickness is not being affected by growth plate length.

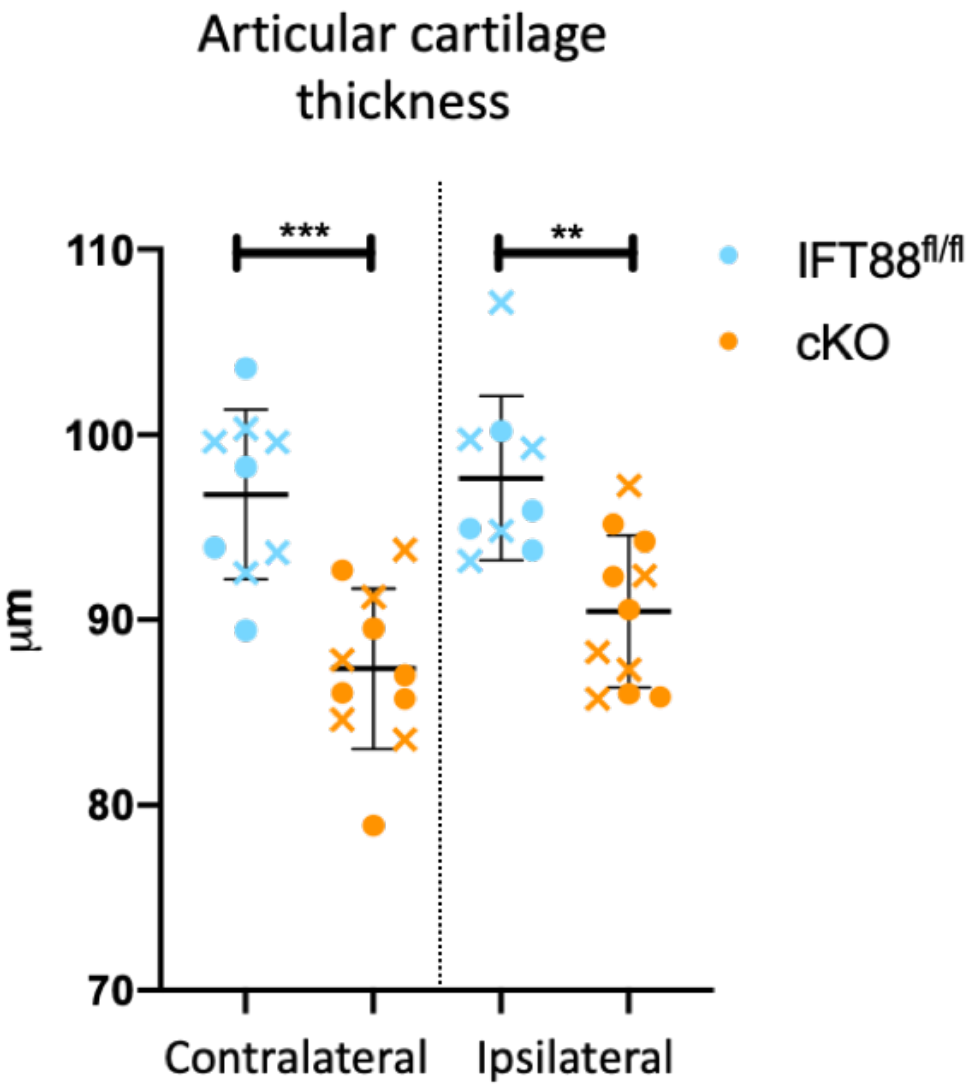


Figure 7.3.2.3: Articular cartilage measurements of contralateral and ipsilateral knee joints. Measurements of tibial articular cartilage thickness taken from contralateral and ipsilateral knee joints (18 measurements per n). Crosses are measurements taken from animals with abnormal growth plates as seen by histology. Data represents the mean ± SD (n=9 controls, n=11 cKO). Statistical significance was determined using a Mann-Whitney U test where **=p<0.01, ***=p<0.001.

7.3.2.3 Lateral and medial cartilage thickness measurements

There was no difference in total cartilage thickness between contralateral and ipsilateral control animals. However, in the previous chapter, differences in cartilage thickness were observed between the lateral and medial side. In order to investigate whether

there were any differences between lateral and medial cartilage thickness in contralateral and ipsilateral joints, measurements were split between lateral and medial plateaus. However, in control (*IFT88*$^{fl/fl}$) animals, no difference in thickness was observed in medial or lateral cartilage between contralateral and ipsilateral joints (Fig. 7.3.2.4).

Therefore, it is difficult to make interpretations about the cKO experimental group. The cartilage of cKO animals was thinner than controls on every plateau in both the contralateral and ipsilateral circumstances, apart from the lateral plateau in the ipsilateral circumstance where no difference in thickness was observed. In naïve control animals (Chapter 6), there is also no difference in lateral cartilage thickness between control and cKO animals. In contrast, the lateral cartilage of contralateral joints is thinner in cKO animals compared with controls and the naïve situation (Chapter 6).

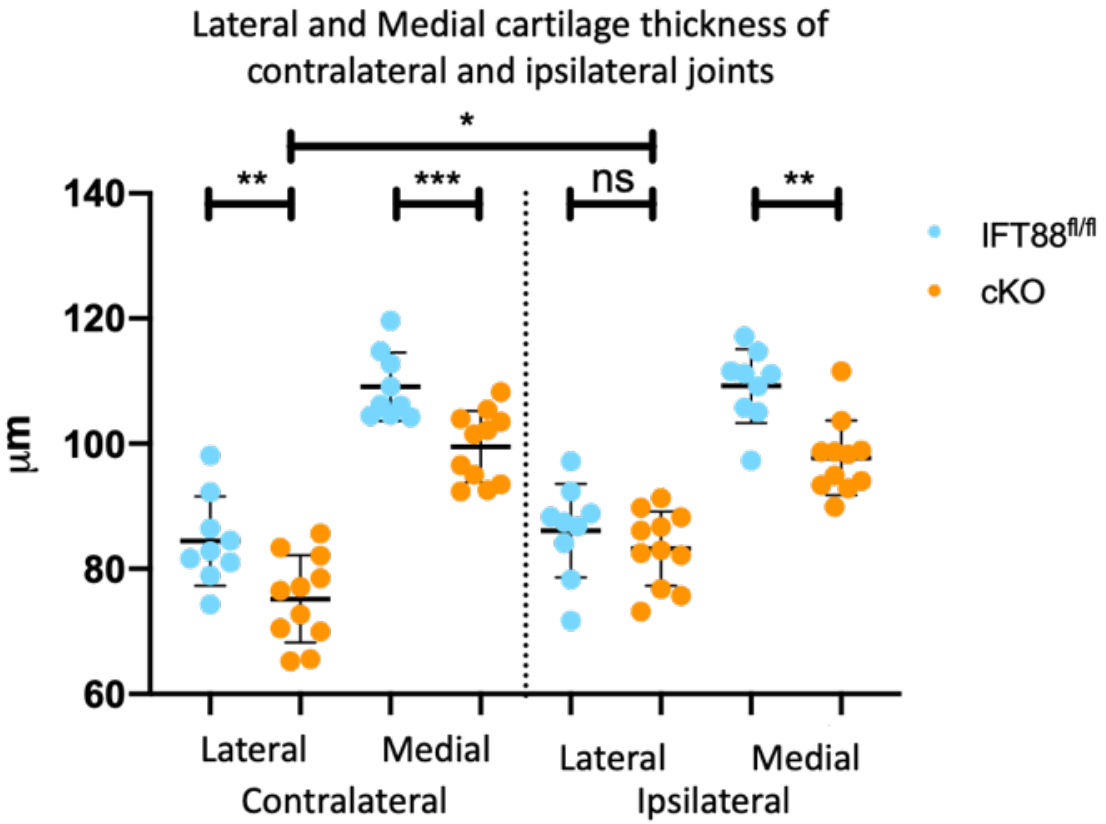


Figure 7.3.2.4: Lateral and medial cartilage measurements of contralateral and ipsilateral knee joints. Lateral and medial measurements of tibial articular cartilage thickness taken from contralateral and ipsilateral knee joints were plotted. (6 measurements per n). Data represents the mean ± SD (n=9 controls, n=11 cKO). Statistical significance was determined using a Mann-Whitney U test where *=p<0.05, **=p<0.01, ***=p<0.001.

7.3.2.4 Uncalcified and calcified cartilage measurements

As shown in Chapter 6, deletion of IFT88 at 8-weeks of age inhibited thickening of medial cartilage between 8- and 10-weeks. This was largely attributable to thinner calcified cartilage, analogous to that seen in immobilised (unloaded) large animal studies of cartilage (Palmoski and Brandt, 1984). Here, it was hypothesised that removal of mechanics would result in perturbed adaptation of articular cartilage between 8- and 10-weeks of age,

resulting in reduced calcification of the cartilage. Despite not seeing differences between control ipsilateral and contralateral total cartilage thickness or differences between lateral and medial thickness, it was hypothesised that perhaps calcification had still been affected. Measurements of uncalcified cartilage and calcified cartilage on both the lateral and medial sides were compared between calcified and uncalcified cartilage.

There was no difference in uncalcified cartilage thickness between the contralateral or ipsilateral joints on the lateral or medial side in control or cKO animals (Fig. 7.3.2.5 A). The same was true for calcified cartilage for control animals (Fig. 7.3.2.5 B). However, whilst there was no difference in medial calcified cartilage, there was a difference in lateral calcified cartilage thickness between contralateral and ipsilateral cartilage in cKO animals. Lateral contralateral calcified cartilage was ~10% thinner than ipsilateral.

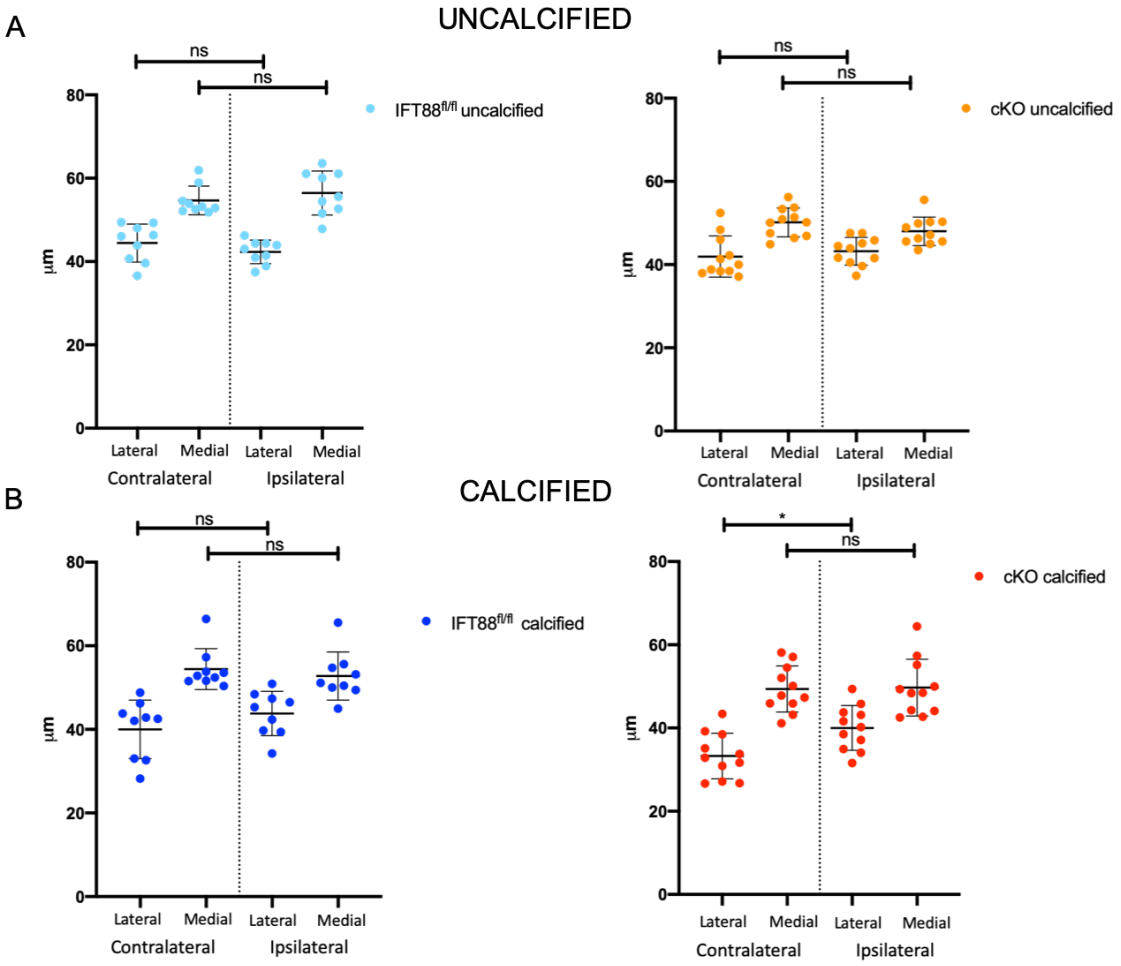


Figure 7.3.2.5: Uncalcified and calcified cartilage measurements of contralateral and ipsilateral knee joints. Uncalcified cartilage measurements of contralateral and ipsilateral tibial articular cartilage of control (light blue) and cKO (orange) animals (A). Calcified cartilage measurements of contralateral and ipsilateral tibial articular cartilage of control (dark blue) and cKO (red) animals (B). 18 measurements per n. Data represents the mean ± SD (n=9 controls, n=11 cKO). Statistical significance was determined using a Mann-Whitney U test where *=p<0.05.

7.3.2.5 Comparing articular cartilage thickness in contralateral and ipsilateral joints with naive joints

In Chapter 6, deletion of IFT88 resulted in an inhibition of cartilage thickening between 8- and 10-weeks of age. In the naïve circumstance there is ~10% thinner cartilage in cKO animals compared with controls. In order to investigate whether

contralateral and ipsilateral cartilage of control animals was thinner than naïve cartilage (historic, from Chapter 6, Fig. 6.3.3.1) and whether in cKO animals this effect was exacerbated, the thickness of articular cartilage between naïve 10-week old mice (IFT88 deleted at 8-weeks), contralateral and ipsilateral joints was compared (Fig. 7.3.2.6). In control (*IFT88*$^{fl/fl}$) mice, there was no difference in articular cartilage thickness between naïve, contralateral and ipsilateral joints. Similarly, there was no obvious difference in the thickness of cartilage between the groups in cKO animals.

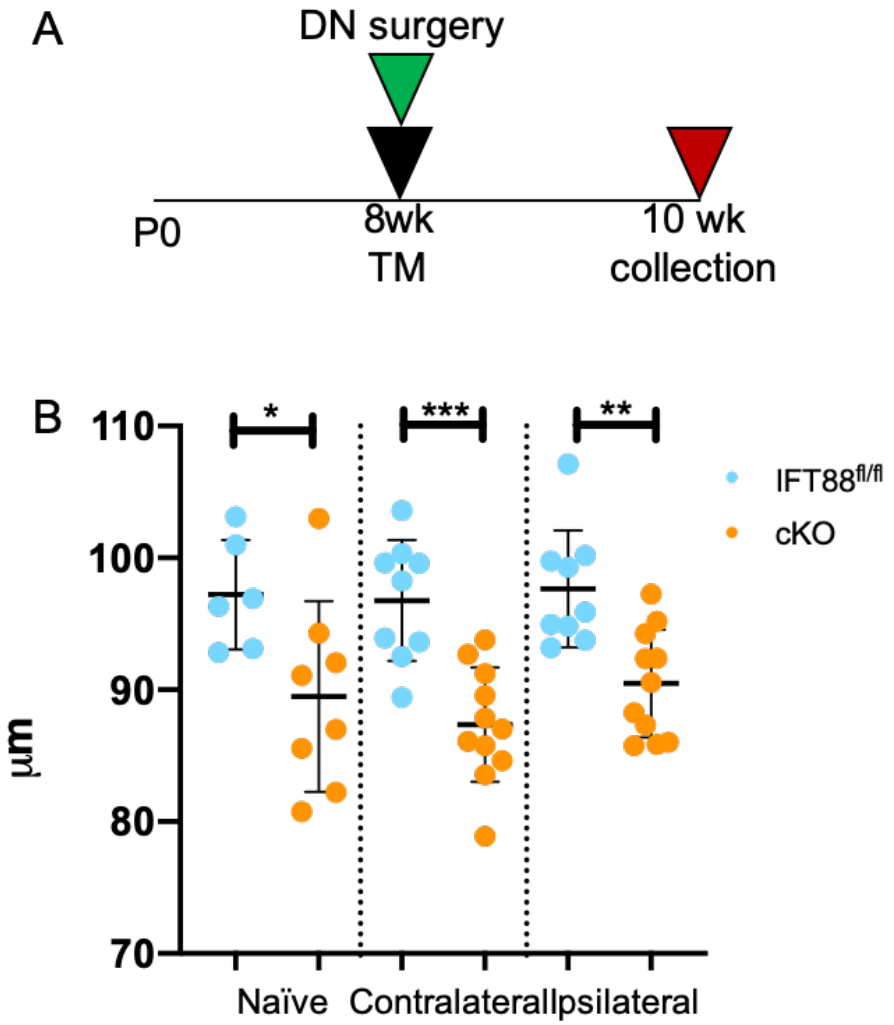


Figure 7.3.2.6: Total cartilage thickness measurements from naive contralateral and ipsilateral hindlimbs. A) Experimental time line. Non-operated animals were treated with tamoxifen (TM, black arrow) at 8 weeks of age and collected at 10 weeks of age. Animals underwent double neurectomy surgery (DN, green arrow) at 8 weeks of age at the same time as TM administration and were collected at 10 weeks of age. Operated joints are ipsilateral, whilst contralateral joints are the non-operated predominant load bearing joint. B) Non-operated (naïve) total cartilage thickness measurements (historic, from Chapter 6, Fig. 6.3.3.1) were compared with total contralateral and ipsilateral hindlimb cartilage thickness. Data represents the mean ± SD. Statistical significance was determined using a Mann-Whitney U test where *=p<0.05, **=p<0.01, ****p=<0.0001.

7.4 Discussion

7.4.1 Aims and hypothesis

In this chapter, I aimed to explore whether IFT88, and by extension the primary cilium, has a role as a mechanotransducer in chondrocytes, mediating mechanics to regulate cartilage health. At the level of the chondrocyte, we hypothesised that removal of IFT88 renders the cell less mechanoresponsive to compression. I employed two different models which changed *in vivo* mechanics within the joint to both examine their effects on my previous output measures, and to examine the effects of removal of IFT88 in these contexts. I hypothesised that DMM surgery would result in exacerbated disease in cKO animals as we observed articular cartilage thinning in naïve animals between 10-22 weeks of age. Additionally, I hypothesised that by removing compressive load, thickening and maturation of articular cartilage between 8- and 10-weeks of age would be inhibited in control animals.

7.4.2 Findings from mechanical models

Firstly, I destabilised the joint, introducing shear stress, using the DMM model. We found increased osteoarthritic disease in the operated knee (DMM) of cKO animals (as denoted by OARSI score) compared with $IFT88^{fl/fl}$ controls, 12-weeks post-DMM, but not 8

weeks post-DMM. Cartilage of cKO animals by 10-weeks of age is thinner than that of controls and continues to atrophy predisposing a subset of animals to OA disease by 34 weeks of age. It is hence reassuring to observe elevated OA disease 12-weeks post-DMM in cKO animals in comparison with controls.

Secondly, we administered tamoxifen at 8-weeks of age, followed by double neurectomy surgery, immobilising one limb. Mice were left for 2-weeks post-surgery and collected at 10-weeks of age. By removing compressive loads by double neurectomy surgery, we hoped to understand whether 'off-loading' the cartilage would recapitulate the thinner articular cartilage phenotype observed in cKO animals. We expected to see thinner ipsilateral cartilage in control animals in comparison with its contralateral. However, we did not see any changes to total articular cartilage thickness in control animals between contralateral and ipsilateral hindlimbs. Separating out these measurements into medial and lateral plateaus also revealed no differences between control contralateral and ipsilateral hindlimbs. Likewise, no changes were observed in calcified or uncalcified cartilage measurements between control contralateral and ipsilateral hindlimbs. I also compared these total cartilage thickness measurements with that of previous historical naïve measurements and found no difference in cartilage thickness in naïve, contralateral or ipsilateral control animals. As the

ipsilateral joint showed no thinning, it is difficult to make any interpretations about the role of IFT88. Despite this, it was comforting to see a reproduction of previous data, observing thinner articular cartilage in cKO animals compared with controls.

The double neurectomy surgery as a method of joint immobilisation has, to our knowledge, not previously been used to investigate cartilage atrophy. Interestingly, a recent paper compared different methods of joint immobilisation by surgical installation of pins, and hindlimb unloading, by lifting the tail so hindlimbs can no longer touch the ground, in WT mice over 8-weeks (Nomura et al., 2017). They found no changes in total cartilage thickness until at least 4-weeks post-removal of compressive loads, and only small changes to the uncalcified region 2-weeks post-unloading. Hence, we may not have expected thinner cartilage to arise from our unloading experiment earlier than 4-weeks of age. Additionally, Nomura et al. 2017 found these cartilage changes post-immobilisation to be associated with both decreased proteoglycan and aggrecan staining in the uncalcified cartilage region by immunohistochemistry, and elevated ADAMTS-5 activity. They also found changes to the bone density of the epiphysis as a result of the unloading. Future work in our double neurectomy model could explore changes to the matrix by IHC. Bone density can also be assessed to quantify mechanical loading.

7.4.3 Response of growth plate to off-loading model

In Chapter 5, I described that in naïve mice, including at 10-weeks of age (tamoxifen treatment at 8-weeks), cKO animals had longer growth plates than controls, with pronounced bilateral holes in the highest loaded regions of the growth plate. Whilst it was not statistically significant, contralateral growth plate measurements had a larger spread than the ipsilateral growth plate measurements in both control and cKO animals. Interestingly, following double neurectomy, we found bilateral cartilaginous holes in the contralateral hindlimbs of both control and cKO animals in 50% of animals reminiscent of that observed in our 10-week old naïve cKO mice (Chapter 5). In this model the contralateral is the weight bearing hindlimb and hence could be experiencing a higher mechanical load than it would normally. These results suggest that IFT88, and by extension the primary cilium, could be responsible for dampening mechanical cues in the final stages of endochondral ossification affecting mineralisation and subsequent ossification of growth plate cartilage in the highest loaded regions. Recently, work has implicated another IFT protein, IFT80, to be important for fracture healing and the ossification of new reparative cartilage (Liu et al., 2019). Future work will explore pathways that may be mechanosensitive and key to mineralisation of the growth plate.

7.4.4 Interpreting effect of IFT88 deletion in articular cartilage

Total cartilage thickness of control animals did not change in the contralateral or the ipsilateral joint. This suggests that removal of mechanics over a 2-week period is not as influential as IFT88 deletion, implicating a non-mechanical component. We cannot rule out the possibility that deletion of IFT88 and by extension the primary cilium is influencing Hh signalling in the articular cartilage. Elevated Hh signalling has been shown to both exacerbate disease resulting in cartilage loss (Lin et al., 2009) and increase articular cartilage thickness during development (Chang et al., 2012), suggesting that the role of IFT88/the primary cilium could have an evolving role in development, homeostasis and disease through the tuning of Hh signalling. Indeed, Hh is important within growth plate development to stimulate the differentiation of hypertrophic chondrocytes that calcify their matrix.

Evidence presented in this thesis chapter could argue the role of the primary cilium in the integration of mechanically regulated Hh signalling *in vivo*, a phenomenon already proposed *in vitro* (Thompson et al., 2014b). Control animals exhibited longer growth plates and cartilaginous bilateral holes in the highest loaded regions of the joint, similar to that seen in cKO animals (Chapter 5). Perhaps, pathophysiological mechanics influences

mechanically regulated Hh signalling, disrupting the PTHrP-Hh feedback loop of the growth plate, resulting in impaired growth plate closure. Future work will attempt to understand if Hh signalling is disturbed in cKO mice by isolation of RNA from micro-dissected cartilage for RTPCR analysis.

7.5 Summary

Here I have begun to investigate the mechanism behind the changes in growth plate and articular cartilage shown in earlier chapters, testing the hypothesis that IFT88 regulates the mechanoadaptive response of cartilage to *in vivo* mechanics. I first investigated the role of IFT88 in mediating sheer stresses (DMM) and removal of compressive loads (double neurectomy) in both control and cKO mice. I found exacerbated disease in cKO animals compared with controls 12-weeks post-DMM. By removing compressive loads in the double neurectomy model, we found no changes to the total articular cartilage thickness in controls. However, double neurectomy resulted in longer growth plates with bi-lateral holes in the contralateral (compensatory increased weight bearing) joints of both controls and cKO animals, implicating IFT88 as a mediator of mechanics in the final stages of growth plate closure and endochondral ossification.

8

General Discussion

If I have seen further, it is by standing on the shoulders of Giants- Isaac Newton

Contents

8.1 Project Rationale 318

8.2 IFT88 as a novel regulator of chondrocyte protease activity 320

8.3 The peri-ciliary region as a 'hotspot' for endocytotic clearance 320

8.4 The role of IFT88 in the adolescent growth plate . . . 325

8.5 The role of IFT88 in articular cartilage 329

8.6 IFT88 supports mechanotransduction *in vivo* 331

8.7 IFT88 and the remodelling of cartilage matrix 333

8.8 Preliminary studies linking *in vivo* phenotypes to *in vitro* protease activity and LRP-1 localisation 336

8.9 Non-canonical roles 339

8.10 Future Work 342

8.11 Concluding remarks 343

8.1 Project Rationale

Mutations to ciliary proteins result in rare congenital diseases, known as ciliopathies, that present with musculoskeletal phenotypes.

These diseases, and the genetic models designed to mimic them, comprise, but are not limited to, craniofacial abnormalities (Singer et al., 2019; Tian et al., 2017), aberrant limb patterning (Haycraft and Serra, 2008) and stunted long bone growth (Haycraft et al., 2007b; McGlashan et al., 2007; Song et al., 2007).

Beyond the ciliopathies, there are many unanswered questions in musculoskeletal biology and disease that study of the cilium and ciliary proteins, such as IFT88, may be pertinent to. In cartilage these include questions such as how is the careful balance of matrix turnover regulated? How are the matrix proteases, responsible for both developmental and pathological remodelling of the tissue, kept in check? How do chondrocytes integrate extrinsic cues such as mechanics with their intrinsic programs of cell signalling and behaviour? Understanding the role of the primary cilium in the musculoskeletal system, and in particular cartilage biology, could be important for elucidating new pathways to be exploited in cartilage homeostasis, regeneration and fracture repair. When I began this project however, we knew little about the role of the cilium, or core ciliary proteins such as IFT88, in cartilage, beyond embryonic and peri-natal development.

8.2 IFT88 as a novel regulator of chondrocyte protease activity

In Chapter 3, I explored the role of IFT88 in the post-translational regulation of aggrecanase activity using a mouse chondrocyte cell line harbouring a mutation to IFT88 (ORPK). I described that ORPK chondrocytes exhibited elevated aggrecan degradation, previously identified to be regulated independent of transcriptional control (Coveney et al., 2018). This increased activity was associated with reduced, LRP-1-mediated, endocytotic clearance of ADAMTS-5, and a disruption to the normal, wild type, surface localisation and maintenance of this receptor. Due to the potent nature of these proteases, even a small reduction in the rate of clearance from the extracellular matrix (ECM) could result in significant degradation of cartilage over an extended period of time, for example the pre-symptomatic period in OA.

8.3 The peri-ciliary region as a 'hotspot' for endocytotic clearance

One of the most striking results of this chapter, and the work of others that preceded it, was the observation of apparent polarised endocytosis of FLAG tagged TS-5 ligand (TS-5-FLAG) (Coveney et al., 2018; Yamamoto et al., 2013a), which coincided with

polarised localisation of LRP-1β to the base of the primary cilium and surrounding cell membrane. Subsequent work in the Wann laboratory has also identified a putative hotspot of recycling early endosomes at the base of the chondrocyte cilium. Evolutionarily, cilia and flagella are highly conserved microtubule organelles, with structural similarities. At the base of the Trypanosome flagellum is a pit known as the flagellum pocket, and is the only site of endocytosis in this organism. On deletion of IFT88 in trypanosomes, the pocket structure is altered and endocytosis is impaired (Absalon et al., 2008). Primary cilia form an analogous ciliary pocket, historically hypothesised to be a site of endocytosis (Molla-Herman et al., 2010). However, subsequent research focus has largely been on the endocytotic recycling of ciliary proteins and ciliogenesis (Pedersen et al., 2016). For example, research has proposed that TGF-β signalling is regulated by clathrin mediated endocytosis at the ciliary pocket (Clement et al., 2013a). Furthermore, a caveolin-enriched microdomain was described at the ciliary transition zone and demonstrated to regulate Hh signalling within the ciliary axoneme (Schou et al., 2017). LRP-1 and its cargos, including proteases, are endocytosed by clathrin mediated endocytosis (Yamamoto et al., 2016; Yamamoto et al., 2013a). Hence, our current thinking is that our data support the idea of a conserved role for the ciliary

pocket as a site of organised endocytosis in chondrocytes, post-transcriptionally regulating extracellular protease activity. Further work, using higher resolution microscopy than that used in this thesis, will be required in order to determine whether LRP-1 lines the ciliary pocket or is rapidly recycled in the peri-ciliary environment.

In this thesis I also used an immortalised mouse chondrocyte cell line harbouring a hypomorphic mutation to IFT88, known as the ORPK chondrocyte cell line. The ORPK chondrocyte line is very useful and highly tractable, but has limitations due to the complex and far-reaching effects of this mutation. Ongoing work in the Wann laboratory is now targeting other ciliary proteins including the master ciliogenesis kinase TTBK2 to understand the molecular interface between the ciliome and LRP-1 mediated endocytosis. In the non-ciliary context of the immunological synapse, other IFTs working alongside IFT88 including IFT20, IFT57 and IFT52 have been associated with polarised recycling of receptors (Galgano et al., 2017; Griffiths et al., 2010; Stinchcombe and Griffiths, 2014).

The primary cilium and IFT88 are most famous for their role in the regulation of the Hh signalling pathway during development (Goetz and Anderson, 2010; Huangfu et al., 2003). During ciliogenesis, IFT88 associates with centrosomes and is an absolute requirement for ciliary assembly in many cell types. IFT88

moves along the axonemal microtubules to transport Hh pathway components (Clement et al., 2009b). ORPK chondrocytes harbour a hypomorphic mutation to IFT88, eliminating the formation of a primary cilium by ~85%. This loss of cilia affects this ciliary trafficking of Hh pathway constituents including, patched, smoothened and Gli transcription factors (Haycraft et al., 2005; Rohatgi et al., 2007b). Recently, the Hh pathway has been linked to altered matrix catabolism and OA, demonstrated by decreased severity of surgically induced OA progression on attenuation of the Hh pathway (Lin et al., 2009). However, this particular group went on to show that Hh signalling is important for the regulation of cholesterol accumulation in chondrocytes, which is associated with OA severity, resulting in atypical aggrecanase activity (Ali et al., 2016). Interestingly, a recent paper suggests that Hh signalling regulates the expression of an inhibitor of aggrecanase activity, TIMP-3 (Kopinke et al., 2017).

In addition to limited ligand response (Thompson et al., 2014b), ORPK chondrocytes have diminished constitutive Hh signalling in comparison with WT chondrocytes, as measured by the baseline expression of Gli1 and Ptch1 (Coveney et al., 2018). Chondrocytes stimulated with recombinant Ihh do not increase expression of ADAMTS-5 or MMP-13 (another crucial OA associated protease) (Thompson et al., 2015b) and we do not see constitutive changes

to the expression of either of these enzymes in the ORPK line (Coveney et al., 2018). Interestingly, deletion of IFT88 in WT chondrocytes did not lead to the same levels of aggrecan neoepitope production as the hypomorphic mutation. This suggests that the ORPK mutation may be having a more prominent effect on cellular processes than total loss of IFT88 may have been having.

As with all research seeking to understand the role of ciliary proteins and by extension the primary cilium itself, we must be wary of over interpreting altered cell behaviours or indeed tissue and/or genetic model phenotypes as solely due to the primary cilium (Hua and Ferland, 2018). We cannot dismiss the potential non-ciliary functions of IFT88. T cells, possess ciliary machinery, often concentrated at the immunological synapse, but do not assemble a primary cilium (Stinchcombe and Griffiths, 2014). However, as mentioned earlier, perhaps analogously to the ciliary pocket the immunological synapse, recycles T-cell antigen receptors through the recycling of endosomes (Huppa and Davis, 2003). The immunological synapse is also highly polarised and membranous, and cytoskeletal changes occur during the formation of a synapse when docking to antigen presenting cells. This rearrangement of machinery is very similar to that observed at the base of the primary cilium and the ciliary pocket (Angus and Griffiths, 2013; Stinchcombe and Griffiths, 2014).

8.4 The role of IFT88 in the adolescent growth plate

Cartilage is capable of repair and turnover, but components of the ECM, specifically collagens, have been shown to reside within the cartilage for decades (Heinemeier et al., 2016). The growth plate has been the focus of cartilage research, beyond interests in skeletal growth, as its dynamic remodelling during endochondral ossification could illuminate targetable mechanisms that could be exploited for the treatment of degenerative cartilage diseases (Javaheri et al., 2018). The main aim of my project was to understand whether IFT88, and by extension the primary cilium, remained important for post-natal cartilage i.e during adolescence, adulthood and potentially therefore in the disease context. In order to address this question, I used a mouse model, which, enabled me to specifically target IFT88 in aggrecan expressing chondrocytes, at specific time-points. Deletion of IFT88 in the later phases of post-natal skeletal development resulted in impaired growth plate closure with longer growth plates observed in cKO animals, some presenting with large bilateral cartilaginous filled holes throughout adolescence, a phenomenon absent in controls. These cartilaginous holes were found to be filled with ColX expressing hypertrophic chondrocytes suggesting they had differentiated correctly, but that subsequent downstream processes, such as calcification of the

ECM, cartilage remodelling and vascular invasion had failed to be initiated.

As previously mentioned in this thesis, Hh signalling is dependent on IFT88 and the primary cilium. In the growth plate, Ihh is an important signalling molecule, released from hypertrophic chondrocytes, driving the hypertrophic differentiation of chondrocytes, the creation of ColX and forming a platform for vascular invasion and subsequent bone formation. It also stimulates resting and proliferating chondrocytes to secrete PTHrP promoting proliferation, which in turn inhibits hypertrophic differentiation. This careful balance of signalling between Ihh and PTHrP results in a feedback axis of signalling ensuring both growth plate ossification and thereby bone growth, and also growth plate renewal. Disruption of this axis can lead to aberrant endochondral ossification, accelerated growth plate closure and dwarfism.

Ihh is not only required for growth plate formation and for the stimulation of chondrocytes to undergo hypertrophy, but is also important for osteoblast differentiation (Hilton et al., 2005). PTHrP is also important for vascular invasion and bone formation (Lanske et al., 1999b). Ihh is a mechanically regulated gene (Wu et al., 2001). If mechanically induced expression of Ihh is altered, PTHrP may not be stimulated properly resulting in possibly higher levels of expression. Further investigation of this apparent failed growth

plate closure phenotype as a result of IFT88 removal could be considered in the context of angiogenic markers and vascular invasion.

However, mechanisms by which vascular invasion occurs at the interface between hypertrophic chondrocytes and the bone remain not well understood. Cartilage is a highly avascular tissue, in contrast to bone which is one of the most highly vascularised tissues in the body, requiring a drastic change to its physiology during endochondral ossification. This transformation of the cartilage composition at the site of hypertrophic chondrocytes is vital for angiogenesis and hence bone formation (Vu et al., 1998). Angiogenesis requires the extracellular matrix to be proteolytically modified to allow the invasion of endothelial cells, which in turn mobilises crucial signalling molecules and is associated with MMP activity (Birkedal-Hansen, 1993; Karelina et al., 1995). In particular, MMP-9 is also highly expressed in embryonic development where high levels of tissue remodelling occurs (Vu et al., 1998). Future work to understand the role of IFT88 within the growth plate might include staining for MMPs, such as MMP-9 and angiogenic factors, such as VEGFR.

IFT proteins have been previously associated with cartilage and ossification. Recently, another IFT-B complex protein, IFT80, has been shown to be crucial for fracture repair processes, including for

the recruitment of blood vessels that assist with the replacement of the ECM with bone. Deletion of IFT80 resulted in a down regulation of VEGF and results in porous low-density bone formation (Liu et al., 2019). As matrix and bone remodelling processes occur during the dynamic phase of growth plate closure, deletion of IFT88 could also affect vascularisation of the ECM and subsequent bone formation. Indeed, we found decreased bone density in recently formed bone in our cKO animals compared with controls.

Interestingly, the observed growth plate phenotype in cKO animals is reminiscent of that seen in human chondrodysplasias. Previous research showed that single nucleotide polymorphisms (SNPs) in the flagellum protein SPAG17 were linked to human height and skeletal dysplasias (Cordova-Fletes et al., 2018; Zhao et al., 2010). More recently, mutations to SPAG17 have been linked to skeletal malformations (Teves et al., 2015) and substantial matrix changes leading to fibrosis (Teves et al., 2019). It is currently unclear how SPAG17 is causing defects in endochondral ossification and limb formation, but there is significant overlap with ciliary and Hh related phenotypes in these models.

8.5 The role of IFT88 in articular cartilage

In this thesis, we found that deletion of IFT88 during adolescent development resulted in inhibited articular cartilage thickening during adolescence, followed by dramatic articular cartilage thinning in adulthood. These results are in contrast to previous studies which targeted IFT88 and IFTs earlier in development, and reported increased articular cartilage thickness post-deletion (Chang et al., 2012; Yuan and Yang, 2015a). As described in this thesis, during articular cartilage maturation, the cartilage slowly calcifies to result in an articular cartilage composition of 60% calcified cartilage and 40% uncalcified cartilage. On deletion of IFT88, we found thinner articular cartilage in cKO animals was predominantly owing to loss of calcified articular cartilage, leaving uncalcified cartilage largely unaffected. This resulted in articular cartilage composition being more uncalcified than calcified, reminiscent of immature articular cartilage earlier in development. Further, cartilage atrophy resulting from loss of IFT88 predisposed the articular cartilage to osteoarthritic like disease, with some animals developing total loss of cartilage and gross osteophyte formation. We have found IFT88 to be chondro-protective, important for maintaining articular cartilage thickness and protecting it against degradative processes.

Ihh signalling has been shown to be very important for cartilage development and Ihh knockouts during development can exhibit dwarfed limbs as a result of premature growth plate closure (Maeda et al., 2007). As these two phenotypes of thicker articular cartilage (Chang et al., 2012, Yuan and Yang, 2015a), and premature closure of growth plate cartilage (Maeda et al., 2007) are so different from those observed in this thesis (Chapter 5 and Chapter 6), it suggests a potential diminishing or evolving role of Ihh in the articular cartilage and growth plate as it matures, but also suggests other signalling pathways including mechanotransduction could be more influential. While Ihh is important for growth plate development, it has also been shown to be crucial for the calcification of cartilage (St-Jacques et al., 1999). Ihh is also thought to act as a mechanotransduction mediator, translating mechanical forces into cartilage formation (Ng et al., 2006). Hence Hh signalling could still be important in adult cartilage and this work could point to the strong inter-relationship between mechanics, Ihh, and the primary cilium. Particularly, Hh could be important for hypertrophic chondrocytes of deep zone cartilage in the calcification of their surrounding matrix, similar to the process of ossification in growth plate cartilage.

8.6 IFT88 supports mechanotransduction *in vivo*

In order to more specifically address whether deletion of IFT88 had an impact on the ability of the chondrocyte to respond to mechanical cues, we challenged naïve and cKO joints with shear stress using the DMM model, and removal of compressive load, using the double neurectomy model.

We hypothesised that if IFT88, and by extension the primary cilium, were important for the transduction of mechanical cues, and observed cartilage thinning in the cKO animals was owing to failed transduction of these mechanical cues, removing compressive loads would result in a recapitulation of the cartilage thinning phenotype in control animals. To investigate the potential role of mechanics in articular cartilage adaptation we performed the double neurectomy surgery to reduce compressive load in the ipsilateral hindlimb. We found that reduced load bearing, had no effect on articular cartilage thickness in control animals. Removal of mechanics for two-weeks, failed to recapitulate observed thinner cartilage in cKO animals over the same period in control animals. As such, we were unable to interpret other changes that might have occurred in the cKO animals. Previous work found that cartilage thinning was not observed until 4-weeks post off-loading, so perhaps we are observing the earliest response of cartilage to this change

in load bearing. Additionally, as we saw thinner cartilage in cKO animals within two-weeks, we hypothesise that there must be another mechanism working in conjunction with impaired mechanotransduction leading to this relatively rapid phenotype.

Unexpectedly but intriguingly, the double neurectomy experiment resulted in a pronounced growth plate phenotype in 50% of our animals contralateral hindlimbs (Fig. 7.3.2.1), reminiscent of that observed in our 10-week old naïve (non-operated) cKO mice. The growth plates of ipsilateral (operated) hindlimbs were unaffected (Fig. 7.3.2.1.). The contralateral is the weight bearing non-operated hindlimb and hence could be experiencing a higher mechanical load than it would normally. These results indicate that mechanics could remain important to the final stages of growth plate closure, between 8- and 10-weeks of age, and that overloading the joint results in a phenotype highly reminiscent of that seen in cKO mice at the same time point. These results suggests that IFT88, and by extension the primary cilium, could be responsible for dampening mechanical cues in the final stages of endochondral ossification affecting mineralisation and subsequent ossification of growth plate cartilage in the highest loaded regions. Recently, work has implicated another IFT protein, IFT80, to be important for fracture healing and the ossification of new reparative cartilage (Liu, Alharbi et al. 2019). Future work will include physiological

loading (wheel exercise) of control and cKO animals to see if this longer growth plate phenotype is recapitulated. Previous work in mouse models has shown longer ulna growth plates as a result of loading models (Ohashi et al., 2002). In addition, future work will explore pathways that may be mechanosensitive and key to mineralisation of the growth plate.

The difference in the response to mechanics between the articular cartilage and the growth plate indicates that the role of IFT88 is different between the two cartilaginous tissues. Despite the fact that chondrocytes reside in both tissues, we hypothesise mechanical loading of the joint through weight bearing or increased weight bearing appears to be the mechanism by which IFT88 regulates growth plate length during the final stages of growth plate closure. In contrast, removal of mechanics did not recapitulate the observed loss of articular cartilage in the cKO animals, suggesting the role of IFT88 is different or more important for other signalling pathways rather than mechanics, including inflammation (Sheffield et al., 2018).

8.7 IFT88 and the remodelling of cartilage matrix

Herein, we investigated the relative contributions of uncalcified and calcified cartilage as the articular cartilage develops and how the removal of IFT88 affects those contributions. This adaptation

and changes to the cartilage matrix appears to be important for the mechanical properties and function of the tissue. Chondrocytes situated within the calcified deep zone of the cartilage will experience different strains exerted by the stiffer matrix than chondrocytes situated in the less stiff uncalcified matrix. The differences in stiffness of the matrix in distinct zones of the cartilage results in discrete deformations to the PCM dependent on zone (Choi et al., 2007). Superficial zone cartilage has a much lower modulus than deep zone cartilage. Chondrocytes in chondrons surrounded by a PCM are protected from high or injurious strains within the superficial zone, whereas the PCM in deep zone cartilage acts to amplify these strains, relative to the ECM, to the chondrocyte (Sanchez-Adams et al., 2014). Hence, the composition of the cartilage and the differences in the matrix observed between superficial and deep zone could have crucial roles in mechanical transduction to chondrocytes and hence the overall maintenance of the cartilage by chondrocytes. Additionally, changes to calcified and uncalcified cartilage thickness with age could be reflective of an increase in size and weight of the animal (Vincent and Wann, 2018), requiring mechanical changes to the ECM and a move towards a higher modulus protective environment for chondrocytes found in the calcified cartilage.

The calcification of cartilage is an intricate process regulated

by several transcription factors which include runt-related transcription factor 2 (Runx-2). Runx-2 is a major regulator of chondrocyte hypertrophy (Nonaka et al., 1998) and its expression is dependent on Ihh signalling (St-Jacques et al., 1999). As such, Ihh and Runx-2 interact to regulate chondrogenesis (Kim et al., 2013). Deletion of Runx-2 at 5-weeks of age in aggrecan expressing chondrocytes resulted in disruption of TMJ cartilage as early as 4-weeks later. Deletion of Runx-2 resulted in disruption to chondrocyte columns and zonal organisation, significant loss of hypertrophic chondrocytes, and a thinner calcified cartilage zone. The thinner calcified cartilage phenotype is similar to what we observed in our animals. The authors do not comment on the total overall thickness of the cartilage, but observed reduced Ihh staining and reduced ColX staining in the hypertrophic region suggesting failed chondrocytes differentiation (Liao et al., 2019).

There is also a close relationship between the primary cilium and the ECM, with the primary cilium having been shown to interact with the ECM through receptor localisation (McGlashan et al., 2006). Therefore, it is not surprising that human ciliopathies arising from mutations to cilia related proteins present with altered matrix phenotypes. In some ciliopathies, extensive organ fibrosis is observed, including in Bardet-Biedl syndrome (BBS), Polycystic Kidney Disease (PKD) and Nephronophthisis (Gallagher et al.,

2008; Stroope et al., 2010; Togawa et al., 2011). These diseases implicate cilia proteins, and by extension the primary cilium, in fibrotic disease and hence ECM homeostasis. Beyond hedgehog signalling, perturbations to IFT88 lead to cytoskeletal changes, which could alter mechanical signals being transduced to the cells (McGlashan et al., 2007). As yet, I have not had a chance to explore this further.

8.8 Preliminary studies linking *in vivo* phenotypes to *in vitro* protease activity and LRP-1 localisation

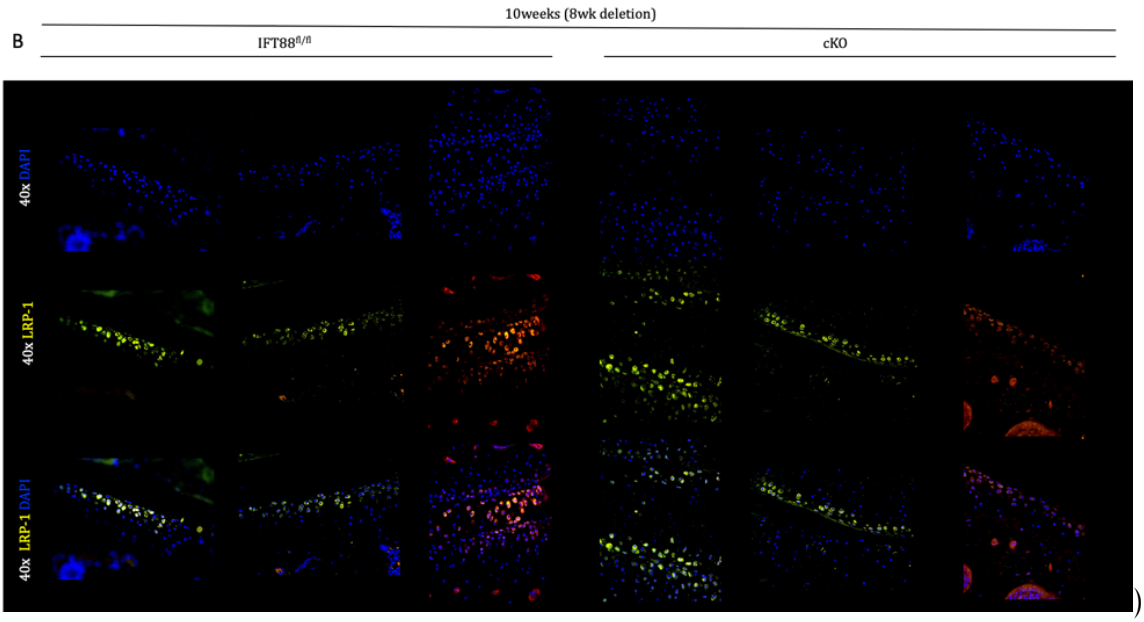
Interestingly, recent work implicated loss of aggrecan and increased ADAMTS-5 presence in cartilage thinning and atrophy during a model of joint immobilisation (Nomura et al., 2017). Previously, within this thesis, I described a putative relationship between the rate of ADAMTS-5 endocytosis, and the primary cilium (Chapter 3) (Coveney et al., 2018). Cells with perturbed ciliogenesis, as a result of a hypomorphic mutation to IFT88, exhibited elevated AGEG neoepitopes when co-cultured with aggrecan and a reduced rate of clearance of ADAMTS-5 (Chapter 3). The aggrecan neoepitope NITEGE is the fragment left bound to the ECM when cleaved by ADAMTS-5 and can be probed for within histological sections (Chambers et al., 2001). Hence, we investigated whether there were any changes to articular cartilage NITEGE fragment

formation in IFT88 deleted mice where cartilage was thinner in comparison to controls. NITEGE staining was localised to the superficial zone/uncalcified region of cartilage similar to that found in Nomura et al (2017). However, we found no obvious changes to NITEGE expression in these tissue sections, though further work and repeats will be required to enable us to conclude the thinning is not associated with increased proteoglycan catabolism.

Previous work in this thesis (see Chapter 3) observed a relationship between the primary cilium and LRP-1β staining (Coveney et al., 2018). LRP-1 was found to localise to the side of the cell where the cilium was assembled, whereas cells harbouring a hypomorphic mutation to IFT88 (ORPK), had no polarised relationship with LRP-1. LRP-1 is a cell surface receptor responsible for the endocytosis of many ligands including the aggrecanase ADAMTS-5 (Yamamoto et al., 2016). Prolonged exposure of the cartilage to this aggrecanase could lead to elevated cartilage degradation and could explain observed thinner cartilage. However, we found no elevated neoepitope staining in our histological sections to support this hypothesis, though our n is limited at this stage. We hence investigated whether IFT88 deletion perturbed LRP-1 localisation both *in vitro* and *in vivo*.

To investigate whether the deletion of IFT88 had altered LRP-1 localisation *in vitro*, I isolated and cultured rib chondrocytes

from control and cKO mice, and treated with tamoxifen (4-OH). There was a striking relationship between LRP-1β staining and the primary cilium, which deletion of IFT88 by use of tamoxifen *in vitro* did not perturb. However, these cells still assembled a primary cilium. We hypothesise formation of the ciliary structure is important for the localisation of LRP-1β and disrupted staining would only occur when a cilium is absent. Further work will be needed to understand whether deletion of IFT88 in these chondrocytes is sufficient to alter cilia assembly and hence LRP-1β distribution. To investigate whether the deletion of IFT88 had altered LRP-1 localisation *in vivo*, unstained coronal histological sections were stained for the transmembrane component, LRP-1β. LRP-1β staining when observed at 40x revealed no discernible changes to LRP-1β staining in the articular surface of cKO animals compared with controls (Fig. 8.8.0.1). However, this does not necessarily mean that there is no change to the localisation of LRP-1β; the thickness of the slices and orientation of the sections could inhibit any clear differences being determined. Therefore, further work to understand this mechanism *in vivo* will be needed.



)

Figure 8.8.0.1: No observed differences in LRP-1 staining on deletion of IFT88. Coronal sections of the knee joint showing the medial compartment (20x). On top are nuclear stained sections with DAPI (blue). In the middle LRP-1 (yellow) staining. On the bottom are merged images of DAPI and LRP-1 in both control and cKO animals at 10-weeks of age (deletion at 8-weeks)

8.9 Non-canonical roles

Beyond the primary cilium, IFT88 has been implicated in cell division and cytoskeletal changes. In the growth plate, IFT88 disruption led to reduced growth plate length, failed hypertrophic differentiation and changes to actin (McGlashan et al., 2007). Furthermore, these cytoskeletal changes including actin organisation and stiffness of the actin cortex, were associated with disrupted cell biomechanics (Wang et al., 2016). Together, these studies imply that disruption to IFT88 results in cytoskeletal changes, in turn leading changes to mechanical stresses imposed on the chondrocyte induced by deformation of cartilage under

loading, or inflicted by the stiffness of the matrix. Deletion of IFT88 in cKO animals could have resulted in similar changes to cytoskeletal organisation resulting in changes to the mechanics inflicted upon the cell leading to failed differentiation in highest loaded regions of the articular cartilage (medial side) or during growth-plate development. Additionally, we observed changes to the composition of the cartilage, with loss of calcified cartilage. These ECM changes could also change the mechanical stiffness of surrounding cartilage and in conjunction with cytoskeletal changes, could result in failed differentiation. Hence, the phenotype we observe as a result of IFT88 deletion could potentially be independent of the primary cilium. Further work would be required to investigate this further.

Interestingly, other signalling pathways have also been associated with cytoskeletal changes and mechanics. The Hippo pathway is most famous for its regulation of organ size (Pan, 2007; Yu et al., 2015), influencing cellular phenotypes through inhibition of its co-activator transcription factor proteins, yes associated protein (YAP) and PDZ-binding motif (TAZ) (Misra and Irvine, 2018). In cartilage, Yap1 has been found to inhibit chondrocyte differentiation by suppression of ColX through interreacting with Runx-2. Yap1 has also been found to attenuate chondrocyte maturation and endochondral ossification during

skeletal development (Deng et al., 2016). Furthermore, at the level of articular cartilage, YAP was found to be chondroprotective in a model of OA (Deng et al., 2018). The localisation and activity of YAP/TAZ is carefully regulated by mechanical forces to include those induced by stress, strain, stiffness of the extracellular environment and even cell geometry (Dupont et al., 2011; Zhao et al., 2008). The YAP/TAZ response to mechanical forces also depends upon the activity of Rho GTPases and the reorganisation of the actin cytoskeleton (Aragona et al., 2013; Reginensi et al., 2013). Changes to the ECM such as calcification, as seen in this thesis as a result of IFT88 deletion, and cytoskeletal changes observed as a result of perturbed IFT88 (McGlashan et al., 2007) could result in changes to the mechanics experienced by chondrocytes affecting the YAP/TAZ pathway.

There are also IFT proteins known to have non-ciliary roles. The IFT protein IFT20, also a component of the IFT-B complex, has non-ciliary roles including trafficking of proteins from the Golgi apparatus to the cilium (Nishita et al., 2017). IFT20 has been implicated in canonical and non-canonical IFT in craniofacial skeletal development (Noda et al., 2016). Deletion of IFT20 in TMJ cartilage at 5-weeks of age results in thinner articular cartilage and loss of proteoglycan staining compared with controls (Kitami et al., 2019), similar to what we find in our cKO animals. This

was associated with loss of primary cilia, reduced proliferation, and decreased Golgi size. Owing to disruption of primary cilia, Hh signalling was also impaired and resulted in impaired hypertrophic chondrocyte differentiation. Hence, perhaps, disruption of IFT88 both impairs Hh signalling and results in cytoskeletal changes impacting the cellular response to mechanical cues.

8.10 Future Work

In this thesis I investigated the importance of IFT88 to post-natal cartilage and began to try to understand the mechanisms by how removal of IFT88 could be regulating cartilage thickness and calcification and hence adaptation of maturing and adult cartilage. Deletion of IFT88 at 8-weeks of age, whilst sexual maturity has been reached and skeletal maturity has almost been completed, appears to be just prior to the maturation of cartilage, where it is transitioning from being predominantly uncalcified to predominantly calcified. To address the possible affects IFT88 deletion and ciliary disruption was having on Hh signalling we have two outstanding experiments:

1. To micro-dissect articular cartilage from 10-week old mice 2-weeks post tamoxifen treatment for RTPCR analysis to understand both the level of deletion specifically within adult articular cartilage and also what genes are being regulated

by the deletion of IFT88. We hope to be able to assess the regulation of Hh components

2. To isolate and culture mouse rib chondrocytes and stimulate with Hh ligand *in vitro* post-tamoxifen administration to ascertain whether deletion of IFT88 in this Cre model affects the Hh signalling pathway.

Additionally, owing to the articular cartilage compositional changes observed as a result of off-loading (ipsilateral) and over-loading (contralateral) in the double neurectomy experiment, we would like to explore the role of mechanics further within articular cartilage. This will involve introducing higher mechanical loads to the joints between 8- and 10-weeks of age.

1. To introduce elevated mechanics by placing a wheel within the cage. Mice will exercise more than naïve animals, introducing more mechanics to the joint.

8.11 Concluding remarks

In this thesis I aimed to understand whether IFT88 and, by extension the primary cilium, maintained a role in cartilage beyond peri-natal development. I hope to have convinced readers that the primary cilium and IFT88 could be important for articular cartilage matrix homeostasis and could be a potential target to

modulate the response to mechanics and Hh signalling *in vivo*. Through this thesis I have shown that IFT88 is important for the final stages of growth plate maturation and closure during long bone endochondral ossification. Further, I have shown that IFT88 is crucial to the adaptation of the articular cartilage into adulthood, and a lack of IFT88 leads to atrophy of the articular cartilage predisposing the articular cartilage to osteoarthritic like disease. This work demonstrates that IFT88 and the primary cilium could prove to be a novel target for modulating cartilage thickness and homeostasis to maintain the health of the tissue and avert disease.

A

Appendices

THE FASEB JOURNAL • RESEARCH • www.fasebj.org

Cilia protein IFT88 regulates extracellular protease activity by optimizing LRP-1–mediated endocytosis

Clarissa R. Coveney,* Isabella Collins,* Megan Mc Fie,* Anastasios Chanalaris,* Kazuhiro Yamamoto,*,† and Angus K. T. Wann*,[1]

*Arthritis Research UK Centre for Osteoarthritis Pathogenesis, Kennedy Institute, Nuffield Department for Orthopaedics, Rheumatology, and Musculoskeletal Sciences, University of Oxford, Oxford, United Kingdom; and †Institute of Ageing and Chronic Disease, University of Liverpool, Liverpool, United Kingdom

ABSTRACT: Matrix protease activity is fundamental to developmental tissue patterning and remains influential in adult homeostasis. In cartilage, the principal matrix proteoglycan is aggrecan, the protease-mediated catabolism of which defines arthritis; however, the pathophysiologic mechanisms that drive aberrant aggrecanolytic activity remain unclear. Human ciliopathies exhibit altered matrix, which has been proposed to be the result of dysregulated hedgehog signaling that is tuned within the primary cilium. Here, we report that disruption of intraflagellar transport protein 88 (IFT88), a core ciliary trafficking protein, increases chondrocyte aggrecanase activity *in vitro*. We find that the receptor for protease endocytosis in chondrocytes, LDL receptor–related protein 1 (LRP-1), is unevenly distributed over the cell membrane, often concentrated at the site of cilia assembly. Hypomorphic mutation of IFT88 disturbs this apparent hot spot for protease uptake, increases receptor shedding, and results in a reduced rate of protease clearance from the extracellular space. We propose that IFT88 and/or the cilium regulates the extracellular remodeling of matrix—independently of Hedgehog regulation—by enabling rapid LRP-1–mediated endocytosis of proteases, potentially by supporting the creation of a ciliary pocket. This result highlights new roles for the cilium's machinery in matrix turnover and LRP-1 function, with potential relevance in a range of diseases.—Coveney, C. R., Collins, I., Mc Fie, M., Chanalaris, A., Yamamoto, K., Wann, A. K. T. Cilia protein IFT88 regulates extracellular protease activity by optimizing LRP-1–mediated endocytosis. FASEB J. 32, 6771–6782 (2018). www.fasebj.org

KEY WORDS: primary cilium · chondrocyte · cartilage · matrix · osteoarthritis

A range of cellular activities—beyond those that govern transcription, expression, and secretion—regulate tissue patterning and homeostasis. For example, receptor-mediated endocytosis exerts influence by removing signaling ligands (1) and enzymes (2, 3) from the extracellular space. Control of extracellular protease enzymes is critical in tissue remodeling, particularly in matrix-rich tissues, such as cartilage, where matrix anabolism and catabolism are carefully balanced by the only cell type present, the chondrocyte (4). Proteases have potent biochemical catabolic activity, which is kept strictly regulated in physiologic conditions. Musculoskeletal diseases, such as osteoarthritis (OA), are defined—and often diagnosed—by the catabolic destruction of cartilage tissue that lines the articular surfaces of joints without compensatory anabolic repair (5). Triggers and mechanisms of many forms of arthritis are still uncertain; however, there is broad agreement that increased protease activity drives pathologic cartilage matrix destruction (6, 7). Therefore, unveiling mechanisms for the physiologic regulation and pathologic dysregulation of protease activity remains critical to the understanding and treatment of arthritis and other diseases in which matrix turnover is altered.

In articular cartilage, extracellular matrix consists predominantly of collagen fibrils and proteoglycans, which form a tissue with the tensile strength and hydration that allows it to withstand constant mechanical challenge while also enabling smooth articulation. The activity of proteases, including the aggrecan proteoglycan-degrading aggrecanases, members of the a disintegrin and metalloproteinase with thrombospondin motifs (ADAMTS) family and collagenase members of the matrix metalloproteinase

ABBREVIATIONS: ADAM, a disintegrin and metalloproteinase; ADAMTS, a disintegrin and metalloproteinase with thrombospondin motif; EEA-1, early endosome antigen 1; GLI2, glioma-associated oncogene family zinc finger 2; Hh, Hedgehog; IFT88, intraflagellar transport protein 88; LRP-1, LDL receptor–related protein 1; MMP, matrix metalloproteinase; MTOC, microtubule organizing center; OA, osteoarthritis; *ORPK*, Oak ridge polycystic kidney; PTCH1, patched-1; RAP, human receptor-associated protein; TIMP3, tissue inhibitor of metalloproteinase 3

[1] Correspondence: Kennedy Institute of Rheumatology, University of Oxford, Roosevelt Dr., Headington, Oxford OX3 7FY, United Kingdom. E-mail: angus.wann@kennedy.ox.ac.uk

This is an Open Access article distributed under the terms of the Creative Commons Attribution 4.0 International (CC BY 4.0) (http://creativecommons.org/licenses/by/4.0/) which permits unrestricted use, distribution, and reproduction in any medium, provided the original work is properly cited.

doi: 10.1096/fj.201800334

www.fasebj.org by Oxford Univ Lib Serv - Bodleian Lib (129.67.90.252) on October 30, 2019. The FASEB Journal Vol. ${article.issue.getVolume()}, No. ${article.issue.getIssueNumbe

(MMP) family, are highly significant in arthritis (6, 7). *In vitro* studies, mouse models of OA, and late-stage clinical disease samples all implicate these enzymes in matrix destruction and pathogenesis; however, mRNA levels of the major aggrecanases of relevance—for example, *ADAMTS5*—do not always correlate to cartilage destruction. A number of upstream signaling pathways are implicated in their regulation, including NF-κB (8) and JNK (9). Recently, it has been demonstrated that extracellular protease levels—and most importantly, their activities—are regulated by cell uptake *via* the LDL receptor–related protein 1 (LRP-1) system (9–13). Reduced LRP-1–mediated uptake and shedding of the α (heavy chain) portion of LRP-1 is reported in OA chondrocytes and has been proposed to underlie the increased protease activity in the disease (12).

Chondrocytes, like most cell types, assemble a single primary cilium (14, 15), an organelle that became the subject of a number of reports after the discovery of the human ciliopathies at the turn of the 21st century (16). Congenital ciliopathies stem from mutations to proteins associated with the cilium, a collective termed the ciliome. The full ciliome is likely still unknown, but includes genes and proteins that are associated with ciliogenesis, ciliary structure, trafficking within the ciliary compartment, or receptors or signaling proteins that are enriched within the ciliary compartment. One of the first ciliary components defined in mammalian cells, intraflagellar transport protein 88 (IFT88), is a core anterograde or type B trafficking protein—carrying proteins to the tip of the primary cilium—and is therefore critical for ciliary assembly and function (17, 18). The most famous roles for the cilium, and certainly IFT, include the transduction of signaling downstream to Hedgehog (Hh) ligands (19), mechanical stimuli (20), and growth factors (21–23); however, the ciliome is now associated with the regulation of a plethora of cell biology through both ciliary and potentially nonciliary mechanisms. Microscopy studies of cilia in culture and *in situ*, including in tissues of the joint, such as synovium and cartilage, describe the association between the cilium, particularly the ciliary pocket, and vesicles of the endocytosis system (24–26). This is functionally important for cilia, downstream to growth factors and Hh (22, 27); however, it remains unknown whether the ciliary pocket is as important to global cellular endocytosis in mammalian cells as the analogous flagellar pocket is for trypanosomes (28).

Many ciliopathies have striking musculoskeletal phenotypes (29). When core ciliome components, including IFT88, have been deleted during development in murine models, skeletal morphology and organization is grossly disrupted, including at the level of matrix deposition and thus potentially turnover (30–34). Whereas Hh signaling is activated in OA (35), the activation of the pathway alone does not drive cartilage catabolism (36). In chondrocytes, ciliary IFT is also important for the cellular response to pathophysiologically relevant stimuli, such as mechanics, inflammatory cytokines, and osmotic flux (25, 37–40). Here, we experimentally examined whether the ciliome, specifically IFT88, directly regulates matrix catabolism independent of transducing pathophysiologic stimuli.

MATERIALS AND METHODS

Primary Abs, substrates, recombinant proteins, and inhibitors

The following primary Abs were used in this study: Aggrecan (6-B-4) (Abcam, Cambridge, MA, USA), ARGXX (BC-3) (Abcam), phospho-JNK1/2 (Thermo Fisher Scientific, Waltham, MA, USA) β-actin (Cell Signaling Technology, Danvers, MA, USA), FLAG-M2 (MilliporeSigma, Burlington, MA, USA), acetylated α-tubulin (6-11B-1) (MilliporeSigma), early endosome antigen 1 (EEA-1; Abcam), LRP-1 β-light chain (Abcam), LRP-1 α-heavy chain (8G1) (Abcam), a disintegrin and metalloproteinase (ADAM)-17 (Abcam), MMP-13 (Santa Cruz Biotechnology, Dallas, TX, USA), MMP14 (anti-catalytic domain EP1264Y) (Abcam), mouse monoclonal anti–MT1-MMP hemopexin domain 222-1D8 (a gift from Yoshi Itoh, Kennedy Institute) generated as previously described (41), and arl13b (ProteinTech, Rosemont, IL, USA). Anti-AGEG was a kind gift from Hideaki Nagase (University of Oxford). Purified aggrecan from bovine cartilage came from MilliporeSigma. Recombinant human C-terminal His-tagged human receptor-associated protein (RAP) was produced in *Escherichia coli* using a pET3a-based expression vector and purified as described previously (13). The domain deletion mutant, ADAMTS-5 (TS5-3)-flag, is described in Gendron *et al*. (42), and recombinant MMP-13 is described in Yamamoto *et al*. (43). Recombinant IL-1β was purchased from PeproTech (London, United Kingdom).

Cell culture

The majority of experiments used a chondrocyte cell line as described in Results and previously (37). The line was maintained and immortalized at 33°C in low-glucose DMEM that was supplemented with 10% (v/v) fetal calf serum, 2.5 mM L-glutamine, 88 U/ml penicillin, 90 μg/ml streptomycin, and 10 ng/ml IFN-γ. Experiments were conducted using primary cells by removing IFN-γ and culturing at 37°C. For experiments that used primary human chondrocytes, cartilage samples were obtained from the Oxford Musculoskeletal Biobank, collected with informed donor consent before knee replacement surgery, in full compliance with national and institutional ethical requirements, the United Kingdom Human Tissue Act, and the Declaration of Helsinki (HTA License 12217 and Oxford REC C 09/H0606/11). Cartilage explants were removed from the joints immediately after surgery, diced, and subjected to collagenase digestion (type A; Roche, Basel, Switzerland) at 2 mg/ml overnight at 37°C in primary medium [low-glucose DMEM that was supplemented with 10% (v/v) fetal calf serum, 2.5 mM L-glutamine, 88 U/ml penicillin, 90 μg/ml streptomycin, and 16 mM HEPES]. Tissue suspension was then filtered through a 70-μm filter. Cells were then resuspended in primary medium, counted, and seeded onto 13-mm glass coverslips at 2×10^4/cm, then cultured for up to 48 h or to confluence to ensure quiescence.

Aggrecanase assays

We used a system of coculture with aggrecan as described previously (9). Chondrocytes were cultured in serum-free medium that contained 50 μg/ml bovine aggrecan using IL-1β (50 ng/ml) as a positive control, and medium was collected at time points after this in a 24-h period. Before analysis, 150 μl of medium sample was deglycosylated overnight at 37°C using Chondroitinase ABC (0.0013 U/mg GAG; MilliporeSigma) and endo-β-galactosidase

www.fasebj.org by Oxford Univ Lib Serv - Bodleian Lib (129.67.90.252) on October 30, 2019. The FASEB Journal Vol. ${article.issue.getVolume()}, No. ${article.issue.getIssueNumbe

from *Bacteroides fragilis* (0.0007 U/mg GAG; MilliporeSigma) added in 50 μl of digestion buffer that consisted of Tris (50 mM), EDTA (25 mM), and 50 mM sodium acetate (pH 7.5). Proteins were precipitated with 1 ml of ice-cold acetone and the pellet was air dried before resuspension in 50 μl Laemmli loading buffer (Bio-Rad, Hercules, CA, USA) that contained 2-ME (1:10) for loading. Fragments that were generated by cleaving at the Glu^{1819}-Ala^{1820} bond in aggrecan were detected using a polyclonal rabbit Ab directed at N-terminal AGEG. Samples were run on 4–12% NuPAGE Bis-Tris gels, then transferred to PVDF membrane. Bands were detected using ECL Plus Reagent, imaged on a Syngene G:Box imager (Fredrick, MD, USA).

Quantitative RT-PCR

Cells were cultured per aggrecanase experiments, then RNA was isolated using an RNAeasy Mini Kit (Qiagen, Germantown, MD, USA). RNA was resuspended in RNAase-free water and yields and indicative purity were checked using Nanodrop (Thermo Fisher Scientific). One microgram of RNA was used to synthesize cDNA, and reverse transcription was performed using the ABI High Capacity Kit (Thermo Fisher Scientific) following the manufacturer's instructions. Real-time RT-PCR was performed using the TaqMan (FAM dye) Universal Master Mix II (Thermo Fisher Scientific). Each reaction consisted of 0.5 μl cDNA template, 5 μl Master Mix, 0.5 μl primer, and 4 μl nuclease-free water. Samples were loaded in a 384-well plate and thermocycling was performed on a ViiA7 Real-Time RT-PCR System (Thermo Fisher Scientific) using the following protocol: hold 2 min at 50°C; hold 10 min at 95°C; 40 cycles: 15 s at 95°C, 1 min at 60°C; hold at 4°C. Data were captured and primary analysis was performed using Expression Suite Software (v.1.1; Applied Biosystems, Foster City, CA, USA) using the $\Delta\Delta C_t$ method using 18S as a normalizing gene. TaqMan assays (**Table 1**) were purchased from Thermo Fisher Scientific.

Western blotting

Cell lysates

Cells were kept on ice and washed quickly in ice-cold PBS before ice-cold lysis buffer (150 mM sodium chloride, 1% Triton X-100, 50 mM Tris, pH 8, a cocktail of protease inhibitors; Roche) was added to cells for 5 min. Cells were removed from the culture surface using a cell scraper before being left for an additional 5 min and homogenized using a 21-gauge needle. Samples were spun at 10,000 rpm for 15 min at 4°C before the supernatant cytoplasmic fraction was frozen and stored at −20°C.

Conditioned medium

Cells were cultured as per before aggrecanase experiments, then serum-free medium was collected after 24 h and stored at −20°C. Proteins were resolved by Bis-Tris gels, with the exception of LRP-1α for which samples were run, undenatured, on TCA gels. For endocytosis assays and LRP-1β expression, near-infrared secondary Abs (Li-Cor, Cambridge, United Kingdom) were used, multiplexing target protein with a reference where possible, and ImageJ (National Institutes of Health, Bethesda, MD, USA) was used to quantify immunoreactive bands. Other blots—neoepitopes, shed LRP-1, and sheddase expression—used horseradish peroxidase secondary Abs and ECL Plus detection.

Endocytosis uptake assays

Cells were cultured as previously described. After 72 h, cells were washed with PBS and cultured in serum-free medium for 24 h before medium was replaced, again with serum-free medium, for the duration of uptake experiments. Cells were cultured with serum-free medium with a final concentration of 20 nM FLAG-tagged ADAMTS-5 or 10 nM Pro-MMP-13. Where the experimental design required, cells were coincubated with a final concentration of 500 nM RAP for 20 min before the addition of ligands. Medium samples were collected straight into Laemmli loading buffer (Bio-Rad), boiled for 5 min, and frozen.

Immunofluorescence

Cells were cultured to confluence on 1.9-cm^2 glass coverslips. For total cell staining, coverslip cultures were fixed using 4% paraformaldehyde at 37°C for 7 min, followed by permeabilization with 0.5% Triton X-100, and were blocked with 5% goat serum. Coverslips were incubated overnight at 4°C with primary Abs, depending on the protein of interest: acetylated α-tubulin (1:2000), arl13b (1:1000), LRP-1 (1:1000), FLAG-TS-5 (1:500), and EEA-1 (1:500). Coverslips were washed and incubated for 45 min in the dark at 25°C with Alexa Fluor 488 anti-mouse conjugate (Thermo Fisher Scientific) and Alexa Fluor 555 anti-rabbit conjugate (Thermo Fisher Scientific) before mounting with DAPI (1:5000) counterstain (Thermo Fisher Scientific). For surface staining, coverslip cultures were only fixed for 1 min and no permeabilization was conducted before blocking with 5% goat serum. Samples were then treated the same as previously described. Coverslips were mounted onto slides using Prolong Gold (Thermo Fisher Scientific and sealed. For FLAG-TS-5 uptake/cilia length studies, wild-type cells were treated with FLAG-TS-5 over a 60-min time course before fixation as per total cell protocols. Images shown are from 40-min time point.

Imaging and analysis images were acquired using an Olympus FluoView FV1000 Confocal Microscope (Olympus, Tokyo, Japan) with an oil immersion ×63 objective to produce confocal serial sections for maximum-intensity *z*-stack reconstruction of monolayer fields with laser voltage, offset and gain held constant. Cilia length was measured using a medial line that was defined

TABLE 1. *TaqMan probes used for quantitative RT-PCR*

Gene	Catalog reference	Amplicon length (bp)	Reference sequence
RPS18	Mm02601776_m1	74	NM_011296.2
ADAMTS1	Mm00477355_m1	98	NM_009621.4
ADAMTS4	Mm00556068_m1	66	NM_172845.2
ADAMTS5	Mm00478620_m1	103	NM_011782.2
MMP3	Mm00440295_m1	66	NM_010809.1
MMP13	Mm00439491_m1	65	NM_008607.2
TIMP3	Mm00441826_m1	59	NM_011595.2
GLI2	Mm01293116_m1	80	NM_001081125.1
GLI3	Mm00492337_m1	82	NM_008130.2
PTCH1	Mm00436026_m1	69	NM_008957.2

www.fasebj.org by Oxford Univ Lib Serv - Bodleian Lib (129.67.90.252) on October 30, 2019. The FASEB Journal Vol. ${article.issue.getVolume()}, No. ${article.issue.getIssueNumbe

along the center of the cilium using ImageJ software. Analysis of LRP-1β signal distribution was conducted using two methods. The first used solely the LRP-1β signal for each field and an ImageJ histogram analysis was run before plotting the pixel intensity data in Prism 6 (GraphPad Software, La Jolla, CA, USA). A second manual approach classified single-cell LRP-1β signal into one of 4 groups: *1*) singular focal staining, *2*) majority of staining in 1 quadrant, *3*) in 1 hemisphere, or *4*) evenly distributed. Quadrants were assigned, square to edge of image and centered on nuclei. These were subsequently analyzed as contingency data using a χ^2 test.

Data presentation and statistics

Graphs were generated in Prism 6. All data analyses were performed in Prism. Parametric and nonparametric tests were chosen after D'Agostino-Pearson omnibus normality tests. Statistical tests were used as described in Results.

RESULTS

Hypomorphic mutation to IFT88 results in constitutive aggrecanase activity

Our first aim was to assess whether protease activity changed upon experimental disruption of the ciliome *in vitro*. The IFT88 Oak Ridge Polycystic Kidney ($IFT88^{ORPK}$) mutation is hypomorphic, which results in a shortened form of the protein, but is not 100% penetrant in terms of cilia phenotype (15% of chondrocytes *in vitro* assemble stunted cilia) (33, 37). Using a previously described coculture system (9), we added bovine aggrecan to wild-type and $IFT88^{ORPK}$ mouse chondrocyte cultures and probed the culture medium for aggrecan and aggrecanase neoepitopes.

Treatment with IL-1β for 24 h resulted in the appearance of a 35-kDa aggrecan fragment, which was indicative of proteolysis of full-length aggrecan (~250 kDa, core protein). An identical band appeared without cytokine stimulation after 12 h in wild-type cultures but earlier, at 6 h, in $IFT88^{ORPK}$ cultures that remained more pronounced in $IFT88^{ORPK}$ at all time points (**Fig. 1*A***). $IFT88^{ORPK}$ chondrocytes also had increased production of aggrecan neoepitopes, AGEG and ARGS (Fig. 1*B*), at 24 h. Neoepitope bands were comparable in size to those produced by primary human articular chondrocytes that were isolated from osteoarthritic joints and wild-type mouse chondrocytes that were treated with IL-1β for 24 h (Fig. 1*B*). Relative aggrecanase activity, assessed by probing for AGEG over 24 h, was consistently higher in $IFT88^{ORPK}$ cultures, apparent first at 12 h when there was little measurable activity in WT cultures (Fig. 1*C*). To explore the underlying mechanism for this enhanced aggrecanase activity, we first investigated the gene expression profiles of a number of cartilage proteases using quantitative RT-PCR. We found no transcriptional signature to explain this increased activity. There were no increases in *ADAMTS1*, *-4* or, *-5*; *MMP3* or *-13*; or indeed a difference in mRNA levels of the tissue inhibitor of metalloproteases (*TIMP3*; Fig. 1*D*). RT-PCR analysis also demonstrated that, in these experimental conditions, $IFT88^{ORPK}$ mutation results in the down-regulation of the Hh pathway, previously proposed to drive cartilage destruction in OA (35), as indicated by reduced expression of pathway target patched-1 (*PTCH1*) and transcription factor glioma-associated oncogene family zinc finger 2 (*GLI2*) (P = 0.0004 and 0.008, respectively, multiple Student's t test corrected using Holm-Sidak method; n = 3; Fig. 1*E*). We have previously reported that this mutation influences the response of chondrocytes to cytokines by regulating NF-κB signaling, itself a proposed regulator of aggrecanase transcription (8); however, as reported (38), there is no constitutive pathway activation. Similarly, here we found no constitutive JNK pathway activity (Fig. 1*F*), also previously linked to aggrecanase activity (9). These data implied that IFT88 regulates aggrecanase activity by post-transcriptional means.

Polarized endocytosis of ADAMTS-5 at the primary cilium

Recent research has shown that chondrocyte aggrecanase activity is regulated post-transcription by endocytotic clearance *via* the LRP-1 system (13), disturbed in OA (44). The primary cilium has been described as a site that is enriched for endocytotic activity *in situ* (25). To investigate the possibility that the disruption of IFT88 and the primary cilium might affect LRP-1–mediated endocytosis of aggrecanases, we cocultured cells with FLAG-tagged, ADAMTS-5 (TS5-3) (42), termed FLAG-TS-5, and monitored uptake. We first cultured chondrocytes on glass coverslips to observe uptake by microscopy. Cell-associated signal was visible from 30 min after the addition of ligand to cultures. At 40 min, wild-type chondrocytes exhibited greater levels of cell-associated FLAG-TS-5 than $IFT88^{OPRK}$ chondrocytes (**Fig. 2*A***, green signal). We also observed that, in wild-type cells, this signal was preferentially localized to one side of the cell, at its center, the site of ciliary assembly (red, anti-arl13b signal Fig. 2*A*, expanded image). While imaging aggrecanase uptake, we observed an increase in cilia length (15% increase in median length, Fig. 2*B*). This implied an interplay between ciliary IFT and the uptake of ADAMTS-5.

Endocytosis of protease impaired by IFT88 mutation

To explore in a more quantitative manner the possibility that IFT88 regulates the rate of endocytotic clearance of proteases, we measured extracellular (culture medium) levels of recombinant FLAG-TS-5 over time. After its addition to cells, levels of extracellular FLAG-TS-5 rapidly dropped, with signal often absent by 80 min (Fig. 2*C*). Quantification of repeat experiments (Fig. 2*D*) demonstrated that this uptake was partially blocked by the LRP-1 antagonist, RAP, and that extracellular FLAG-TS-5 levels were consistently higher in $IFT88^{ORPK}$ cultures. The extracellular half-life of FLAG-TS-5 in $IFT88^{ORPK}$ cultures was double that of wild-type cultures, which was indicative of a reduced rate of LRP-1–mediated endocytotic uptake. The extracellular half-life was similar or greater to that observed in wild-type cells inhibited by RAP. Rates of uptake in $IFT88^{ORPK}$ cultures were unaffected by the

www.fasebj.org by Oxford Univ Lib Serv - Bodleian Lib (129.67.90.252) on October 30, 2019. The FASEB Journal Vol. ${article.issue.getVolume()}, No. ${article.issue.getIssueNumbe

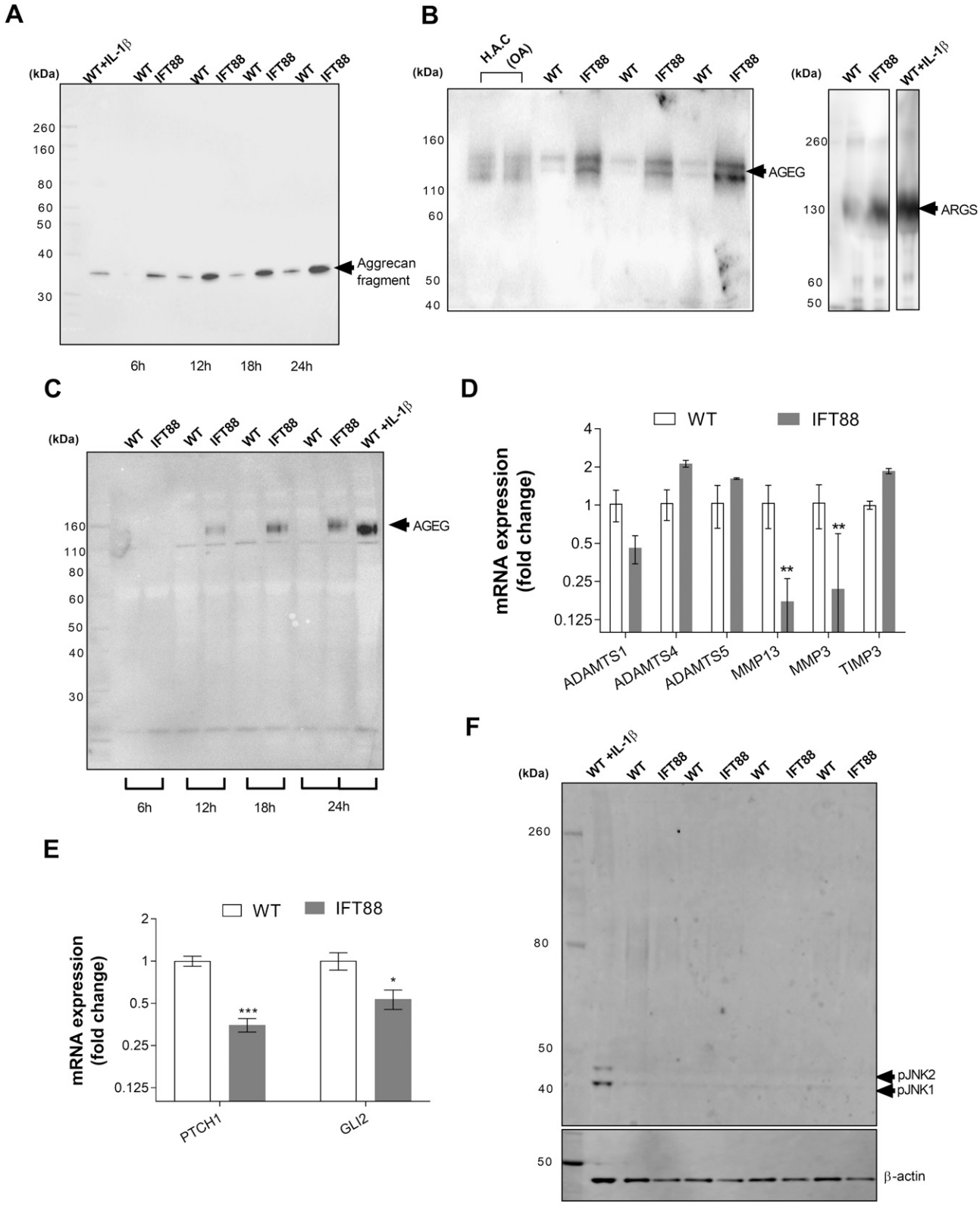


Figure 1. IFT88 mutation results in constitutive catabolic activity without associated transcriptional regulation. Wild-type (WT) and IFT88^{ORPK} chondrocytes were cultured with full-length aggrecan medium collected at intervals. *A*) Western blot analysis of conditioned medium, probing for aggrecan showing 35-kDa fragment in cultures that were treated with 10 ng/ml IL-1β and over time in unstimulated cultures. *B, C*) Western blot analysis showing the presence of AGEG and ARGS neoepitopes in conditioned medium after 24 h (*B*), and AGEG over a time course (*C*). *D, E*) Quantitative RT-PCR analysis of WT and IFT88 chondrocytes from identical experiments. Data shown are mean ΔC_t normalized to average WT ± SD. ***$P = 0.0004$, *$P = 0.008$ for PTCH1 and GLI2, respectively, multiple Student's t test corrected by Holm-Sidak method; $n = 3$). *F*) Western blot analysis of cell lysates probed for pJNK1 and pJNK2, with positive control WT cells treated with 10 ng/ml IL-1β and lysate collected at 10 min ($n = 4$).

www.fasebj.org by Oxford Univ Lib Serv - Bodleian Lib (129.67.90.252) on October 30, 2019. The FASEB Journal Vol. ${article.issue.getVolume()}, No. ${article.issue.getIssueNumbe

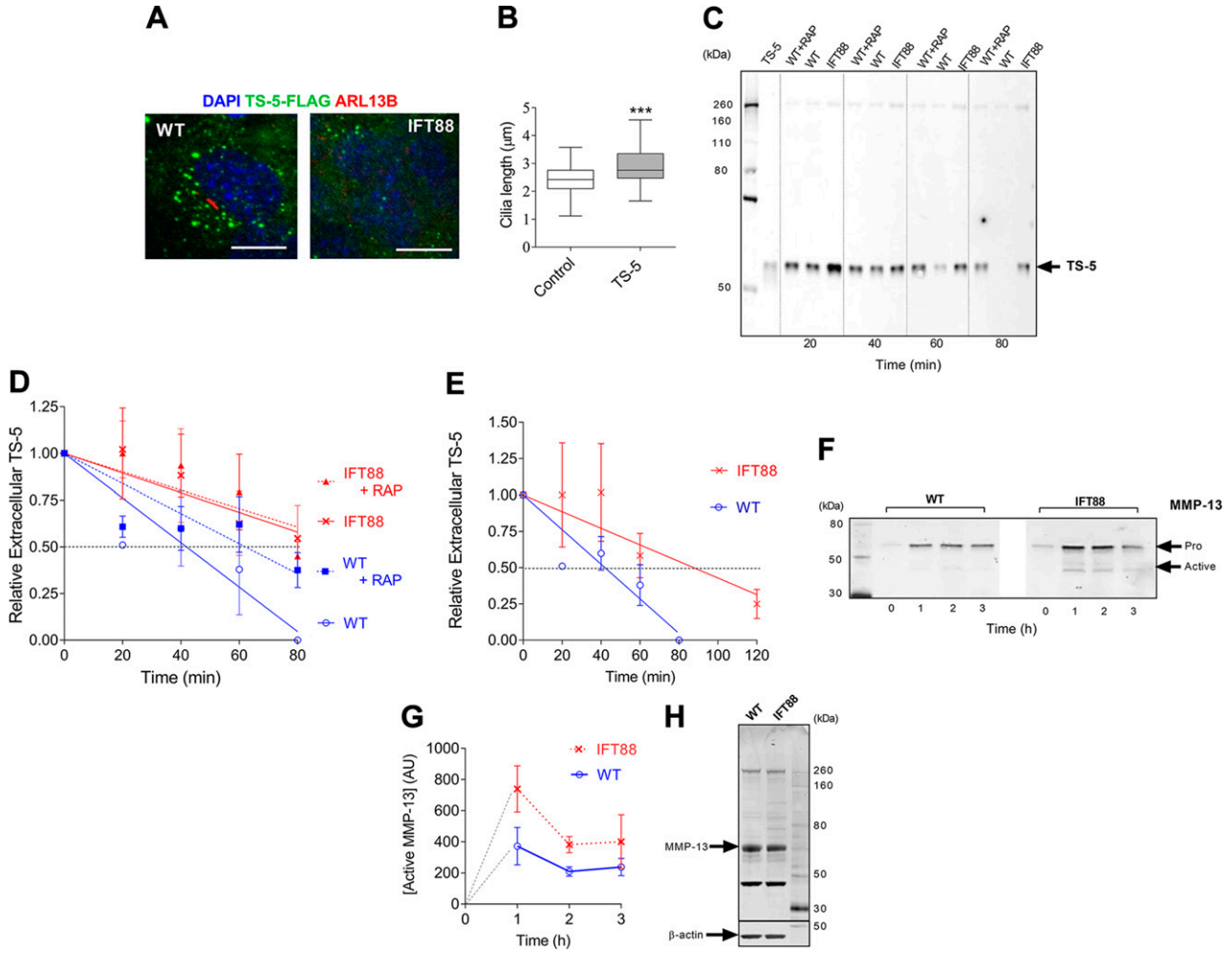


Figure 2. Perturbation of IFT88 impairs chondrocyte endocytosis of proteases. Cells were cultured with recombinant proteases—either FLAG-TS-5 or full-length MMP-13—and uptake of proteases was monitored by microscopy or measurement of FLAG-TS-5 in extracellular media by Western blot. *A*) Confocal fluorescent microscopy of wild-type (WT) and IFT88^{ORPK} cells on exposure to FLAG-TS-5 (green). Primary cilia (red) were labeled with anti-arl13b and nuclei with DAPI (blue). Scale bar, 10 μm. Image captured after 40 min of incubation. *B*) Cilia length data as shown by box plot with Tukey whiskers. ***$P \leq 0.001$ (Mann-Whitney *U* test, control $n = 61$ cilia; FLAG-TS-5, $n = 62$ cilia). Images also taken at the 40-min incubation time point. *C*, *D*) Western blot analysis of extracellular FLAG-TS-5 over time (*C*) and quantification of data (data are shown as mean normalized to 0 time-point, ± SD, $n = 6$; *D*). *E*) Quantification of repeat study comparing WT and IFT88^{ORPK} cells over an extended time course (means ± SD, $n = 3$). *F*, *G*) Western blot for rMMP-13 uptake showing both full-length (pro) and cleaved (active) MMP-13 (*F*) and quantification of data (means ± SD, $n = 3$; *G*). *H*) Western blot for MMP13 expression in cell lysates.

addition of RAP. An extended time course revealed that there was, on average, still 25% of FLAG-TS-5 remaining at 2 h after addition to IFT88^{ORPK} cells, 40 min after the signal became unmeasurable in wild-type cells (Fig. 2*E*). Repeat studies using recombinant MMP-13, also an LRP-1 ligand, demonstrated a reduced rate of uptake for MMP-13 in IFT88^{ORPK} cultures (Fig. 2*F*), associated with the accumulation of cleaved, active MMP-13 (quantified in Fig. 2*G*). Importantly, both cell types secreted low amounts of endogenous MMP-13 protein into the culture medium. Furthermore, in contrast to mRNA levels, protein expression was unchanged in IFT88^{ORPK} lysates (Fig. 2*H*).

Disruption of IFT88 stimulates LRP-1 shedding

The light chain (β) of LRP-1 is cleaved by sheddases at the cell surface, and the entire heavy chain (α) is released into the extracellular milieu, a process that is enhanced in OA and that leads not only to reduced uptake of ligands by endocytosis, but also to enhanced extracellular activity of proteases by binding to the protease (12). We hypothesized that this LRP-1 may have been shed and present at higher levels with disruption of IFT. By probing conditioned media, we found that extracellular amounts of high-MW LRP-1α subunit were higher in IFT88^{ORPK} cultures (**Fig. 3*A***), which indicated that the mutation is associated with enhanced shedding of LRP-1. Previous studies identified 2 sheddases of LRP-1 in chondrocytes, ADAM-17 and MMP-14 (12). Kidney epithelial cells with the identical IFT88^{ORPK} mutation have previously been described to have elevated ADAM-17 (45), but, in contrast, we found that IFT88^{ORPK} chondrocytes expressed similar or lower levels of ADAM-17 than wild-type chondrocytes (Fig. 3*B*); however, we found increased cellular expression of MMP-14 in

www.fasebj.org by Oxford Univ Lib Serv - Bodleian Lib (129.67.90.252) on October 30, 2019. The FASEB Journal Vol. ${article.issue.getVolume()}, No. ${article.issue.getIssueNumbe

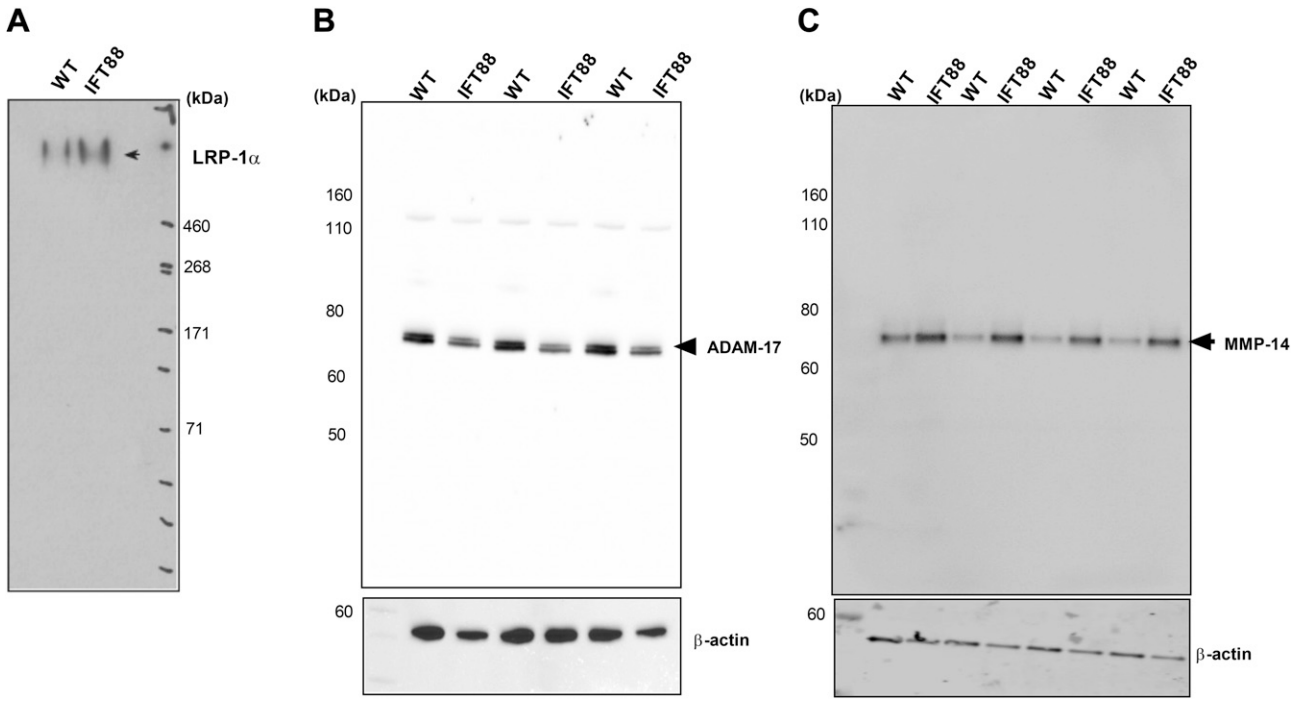


Figure 3. IFT88 mutation results in LRP-1 shedding. *A*) Western blot for extracellular (shed) LRP-1α in conditioned medium of cultures. *B, C*) Western blot of cell lysates that demonstrates the cellular expression of sheddases ADAM-17 ($n = 3$; *B*) and MMP-14 ($n = 4$; *C*), respectively. Conditioned medium and lysates for all groups were collected after 24 h of culture.

IFT88^{ORPK} chondrocytes compared with wild-type cells (Fig. 3*C*).

Spatial association between microtubule organizing center/primary cilium and LRP-1

In light of the observation that FLAG-TS-5 accumulated in a polarized fashion in chondrocytes (Fig. 2*A*), and previous reports of endocytosis at the base of the primary cilium (24, 25), we next explored LRP-1 distribution by microscopy. Both human primary and murine chondrocytes were stained with an Ab to the light (β) chain of LRP-1 (red), which includes the transmembrane and short cytoplasmic domains. We also colabeled primary cilia; staining for acetylated α-tubulin (green) and nuclei are blue throughout (DAPI). In both human primary chondrocytes (**Fig. 4*A***) and mouse wild-type chondrocytes, (**Figs**. 4*B* and **5*A***, wide-field), LRP-1β was predominantly expressed in a perinuclear manner and associated with the microtubule network, but often formed into bright clusters and concentrations near the microtubule organizing center (MTOC), the site of cilia assembly. LRP-1β expression, on occasion, was nearly exclusively confined to a singular signal at the ciliary base, but more commonly observed to be highly polarized to this area (as described and quantified in Fig. 5). Preparation of samples—without a permeabilization step and with only a brief paraformaldehyde fixation—resulted in staining bias toward near cell surface only. This was validated by the observation that cytoplasmic signal—indicated by acetylated α-tubulin—becomes barely visible apart from cytokinetic bridges (Fig. 4*C*, black and white images). In these conditions, LRP-1β distribution displayed the same polarized distribution, which implied the periciliary organization of LRP-1 on the membrane (Fig. 4*C*, red signal). In contrast, cytoplasmic early EEA-1, which is reflective of internalized early endosomes, was not similarly polarized (Fig. 4*D*, red signal).

IFT88^{ORPK} mutation disrupts LRP-1 organization

In IFT88^{ORPK} chondrocytes, LRP-1β expression was more homogenously distributed over the cells compared with wild-type cells, although some polarization of signal is still observed in one quadrant of the cell and sometimes at the site of MTOC (Fig. 5*A, C, E*). This staining was imaged in multiple fields from multiple cell preparations ($n \geq 7$ fields, >300 cells), all of which demonstrated qualitative changes to the surface distribution of LRP-1β. ImageJ analysis of the frequency distribution of LRP-1β signal in these whole-field images indicated a change in the frequency of distribution of signal intensity between wild-type and IFT88^{ORPK} populations (Fig. 5*B*). Additional classification of fields of cells into 4 subtypes of LRP-1β distribution revealed a statistically significant difference between wild-type and IFT88^{ORPK} cells ($P \leq 0.0001$, χ^2 test; $n = 7$ fields, at least 265 cells/population). Approximately 75% of wild-type cells had the majority of the LRP-1β signal in one quadrant of the cell or a single focal point at the site of ciliary assembly. In comparison, >80% of IFT88^{ORPK} cells had even distribution or a hemispherical polarization (Fig. 5*D*). Total LRP-1β protein expression, as measured by Western blot, was not different (Fig. 5*F*). In cell preparations, ciliation in wild-type cells can range from 50 to 80%, increasing with cell quiescence. In adult mouse cartilage

www.fasebj.org by Oxford Univ Lib Serv - Bodleian Lib (129.67.90.252) on October 30, 2019. The FASEB Journal Vol. ${article.issue.getVolume()}, No. ${article.issue.getIssueNumbe

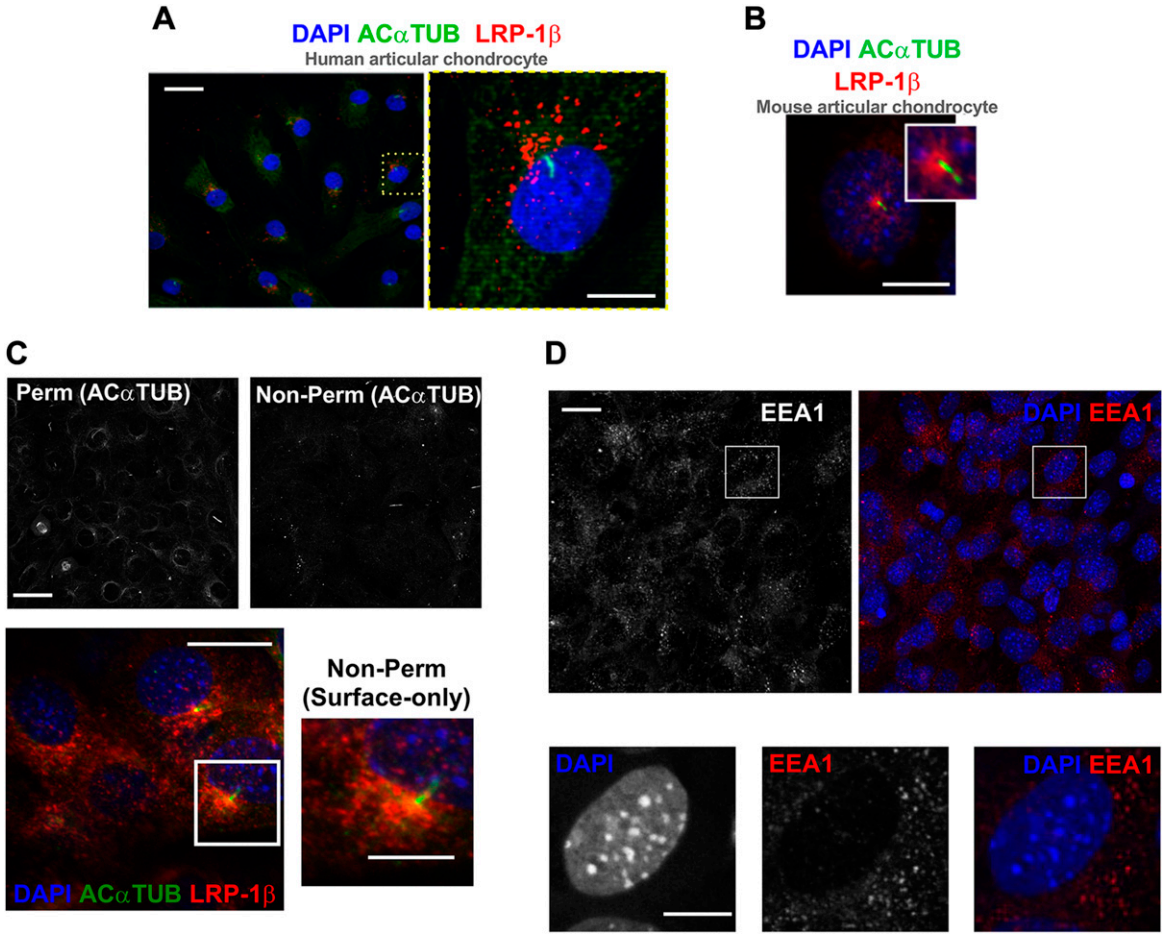


Figure 4. Membranous hot spot of LRP-1β associated with primary cilium. *A*) Immunofluorescent staining of primary cilia (green) and LRP-1β (red) in human articular chondrocytes. *B*) Immunofluorescent staining of LRP-1β (red) and primary cilia (green) in wild-type (WT) mouse chondrocytes. *C*) Immunofluorescence images shows surface-only staining of LRP-1β (red) in WT cells that concentrated at the base of the primary cilium (green) in cells without permeabilization as validated by the absence of a majority of acetylated α-tubulin signal (black and white images above). *D*) Immunofluorescence of EEA-1 (red) in mouse WT chondrocytes. Nuclei were labeled with DAPI. Scale bars, 10 μm.

tissue, cilia prevalence is usually high [>50% and polarized in position (33)]. In culture, when ciliation was greatest (70–80% prevalence) a ciliary axoneme-associated signal for LRP-1β was commonly observed (Fig. 5*G*).

To summarize, we find that hypomorphic mutation to IFT88 in chondrocytes results in marked increases in aggrecanase activity, seemingly independent of transcriptional regulation. This is associated with reduced endocytotic clearance of protease, potentially as a critical organization of membrane LRP-1 is disrupted. Disruption of this organization of membranous LRP-1β is also associated with the shedding of LRP-1α, which likely contributes to the endocytotic and aggrecanase phenotypes. We propose that the polarized, periciliary region is important for efficient, rapid endocytosis of protease and is important to the regulation of matrix remodeling.

DISCUSSION

Previous studies have linked the primary cilium and/or its associated core protein machinery with musculoskeletal development (46), matrix patterning (33), and turnover processes (32), as well as, potentially, the development of OA *via* ciliary-regulated Hh signaling (32, 35). A key component of the cilium's machinery, IFT88 is highly influential in cartilage (33) and transduces the chondrocyte response to mechanical (37) and inflammatory cues (39). Although canonical, ciliary Hh signaling is hugely influential, activation of Hh alone does not activate cartilage catabolism *in vitro* (36). Here, we directly explored the role of the cilium in the regulation of protease activity. Hypomorphic disruption of IFT88 increased the constitutive catabolic activity of chondrocytes *in vitro*. The IFT88^{ORPK} mutation, which results in changes to matrix patterning in cartilage *in vivo* (33), renders cells unable to express full-length IFT88 and assemble a primary cilium. This has also previously been associated with the regulation of multiple chondrocyte responses (37–39, 47–49), most of which are proposed to be indicative of roles for the cilium. Importantly, however, IFT88, and indeed this mutation, are both associated with cell biology that is not proven to be attributable to cilia function—for example, migration (50), cell division (51), and planar cell polarity (52).

www.fasebj.org by Oxford Univ Lib Serv - Bodleian Lib (129.67.90.252) on October 30, 2019. The FASEB Journal Vol. ${article.issue.getVolume()}, No. ${article.issue.getIssueNumbe

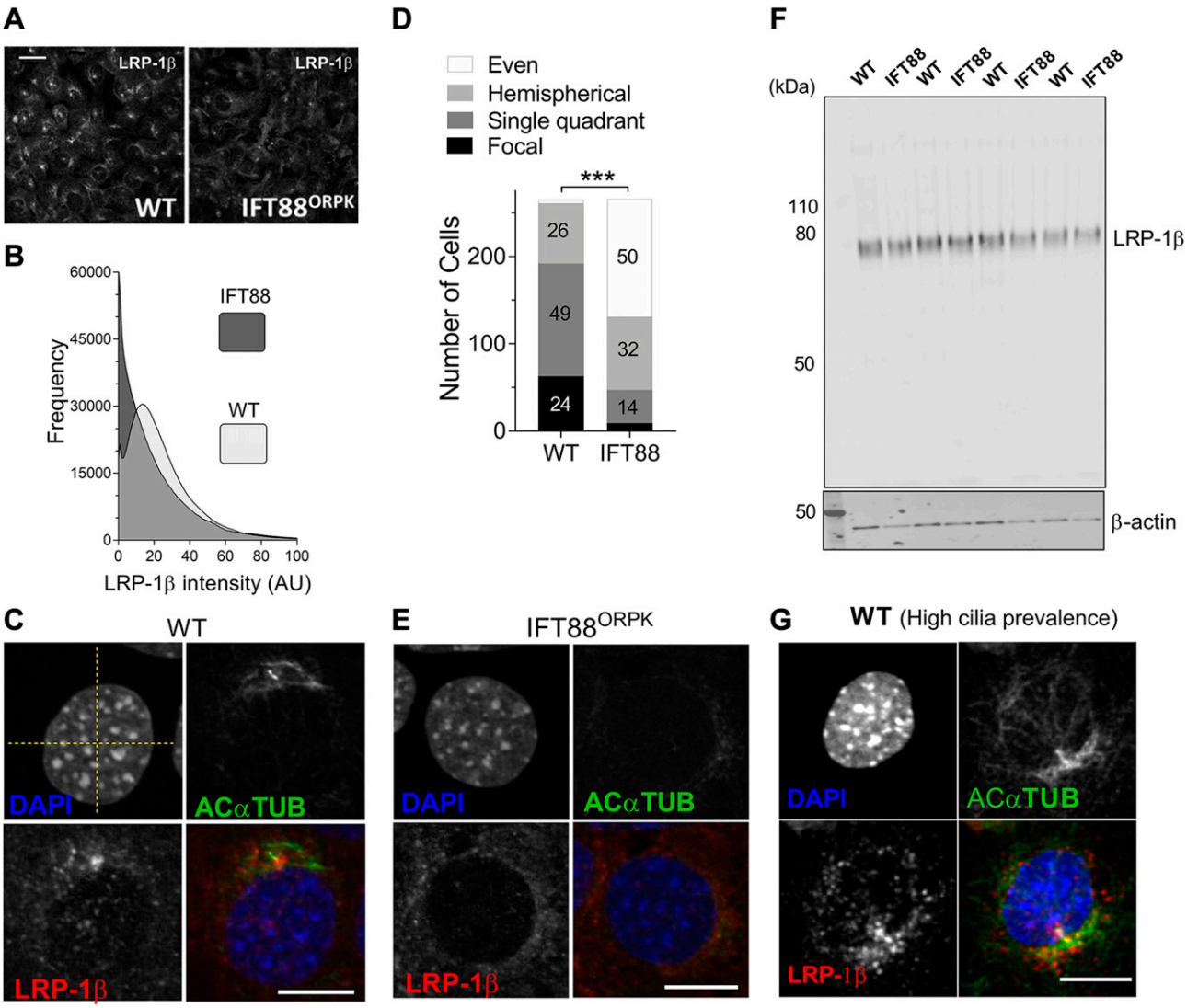


Figure 5. IFT88 mutation disturbs hot spot that is possibly associated with the ciliary pocket. *A*) Fluorescent microscopy of wild-type (WT) and IFT88^{ORPK} cultures demonstrates the LRP-1β signal distribution in field of cells. *B*) Frequency histogram of LRP-1β signal intensity distribution for 6 fields of cells (~n = 300 cells). *C*, *E*) Single-cell confocal images of WT (focal distribution; *C*) and IFT88^{ORPK} (even distribution; *E*) cells. Yellow dashed lines were used to define quadrants centered on nuclei. *D*) Contingency data from a classification analysis from 7 fields of WT and IFT88^{ORPK} cultures that describe numbers in each group (percentages shown on bars, with the exception of WT even distribution, which had 1% frequency, and IFT88^{ORPK} single focal distribution, which had 4% frequency) of each type of staining within total populations. Statistical difference is from a χ^2 analysis. ***$P < 0.0001$. *F*) Western blot analysis of LRP-1β total protein expression (n = 4 repeats). *G*) LRP-1β (red) signal localized along length of the cilium (green), potentially lining a ciliary pocket (representative of single quadrant distribution for classification data). Scale bars, 10 μm.

Weak inherent gelatinase activity and collagenase activity in these cells make it difficult to assess these protease activities by zymography and collagen II coculture, respectively; however, using a recently developed technique (9) that allows for the assessment of aggrecan degradation by quantifying the production of aggrecan neoepitopes, we observed increased constitutive aggrecanase activity stimulated in IFT88^{ORPK} chondrocytes. This activity was comparable to that of human primary chondrocytes from the clinical OA setting or mouse chondrocytes that are stimulated with the inflammatory cytokine, IL-1β. Relative rates of AGEG production between wild-type and IFT88^{ORPK} cells seemed to diverge over a 24-h time course, which implies an immediate inherent difference in the cells, which we would now propose to be impaired receptor-mediated endocytosis of aggrecanase enzymes, and a synergistic factor, which we propose to be LRP-1 shedding. In OA, tissue damage is not always directly associated with increased gene expression of catabolic enzymes. In our experimental setting, ADAMTS expression was unchanged, whereas MMP expression was reduced. A number of candidate pathways lie upstream in the regulation of aggrecanase activity. The NF-κB pathway is upstream of aggrecanase transcription (8), and its activity is regulated by IFT88, but only in response to cytokine (38). Recently, in chondrocytes, the JNK2 pathway has been linked to OA protease activity (9); however, we find that IFT88^{ORPK} cells do not have constitutive JNK2

www.fasebj.org by Oxford Univ Lib Serv - Bodleian Lib (129.67.90.252) on October 30, 2019. The FASEB Journal Vol. ${article.issue.getVolume()}, No. ${article.issue.getIssueNumbe

activity. Another possibility is the constitutive activation of the Hh pathway, recently linked to altered matrix catabolism and OA. Its activation results in spontaneous OA and pathway attenuation reduces the severity of surgically induced OA (35); however, this might not be a direct effect on aggrecanase activity as this group went on to demonstrate that Hh signaling regulates cholesterol accumulation in chondrocytes, associated with OA severity (53). IFT88 transduces Hh signal by ciliary trafficking of patched, smoothened, and the resultant modification of Gli transcription factors (54, 55). In our experimental conditions, the pathway is inhibited, likely owing to low-level Hh activation that is diminished by the loss of cilia; ~85% of chondrocytes with this mutation do not assemble a primary cilium. In the absence of a likely post-transcriptional mechanisms.

Recent studies have linked increases in protease ativity in cartilage to the LRP-1 endocytosis system (11–13). More broadly, links between the cilium and endocytosis have also been described (14, 22, 24–27). In particular, Schou *et al.* (27) describes a caveolin-enriched microdomain at the ciliary transition zone that regulates Hh signal transduction within the ciliary axoneme. This endocytotic domain requires the novel ciliary kinesin-3 member kinesin family member 13B, which, of interest, also regulates LRP-1 (56); however, a functional link between ciliary machinery and the regulation of global cell endocytosis remains unreported. We propose that our findings link IFT88 and, by extension, potentially the primary cilium to increased matrix turnover that is similar to that observed in OA *via* an LRP-1 regulatory axis. Cilia are highly conserved in their structure throughout evolution; primary and motile cilia bear great similarities to prokaryotic and eukaryotic flagella. Trypanosomes are unicellular parasitic protozoa that assemble a flagellum for locomotion. Interestingly, the only site for endocytosis in trypanosomes is the flagellum pocket at the base of the flagellum structure, and on the deletion of IFT88, while a pocket is still assembled, endocytosis function is impaired (28). In chondrocytes, *in vitro*, we find that labeled ADAMTS-5 is taken up preferentially to 1 segment of the cell. Moreover, relative rates of endocytosis of both ADAMTS-5 and MMP-13 are reduced when IFT88 is disrupted, an effect that is comparable to that of LRP-1 inhibition by RAP. The experimental concentration of ligands is high compared with likely pathophysiologic levels. Nevertheless, an extension of protease half-life in cartilage that is comparable to that observed in these experiments is likely influential, increasing exposure time of the extracellular matrix to proteases. We also found increased LRP-1 shedding when IFT88 was disrupted. This, combined with reduced clearance, is likely to amplify the catabolic activity of the cells, as shed LRP-1α binds proteases and further increases their activity (12). IFT88^{ORPK} chondrocytes express elevated levels of MMP-14, a sheddase that has been identified as disturbing the LRP-1 system in OA (12). Strikingly, we find the transmembrane-containing β chain of the LRP-1 receptor is concentrated in the region around the cilium. This distribution varies in different culture conditions but is pronounced in quiescent cells of the line used here and freshly isolated primary human chondrocytes. The IFT88^{ORPK} mutation disrupts this LRP-1β organization without an effect on the amount of protein. We find that the surface population of this receptor displays this polarized distribution, often forming a hot spot for endocytotic clearance, rather than being purely reflective of a predictable relative concentration of all vesicular trafficking in the area around the MTOC. In cells that demonstrate highly concentrated LRP-1, we see staining that is supportive of a working hypothesis that LRP-1 lines the ciliary pocket region, but higher resolution microscopy will be required to determine if this is the case. Given the generalized associations between the cilium and endocytosis recognized by others, we do not interpret our results to be specific to LRP-1 or its ligands, but in the chondrocyte, these are particularly physiologically and disease relevant, hence our focus here. We cannot rule out a nonciliary mechanism. IFTs are linked to endocytosis independent of cilia. In T cells that do not form a cilium, but rather form an immune synapse responsible for the recycling of endosome-associated T-cell antigen receptors, IFT88 has been associated with polarized receptor recycling alongside IFT20, IFT57, and IFT52 (57–60). Ongoing studies are exploring the roles of other components of the ciliome in protease activity and endocytosis.

In summary, the current study makes a functional link between IFT and protease activity in chondrocytes *via* a regulatory axis that is highly relevant to osteoarthritis; however, this link between IFT and LRP-1–mediated endocytosis may be relevant in other pathophysiologic scenarios in which LRP-1 plays putative roles, such as in atherosclerotic and neuronal plaques (61). Additional studies are required to dissect this mechanism in detail, especially to identify a means by which to exploit this putative regulation of endocytosis by IFT. FJ

ACKNOWLEDGMENTS

The authors thank the Oxford Musculoskeletal Biobank (University of Oxford) forproviding human cartilage samples; and Hideaki Nagase, Yoshi Itoh, Linda Troeberg, Heba Ismail, and Tonia Vincent (University of Oxford) for providing key reagents, Abs, and critical comments throughout the development of this manuscript. This work was supported by the Arthritis Research United Kingdom (ARUK) Centre for Osteoarthritis Pathogenesis (Grant 20205), including a small project initiative awarded to A.K.T.W. and K.Y. that supported M.M.F.; a Kennedy Trust for Rheumatology Research (KTRR) Prize Studentship supporting C.R.C.; and an ARUK studentship awarded to A.K.T.W. (Grant 21546, supporting I.C.), and ARUK grant (Grant 20887) awarded to Linda Troeberg (supporting A.C.), an ARUK Career Development Fellowship (Grant 21447, supporting K.Y.), and a KTRR/ARUK Career Development Fellowship supporting A.K.T.W. The authors declare no conflicts of interest.

AUTHOR CONTRIBUTIONS

C. R. Coveney, I. Collins, M. Mc Fie, A. Chanalaris, K. Yamamoto, and A. K. T. Wann conceived and designed experiments; C. R. Coveney, I. Collins, M. Mc Fie, A. Chanalaris, and A. K. T. Wann performed experiments; K. Yamamoto contributed reagents and analytic tools; C. R.

www.fasebj.org by Oxford Univ Lib Serv - Bodleian Lib (129.67.90.252) on October 30, 2019. The FASEB Journal Vol. ${article.issue.getVolume()}, No. ${article.issue.getIssueNumbe

Coveney, I. Collins, M. Mc Fie, A. Chanalaris, K. Yamamoto, and A. K. T. Wann analyzed data; C. R. Coveney and A. K. T. Wann wrote the manuscript; and all authors revised, read, and approved the final manuscript.

REFERENCES

1. Christ, A., Christa, A., Klippert, J., Eule, J. C., Bachmann, S., Wallace, V. A., Hammes, A., and Willnow, T. E. (2015) LRP2 acts as SHH clearance receptor to protect the retinal margin from mitogenic stimuli. *Dev. Cell* **35**, 36–48
2. Emonard, H., Bellon, G., Troeberg, L., Berton, A., Robinet, A., Henriet, P., Marbaix, E., Kirkegaard, K., Patthy, L., Eeckhout, Y., Nagase, H., Hornebeck, W., and Courtoy, P. J. (2004) Low density lipoprotein receptor-related protein mediates endocytic clearance of pro-MMP-2.TIMP-2 complex through a thrombospondin-independent mechanism. *J. Biol. Chem.* **279**, 54944–54951
3. Yang, Z., Strickland, D. K., and Bornstein, P. (2001) Extracellular matrix metalloproteinase 2 levels are regulated by the low density lipoprotein-related scavenger receptor and thrombospondin 2. *J. Biol. Chem.* **276**, 8403–8408
4. Muir, H. (1995) The chondrocyte, architect of cartilage. Biomechanics, structure, function and molecular biology of cartilage matrix macromolecules. *BioEssays* **17**, 1039–1048
5. Glyn-Jones, S., Palmer, A. J., Agricola, R., Price, A. J., Vincent, T. L., Weinans, H., and Carr, A. J. (2015) Osteoarthritis. *Lancet* **386**, 376–387
6. Glasson, S. S., Askew, R., Sheppard, B., Carito, B., Blanchet, T., Ma, H. L., Flannery, C. R., Peluso, D., Kanki, K., Yang, Z., Majumdar, M. K., and Morris, E. A. (2005) Deletion of active ADAMTS5 prevents cartilage degradation in a murine model of osteoarthritis. *Nature* **434**, 644–648
7. Little, C. B., Barai, A., Burkhardt, D., Smith, S. M., Fosang, A. J., Werb, Z., Shah, M., and Thompson, E. W. (2009) Matrix metalloproteinase 13-deficient mice are resistant to osteoarthritic cartilage erosion but not chondrocyte hypertrophy or osteophyte development. *Arthritis Rheum.* **60**, 3723–3733
8. Kobayashi, H., Hirata, M., Saito, T., Itoh, S., Chung, U. I., and Kawaguchi, H. (2013) Transcriptional induction of ADAMTS5 protein by nuclear factor-κB (NF-κB) family member RelA/p65 in chondrocytes during osteoarthritis development. *J. Biol. Chem.* **288**, 28620–28629
9. Ismail, H. M., Yamamoto, K., Vincent, T. L., Nagase, H., Troeberg, L., and Saklatvala, J. (2015) Interleukin-1 acts *via* the JNK-2 signaling pathway to induce aggrecan degradation by human chondrocytes. *Arthritis Rheumatol.* **67**, 1826–1836
10. Scilabra, S. D., Troeberg, L., Yamamoto, K., Emonard, H., Thøgersen, I., Enghild, J. J., Strickland, D. K., and Nagase, H. (2013) Differential regulation of extracellular tissue inhibitor of metalloproteinases-3 levels by cell membrane-bound and shed low density lipoprotein receptor-related protein 1. *J. Biol. Chem.* **288**, 332–342
11. Yamamoto, K., Owen, K., Parker, A. E., Scilabra, S. D., Dudhia, J., Strickland, D. K., Troeberg, L., and Nagase, H. (2014) Low density lipoprotein receptor-related protein 1 (LRP1)-mediated endocytic clearance of a disintegrin and metalloproteinase with thrombospondin motifs-4 (ADAMTS-4): functional differences of non-catalytic domains of ADAMTS-4 and ADAMTS-5 in LRP1 binding. *J. Biol. Chem.* **289**, 6462–6474
12. Yamamoto, K., Santamaria, S., Botkjaer, K. A., Dudhia, J., Troeberg, L., Itoh, Y., Murphy, G., and Nagase, H. (2017) Inhibition of shedding of low-density lipoprotein receptor-related protein 1 reverses cartilage matrix degradation in osteoarthritis. *Arthritis Rheumatol.* **69**, 1246–1256
13. Yamamoto, K., Troeberg, L., Scilabra, S. D., Pelosi, M., Murphy, C. L., Strickland, D. K., and Nagase, H. (2013) LRP-1-mediated endocytosis regulates extracellular activity of ADAMTS-5 in articular cartilage. *FASEB J.* **27**, 511–521
14. Jensen, C. G., Poole, C. A., McGlashan, S. R., Marko, M., Issa, Z. I., Vujcich, K. V., and Bowser, S. S. (2004) Ultrastructural, tomographic and confocal imaging of the chondrocyte primary cilium *in situ*. *Cell Biol. Int.* **28**, 101–110
15. Poole, C. A., Jensen, C. G., Snyder, J. A., Gray, C. G., Hermanutz, V. L., and Wheatley, D. N. (1997) Confocal analysis of primary cilia structure and colocalization with the Golgi apparatus in chondrocytes and aortic smooth muscle cells. *Cell Biol. Int.* **21**, 483–494
16. Satir, P., Pedersen, L. B., and Christensen, S. T. (2010) The primary cilium at a glance. *J. Cell Sci.* **123**, 499–503
17. Haycraft, C. J., Swoboda, P., Taulman, P. D., Thomas, J. H., and Yoder, B. K. (2001) The *C. elegans* homolog of the murine cystic kidney disease gene Tg737 functions in a ciliogenic pathway and is disrupted in osm-5 mutant worms. *Development* **128**, 1493–1505
18. Taulman, P. D., Haycraft, C. J., Balkovetz, D. F., and Yoder, B. K. (2001) Polaris, a protein involved in left-right axis patterning, localizes to basal bodies and cilia. *Mol. Biol. Cell* **12**, 589–599
19. Bangs, F., and Anderson, K. V. (2017) Primary cilia and mammalian hedgehog signaling. *Cold Spring Harb. Perspect. Biol.* **9**, a028175
20. Praetorius, H. A., and Spring, K. R. (2003) The renal cell primary cilium functions as a flow sensor. *Curr. Opin. Nephrol. Hypertens.* **12**, 517–520
21. Schneider, L., Clement, C. A., Teilmann, S. C., Pazour, G. J., Hoffmann, E. K., Satir, P., and Christensen, S. T. (2005) PDGFRalphaalpha signaling is regulated through the primary cilium in fibroblasts. *Curr. Biol.* **15**, 1861–1866
22. Clement, C. A., Ajbro, K. D., Koefoed, K., Vestergaard, M. L., Veland, I. R., Henriques de Jesus, M. P., Pedersen, L. B., Benmerah, A., Andersen, C. Y., Larsen, L. A., and Christensen, S. T. (2013) TGF-β signaling is associated with endocytosis at the pocket region of the primary cilium. *Cell Rep.* **3**, 1806–1814
23. Zhu, D., Shi, S., Wang, H., and Liao, K. (2009) Growth arrest induces primary-cilium formation and sensitizes IGF-1-receptor signaling during differentiation induction of 3T3-L1 preadipocytes. *J. Cell Sci.* **122**, 2760–2768
24. Molla-Herman, A., Ghossoub, R., Blisnick, T., Meunier, A., Serres, C., Silbermann, F., Emmerson, C., Romeo, K., Bourdoncle, P., Schmitt, A., Saunier, S., Spassky, N., Bastin, P., and Benmerah, A. (2010) The ciliary pocket: an endocytic membrane domain at the base of primary and motile cilia. *J. Cell Sci.* **123**, 1785–1795
25. Rich, D. R., and Clark, A. L. (2012) Chondrocyte primary cilia shorten in response to osmotic challenge and are sites for endocytosis. *Osteoarthritis Cartilage* **20**, 923–930
26. Rattner, J. B., Sciore, P., Ou, Y., van der Hoorn, F. A., and Lo, I. K. (2010) Primary cilia in fibroblast-like type B synoviocytes lie within a cilium pit: a site of endocytosis. *Histol. Histopathol.* **25**, 865–875
27. Schou, K. B., Mogensen, J. B., Morthorst, S. K., Nielsen, B. S., Aleliunaite, A., Serra-Marques, A., Fürstenberg, N., Saunier, S., Bizet, A. A., Veland, I. R., Akhmanova, A., Christensen, S. T., and Pedersen, L. B. (2017) KIF13B establishes a CAV1-enriched microdomain at the ciliary transition zone to promote Sonic hedgehog signalling. *Nat. Commun.* **8**, 14177
28. Absalon, S., Blisnick, T., Bonhivers, M., Kohl, L., Cayet, N., Toutirais, G., Buisson, J., Robinson, D., and Bastin, P. (2008) Flagellum elongation is required for correct structure, orientation and function of the flagellar pocket in *Trypanosoma brucei*. *J. Cell Sci.* **121**, 3704–3716
29. Huber, C., and Cormier-Daire, V. (2012) Ciliary disorder of the skeleton. *Am. J. Med. Genet. C. Semin. Med. Genet.* **160C**, 165–174
30. Koyama, E., Young, B., Nagayama, M., Shibukawa, Y., Enomoto-Iwamoto, M., Iwamoto, M., Maeda, Y., Lanske, B., Song, B., Serra, R., and Pacifici, M. (2007) Conditional Kif3a ablation causes abnormal hedgehog signaling topography, growth plate dysfunction, and excessive bone and cartilage formation during mouse skeletogenesis. *Development* **134**, 2159–2169
31. Kaushik, A. P., Martin, J. A., Zhang, Q., Sheffield, V. C., and Morcuende, J. A. (2009) Cartilage abnormalities associated with defects of chondrocytic primary cilia in Bardet-Biedl syndrome mutant mice. *J. Orthop. Res.* **27**, 1093–1099
32. Chang, C. F., Ramaswamy, G., and Serra, R. (2012) Depletion of primary cilia in articular chondrocytes results in reduced Gli3 repressor to activator ratio, increased Hedgehog signaling, and symptoms of early osteoarthritis. *Osteoarthritis Cartilage* **20**, 152–161
33. McGlashan, S. R., Haycraft, C. J., Jensen, C. G., Yoder, B. K., and Poole, C. A. (2007) Articular cartilage and growth plate defects are associated with chondrocyte cytoskeletal abnormalities in Tg737orpk mice lacking the primary cilia protein polaris. *Matrix Biol.* **26**, 234–246
34. Yuan, X., and Yang, S. (2015) Deletion of IFT80 impairs epiphyseal and articular cartilage formation due to disruption of chondrocyte differentiation. *PLoS One* **10**, e0130618
35. Lin, A. C., Seeto, B. L., Bartoszko, J. M., Khoury, M. A., Whetstone, H., Ho, L., Hsu, C., Ali, S. A., and Alman, B. A. (2009) Modulating hedgehog signaling can attenuate the severity of osteoarthritis. *Nat. Med.* **15**, 1421–1425

www.fasebj.org by Oxford Univ Lib Serv - Bodleian Lib (129.67.90.252) on October 30, 2019. The FASEB Journal Vol. ${article.issue.getVolume()}, No. ${article.issue.getIssueNumbe

36. Thompson, C. L., Patel, R., Kelly, T. A., Wann, A. K., Hung, C. T., Chapple, J. P., and Knight, M. M. (2015) Hedgehog signalling does not stimulate cartilage catabolism and is inhibited by interleukin-1β. *Arthritis Res. Ther.* **17**, 373
37. Wann, A. K., Zuo, N., Haycraft, C. J., Jensen, C. G., Poole, C. A., McGlashan, S. R., and Knight, M. M. (2012) Primary cilia mediate mechanotransduction through control of ATP-induced Ca^{2+} signaling in compressed chondrocytes. *FASEB J.* **26**, 1663–1671
38. Wann, A. K., Chapple, J. P., and Knight, M. M. (2014) The primary cilium influences interleukin-1β-induced NFκB signalling by regulating IKK activity. *Cell. Signal.* **26**, 1735–1742
39. Wann, A. K., and Knight, M. M. (2012) Primary cilia elongation in response to interleukin-1 mediates the inflammatory response. *Cell. Mol. Life Sci.* **69**, 2967–2977
40. Phan, M. N., Leddy, H. A., Votta, B. J., Kumar, S., Levy, D. S., Lipshutz, D. B., Lee, S. H., Liedtke, W., and Guilak, F. (2009) Functional characterization of TRPV4 as an osmotically sensitive ion channel in porcine articular chondrocytes. *Arthritis Rheum.* **60**, 3028–3037
41. Itoh, Y., Takamura, A., Ito, N., Maru, Y., Sato, H., Suenaga, N., Aoki, T., and Seiki, M. (2001) Homophilic complex formation of MT1-MMP facilitates proMMP-2 activation on the cell surface and promotes tumor cell invasion. *EMBO J.* **20**, 4782–4793
42. Gendron, C., Kashiwagi, M., Lim, N. H., Enghild, J. J., Thøgersen, I. B., Hughes, C., Caterson, B., and Nagase, H. (2007) Proteolytic activities of human ADAMTS-5: comparative studies with ADAMTS-4. *J. Biol. Chem.* **282**, 18294–18306
43. Yamamoto, K., Okano, H., Miyagawa, W., Visse, R., Shitomi, Y., Santamaria, S., Dudhia, J., Troeberg, L., Strickland, D. K., Hirohata, S., and Nagase, H. (2016) MMP-13 is constitutively produced in human chondrocytes and co-endocytosed with ADAMTS-5 and TIMP-3 by the endocytic receptor LRP1. *Matrix Biol.* **56**, 57–73
44. Hashimoto, K., Fukuda, K., Yamazaki, K., Yamamoto, N., Matsushita, T., Hayakawa, S., Munakata, H., and Hamanishi, C. (2006) Hypoxia-induced hyaluronan synthesis by articular chondrocytes: the role of nitric oxide. *Inflamm. Res.* **55**, 72–77
45. Beck Gooz, M., Maldonado, E. N., Dang, Y., Amria, M. Y., Higashiyama, S., Abboud, H. E., Lemasters, J. J., and Bell, P. D. (2014) ADAM17 promotes proliferation of collecting duct kidney epithelial cells through ERK activation and increased glycolysis in polycystic kidney disease. *Am. J. Physiol. Renal Physiol.* **307**, F551–F559
46. Haycraft, C. J., Zhang, Q., Song, B., Jackson, W. S., Detloff, P. J., Serra, R., and Yoder, B. K. (2007) Intraflagellar transport is essential for endochondral bone formation. *Development* **134**, 307–316
47. Thompson, C. L., Plant, J. C., Wann, A. K., Bishop, C. L., Novak, P., Mitchison, H. M., Beales, P. L., Chapple, J. P., and Knight, M. M. (2017) Chondrocyte expansion is associated with loss of primary cilia and disrupted hedgehog signalling. *Eur. Cell. Mater.* **34**, 128–141
48. Wann, A. K., Thompson, C. L., Chapple, J. P., and Knight, M. M. (2013) Interleukin-1β sequesters hypoxia inducible factor 2α to the primary cilium. *Cilia* **2**, 17
49. Thompson, C. L., Chapple, J. P., and Knight, M. M. (2014) Primary cilia disassembly down regulates mechanosensitive hedgehog signalling: a feedback mechanism controlling ADAMTS-5 expression in chondrocytes. *Osteoarthritis Cartilage* **22**, 490–498
50. Boehlke, C., Janusch, H., Hamann, C., Powelske, C., Mergen, M., Herbst, H., Kotsis, F., Nitschke, R., and Kuehn, E. W. (2015) A cilia independent role of Ift88/polaris during cell migration. *PLoS One* **10**, e0140378
51. Delaval, B., Bright, A., Lawson, N. D., and Doxsey, S. (2011) The cilia protein IFT88 is required for spindle orientation in mitosis. *Nat. Cell Biol.* **13**, 461–468
52. Borovina, A., and Ciruna, B. (2013) IFT88 plays a cilia- and PCP-independent role in controlling oriented cell divisions during vertebrate embryonic development. *Cell Reports* **5**, 37–43
53. Ali, S. A., Al-Jazrawe, M., Ma, H., Whetstone, H., Poon, R., Farr, S., Naples, M., Adeli, K., and Alman, B. A. (2016) Regulation of cholesterol homeostasis by hedgehog signaling in osteoarthritic cartilage. *Arthritis Rheumatol.* **68**, 127–137
54. Rohatgi, R., Milenkovic, L., and Scott, M. P. (2007) Patched1 regulates hedgehog signaling at the primary cilium. *Science* **317**, 372–376
55. Haycraft, C. J., Banizs, B., Aydin-Son, Y., Zhang, Q., Michaud, E. J., and Yoder, B. K. (2005) Gli2 and Gli3 localize to cilia and require the intraflagellar transport protein polaris for processing and function. *PLoS Genet.* **1**, e53
56. Kanai, Y., Wang, D., and Hirokawa, N. (2014) KIF13B enhances the endocytosis of LRP1 by recruiting LRP1 to caveolae. *J. Cell Biol.* **204**, 395–408
57. Finetti, F., Paccani, S. R., Rosenbaum, J., and Baldari, C. T. (2011) Intraflagellar transport: a new player at the immune synapse. *Trends Immunol.* **32**, 139–145
58. Griffiths, G. M., Tsun, A., and Stinchcombe, J. C. (2010) The immunological synapse: a focal point for endocytosis and exocytosis. *J. Cell Biol.* **189**, 399–406
59. Stinchcombe, J. C., and Griffiths, G. M. (2014) Communication, the centrosome and the immunological synapse. *Philos. Trans. R. Soc. Lond. B Biol. Sci.* **369**, 20130463
60. Galgano, D., Onnis, A., Pappalardo, E., Galvagni, F., Acuto, O., and Baldari, C. T. (2017) The T cell IFT20 interactome reveals new players in immune synapse assembly. *J. Cell Sci.* **130**, 1110–1121
61. Lillis, A. P., Van Duyn, L. B., Murphy-Ullrich, J. E., and Strickland, D. K. (2008) LDL receptor-related protein 1: unique tissue-specific functions revealed by selective gene knockout studies. *Physiol. Rev.* **88**, 887–918

Received for publication March 5, 2018.
Accepted for publication June 4, 2018.

www.fasebj.org by Oxford Univ Lib Serv - Bodleian Lib (129.67.90.252) on October 30, 2019. The FASEB Journal Vol. ${article.issue.getVolume()}, No. ${article.issue.getIssueNumbe

Bibliography

Absalon, S., Blisnick, T., Bonhivers, M., et al. (2008). "Flagellum elongation is required for correct structure, orientation and function of the flagellar pocket in Trypanosoma brucei". *J Cell Sci* 121: pp. 3704–16.

Akiyama, H., Chaboissier, M. C., Martin, J. F., et al. (2002). "The transcription factor Sox9 has essential roles in successive steps of the chondrocyte differentiation pathway and is required for expression of Sox5 and Sox6". *Genes Dev* 16: pp. 2813–28.

Akiyama, H., Kim, J. E., Nakashima, K., et al. (2005). "Osteo-chondroprogenitor cells are derived from Sox9 expressing precursors". *Proc Natl Acad Sci U S A* 102: pp. 14665–70.

Alenghat, F. J., Tytell, J. D., Thodeti, C. K., et al. (2009). "Mechanical control of cAMP signaling through integrins is mediated by the heterotrimeric Galphas protein". *J Cell Biochem* 106: pp. 529–38.

Ali, S. A., Al-Jazrawe, M., Ma, H., et al. (2016). "Regulation of Cholesterol Homeostasis by Hedgehog Signaling in Osteoarthritic Cartilage". *Arthritis Rheumatol* 68: pp. 127–37.

Amano, K., Densmore, M. J., and Lanske, B. (2015). "Conditional Deletion of Indian Hedgehog in Limb Mesenchyme Results in Complete Loss of Growth Plate Formation but Allows Mature Osteoblast Differentiation". *J Bone Miner Res* 30: pp. 2262–72.

Amano, K., Densmore, M., Fan, Y., et al. (2016). "Ihh and PTH1R signaling in limb mesenchyme is required for proper segmentation and subsequent formation and growth of digit bones". *Bone* 83: pp. 256–66.

Anderson, J. and Breidahl, P. (1981). "Cartilage atrophy following spinal cord damage". *Australas Radiol* 25: pp. 98–103.

Angus, K. L. and Griffiths, G. M. (2013). "Cell polarisation and the immunological synapse". *Curr Opin Cell Biol* 25: pp. 85–91.

Aragona, M., Panciera, T., Manfrin, A., et al. (2013). "A mechanical checkpoint controls multicellular growth through YAP/TAZ regulation by actin-processing factors". *Cell* 154: pp. 1047–1059.

Beaucage, K. L., Pollmann, S. I., Sims, S. M., et al. (2016). "Quantitative in vivo micro-computed tomography for assessment of age-dependent changes in murine whole-body composition". *Bone Rep* 5: pp. 70–80.

Berendsen, A. D. and Olsen, B. R. (2015). "Bone development". *Bone* 80: pp. 14–8.

Bi, W., Deng, J. M., Zhang, Z., et al. (1999). "Sox9 is required for cartilage formation". *Nat Genet* 22: pp. 85–9.

Bielefeld, K. A., Amini-Nik, S., and Alman, B. A. (2013). "Cutaneous wound healing: recruiting developmental pathways for regeneration". *Cell Mol Life Sci* 70: pp. 2059–81.

Birkedal-Hansen, H. (1993). "Role of matrix metalloproteinases in human periodontal diseases". *J Periodontol* 64: pp. 474–84.

Blease, A., Das Neves Borges, P., Curtinha, M., et al. (2018). "Studying Osteoarthritis Pathogenesis in Mice". *Curr Protoc Mouse Biol* 8: e50.

Bloecker, K., Wirth, W., Hudelmaier, M., et al. (2012). "Morphometric differences between the medial and lateral meniscus in healthy men - a three-dimensional

analysis using magnetic resonance imaging". *Cells Tissues Organs* 195: pp. 353–64.

Borovina, A. and Ciruna, B. (2013). "IFT88 plays a cilia- and PCP-independent role in controlling oriented cell divisions during vertebrate embryonic development". *Cell Rep* 5: pp. 37–43.

Brandt, K. D., Dieppe, P., and Radin, E. (2009). "Etiopathogenesis of osteoarthritis". *Med Clin North Am* 93: pp. 1–24, xv.

Brinkmann, H. and Philippe, H. (2007). "The diversity of eukaryotes and the root of the eukaryotic tree". *Adv Exp Med Biol* 607: pp. 20–37.

Brown, T. D., Johnston, R. C., Saltzman, C. L., et al. (2006). "Posttraumatic osteoarthritis: a first estimate of incidence, prevalence, and burden of disease". *J Orthop Trauma* 20: pp. 739–44.

Bruns, J., Volkmer, M., and Luessenhop, S. (1994). "Pressure distribution in the knee joint". *Archives of Orthopaedic and Trauma Surgery* 113: pp. 204–209.

Burleigh, A., Chanalaris, A., Gardiner, M. D., et al. (2012). "Joint immobilization prevents murine osteoarthritis and reveals the highly mechanosensitive nature of protease expression in vivo". *Arthritis Rheum* 64: pp. 2278–88.

Capecchi, M. R. (2005). "Gene targeting in mice: functional analysis of the mammalian genome for the twenty-first century". *Nat Rev Genet* 6: pp. 507–12.

Chambers, M. G., Cox, L., Chong, L., et al. (2001). "Matrix metalloproteinases and aggrecanases cleave aggrecan in different zones of normal cartilage but colocalize in the development of osteoarthritic lesions in STR/ort mice". *Arthritis Rheum* 44: pp. 1455–65.

Chang, C. F., Ramaswamy, G., and Serra, R. (2012). "Depletion of primary cilia in articular chondrocytes results in reduced Gli3 repressor to activator ratio, increased Hedgehog signaling, and symptoms of early osteoarthritis". *Osteoarthritis Cartilage* 20: pp. 152–61.

Chekuri, A., Guru, A. A., Biswas, P., et al. (2018). "IFT88 mutations identified in individuals with non-syndromic recessive retinal degeneration result in abnormal ciliogenesis". *Hum Genet* 137: pp. 447–458.

Chen, C. G., Thuillier, D., Chin, E. N., et al. (2012). "Chondrocyte-intrinsic Smad3 represses Runx2-inducible matrix metalloproteinase 13 expression to maintain articular cartilage and prevent osteoarthritis". *Arthritis Rheum* 64: pp. 3278–89.

Chen, M., Lichtler, A. C., Sheu, T. J., et al. (2007). "Generation of a transgenic mouse model with chondrocyte-specific and tamoxifen-inducible expression of Cre recombinase". *Genesis* 45: pp. 44–50.

Choi, J. B., Youn, I., Cao, L., et al. (2007). "Zonal changes in the three-dimensional morphology of the chondron under compression: the relationship among cellular, pericellular, and extracellular deformation in articular cartilage". *J Biomech* 40: pp. 2596–603.

Christensen, S. T., Clement, C. A., Satir, P., et al. (2012). "Primary cilia and coordination of receptor tyrosine kinase (RTK) signalling". *J Pathol* 226: pp. 172–84.

Claes, L. E. and Heigele, C. A. (1999). "Magnitudes of local stress and strain along bony surfaces predict the course and type of fracture healing". *J Biomech* 32: pp. 255–66.

Clapham, D. E. (2003). "TRP channels as cellular sensors". *Nature* 426: pp. 517–24.

Clement, C. A., Kristensen, S. G., Mollgard, K., et al. (2009a). "The primary cilium coordinates early cardiogenesis and hedgehog signaling in cardiomyocyte differentiation". *J Cell Sci* 122: pp. 3070–82.

Clement, C. A., Larsen, L. A., and Christensen, S. T. (2009b). "Using nucleofection of siRNA constructs for knockdown of primary cilia in P19.CL6 cancer stem cell differentiation into cardiomyocytes". *Methods Cell Biol* 94: pp. 181–97.

Clement, C. A., Ajbro, K. D., Koefoed, K., et al. (2013a). "TGF-beta signaling is associated with endocytosis at the pocket region of the primary cilium". *Cell Rep* 3: pp. 1806–14.

Clement, C. A., Ajbro, K. D., Koefoed, K., et al. (2013b). "TGF-beta signaling is associated with endocytosis at the pocket region of the primary cilium". *Cell Rep* 3: pp. 1806–14.

Corbit, K. C., Aanstad, P., Singla, V., et al. (2005). "Vertebrate Smoothened functions at the primary cilium". *Nature* 437: pp. 1018–21.

Corbit, K. C., Shyer, A. E., Dowdle, W. E., et al. (2008). "Kif3a constrains beta-catenin-dependent Wnt signalling through dual ciliary and non-ciliary mechanisms". *Nat Cell Biol* 10: pp. 70–6.

Cordova-Fletes, C., Becerra-Solano, L. E., Rangel-Sosa, M. M., et al. (2018). "Uncommon runs of homozygosity disclose homozygous missense mutations in two ciliopathy-related genes (SPAG17 and WDR35) in a patient with multiple brain and skeletal anomalies". *Eur J Med Genet* 61: pp. 161–167.

Corrigan, M. A., Johnson, G. P., Stavenschi, E., et al. (2018). "TRPV4-mediates oscillatory fluid shear mechanotransduction in mesenchymal stem cells in part via the primary cilium". *Sci Rep* 8: p. 3824.

Coveney, C. R., Collins, I., Mc Fie, M., et al. (2018). "Cilia protein IFT88 regulates extracellular protease activity by optimizing LRP-1-mediated endocytosis". *Faseb j*: fj201800334.

Crombrugghe, B. de, Lefebvre, V., and Nakashima, K. (2001). "Regulatory mechanisms in the pathways of cartilage and bone formation". *Curr Opin Cell Biol* 13: pp. 721–7.

DeFrate, L. E., Kim-Wang, S. Y., Englander, Z. A., et al. (2019). "Osteoarthritis year in review 2018: mechanics". *Osteoarthritis Cartilage* 27: pp. 392–400.

Delaval, B., Bright, A., Lawson, N. D., et al. (2011). "The cilia protein IFT88 is required for spindle orientation in mitosis". *Nat Cell Biol* 13: pp. 461–468.

Delling, M., DeCaen, P. G., Doerner, J. F., et al. (2013a). "Primary cilia are specialized calcium signalling organelles". *Nature* 504: pp. 311–4.

Delling, M., DeCaen, P. G., Doerner, J. F., et al. (2013b). "Primary cilia are specialized calcium signalling organelles". *Nature* 504: pp. 311–4.

Delling, M., Indzhykulian, A. A., Liu, X., et al. (2016b). "Primary cilia are not calcium-responsive mechanosensors". *Nature*.

Delling, M., Indzhykulian, A. A., Liu, X., et al. (2016a). "Primary cilia are not calcium-responsive mechanosensors". *Nature* 531: pp. 656–60.

Deng, Y., Wu, A., Li, P., et al. (2016). "Yap1 Regulates Multiple Steps of Chondrocyte Differentiation during Skeletal Development and Bone Repair". *Cell Rep* 14: pp. 2224–2237.

Deng, Y., Lu, J., Li, W., et al. (2018). "Reciprocal inhibition of YAP/TAZ and NF-kappaB regulates osteoarthritic cartilage degradation". *Nat Commun* 9: p. 4564.

Desai, B. N. and Clapham, D. E. (2005). "TRP channels and mice deficient in TRP channels". *Pflugers Arch* 451: pp. 11–8.

Dinsmore, C. and Reiter, J. F. (2016). "Endothelial primary cilia inhibit atherosclerosis". *EMBO Rep*.

Donnelly, E., Ascenzi, M. G., and Farnum, C. (2010). "Primary cilia are highly oriented with respect to collagen direction and long axis of extensor tendon". *J Orthop Res* 28: pp. 77–82.

Duke, J., Janer, L., Campbell, M., et al. (1985). "Microprobe analyses of epiphyseal plates from Spacelab 3 rats". *Physiologist* 28: S217–8.

Duke, P. J., Durnova, G., and Montufar-Solis, D. (1990). "Histomorphometric and electron microscopic analyses of tibial epiphyseal plates from Cosmos 1887 rats". *Faseb j* 4: pp. 41–6.

Dupont, S., Morsut, L., Aragona, M., et al. (2011). "Role of YAP/TAZ in mechanotransduction". *Nature* 474: pp. 179–83.

Fang, H. and Beier, F. (2014). "Mouse models of osteoarthritis: modelling risk factors and assessing outcomes". *Nat Rev Rheumatol* 10: pp. 413–21.

Follit, J. A., Tuft, R. A., Fogarty, K. E., et al. (2006). "The intraflagellar transport protein IFT20 is associated with the Golgi complex and is required for cilia assembly". *Mol Biol Cell* 17: pp. 3781–92.

Fosang, A. J., Neame, P. J., Last, K., et al. (1992). "The interglobular domain of cartilage aggrecan is cleaved by PUMP, gelatinases, and cathepsin B". *J Biol Chem* 267: pp. 19470–4.

Fosang, A. J., Rogerson, F. M., East, C. J., et al. (2008). "ADAMTS-5: the story so far". *Eur Cell Mater* 15: pp. 11–26.

Galea, G. L., Lanyon, L. E., and Price, J. S. (2017). "Sclerostin's role in bone's adaptive response to mechanical loading". *Bone* 96: pp. 38–44.

Galgano, D., Onnis, A., Pappalardo, E., et al. (2017). "The T cell IFT20 interactome reveals new players in immune synapse assembly". *J Cell Sci* 130: pp. 1110–1121.

Gallagher, A. R., Esquivel, E. L., Briere, T. S., et al. (2008). "Biliary and pancreatic dysgenesis in mice harboring a mutation in Pkhd1". *Am J Pathol* 172: pp. 417–29.

Gerdes, J. M., Liu, Y., Zaghloul, N. A., et al. (2007). "Disruption of the basal body compromises proteasomal function and perturbs intracellular Wnt response". *Nat Genet* 39: pp. 1350–60.

Glasson, S. S., Askew, R., Sheppard, B., et al. (2004). "Characterization of and osteoarthritis susceptibility in ADAMTS-4-knockout mice". *Arthritis Rheum* 50: pp. 2547–58.

Glasson, S. S., Askew, R., Sheppard, B., et al. (2005a). "Deletion of active ADAMTS5 prevents cartilage degradation in a murine model of osteoarthritis". *Nature* 434: pp. 644–8.

Glasson, S. S., Askew, R., Sheppard, B., et al. (2005b). "Deletion of active ADAMTS5 prevents cartilage degradation in a murine model of osteoarthritis". *Nature* 434: pp. 644–8.

Glasson, S. S., Blanchet, T. J., and Morris, E. A. (2007). "The surgical destabilization of the medial meniscus (DMM) model of osteoarthritis in the 129/SvEv mouse". *Osteoarthritis Cartilage* 15: pp. 1061–9.

Glasson, S. S., Chambers, M. G., Van Den Berg, W. B., et al. (2010). "The OARSI histopathology initiative - recommendations for histological assessments of osteoarthritis in the mouse". *Osteoarthritis Cartilage* 18 Suppl 3: S17–23.

Glyn-Jones, S., Palmer, A. J., Agricola, R., et al. (2015). "Osteoarthritis". *Lancet*.

Goetz, S. C. and Anderson, K. V. (2010). "The primary cilium: a signalling centre during vertebrate development". *Nat Rev Genet* 11: pp. 331–44.

Griffiths, G. M., Tsun, A., and Stinchcombe, J. C. (2010). "The immunological synapse: a focal point for endocytosis and exocytosis". *J Cell Biol* 189: pp. 399–406.

Grodzinsky, A. J., Levenston, M. E., Jin, M., et al. (2000). "Cartilage tissue remodeling in response to mechanical forces". *Annu Rev Biomed Eng* 2: pp. 691–713.

Guilak, F. (2011). "Biomechanical factors in osteoarthritis". *Best Pract Res Clin Rheumatol* 25: pp. 815–23.

Handley, C. J., Mok, M. T., Ilic, M. Z., et al. (2001). "Cathepsin D cleaves aggrecan at unique sites within the interglobular domain and chondroitin sulfate attachment regions that are also cleaved when cartilage is maintained at acid pH". *Matrix Biol* 20: pp. 543–53.

Hartmann, M., Herrlich, A., and Herrlich, P. (2013). "Who decides when to cleave an ectodomain?" *Trends Biochem Sci* 38: pp. 111–20.

Haycraft, C. J. and Serra, R. (2008). "Cilia involvement in patterning and maintenance of the skeleton". *Curr Top Dev Biol* 85: pp. 303–32.

Haycraft, C. J., Banizs, B., Aydin-Son, Y., et al. (2005). "Gli2 and Gli3 localize to cilia and require the intraflagellar transport protein polaris for processing and function". *PLoS Genet* 1: e53.

Haycraft, C. J., Zhang, Q., Song, B., et al. (2007a). "Intraflagellar transport is essential for endochondral bone formation". *Development* 134: pp. 307–16.

Haycraft, C. J., Zhang, Q., Song, B., et al. (2007b). "Intraflagellar transport is essential for endochondral bone formation". *Development* 134: pp. 307–16.

Heinemeier, K. M., Schjerling, P., Heinemeier, J., et al. (2016). "Radiocarbon dating reveals minimal collagen turnover in both healthy and osteoarthritic human cartilage". *Sci Transl Med* 8: 346ra90.

Henry, S. P., Jang, C. W., Deng, J. M., et al. (2009). "Generation of aggrecan-CreERT2 knockin mice for inducible Cre activity in adult cartilage". *Genesis* 47: pp. 805–14.

Hilton, M. J., Tu, X., Cook, J., et al. (2005). "Ihh controls cartilage development by antagonizing Gli3, but requires additional effectors to regulate osteoblast and vascular development". *Development* 132: pp. 4339–51.

Holder, N. (1977). "An experimental investigation into the early development of the chick elbow joint". *J Embryol Exp Morphol* 39: pp. 115–27.

Hou, X., Mrug, M., Yoder, B. K., et al. (2002). "Cystin, a novel cilia-associated protein, is disrupted in the cpk mouse model of polycystic kidney disease". *J Clin Invest* 109: pp. 533–40.

Hua, K. and Ferland, R. J. (2018). "Primary cilia proteins: ciliary and extraciliary sites and functions". *Cell Mol Life Sci* 75: pp. 1521–1540.

Huangfu, D. and Anderson, K. V. (2005). "Cilia and Hedgehog responsiveness in the mouse". *Proc Natl Acad Sci U S A* 102: pp. 11325–30.

Huangfu, D., Liu, A., Rakeman, A. S., et al. (2003). "Hedgehog signalling in the mouse requires intraflagellar transport proteins". *Nature* 426: pp. 83–7.

Huppa, J. B. and Davis, M. M. (2003). "T-cell-antigen recognition and the immunological synapse". *Nat Rev Immunol* 3: pp. 973–83.

Ismail, H. M., Yamamoto, K., Vincent, T. L., et al. (2015a). "Interleukin-1 Acts via the JNK-2 Signaling Pathway to Induce Aggrecan Degradation by Human Chondrocytes". *Arthritis Rheumatol* 67: pp. 1826–36.

Ismail, H. M., Miotla-Zarebska, J., Troeberg, L., et al. (2015b). "JNK2 controls aggrecan degradation in murine articular cartilage and the development of experimental osteoarthritis". *Arthritis Rheumatol*.

Javaheri, B., Caetano-Silva, S. P., Kanakis, I., et al. (2018). "The Chondro-Osseous Continuum: Is It Possible to Unlock the Potential Assigned Within?" *Front Bioeng Biotechnol* 6: p. 28.

Jensen, C. G., Poole, C. A., McGlashan, S. R., et al. (2004). "Ultrastructural, tomographic and confocal imaging of the chondrocyte primary cilium in situ". *Cell Biol Int* 28: pp. 101–10.

Jin, Y., Cong, Q., Gvozdenovic-Jeremic, J., et al. (2018). "Enpp1 inhibits ectopic joint calcification and maintains articular chondrocytes by repressing hedgehog signaling". *Development* 145.

Joukov, V. and De Nicolo, A. (2019). "The Centrosome and the Primary Cilium: The Yin and Yang of a Hybrid Organelle". *Cells* 8.

Jurvelin, J., Kiviranta, I., Tammi, M., et al. (1986). "Effect of physical exercise on indentation stiffness of articular cartilage in the canine knee". *Int J Sports Med* 7: pp. 106–10.

Kamkin, A. and Kiseleva, I. (2005). "Mechanosensitivity of Cells from Various Tissues". *Mechanosensitivity in Cells and Tissues*. Ed. by A. Kamkin and I. Kiseleva. Moscow: Academia Academia Publishing House Ltd.

Karelina, T. V., Goldberg, G. I., and Eisen, A. Z. (1995). "Matrix metalloproteinases in blood vessel development in human fetal skin and in cutaneous tumors". *J Invest Dermatol* 105: pp. 411–7.

Kaushik, A. P., Martin, J. A., Zhang, Q., et al. (2009). "Cartilage abnormalities associated with defects of chondrocytic primary cilia in Bardet-Biedl syndrome mutant mice". *J Orthop Res* 27: pp. 1093–9.

Kim, E. J., Cho, S. W., Shin, J. O., et al. (2013). "Ihh and Runx2/Runx3 signaling interact to coordinate early chondrogenesis: a mouse model". *PLoS One* 8: e55296.

Kitami, M., Yamaguchi, H., Ebina, M., et al. (2019). "IFT20 is required for the maintenance of cartilaginous matrix in condylar cartilage". *Biochem Biophys Res Commun* 509: pp. 222–226.

Kiviranta, I., Jurvelin, J., Tammi, M., et al. (1987). "Weight bearing controls glycosaminoglycan concentration and articular cartilage thickness in the knee joints of young beagle dogs". *Arthritis Rheum* 30: pp. 801–9.

Kiviranta, I., Tammi, M., Jurvelin, J., et al. (1988). "Moderate running exercise augments glycosaminoglycans and thickness of articular cartilage in the knee joint of young beagle dogs". *J Orthop Res* 6: pp. 188–95.

Klein-Nulend, J., Veldhuijzen, J. P., and Burger, E. H. (1986). "Increased calcification of growth plate cartilage as a result of compressive force in vitro". *Arthritis Rheum* 29: pp. 1002–9.

Ko, J. Y. and Park, J. H. (2013). "Mouse models of polycystic kidney disease induced by defects of ciliary proteins". *BMB Rep* 46: pp. 73–9.

Kobayashi, H., Hirata, M., Saito, T., et al. (2013). "Transcriptional induction of ADAMTS5 protein by nuclear factor-kappaB (NF-kappaB) family member RelA/p65 in chondrocytes during osteoarthritis development". *J Biol Chem* 288: pp. 28620–9.

Kopinke, D., Roberson, E. C., and Reiter, J. F. (2017). "Ciliary Hedgehog Signaling Restricts Injury-Induced Adipogenesis". *Cell* 170: 340–351.e12.

Kottgen, M., Buchholz, B., Garcia-Gonzalez, M. A., et al. (2008). "TRPP2 and TRPV4 form a polymodal sensory channel complex". *J Cell Biol* 182: pp. 437–47.

Koyama, E., Young, B., Nagayama, M., et al. (2007). "Conditional Kif3a ablation causes abnormal hedgehog signaling topography, growth plate dysfunction, and excessive bone and cartilage formation during mouse skeletogenesis". *Development* 134: pp. 2159–69.

Kronenberg, H. M. (2003). "Developmental regulation of the growth plate". *Nature* 423: pp. 332–6.

Kusumbe, A. P., Ramasamy, S. K., and Adams, R. H. (2014). "Coupling of angiogenesis and osteogenesis by a specific vessel subtype in bone". *Nature* 507: pp. 323–328.

Ladenhauf, H. N., Seitlinger, G., and Green, D. W. (2019). "Osgood-Schlatter disease: a 2020 update of a common knee condition in children". *Curr Opin Pediatr*.

Lanske, B., Amling, M., Neff, L., et al. (1999a). "Ablation of the PTHrP gene or the PTH/PTHrP receptor gene leads to distinct abnormalities in bone development". *J Clin Invest* 104: pp. 399–407.

Lanske, B., Amling, M., Neff, L., et al. (1999b). "Ablation of the PTHrP gene or the PTH/PTHrP receptor gene leads to distinct abnormalities in bone development". *J Clin Invest* 104: pp. 399–407.

Lee, S. H. and Somlo, S. (2014). "Cyst growth, polycystins, and primary cilia in autosomal dominant polycystic kidney disease". *Kidney Res Clin Pract* 33: pp. 73–8.

Lehman, J. M., Michaud, E. J., Schoeb, T. R., et al. (2008). "The Oak Ridge Polycystic Kidney mouse: modeling ciliopathies of mice and men". *Dev Dyn* 237: pp. 1960–71.

Leroux, M. A., Cheung, H. S., Bau, J. L., et al. (2001). "Altered mechanics and histomorphometry of canine tibial cartilage following joint immobilization". *Osteoarthritis Cartilage* 9: pp. 633–40.

Leucht, P., Monica, S. D., Temiyasathit, S., et al. (2013). "Primary cilia act as mechanosensors during bone healing around an implant". *Med Eng Phys* 35: pp. 392–402.

Liao, L., Zhang, S., Zhou, G. Q., et al. (2019). "Deletion of Runx2 in condylar chondrocytes disrupts TMJ tissue homeostasis". *J Cell Physiol* 234: pp. 3436–3444.

Lin, A. C., Seeto, B. L., Bartoszko, J. M., et al. (2009). "Modulating hedgehog signaling can attenuate the severity of osteoarthritis". *Nat Med* 15: pp. 1421–5.

Little, C. B. and Hunter, D. J. (2013). "Post-traumatic osteoarthritis: from mouse models to clinical trials". *Nat Rev Rheumatol* 9: pp. 485–97.

Little, C. B., Meeker, C. T., Golub, S. B., et al. (2007). "Blocking aggrecanase cleavage in the aggrecan interglobular domain abrogates cartilage erosion and promotes cartilage repair". *J Clin Invest* 117: pp. 1627–36.

Little, C. B., Barai, A., Burkhardt, D., et al. (2009). "Matrix metalloproteinase 13-deficient mice are resistant to osteoarthritic cartilage erosion but not chondrocyte hypertrophy or osteophyte development". *Arthritis Rheum* 60: pp. 3723–33.

Liu, F., Kozanek, M., Hosseini, A., et al. (2010). "In vivo tibiofemoral cartilage deformation during the stance phase of gait". *J Biomech* 43: pp. 658–65.

Liu, H., Kiseleva, A. A., and Golemis, E. A. (2018). "Ciliary signalling in cancer". *Nat Rev Cancer* 18: pp. 511–524.

Liu, M., Alharbi, M., Graves, D., et al. (2019). "IFT80 is required for fracture healing through controlling the regulation of TGFbeta signaling in chondrocyte differentiation and function". *J Bone Miner Res*.

Lo Cascio, L., Liu, K., Nakamura, H., et al. (2014). "Generation of a mouse line harboring a Bi-transgene expressing luciferase and tamoxifen-activatable creER(T2) recombinase in cartilage". *Genesis* 52: pp. 110–9.

Loeser, R. F., Goldring, S. R., Scanzello, C. R., et al. (2012). "Osteoarthritis: a disease of the joint as an organ". *Arthritis Rheum* 64: pp. 1697–707.

Logan, M., Martin, J. F., Nagy, A., et al. (2002). "Expression of Cre Recombinase in the developing mouse limb bud driven by a Prxl enhancer". *Genesis* 33: pp. 77–80.

Mackie, E. J., Tatarczuch, L., and Mirams, M. (2011). "The skeleton: a multi-functional complex organ: the growth plate chondrocyte and endochondral ossification". *J Endocrinol* 211: pp. 109–21.

Maeda, Y., Nakamura, E., Nguyen, M. T., et al. (2007). "Indian Hedgehog produced by postnatal chondrocytes is essential for maintaining a growth plate and trabecular bone". *Proc Natl Acad Sci U S A* 104: pp. 6382–7.

Mak, K. K., Chen, M. H., Day, T. F., et al. (2006). "Wnt/beta-catenin signaling interacts differentially with Ihh signaling in controlling endochondral bone and synovial joint formation". *Development* 133: pp. 3695–707.

Mak, K. K., Kronenberg, H. M., Chuang, P. T., et al. (2008). "Indian hedgehog signals independently of PTHrP to promote chondrocyte hypertrophy". *Development* 135: pp. 1947–56.

Malone, A. M., Anderson, C. T., Tummala, P., et al. (2007). "Primary cilia mediate mechanosensing in bone cells by a calcium-independent mechanism". *Proc Natl Acad Sci U S A* 104: pp. 13325–30.

Mansfield, J. C., Mandalia, V., Toms, A., et al. (2019). "Collagen reorganization in cartilage under strain probed by polarization sensitive second harmonic generation microscopy". *J R Soc Interface* 16: p. 20180611.

Masuyama, R., Vriens, J., Voets, T., et al. (2008). "TRPV4-mediated calcium influx regulates terminal differentiation of osteoclasts". *Cell Metab* 8: pp. 257–65.

McCulloch, R. S., Mente, P. L., O'Nan, A. T., et al. (2018). "Articular cartilage gene expression patterns in the tissue surrounding the impact site following applications of shear and axial loads". *BMC Musculoskelet Disord* 19: p. 449.

McGlashan, S. R., Jensen, C. G., and Poole, C. A. (2006). "Localization of extracellular matrix receptors on the chondrocyte primary cilium". *J Histochem Cytochem* 54: pp. 1005–14.

McGlashan, S. R., Haycraft, C. J., Jensen, C. G., et al. (2007). "Articular cartilage and growth plate defects are associated with chondrocyte cytoskeletal abnormalities in Tg737orpk mice lacking the primary cilia protein polaris". *Matrix Biol* 26: pp. 234–46.

McGlashan, S. R., Knight, M. M., Chowdhury, T. T., et al. (2010). "Mechanical loading modulates chondrocyte primary cilia incidence and length". *Cell Biol Int* 34: pp. 441–6.

Melrose, J., Shu, C., Whitelock, J. M., et al. (2016). "The cartilage extracellular matrix as a transient developmental scaffold for growth plate maturation". *Matrix Biol* 52-54: pp. 363–83.

Meyer, C. J., Alenghat, F. J., Rim, P., et al. (2000). "Mechanical control of cyclic AMP signalling and gene transcription through integrins". *Nat Cell Biol* 2: pp. 666–8.

Misra, J. R. and Irvine, K. D. (2018). "The Hippo Signaling Network and Its Biological Functions". *Annu Rev Genet* 52: pp. 65–87.

Mitchell, P. G., Magna, H. A., Reeves, L. M., et al. (1996). "Cloning, expression, and type II collagenolytic activity of matrix metalloproteinase-13 from human osteoarthritic cartilage". *J Clin Invest* 97: pp. 761–8.

Mitsuyama, H., Healey, R. M., Terkeltaub, R. A., et al. (2007). "Calcification of human articular knee cartilage is primarily an effect of aging rather than osteoarthritis". *Osteoarthritis Cartilage* 15: pp. 559–65.

Mizuhashi, K., Ono, W., Matsushita, Y., et al. (2018). "Resting zone of the growth plate houses a unique class of skeletal stem cells". *Nature* 563: pp. 254–258.

Molla-Herman, A., Ghossoub, R., Blisnick, T., et al. (2010). "The ciliary pocket: an endocytic membrane domain at the base of primary and motile cilia". *J Cell Sci* 123: pp. 1785–95.

Moore, E. R. and Jacobs, C. R. (2018). "The primary cilium as a signaling nexus for growth plate function and subsequent skeletal development". *J Orthop Res* 36: pp. 533–545.

Moskowitz, R. W. (1972). "Experimental models of degenerative joint disease". *Semin Arthritis Rheum* 2: pp. 95–116.

Murray, P. D. and Drachman, D. B. (1969). "The role of movement in the development of joints and related structures: the head and neck in the chick embryo". *J Embryol Exp Morphol* 22: pp. 349–71.

Muthuri, S. G., McWilliams, D. F., Doherty, M., et al. (2011). "History of knee injuries and knee osteoarthritis: a meta-analysis of observational studies". *Osteoarthritis Cartilage* 19: pp. 1286–93.

Nagao, M., Cheong, C. W., and Olsen, B. R. (2016). "Col2-Cre and tamoxifen-inducible Col2-CreER target different cell populations in the knee joint". *Osteoarthritis Cartilage* 24: pp. 188–91.

Nagel, T. and Kelly, D. J. (2010). "Mechano-regulation of mesenchymal stem cell differentiation and collagen organisation during skeletal tissue repair". *Biomech Model Mechanobiol* 9: pp. 359–72.

Nakamura, E., Nguyen, M. T., and Mackem, S. (2006). "Kinetics of tamoxifen-regulated Cre activity in mice using a cartilage-specific CreER(T) to assay temporal activity windows along the proximodistal limb skeleton". *Dev Dyn* 235: pp. 2603–12.

Nakashima, K., Zhou, X., Kunkel, G., et al. (2002). "The novel zinc finger-containing transcription factor osterix is required for osteoblast differentiation and bone formation". *Cell* 108: pp. 17–29.

Nauli, S. M. and Zhou, J. (2004). "Polycystins and mechanosensation in renal and nodal cilia". *Bioessays* 26: pp. 844–56.

Nauli, S. M., Alenghat, F. J., Luo, Y., et al. (2003). "Polycystins 1 and 2 mediate mechanosensation in the primary cilium of kidney cells". *Nat Genet* 33: pp. 129–37.

Neuhold, L. A., Killar, L., Zhao, W., et al. (2001). "Postnatal expression in hyaline cartilage of constitutively active human collagenase-3 (MMP-13) induces osteoarthritis in mice". *J Clin Invest* 107: pp. 35–44.

Newton, P. T., Li, L., Zhou, B., et al. (2019). "A radical switch in clonality reveals a stem cell niche in the epiphyseal growth plate". *Nature*.

Ng, T. C., Chiu, K. W., Rabie, A. B., et al. (2006). "Repeated mechanical loading enhances the expression of Indian hedgehog in condylar cartilage". *Front Biosci* 11: pp. 943–8.

Nguyen, A. M. and Jacobs, C. R. (2013). "Emerging role of primary cilia as mechanosensors in osteocytes". *Bone* 54: pp. 196–204.

Nilius, B. (2007). "TRP channels in disease". *Biochim Biophys Acta* 1772: pp. 805–12.

Nilsson, O. and Baron, J. (2004). "Fundamental limits on longitudinal bone growth: growth plate senescence and epiphyseal fusion". *Trends Endocrinol Metab* 15: pp. 370–4.

Nishita, M., Park, S. Y., Nishio, T., et al. (2017). "Ror2 signaling regulates Golgi structure and transport through IFT20 for tumor invasiveness". *Sci Rep* 7: p. 1.

Noda, K., Kitami, M., Kitami, K., et al. (2016). "Canonical and noncanonical intraflagellar transport regulates craniofacial skeletal development". *Proc Natl Acad Sci U S A* 113: E2589–97.

Nomura, M., Sakitani, N., Iwasawa, H., et al. (2017). "Thinning of articular cartilage after joint unloading or immobilization. An experimental investigation of the pathogenesis in mice". *Osteoarthritis Cartilage* 25: pp. 727–736.

Nonaka, S., Tanaka, Y., Okada, Y., et al. (1998). "Randomization of left-right asymmetry due to loss of nodal cilia generating leftward flow of extraembryonic fluid in mice lacking KIF3B motor protein". *Cell* 95: pp. 829–37.

Norris, D. P. and Jackson, P. K. (2016). "Cell biology: Calcium contradictions in cilia". *Nature* 531: pp. 582–3.
Ohashi, N., Robling, A. G., Burr, D. B., et al. (2002). "The effects of dynamic axial loading on the rat growth plate". *J Bone Miner Res* 17: pp. 284–92.
Ojanen, S. P., Finnila, M. A. J., Makela, J. T. A., et al. (2019). "Anterior cruciate ligament transection of rabbits alters composition, structure and biomechanics of articular cartilage and chondrocyte deformation 2weeks post-surgery in a site-specific manner". *J Biomech*: p. 109450.
Oka, Y., Murata, K., Kano, T., et al. (2019). "Impact of Controlling Abnormal Joint Movement on the Effectiveness of Subsequent Exercise Intervention in Mouse Models of Early Knee Osteoarthritis". *Cartilage*: p. 1947603519885007.
Ornitz, D. M. and Legeai-Mallet, L. (2017). "Achondroplasia: Development, pathogenesis, and therapy". *Dev Dyn* 246: pp. 291–309.
Ornitz, D. M. and Marie, P. J. (2002). "FGF signaling pathways in endochondral and intramembranous bone development and human genetic disease". *Genes Dev* 16: pp. 1446–65.
Ornitz, D. M. and Marie, P. J. (2019). "Fibroblast growth factors in skeletal development". *Curr Top Dev Biol* 133: pp. 195–234.
Osborne, A. C., Lamb, K. J., Lewthwaite, J. C., et al. (2002). "Short-term rigid and flaccid paralyses diminish growth of embryonic chick limbs and abrogate joint cavity formation but differentially preserve pre-cavitated joints". *J Musculoskelet Neuronal Interact* 2: pp. 448–56.
Palmoski, M., Perricone, E., and Brandt, K. D. (1979). "Development and reversal of a proteoglycan aggregation defect in normal canine knee cartilage after immobilization". *Arthritis Rheum* 22: pp. 508–17.
Palmoski, M. J. and Brandt, K. D. (1984). "Effects of static and cyclic compressive loading on articular cartilage plugs in vitro". *Arthritis Rheum* 27: pp. 675–81.
Pan, D. (2007). "Hippo signaling in organ size control". *Genes Dev* 21: pp. 886–97.
Park, H., Kong, S. Y., Kim, H. W., et al. (2012). "Altered cellular kinetics in growth plate according to alterations in weight bearing". *Yonsei Med J* 53: pp. 618–24.
Pedersen, L. B., Mogensen, J. B., and Christensen, S. T. (2016). "Endocytic Control of Cellular Signaling at the Primary Cilium". *Trends Biochem Sci* 41: pp. 784–97.
Pitsillides, A. A. (2006). "Early effects of embryonic movement: 'a shot out of the dark'". *J Anat* 208: pp. 417–31.
Pool W. H., J. (1974). "Cartilage atrophy". *Radiology* 112: pp. 47–50.
Poole, C. A. (1991). *The growth plate: Cellular physiology, cartilage assembly and mineralization. In Cartilage: Molecular aspects*. CRC Press: pp. 179–212.
Poole, C. A., Jensen, C. G., Snyder, J. A., et al. (1997). "Confocal analysis of primary cilia structure and colocalization with the Golgi apparatus in chondrocytes and aortic smooth muscle cells". *Cell Biol Int* 21: pp. 483–94.
Poole, C. A., Zhang, Z. J., and Ross, J. M. (2001). "The differential distribution of acetylated and detyrosinated alpha-tubulin in the microtubular cytoskeleton and primary cilia of hyaline cartilage chondrocytes". *J Anat* 199: pp. 393–405.
Praetorius, H. A. and Spring, K. R. (2001). "Bending the MDCK cell primary cilium increases intracellular calcium". *J Membr Biol* 184: pp. 71–9.
Praetorius, H. A. and Spring, K. R. (2003). "The renal cell primary cilium functions as a flow sensor". *Curr Opin Nephrol Hypertens* 12: pp. 517–20.

Racunica, T. L., Teichtahl, A. J., Wang, Y., et al. (2007). "Effect of physical activity on articular knee joint structures in community-based adults". *Arthritis Rheum* 57: pp. 1261–8.

Rais, Y., Reich, A., Simsa-Maziel, S., et al. (2015). "The growth plate's response to load is partially mediated by mechano-sensing via the chondrocytic primary cilium". *Cell Mol Life Sci* 72: pp. 597–615.

Ratliff, A. H. (1959). "The short leg in poliomyelitis". *J Bone Joint Surg Br* 41-b: pp. 56–69.

Rattner, J. B., Sciore, P., Ou, Y., et al. (2010). "Primary cilia in fibroblast-like type B synoviocytes lie within a cilium pit: a site of endocytosis". *Histol Histopathol* 25: pp. 865–75.

Reginensi, A., Scott, R. P., Gregorieff, A., et al. (2013). "Yap- and Cdc42-dependent nephrogenesis and morphogenesis during mouse kidney development". *PLoS Genet* 9: e1003380.

Reich, A., Jaffe, N., Tong, A., et al. (2005). "Weight loading young chicks inhibits bone elongation and promotes growth plate ossification and vascularization". *J Appl Physiol (1985)* 98: pp. 2381–9.

Reich, A., Sharir, A., Zelzer, E., et al. (2008). "The effect of weight loading and subsequent release from loading on the postnatal skeleton". *Bone* 43: pp. 766–74.

Reich, A., Maziel, S. S., Ashkenazi, Z., et al. (2010). "Involvement of matrix metalloproteinases in the growth plate response to physiological mechanical load". *J Appl Physiol (1985)* 108: pp. 172–80.

Riad, J., Finnbogason, T., and Brostrom, E. (2010). "Leg length discrepancy in spastic hemiplegic cerebral palsy: a magnetic resonance imaging study". *J Pediatr Orthop* 30: pp. 846–50.

Rich, D. R. and Clark, A. L. (2012). "Chondrocyte primary cilia shorten in response to osmotic challenge and are sites for endocytosis". *Osteoarthritis Cartilage* 20: pp. 923–30.

Robert, A., Margall-Ducos, G., Guidotti, J. E., et al. (2007). "The intraflagellar transport component IFT88/polaris is a centrosomal protein regulating G1-S transition in non-ciliated cells". *J Cell Sci* 120: pp. 628–37.

Rohatgi, R., Milenkovic, L., and Scott, M. P. (2007a). "Patched1 regulates hedgehog signaling at the primary cilium". *Science* 317: pp. 372–6.

Rohatgi, R., Milenkovic, L., and Scott, M. P. (2007b). "Patched1 regulates hedgehog signaling at the primary cilium". *Science* 317: pp. 372–6.

Rolfe, R. A., Nowlan, N. C., Kenny, E. M., et al. (2014). "Identification of mechanosensitive genes during skeletal development: alteration of genes associated with cytoskeletal rearrangement and cell signalling pathways". *BMC Genomics* 15: p. 48.

Roos, E. M. and Dahlberg, L. (2005). "Positive effects of moderate exercise on glycosaminoglycan content in knee cartilage: a four-month, randomized, controlled trial in patients at risk of osteoarthritis". *Arthritis Rheum* 52: pp. 3507–14.

Ross, A. J., May-Simera, H., Eichers, E. R., et al. (2005). "Disruption of Bardet-Biedl syndrome ciliary proteins perturbs planar cell polarity in vertebrates". *Nat Genet* 37: pp. 1135–40.

Rountree, R. B., Schoor, M., Chen, H., et al. (2004). "BMP receptor signaling is required for postnatal maintenance of articular cartilage". *PLoS Biol* 2: e355.

Rowan, A. D., Hui, W., Cawston, T. E., et al. (2003). "Adenoviral gene transfer of interleukin-1 in combination with oncostatin M induces significant joint damage in a murine model". *Am J Pathol* 162: pp. 1975–84.

Ruhlen, R. and Marberry, K. (2014). "The chondrocyte primary cilium". *Osteoarthritis Cartilage* 22: pp. 1071–6.

Sahebjam, S., Khokha, R., and Mort, J. S. (2007). "Increased collagen and aggrecan degradation with age in the joints of Timp3(-/-) mice". *Arthritis Rheum* 56: pp. 905–9.

Sanchez-Adams, J., Leddy, H. A., McNulty, A. L., et al. (2014). "The mechanobiology of articular cartilage: bearing the burden of osteoarthritis". *Curr Rheumatol Rep* 16: p. 451.

Sandy, J. D., Flannery, C. R., Neame, P. J., et al. (1992). "The structure of aggrecan fragments in human synovial fluid. Evidence for the involvement in osteoarthritis of a novel proteinase which cleaves the Glu 373-Ala 374 bond of the interglobular domain". *J Clin Invest* 89: pp. 1512–6.

Satir, P. and Christensen, S. T. (2007). "Overview of structure and function of mammalian cilia". *Annu Rev Physiol* 69: pp. 377–400.

Schiedel, F. and Rodl, R. (2012). "Lower limb lengthening in patients with disproportionate short stature with achondroplasia: a systematic review of the last 20 years". *Disabil Rehabil* 34: pp. 982–7.

Schmidts, M. (2014). "Clinical genetics and pathobiology of ciliary chondrodysplasias". *J Pediatr Genet* 3: pp. 46–94.

Schou, K. B., Mogensen, J. B., Morthorst, S. K., et al. (2017). "KIF13B establishes a CAV1-enriched microdomain at the ciliary transition zone to promote Sonic hedgehog signalling". *Nat Commun* 8: p. 14177.

Scilabra, S. D., Troeberg, L., Yamamoto, K., et al. (2013). "Differential regulation of extracellular tissue inhibitor of metalloproteinases-3 levels by cell membrane-bound and shed low density lipoprotein receptor-related protein 1". *J Biol Chem* 288: pp. 332–42.

Sheffield, I. D., McGee, M. A., Glenn, S. J., et al. (2018). "Osteoarthritis-Like Changes in Bardet-Biedl Syndrome Mutant Ciliopathy Mice (Bbs1(M390R/M390R)): Evidence for a Role of Primary Cilia in Cartilage Homeostasis and Regulation of Inflammation". *Front Physiol* 9: p. 708.

Shitama, K. (1979). "Calcification of aging articular cartilage in man". *Acta Orthop Scand* 50: pp. 613–9.

Shwartz, Y., Blitz, E., and Zelzer, E. (2013). "One load to rule them all: mechanical control of the musculoskeletal system in development and aging". *Differentiation* 86: pp. 104–11.

Siljee, J. E., Wang, Y., Bernard, A. A., et al. (2018). "Subcellular localization of MC4R with ADCY3 at neuronal primary cilia underlies a common pathway for genetic predisposition to obesity". *Nat Genet* 50: pp. 180–185.

Singer, D., Thamm, K., Zhuang, H., et al. (2019). "Prominin-1 controls stem cell activation by orchestrating ciliary dynamics". *Embo j* 38.

Song, B., Haycraft, C. J., Seo, H. S., et al. (2007). "Development of the post-natal growth plate requires intraflagellar transport proteins". *Dev Biol* 305: pp. 202–16.

St-Jacques, B., Hammerschmidt, M., and McMahon, A. P. (1999). "Indian hedgehog signaling regulates proliferation and differentiation of chondrocytes and is essential for bone formation". *Genes Dev* 13: pp. 2072–86.

Staines, K. A., Poulet, B., Wentworth, D. N., et al. (2017a). "The STR/ort mouse model of spontaneous osteoarthritis - an update". *Osteoarthritis Cartilage* 25: pp. 802–808.

Staines, K. A., Poulet, B., Wentworth, D. N., et al. (2017b). "The STR/ort mouse model of spontaneous osteoarthritis - an update". *Osteoarthritis Cartilage* 25: pp. 802–808.

Stifter, S. A. and Greter, M. (2020). "STOP floxing around: Specificity and leakiness of inducible Cre/loxP systems". *Eur J Immunol* 50: pp. 338–341.

Stinchcombe, J. C. and Griffiths, G. M. (2014). "Communication, the centrosome and the immunological synapse". *Philos Trans R Soc Lond B Biol Sci* 369.

Stroope, A., Radtke, B., Huang, B., et al. (2010). "Hepato-renal pathology in pkd2ws25/- mice, an animal model of autosomal dominant polycystic kidney disease". *Am J Pathol* 176: pp. 1282–91.

Struglics, A., Larsson, S., Pratta, M. A., et al. (2006). "Human osteoarthritis synovial fluid and joint cartilage contain both aggrecanase- and matrix metalloproteinase-generated aggrecan fragments". *Osteoarthritis Cartilage* 14: pp. 101–13.

Takeda, S., Bonnamy, J. P., Owen, M. J., et al. (2001). "Continuous expression of Cbfa1 in nonhypertrophic chondrocytes uncovers its ability to induce hypertrophic chondrocyte differentiation and partially rescues Cbfa1-deficient mice". *Genes Dev* 15: pp. 467–81.

Tatsumi, S., Ishii, K., Amizuka, N., et al. (2007). "Targeted ablation of osteocytes induces osteoporosis with defective mechanotransduction". *Cell Metab* 5: pp. 464–75.

Tetlow, L. C., Adlam, D. J., and Woolley, D. E. (2001). "Matrix metalloproteinase and proinflammatory cytokine production by chondrocytes of human osteoarthritic cartilage: associations with degenerative changes". *Arthritis Rheum* 44: pp. 585–94.

Tetsunaga, T., Nishida, K., Furumatsu, T., et al. (2011). "Regulation of mechanical stress-induced MMP-13 and ADAMTS-5 expression by RUNX-2 transcriptional factor in SW1353 chondrocyte-like cells". *Osteoarthritis Cartilage* 19: pp. 222–32.

Teves, M. E., Sundaresan, G., Cohen, D. J., et al. (2015). "Spag17 deficiency results in skeletal malformations and bone abnormalities". *PLoS One* 10: e0125936.

Teves, M. E., Strauss J. F., r., Sapao, P., et al. (2019). "The Primary Cilium: Emerging Role as a Key Player in Fibrosis". *Curr Rheumatol Rep* 21: p. 29.

Thompson, C. L., Chapple, J. P., and Knight, M. M. (2014a). "Primary cilia disassembly down-regulates mechanosensitive hedgehog signalling: a feedback mechanism controlling ADAMTS-5 expression in chondrocytes". *Osteoarthritis Cartilage* 22: pp. 490–8.

Thompson, C. L., Chapple, J. P., and Knight, M. M. (2014b). "Primary cilia disassembly down-regulates mechanosensitive hedgehog signalling: a feedback mechanism controlling ADAMTS-5 expression in chondrocytes". *Osteoarthritis Cartilage* 22: pp. 490–8.

Thompson, C. L., Patel, R., Kelly, T. A., et al. (2015a). "Hedgehog signalling does not stimulate cartilage catabolism and is inhibited by Interleukin-1beta". *Arthritis Res Ther* 17: p. 373.

Thompson, C. L., Patel, R., Kelly, T. A., et al. (2015b). "Hedgehog signalling does not stimulate cartilage catabolism and is inhibited by Interleukin-1beta". *Arthritis Res Ther* 17: p. 373.

Tian, H., Feng, J., Li, J., et al. (2017). "Intraflagellar transport 88 (IFT88) is crucial for craniofacial development in mice and is a candidate gene for human cleft lip and palate". *Hum Mol Genet* 26: pp. 860–872.

Togawa, H., Nakanishi, K., Mukaiyama, H., et al. (2011). "Epithelial-to-mesenchymal transition in cyst lining epithelial cells in an orthologous PCK rat model of autosomal-recessive polycystic kidney disease". *Am J Physiol Renal Physiol* 300: F511–20.

Tortorella, C., Piazzolla, G., Spaccavento, F., et al. (2000). "Regulatory role of extracellular matrix proteins in neutrophil respiratory burst during aging". *Mech Ageing Dev* 119: pp. 69–82.

Troeberg, L. and Nagase, H. (2012). "Proteases involved in cartilage matrix degradation in osteoarthritis". *Biochim Biophys Acta* 1824: pp. 133–45.

Vincent, T. L. and Wann, A. K. T. (2018). "Mechanoadaptation: articular cartilage through thick and thin". *J Physiol*.

Vincent, T. L., Williams, R. O., Maciewicz, R., et al. (2012). "Mapping pathogenesis of arthritis through small animal models". *Rheumatology (Oxford)* 51: pp. 1931–41.

Vooijs, M., Jonkers, J., and Berns, A. (2001). "A highly efficient ligand-regulated Cre recombinase mouse line shows that LoxP recombination is position dependent". *EMBO Rep* 2: pp. 292–7.

Vu, T. H., Shipley, J. M., Bergers, G., et al. (1998). "MMP-9/gelatinase B is a key regulator of growth plate angiogenesis and apoptosis of hypertrophic chondrocytes". *Cell* 93: pp. 411–22.

Walsh, M., Connolly, P., Jenkinson, A., et al. (2000). "Leg length discrepancy–an experimental study of compensatory changes in three dimensions using gait analysis". *Gait Posture* 12: pp. 156–61.

Wang, Z., Wann, A. K., Thompson, C. L., et al. (2016). "IFT88 influences chondrocyte actin organization and biomechanics". *Osteoarthritis Cartilage* 24: pp. 544–54.

Wann, A. K., Zuo, N., Haycraft, C. J., et al. (2012). "Primary cilia mediate mechanotransduction through control of ATP-induced Ca2+ signaling in compressed chondrocytes". *Faseb j* 26: pp. 1663–71.

Whittaker, J. L., Woodhouse, L. J., Nettel-Aguirre, A., et al. (2015). "Outcomes associated with early post-traumatic osteoarthritis and other negative health consequences 3-10 years following knee joint injury in youth sport". *Osteoarthritis Cartilage* 23: pp. 1122–9.

Wiegant, K., Intema, F., Roermund, P. M. van, et al. (2015). "Evidence of cartilage repair by joint distraction in a canine model of osteoarthritis". *Arthritis Rheumatol* 67: pp. 465–74.

Wu, Q., Zhang, Y., and Chen, Q. (2001). "Indian hedgehog is an essential component of mechanotransduction complex to stimulate chondrocyte proliferation". *J Biol Chem* 276: pp. 35290–6.

Yamamoto, K., Troeberg, L., Scilabra, S. D., et al. (2013a). "LRP-1-mediated endocytosis regulates extracellular activity of ADAMTS-5 in articular cartilage". *Faseb j* 27: pp. 511–21.

Yamamoto, K., Troeberg, L., Scilabra, S. D., et al. (2013b). "LRP-1-mediated endocytosis regulates extracellular activity of ADAMTS-5 in articular cartilage". *Faseb j* 27: pp. 511–21.

Yamamoto, K., Okano, H., Miyagawa, W., et al. (2016). "MMP-13 is constitutively produced in human chondrocytes and co-endocytosed with ADAMTS-5 and TIMP-3 by the endocytic receptor LRP1". *Matrix Biol*.

Yamamoto, K., Santamaria, S., Botkjaer, K. A., et al. (2017). "Inhibition of shedding of low-density lipoprotein receptor-related protein 1 reverses cartilage matrix degradation in osteoarthritis". *Arthritis Rheumatol*.

Yang, C. Y., Chanalaris, A., and Troeberg, L. (2017). "ADAMTS and ADAM metalloproteinases in osteoarthritis - looking beyond the 'usual suspects'". *Osteoarthritis Cartilage* 25: pp. 1000–1009.

Yang, L., Tsang, K. Y., Tang, H. C., et al. (2014). "Hypertrophic chondrocytes can become osteoblasts and osteocytes in endochondral bone formation". *Proc Natl Acad Sci U S A* 111: pp. 12097–102.

Yu, F. X., Zhao, B., and Guan, K. L. (2015). "Hippo Pathway in Organ Size Control, Tissue Homeostasis, and Cancer". *Cell* 163: pp. 811–28.

Yuan, X. and Yang, S. (2015a). "Deletion of IFT80 Impairs Epiphyseal and Articular Cartilage Formation Due to Disruption of Chondrocyte Differentiation". *PLoS One* 10: e0130618.

Yuan, X. and Yang, S. (2015b). "Deletion of IFT80 Impairs Epiphyseal and Articular Cartilage Formation Due to Disruption of Chondrocyte Differentiation". *PLoS One* 10: e0130618.

Zhao, B., Ye, X., Yu, J., et al. (2008). "TEAD mediates YAP-dependent gene induction and growth control". *Genes Dev* 22: pp. 1962–71.

Zhao, J., Li, M., Bradfield, J. P., et al. (2010). "The role of height-associated loci identified in genome wide association studies in the determination of pediatric stature". *BMC Med Genet* 11: p. 96.

Zhong, Z. A., Sun, W., Chen, H., et al. (2015). "Optimizing tamoxifen-inducible Cre/loxp system to reduce tamoxifen effect on bone turnover in long bones of young mice". *Bone* 81: pp. 614–619.

Zhou, X., Mark, K. von der, Henry, S., et al. (2014). "Chondrocytes transdifferentiate into osteoblasts in endochondral bone during development, postnatal growth and fracture healing in mice". *PLoS Genet* 10: e1004820.

Ziaaldini, M. M., Marzetti, E., Picca, A., et al. (2017). "Biochemical Pathways of Sarcopenia and Their Modulation by Physical Exercise: A Narrative Review". *Front Med (Lausanne)* 4: p. 167.

Zimmermann, K. W. (1898). "Beiträge zur Kenntniss einiger Drüsen und Epithelien". *Archiv für mikroskopische Anatomie* 52: pp. 552–706.